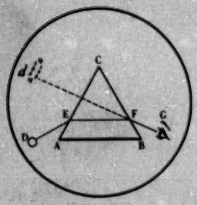

# optics and spectroscopy

volume viii
number 4
april 1960

OPTICAL SOCIETY OF AMERICA

USSR ACADEMY OF SCIENCE

*RUSSIAN EDITORIAL STAFF FOR*
*OPTIKA I SPEKTROSKOPIYA sponsored by*
*USSR ACADEMY OF SCIENCES*

*Editor*: S. E. FRISH

*Assistant Editor*: P. P. FEOFILOV
*Corresponding Secretary*: L. S. SAZONOV

*Associate Editors*:

M. M. GUREVICH M. A. EL'IASHEVICH A. A. LEBEDEV V. P. LINNIK
S. L. MANDEL'SHTAM I. V. OBREIMOV V. K. PROKOF'EV
N. N. SOBOLEV A. N. TERENIN A. I. TUDOROVSKII

Translated from *OPTIKA I SPEKTROSKOPIYA* on the initiative of
THE OPTICAL SOCIETY OF AMERICA, INC.
with a grant-in-aid from
THE NATIONAL SCIENCE FOUNDATION

TRANSLATION EDITORIAL STAFF

*Scientific Editors*

FRED W. BEHNKE, *Perkin-Elmer Corp.*

CYRUS FELDMAN, *Oak Ridge National Laboratory*

GEORGE HERRMAN, *Columbia University*

*Administrative Editor*: PATRICIA R. WAKELING, *OSA*

Published monthly by the Optical Society of America, Inc. Executive office: 1155 Sixteenth Street, N.W., Washington, D.C. Subscriptions for one year to members of the Society: Associates $13.00; Regular members and Fellows $17.00. Subscriptions for non-members of the Society: One year U. S. and Possessions, $25.00; Foreign $26.00. Back numbers: $3.00 per copy. Subscriptions, changes of address and undeliverable copies should be referred to the Executive offices in Washington, D.C. The office of publication is 2500 South State Street, Ann Arbor, Michigan. Second class postage paid at Ann Arbor, Michigan.

Printed in the U.S.A. by Edwards Brothers, Inc., Ann Arbor, Michigan.

# NINETIETH ANNIVERSARY OF V. I. LENIN'S BIRTHDAY

April 22, 1960, was the ninetieth anniversary of the birthday of the great leader of the October Revolution and the founder of the Soviet Socialistic State, Vladimir Il'ich Lenin. As head of the Soviet Nation, Lenin was concerned with all the facets of its life. His untiring attention was directed not only to the solution of the most pressing current political problems, but also to the development of the national economy and culture of the country. In 1918, the first year of the Revolution, Lenin drew up "A Plan for Science and Technology." Soviet science—the characteristic features of which are democracy and availability to all people—came into existence and developed under his direct influence. He wrote "In the past, the whole human mind and all of its genius had been created to give only some people all of the benefits of technology and culture and to deny the most essential things—education and development—to others. Now, all the wonders of technology and all the conquests of culture shall become the property of all people; and henceforth the human mind and genius will never be repressed and exploited."

In the years 1918-1919, the first Soviet Scientific Research Institutes in the field of physics appeared: the Institute of Physics and Biophysics in Moscow, the Physico-Technical Institute, and the State Optical Institute in Leningrad.

In December 1920, on Lenin's initiative the Eighth All Russian Soviet Congress adopted a plan for the electrification of the country—the GOELRO plan—laying the foundation for the development of science and technology, and, therefore, for all the national economy of the young Soviet State.

Among the gigantic heritage left by Vladimir Il'ich Lenin his philosophic writing is exceptionally important to Soviet science. In his famous book "Materialism and Empiriocriticism" Lenin presented a deep analysis of the crisis which physics experienced at the turn of the century. In this book he showed how the direction for the development of science should be based on the application of dialectic materialism, but, while he considered that the principles of dialectic materialistic philosophy form the basis of Soviet science, he also warned against dogmatism and doctrinairism.

Lenin gave the classical definition of matter as a philosophic category which defines an objective reality presenting itself to the senses of the man; a reality that can be copied, photographed, and reflected in our senses, while its existence is independent of them. With exceptional clarity he presented the problem of the dichotomy between the philosophic, gnosiological concept of matter and the concrete concepts of various manifestations of matter in a physics experiment. Nowadays, anybody understanding Lenin's ideas will find it hard to comprehend how the philosophic concept of matter, which follows from the sum total of our knowledge of the real universe, can be confused with its specific manifestations, and how the solution of the gnosiological philosophic problem of the existence of the material universe can depend on the various specific physical discoveries. Nevertheless, the history of

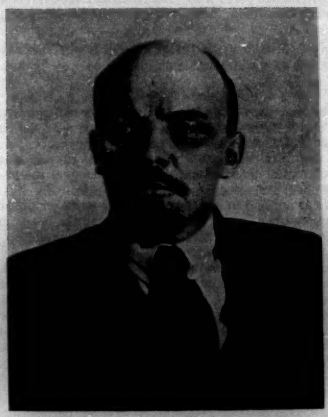

physics shows that these errors were made continually.

Twentieth century physicists studied the properties of atoms and elementary particles, which led to the creation of quantum mechanics, and the relativity theory. Discoveries of the utmost importance were made which forced us to abandon old concepts and which pointed to the unusual nature of intra-atomic processes taking place at high speeds, processes of a different nature from the straightforward developments of classical mechanics. Many bourgeois physicists claimed that these discoveries contradict our materialistic ideas. New idealistic philosophies appeared; sermons against causality and against the objective existence of space and time were heard; erroneous ideas were expressed on the possibility of learning about the universe on the basis of general a priori ideas without the help of experiments and observations. However, Soviet physicists, using Lenin's guiding ideas, were and are thoroughly capable of discovering the true positive content of new theories and to separate it from the idealistic dressing by which it is often concealed.

Lenin gave to Soviet scientists excellent examples of how to expose erroneous idealistic interpretations of new theories, and how to avoid the metaphysical mechanicism which retards science. He showed us what Soviet science should be: it should be uncompromising, free of all shallow and foreign dressings, and concerned primarily with the welfare of the people.

Heeding the counsel of Vladimir Il'ich Lenin, the Soviet prople transformed backward Russia into a powerful socialistic nation. Its scientific and technical accomplishments are justly admired by all progressive people.

# ON THE CALCULATION OF PHOTOIONIZATION ABSORPTION

L. M. Biberman and G. E. Norman

Received 1 July 1959

A method is suggested for calculating the coefficient of absorption due to the photoionization of multielectron atoms.

The literature contains a large number of papers dealing with the absorptivity of hot gases due to the photoionization of excited atoms.

If the distribution of atoms among the excited states is a Boltzmann distribution, then for hydrogen, the resulting absorption coefficient is found as follows: Kramers' formula is applied to all states with the same principal quantum number n, and a summation over the lower excited levels and an integration over the upper excited levels is then carried out.

Unsöld[1] extended the expression which holds for hydrogen to complex atoms. The structural peculiarities of complex atoms were taken into account by introducing an effective nuclear charge $Z^*$ and a factor $\gamma$. $\gamma$ is the ratio of the number of sublevels of a complex atom with a given n and l to an analogous quantity for hydrogen.

The quantity $Z^*$ is defined by the relationship:

$$E_{nl} = -\frac{Z^{*2}}{n^2}, \qquad (1)$$

where $E_{nl}$ is the energy of the state for a given n and l. Because of a more uniform distribution of energy levels, it was possible to extend the integration over all the excited states in the case of complex atoms. As a result, the following expression for the photoionization absorption coefficient was obtained, computed for a single atom: for $\nu \leq \nu_g$

$$\varkappa_T(\nu, T) = 1.8 \cdot 10^{24} \frac{Z^{*2}\gamma_1 T}{\Sigma_0 \cdot \nu^3} e^{-\frac{u}{T}} (e^u - 1) \qquad (2')$$

and for $\nu \geq \nu_g$

$$\varkappa_T(\nu, T) = 1.8 \cdot 10^{24} \frac{Z^{*2}\gamma_1 T}{\Sigma_0 \cdot \nu^3} e^{-\frac{u}{T}} (e^{u_g} - 1), \qquad (2'')$$

where $\nu$ is the absorbed frequency, T is the Kelvin temperature, $\Sigma_0$ is the atomic state sum, $u = h\nu/kT$, and $\nu_1$ and $\nu_g$ are the frequencies corresponding to the photoionization threshold from the ground and excited states respectively.

Expressions (2′) and (2″) are obtained using the same value of $Z^*$ for all levels, in spite of the fact that according to (1), the quantity $Z^*$ depends strongly on n and l. Unsöld,[1] Vitense,[2] Schirmer,[3] and others suggest that $Z^*$ be computed by substituting the ground state energy of the atom in (1); this gives $Z^{*2} = 4$-7. On the other hand, Maecher and Peters[4] assumed that $Z^* = 1$ which gave a better agreement of the theoretical and experimental data.

Thus, there are serious differences of opinion in the literature as to the choice of the value of $Z^*$, an important quantity which, according to Unsöld, takes account of the structural difference between the complex atom and hydrogen.

Recently, Seaton and Burgess,[5] using the quantum defect method, obtained expressions for the photoionization cross section of an arbitrary excited atom whose optical electron is in the state n, l:

$$\varkappa_{nl}(\nu) = 8.57 \cdot 10^{-19} \cdot \frac{E}{E_{nl}^3} \sum_{l'=l\pm 1} C_{l'} \left| g\left(n_l^*; k^2; l'\right)\right|^2, \qquad (3)$$

where

$$g\left(n_l^*; k^2; l'\right) = G_{ll'}\left(n_l^*\right) \cdot \left(\frac{E}{E_{nl}}\right)^{-\gamma_{ll'}(n_l^*)} \cos \pi\left[n_l^* + \mu_{l'}(k^2) + \gamma_{ll'}\right], \qquad (4)$$

and

$$\gamma_{ll'} = a_{ll'} + \frac{b_{ll'}}{n_l^*} + \frac{c_{ll'}}{n_l^{*2}} + \frac{a_{ll'} n_l^* k^2}{1 + n_l^* k^2} + \frac{\beta_{ll'} n_l^{*2} k^2}{1 + n_l^{*2} k^2}. \qquad (5)$$

where $k^2$ and E are the energies of the free electron and the absorbed photon respectively, expressed in Rydberg units, l, l′ are the azimuthal quantum numbers of electrons in their initial and final states, $n_l^*$ is the effective principal quantum number of the initial state determined from Eq. (1) with $Z^* = 1$; $\mu_{l'}(k^2)$ is the quantum defect of the levels l′ extrapolated to positive energies of the optical electron, $\mu_{l'}(k^2) \geq 0$;

$$C_{l+1} = \frac{l+1}{2l+1}; \; C_{l-1} = \frac{l}{2l+1}.$$

In reference 5 the functions $g_{ll'}(n_l^*)$, $\gamma_{ll'}(n_l^*)$ and the coefficients $a_{ll'}$, $b_{ll'}$, $c_{ll'}$, $\alpha_{ll'}$, $\beta_{ll'}$ are tabulated for $1 \leq n_l^* \leq 12$, $0 \leq l \leq 3$, $0 \leq l' \leq 3$.

Naturally, Eqs. (3)-(5) also describe the photoionization of hydrogen. In this case, $n_l^* = n$ and $\mu_{l'} = 0$, and since n is an integer,

$$\left|\cos \pi\left[n_l^* + \mu_{l'}(k^2) + \gamma_{ll'}\right]\right| = \left|\cos \pi \gamma_{ll'}\right|.$$

Cross sections calculated according to (3), (4), and (5) agree with the results obtained using Kramers' formula, which was made more accurate by using the Gaunt factor. The Gaunt factor, as is well known, does not differ much from unity near the series limit.

Using the results of Seaton and Burgess, one can show that the application of Kramers' formula to complex atoms gives quite erroneous results, which cannot be corrected by introducing the constant factor $Z^{*2}$.

Let the effective quantum number $n^*$ correspond to a certain state of the complex atom. Also, let the inequality $n < n_l^* < n + 1$ hold. Calculations show that the magnitude of the photoionization cross section computed for $n_l^*$ does not fall between the corresponding values obtained for n and n + 1; that is, this value is not intermediate between the two corresponding hydrogen cross sections and may be considerably different in its frequency dependence. Mathematically, this result is expressed as the phase change of the cosine in (4) by the amount $\pi[n_l^* + \mu_{l'}(k^2) - n]$. It is clear that the constant factor $Z^{*2}$ cannot account for the phase change in the cosine, which in addition depends on $n_l^*$. Thus it also does not reflect the structural properties of the complex atom.

It should be pointed out that, on the whole, the formulas of Unsöld have neither a theoretical nor an experimental basis.

This report is an attempt to obtain theoretically sound approximate expressions, as simple as possible,

for computing the resulting photoionization cross sections of complex atoms distributed among the excited states according to a Boltzmann distribution.

## DERIVATION OF THE APPROXIMATE FORMULA

The quantum defect decreases sharply with increasing l. This allows us to divide the whole scheme of energy levels of the complex atom into two parts A and B. Group A comprises the levels which have a large quantum defect. The levels of group B have practically no quantum defect, so that the photoionization cross sections of these levels are equal to the corresponding photoionization cross sections of the hydrogen atom. This permits us to take Eq. (2) as the basis of the calculation, letting $Z^* = 1$ and introducing a correction for the difference between the photoionization cross sections of the levels of group A and the corresponding hydrogen cross sections. Thus, the resulting photoionization cross sections of a gas consisting of complex atoms may be written in the form

$$\varkappa(\nu, T) = \varkappa_r(\nu, T; Z^*=1)\left[1 + \frac{\Delta\varkappa(\nu, T)}{\varkappa_r(\nu, T; Z^*=1)}\right]$$

$$= \varkappa_r(\nu, T; Z^*=1)\,\xi(\nu, T), \qquad (6)$$

$$\Delta\varkappa(\nu, T) = \frac{\gamma}{\Sigma_0}\sum_{l=0}^{l_1} 2(2l+1)\sum_{l'=l\pm1}\sum_{n_l^*=n_g^*}^{\infty} a\mathfrak{b}(\nu)\,e^{-\varkappa_l - \varkappa_{nl}}, \qquad (7)$$

where $l_1$ is the largest value of l for the levels of group A and $n_g^*$ is the smallest value of $n_l^*$ corresponding to the absorption of a frequency $\nu$ for a given l.

$$a = 8.57\cdot 10^{-19} E_{nl}^{2\gamma_{ll'}(n_l^*)-2}\cdot E^{1-2\gamma_{ll'}(n_l^*)} G_{ll'}^2(n_l^*)\, C_{l'}, \qquad (8)$$

$$\mathfrak{b}(\nu) = \cos^2\pi\left[\gamma_{ll'} + \mu_{l'}(k^2) - \mu_l(E_{nl})\right] - \cos^2\pi\gamma_{ll'}. \qquad (9)$$

Summation over $n_l^*$ formally extends to $\infty$; however, for large $n_l^*$ several levels in group A and a large number in group B correspond to each value $n_l^*$. Therefore the upper limit of the summation over $n_l^*$ in (7) has little effect on the final result.

Let us make a number of simplifications:

1. From analysis of the Burgess-Seaton formulas it follows that as a rule, the transition probability $l \to l+1$ is large compared to the probability $l \to l-1$. In view of this, we neglect transitions $l \to l-1$.

2. In Eq. (7), instead of summing over $n_l^*$ we integrate over $E_{nl}$ (for a given value of the absorbed frequency). In doing this for a complex atom, a factor

$$1 + \frac{d}{dn_l^*}\mu_l(E_{nl}),$$

appears, which takes account of the change in density distribution in the energy level scheme. This factor depends slightly on $n_l^*$. A considerable simplification is obtained if for all the levels of the group A the integration is carried out for the same value of the lower limit $n_l^* = n_g^*$. This value of n determines the limiting frequency $\nu_g$.

3. Using the data from reference 5, one can show that in the energy range of interest to us, and for the l values which are not too large,

$$K_{ll'} = G_{ll'}^2(n_l^*)\, E_{nl}^{2\gamma_{ll'}(n_l^*)-3.5}$$

depends only slightly on $E_{nl}$. We decided that it is possible to neglect slight changes in this quantity.

4. For $\chi_{ll'}$, which is defined by Eq. (5), we use the approximation for $\nu \leqslant \nu_g$

$$\gamma_{ll'} = a_{ll'} + b_{ll'}\sqrt{E} + c_{ll'}E; \qquad (10)$$

For $\nu \geqslant \nu_g$, $\chi_{ll'}$ is calculated using (5), letting $n_l^* = n_g^*$. Approximation (10) is a good one, because for an arbitrary case it accurately gives the value of $\chi_{ll'}$ for the frequencies near the threshold; as a rule, the largest photoionization cross sections correspond to these frequencies.

5. $E^{1-2\gamma_{ll'}(n_l)}$ is taken outside of the integration sign; this also gives rise to an insignificant error in the final result.

Using the above described simplifications, Eq. (7) is easily computed if for a given l the quantum number defects do not depend on the energy of the level. This holds for oxygen, nitrogen, and carbon, for example. In this case we get

$$\xi(\nu, T) = 1 + 0.11\sum_{l=0}^{l_1}(l+1)\,K_{ll'}\mathfrak{b}(\nu)\,E^{4-2\gamma_{ll'}}. \qquad (11)$$

Figure 1 shows the dependence of $\xi(\nu)$ for oxygen, nitrogen, and carbon.

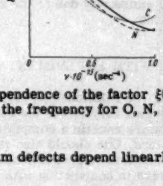


Fig. 1. Dependence of the factor $\xi(\nu)$ (see Eq. 11) on the frequency for O, N, and C atoms.

If the quantum defects depend linearly on $E_{nl}$, then for $\nu \leqslant \nu_g$

$$\xi(\nu, T) = 1 + 0.055\sum_{l=0}^{l_1}(l+1)\,K_{ll'}E^{4-2\gamma_{ll'}}$$

$$\times\left\{(1 + 2f_l E^{1.5})\sin\varphi\cdot\sin 2\pi\left[\gamma_{ll'} + \mu_{l'}(0) - \mu_l(E) + \frac{\varphi}{2\pi}\right]\right.$$

$$\left. - \cos 2\pi\gamma_{ll'} + 2f_l E^{1.5}\right\}, \qquad (12')$$

where

$$\varphi = \arctan\frac{kRe}{kT2\pi(f_l - f_{l'})};\quad \mu_{l'}(k^2) = d_{l'} + f_{l'}k^2;\quad \mu_l(E_{nl}) = d_l - f_l E_{nl}$$

for $\nu \geqslant \nu_g$

$$\xi(\nu, T) = 1 + 0.055\sum_{l=0}^{l_1}(l+1)\,K_{ll'}E^{4-2\gamma_{ll'}}$$

$$\times\left\{(1 + 2f_l E_g^{1.5})\sin\varphi\cdot\sin 2\pi\left[\gamma_{ll'} + \mu_{l'}(E-E_g) - \mu_l(E_g) + \frac{\varphi}{2\pi}\right]\right.$$

$$\left. - \cos 2\pi\gamma_{ll'} + 2f_l E_g^{1.5}\right\}. \qquad (12'')$$

If $\nu \leqslant \nu_g$, then expression (11) or (12'), together with (6), completely determines the absorption coefficient. However, if $\nu > \nu_g$ the corresponding equations determine the absorption of frequency $\nu$ by the levels where $n_l^* > n_g$. In this case we have to take into account the part played by the few levels with $n_l^* < n_g$, using the Seaton-Burgess formulas.

It should be mentioned that in the cases where the

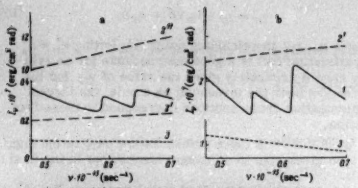

Fig. 2. Experimental and theoretical data on the emissivity of oxygen in a continuous spectrum, calculated for one atom; a—for T = 10,500°K; b—for T = 13,000°K. Curve 1—experiment; curve 2′—calculation according to Unsöld for Z* = 1; curve 2″—the same for Z*² = 5; curve 3—authors' calculation.

levels with the same n and l but with different multiplicities differ greatly in energy, the coefficient $\xi(\nu, T)$ can be computed separately for the group of levels of each multiplicity, taking account of the statistical weight of each of the groups.

The above-mentioned equations for the absorption coefficient, together with the Kirchhof's law, enable us to easily compute the emissivity due to the recombination of electrons with ions.

## COMPARISON WITH EXPERIMENTAL RESULTS

Verification of the relationships given above is complicated by the fact that very few of the experimental papers in the literature contain a complete set of the necessary parameters. One should also recognize that photoionization absorption or recombination luminescence usually appears in conjunction with other incompletely understood processes.

We decided to use Boldt's papers[6, 7] which measure the absolute spectral emissivity of arcs burning in pure nitrogen or oxygen at one atmosphere pressure and at T = 10,500-13,000°K. It should be borne in mind that the intensity measured also includes the luminescence due to the formation of negative ions and free-free electron transitions in the field of atoms and ions.

Figures 2 and 3 show the results of the measurements at 13,000 and 10,500°K for one atom. The spectral emissivity computed according to Unsöld and by means of Eqs. (6) and (11) is also shown in these figures.

Figures 2 and 3 allow us to draw the following conclusions:

(a) For T = 13,000°K, even assuming Z* = 1, the calculation according to Unsöld gives a curve considerably higher than the experimental curve, in spite of the fact that only one of the processes leading to the measured intensity change was accounted for. If, according to references 1 and 2, we let Z*² = 5, as Greenstein[8] did, then there is a deviation of an order of magnitude for C, N, and O.

The curve calculated according to (6) and (11) lies below the experimental curve. This deviation is in agreement with the indirect estimates of the part played by all the other radiation processes which were made by Boldt.

(b) According to Boldt, for T = 10,500°K one should take into account the fact that the creation of negative ions and free-free transitions contribute 60-70% of the measured intensity. Our curves lie below the experimental ones by a corresponding amount. A calculation according to Unsöld again gives results which are too high.

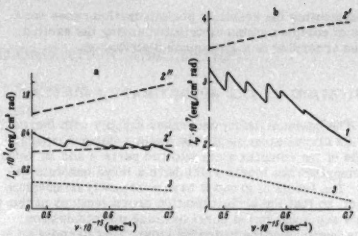

Fig. 3. Experimental and theoretical data on the calculation of emissivity of nitrogen in the continuous spectrum, calculated for one atom; a—for T = 10,500°K; b—for T = 13,000°K. Curve 1—experiment; curve 2′—calculation according to Unsöld for Z* = 1; curve 2″—the same for Z*² = 5; curve 3—calculation of the authors.

Comparison of our calculations with the measurements of the emissivity of an open carbon arc carried out by Maecker and Peters[4] gives analogous results.

In the experimental conditions used in references 6, 7, and 4, a considerable decrease of the ionization potential Δu took place, due to the interaction of atoms with the neighboring charged particles.

The influence of this phenomenon on the degree of ionization was taken into account in the calculation.

The same phenomenon can affect the magnitude of the photoionization cross section; this is usually taken into account by replacing the quantity $u_1$ by the quantity $u_1 - \Delta u$ in (2′). A similar operation carried out in our calculations leads to some increase of the calculated quantities. This, however, does not alter our conclusions. We did not compute a similar correction for the interaction of atoms with neighboring charges, because we feel that this problem should be examined separately.

The proposed equation (6) formally differs from Unsöld's formula only in that the Z*² is replaced by $\xi(\nu, T)$. However, the use of Z*² is based on an analogy which has no foundation, while the quantity $\xi(\nu, T)$ is obtained by simplification of an accurate expression. We should mention here that $\xi(\nu, T)$ depends strongly on the frequency, can depend on the temperature, and in the examples which were considered turned out to be less than unity in magnitude, while Z* is always taken as a constant and is always greater than 1. Even if, contrary to Unsöld's suggestion, we let Z* = 1, the experimental results cannot be explained. We feel that the proposed method for the calculation of photoionization absorption rests on a firmer theoretical basis and gives results much closer to the experimental data.

## REFERENCES

1. A. Unsöld. Ann. Physik **33**, 607 (1938).
2. E. Vitense. Z. Astrophys. **28**, 91 (1951).
3. H. Schirmer. Z. angew. Phys. **6**, 3 (1954).
4. H. Maecker and T. Peters. Z. Physik **139**, 448 (1954).
5. A. Burgess and M. J. Seaton. Revs. Modern Phys. **30**, 992 (1958).
6. G. Boldt. Z. Physik **154**, 319 (1957).
7. G. Boldt. Z. Physik **154**, 330 (1959).
8. J. Greenstein. Astrophys. J. **95**, 299 (1942).

# SPARK DISCHARGE EMISSION IN HELIUM

M. P. Vanyukov, A. A. Mak and V. P. Muratov

Received 24 July 1959

A study was made of the time variation of the profiles of arc and spark lines in the plasma emission of a spark discharge in helium. It was found that values of the concentration of charged particles determined from the width and shift of different lines differed by factors of 2 or 3.

## INTRODUCTION

The emission of a spark discharge in helium can give valuable information concerning the discharge plasma. Because of the availability of data on the atomic constants (oscillator strengths, Stark constants, etc.) it is possible to estimate the temperature of the plasma, the concentration of charged particles, etc., from the intensities, widths, and displacements of the spectral lines. Data on line profiles have already been used for determining the electron concentration in a pulsed discharge in helium[1,2] and also in a shock wave propagated in a helium atmosphere.[3] It is of interest to trace the time variation of the emission spectrum of a spark discharge in helium with the aim of determining, in particular, the concentrations of charged particles in the plasma at different instants of time. The spark discharge in helium is attracting attention at the present time also because of the high temperature which can be attained in its plasma. It has been reported that with an especially developed discharge circuit with low inductance condensers it has been possible to obtain a plasma temperature of the order of 250,000°K.[4,5]

The present communication reports the results of investigations on the time variation of the spectra of a spark discharge in helium; the experiments were carried out with a previously designed photoelectric arrangement with a time resolution of $\sim 5 \times 10^{-8}$ sec and a spectral resolution of 0.2 A.[6,7]

## TIME VARIATION OF THE DISCHARGE SPECTRUM

The spark discharge was produced in a demountable pulse lamp filled with technical grade helium at pressures of 2.5–12 atm; voltages of 2.5–10 kv with a condenser capacity of 0.05 $\mu$f and discharge circuit inductances of 0.18, 3.6, and 25 $\mu$h were used. The plasma emission was recorded in the wavelength region 2500–5500 A. A comparison spectrum was furnished by a Geissler discharge tube, the emission lines of which could be assumed to be unshifted.

Figure 1 shows the spectrum of the spark discharge in helium at various times, t, after the initiation of the discharge. In the first stage of the discharge (up to t = 0.3 $\mu$sec) an intense continuous spectrum is observed, especially in the short wavelength part of the spectral region studied; the intense HeII line at 4686 A and the HeII line at 3203 A stand out from this background. The intensity of the continuous radiation decreases more rapidly with time than the intensity of the ionic lines. The arc lines, HeI 3889, 4471, and 5016 A, appear later, beginning approximately at t = 0.3 $\mu$sec, and their emission continues much longer than that of the spark lines. The HeI 3188 A line in most cases overlaps the HeII 3203 A line.

Figure 2 shows recordings of the line profile of HeII 4686 A for three values of t during the discharge in a

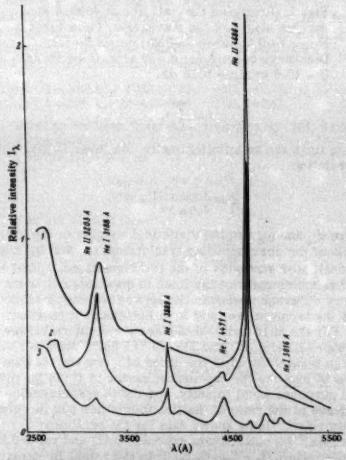


Fig. 1. Spectrum of the emission from a spark discharge in helium at various times after the beginning of the discharge. Time ($\mu$sec): curve 1—0.1; curve 2—0.7; curve 3—4.5. Discharge conditions: p = 5 atm, C = 0.035 $\mu$f, U = 7 kv, L = 0.18 $\mu$h.

circuit with minimum inductance. It was established that the 4686 A line in the first moments is greatly broadened and shifted towards the red, while remaining symmetrical. The existence of considerable displacements of the line (up to 8 A), due to the quadratic Stark effect, is an indication of extremely high intermolecular fields occurring in the first stages of the discharge.[8] It is evident in Fig. 2 that at the instant t = 0.25 $\mu$sec the profile of the line has a flat top; this indicates the existence at this instant of a uniform temperature throughout the plasma, which is completely opaque in the wavelength region around the central part of the line. If the discharge takes place in a circuit with inductance L greater than 3.6 $\mu$h, the HeII 4686 A line does not appear even in the first stage of the discharge.

In investigating line profiles it is essential to know to what extent they are distorted by reabsorption. In the case of the lines 5016 A ($2^1S$-$3^1P$) and 3889 A ($2^3S$-$3^3P$) this question can be resolved by measuring the ratio of the line intensities for given values of t.

The ratio of the integrated intensities

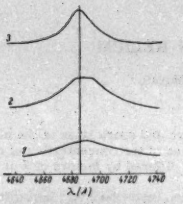


Fig. 2. Profile of the HeII line at 4686 A at various stages of the discharge. Time (μsec): curve 1—0.5; curve 2—0.25; curve 3—1.2. Discharge conditions: p = 12 atm, C = 0.05 μf, U - 10.5 kv, L. = 0.18 μh.

$$I = \int_{-\infty}^{+\infty} I_\lambda d\lambda$$

of two lines for an infinitesimally thin layer is given by the relation

$$\frac{I_{\lambda_1}}{I_{\lambda_2}} = \frac{g_{i_1} f_{k_1 i_1}}{g_{i_2} f_{k_2 i_2}} \left(\frac{\lambda_2}{\lambda_1}\right)^3 e^{-\frac{\Delta E}{kT}}, \qquad (1)$$

where $g_{i_1}$ and $g_{i_2}$ are the statistical weights of the lower levels of the corresponding transitions, $f_{k_1 i_1}$ and $f_{k_2 i_2}$ are the oscillator strengths of the two transitions, $\lambda_1$ and $\lambda_2$ are the wavelengths of the lines in question, $\Delta E$ is the energy difference between the upper levels of the lines, T is the temperature, and k is Boltzmann's constant.

For the 5016 and 3889 A lines the distance between the upper levels, $3^1P$ and $3^3P$, is 645 $cm^{-1}$; thus, for discharge temperatures of the order of a few tens of thousands of degrees the exponential factor in (1) is for practical purposes equal to unity, and the temperature dependence of the ratio of the line intensities can therefore be neglected. Using known data for the oscillator strengths,[9] we obtain from expression (1) and value 0.29 for the ratio $I_1/I_2 = I_{5016}/I_{3889}$. If in the actual light source there is appreciable reabsorption, the experimental value of $I_{5016}/I_{3889}$ should increase with an increase in the opacity of the source, since the 3889 A line is more subject to reabsorption than the 5016 A line. Table 1 gives experimental values of the ratio of the line intensities for different values of t and different values of the circuit inductance.

Table 1

| Circuit inductance (μh) | Time (μsec) | $\frac{I_{5016}}{I_{3889}}$ |
|---|---|---|
| 0.18 | 2.7 | 0.6* |
| 3.6 | 2.7 | 0.26 |
| 3.6 | 5.2 | 0.2 |
| 25 | 2.7 | 0.3 |

*This value is possibly a little high since the neighboring lines of the nitrogen impurity, NII 5001 and 5005 A), can make a contribution to the integrated intensity of the 5016 A line (cf. below).

It is evident from the table that with the lowest inductance in the discharge circuit and for t = 2.7 μsec, the discharge plasma is partially opaque. In the other cases it is certain that there is no appreciable reabsorption.

In the strong electric fields which occur for high concentrations of charged particles in the spark discharge it might be expected that forbidden lines would occur in the spectrum. As an example of this, Fig. 3 shows the recorder trace of the two closely spaces lines HeI 4471 A ($2^3P$-$4^3D$) and HeI 4470 A ($2^3P$-$4^3F$), the latter of which is forbidden under ordinary conditions. In accordance with the different signs of the Stark constants for these two lines, the first is shifted towards the red and the second towards the violet; this is reliable evidence that the width and displacement of the lines are due to the influence of electrical fields on the radiating atom. The shift of the lines, which at t = 2.7 μsec reaches a value of 23 A, decreases with time in conformity with the decrease in the concentration of charged particles. In the first stages of the discharge the intensity of the forbidden line is greater than that of the allowed line. It is interesting to note that under the conditions prevailing in stellar atmospheres no shift of the 4470 A line is observed.[10] Unfortunately, it is difficult to use the profile of the 4471 A line in the quantitative reduction of experimental results, although attempts to do this have been made (e.g., Unsöld[11]). A decrease in the line shifts with time is observed even for the later moments of the discharge also in the case of a circuit with large inductance (L = 3.6 μh).

We will now consider in more detail the line profiles of HeI 5016 A ($2^1S$-$3^1P$) and HeI 3889 A ($2^3S$-$3^3P$), from which we will determine below the concentrations of the charged particles. The broadening of these lines for the concentrations existing in the discharge is determined by the quadratic Stark effect. The symmetry of the lines is disturbed by the presence of statistical wings (Figs. 4 and 5).

Actually the demarcation between the statistical wing and the line core, where the collision theory is applicable, can be determined by the formula[12]

$$\Delta w_g \simeq \frac{\gamma^{1/2}}{(2\pi C)^{1/2}\left(\frac{\pi}{2}\right)^{1/2}}, \qquad (2)$$

where

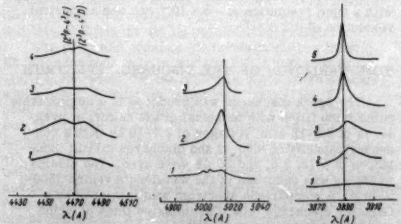


Fig. 3 Fig. 4 Fig. 5

Fig. 3. Profiles of the HeI lines at 4470 and 4471 A at various stages of the discharge. Time (μsec): curve 1—2.7; curve 2—5.2; curve 3—7.2; curve 4—10.2. Discharge conditions: p = 2.5 atm, C = 0.05 μf, U = 4.5 kv, L = 0.18 μh.

Fig. 4. Profile of the HeI line at 5016 A at various stages of the discharge. Time (μsec): curve 1—0.7; curve 2—2.7; curve 3—5.2. Discharge conditions: p = 2.5 atm, C = 0.05 μf, U = 2.5 kv, L = 3.6 μh.

Fig. 5. Profile of the HeI line at 3889 A at various stages of the discharge. Time (μsec): curve 1—0.2; curve 2—0.3 curve 3—0.7; curve 4—5.2; curve 5—9. Discharge conditions: p = 2.5 atm, C = 0.05 μf, U = 3.3 kv, L = 0.18 μh.

$$V = \sqrt{\frac{8}{\pi} RT \frac{1}{\mu}}. \quad (3)$$

For the temperature T = 40,000°K, $V_a = 1.3 \times 10^8$ cm $sec^{-1}$ and $V_i = 2.1 \times 10^8$ cm $sec^{-1}$. Using the values $2.9 \times 10^{-15}$ $cm^4$ $sec^{-1}$ [13] and $0.5 \times 10^{-15}$ $cm^4$ $sec^{-1}$ [9, 14] for the Stark constants of the 5016 A and 3889 A lines, respectively, we obtain from formula (2) the following values of the limits for the statistical wings: for the 5016 A line, $\Delta\lambda_{ge} = 390$ A and $\Delta\lambda_{gi} = 1.6$ A; and for the 3889 A line $\Delta\lambda_{ge} = 420$ A and $\Delta\lambda_{gi} = 1.7$ A.

When the latter data are compared with the magnitude of the asymmetry of the lines shown in Figs. 4 and 5, it is easy to see that the asymmetry can be ascribed to the statistical mechanism of broadening in the field of the ions.

Using the 3889 A line as an example it is also evident how the displacement decreases with increasing time. In the early stages of the development of the 5016 A line the appearance of the nitrogen lines, NII 5001 A and NII 5005 A, can be noted; the technical grade helium contains nitrogen as an impurity.

## THE ELECTRON CONCENTRATION IN THE PLASMA OF THE SPARK DISCHARGE

An estimate of the concentration of charged particles in the plasma of the spark discharge in helium was made using the halfwidths and displacements of the 5016 A and 3889 A lines; the impact theory of Weisskopf and Lindholm[12] was used, and the corrections introduced into the calculation by the nonstationary theory of Vainshtein and Sobel'man[15] were taken into account.

According to the theory of Weisskopf and Lindholm the dependence of the halfwidth $\gamma$ and the displacement $\Delta$ of the line on the concentration N is given by the expressions:

$$\gamma = 38.8 C^{2/3} V^{-1/3} N \quad (4)$$

and

$$\Delta = 33.4 C^{2/3} V^{1/3} N, \quad (5)$$

from which follows the well-known relation between the halfwidth and the shift:

$$\frac{\gamma}{\Delta} = 1.15. \quad (6)$$

For a plasma temperature equal to 40,000°K the theory of Weisskopf and Lindholm gives the following values of the proportionality constants for the concentration in terms of the halfwidth and the displacement, respectively, with $\gamma$ and $\Delta$ expressed in A:

For the 5016 A line

$$\left.\begin{aligned} N &= 0.87 \cdot 10^{18}\ \gamma\ (cm^{-3}), \\ N &= 1 \cdot 10^{18}\ \Delta\ (cm^{-3}); \end{aligned}\right\} \quad (7)$$

For the 3889 A line

$$\left.\begin{aligned} N &= 4.75 \cdot 10^{18}\ \gamma\ (cm^{-3}), \\ N &= 5.5 \cdot 10^{18}\ \Delta\ (cm^{-3}). \end{aligned}\right\} \quad (8)$$

Values of the concentration calculated from (7) and (8) by substituting on the right-hand side experimental values of $\gamma$ and $\Delta$, determined for different parameters of the discharge circuit, are given in Table 2.

According to the nonstationary theory of Vainshtein and Sobel'man the half-width $\gamma$ and the shift $\Delta$ of the line are given by the following expressions:

$$\gamma = 38.8 C^{2/3} V^{1/3} \left[ I'(\beta_a) + \left(\frac{2m}{M}\right)^{1/3} I'(\beta_i) \right] N; \quad (9)$$

$$\Delta = 33.4 C^{2/3} V^{1/3} \left[ I''(\beta_a) + \left(\frac{2m}{M}\right)^{1/3} I''(\beta_i) \right] N. \quad (10)$$

The parameter $\beta$ occurring in (9) and (10) is given by the expression

$$\beta = \frac{2\,(2\pi C)^{1/3} (\Delta E)^{1/3}}{\lambda^2 V^2}. \quad (10a)$$

The calculation of $\beta$ was carried with the assumption that for the $3^1P$ level the perturbing level is $3^1D$, and for $3^3P$ the perturbing level is $3^3D$. The numerical values of the atomic constants were taken from the tables given in reference 9. At a temperature of ~40,000°K the value of $\beta_i$ is $\gg 1$ for both the levels under consideration. The quantity $\beta_a$ has the values $2.3 \times 10^{-2}$ and $9.2 \times 10^{-2}$ for the lines 5016 A and 3889 A, respectively. According to reference 15, for these values of $\beta$ the functions $I'(\beta_a)$ and $I''(\beta_a)$ take the following values

$$\begin{aligned} &\lambda = 5016\ A; \quad I'(\beta_a) = 0.85; \quad I''(\beta_a) = 0.22; \\ &\lambda = 3889\ A; \quad I'(\beta_a) = 1.16; \quad I''(\beta_a) = 0.43. \end{aligned} \quad (10b)$$

Finally, we have from formulas (9) and (10), with $\gamma$ and $\Delta$ expressed in A,

For the 5016 A line

$$\left.\begin{aligned} N &= 0.79 \cdot 10^{18}\ \gamma\ (cm^{-3}); \\ N &= 2.22 \cdot 10^{18} \Delta\ (cm^{-3}); \end{aligned}\right\} \quad (11)$$

For the 3889 A line

$$\left.\begin{aligned} N &= 3.43 \cdot 10^{18} \gamma\ (cm^{-3}); \\ N &= 8.35 \cdot 10^{18} \Delta\ (cm^{-3}). \end{aligned}\right\} \quad (12)$$

Numerical values of the concentration calculated from formulas (11) and (12) are given in Table 2.

Table 2

| Inductance L* (μh) | Time t (μsec) | Wavelength λ (A) | Line halfwidth γ (A) | Line shift Δ (A)** | Electron concentration N ($cm^{-3} \times 10^{-17}$) | | | | γ/Δ |
|---|---|---|---|---|---|---|---|---|---|
| | | | | | Weisskopf-Lindholm | | Vainshtein-Sobel'man | | |
| | | | | | From γ | From Δ | From γ | From Δ | |
| 0.18 | 0.45 | 3889 | 10.5 | 1.5 | 5 | 0.83 | 3.6 | 1.2 | 7 |
| | 0.7 | 3889 | 11 | — | 5.2 | — | 3.7 | — | — |
| | 2.7 | 5016 | 12 | 2.3 | 1.0 | 0.23 | 0.9 | 0.5 | 5.2 |
| | | 3889 | 4.1 | — | 1.95 | — | 1.4 | — | — |
| 3.6 | 0.45 | 3889 | 8 | 1 | 3.8 | 0.55 | 2.7 | 0.83 | 8 |
| | 0.7 | 3889 | 7.5 | — | 3.6 | — | 2.6 | — | — |
| | 2.7 | 5016 | 9.8 | 2.2 | 0.85 | 0.22 | 0.8 | 0.5 | 4.5 |
| | | 3889 | 4.4 | — | 2.1 | — | 1.5 | — | — |
| | 5.2 | 5016 | 7 | — | 0.6 | — | 0.55 | — | — |
| | | 3889 | 3 | — | 1.4 | — | 1.0 | — | — |
| 25 | 0.45 | 3889 | 2.8 | — | 1.3 | — | 0.98 | — | — |
| | 0.7 | 3889 | 2.5 | — | 1.2 | — | 0.85 | — | — |
| | 2.7 | 5016 | 5 | 1 | 0.44 | 0.1 | 0.4 | 0.22 | 5 |
| | | 3889 | 1.9 | — | 0.9 | — | 0.65 | — | — |
| | 5.2 | 5016 | 4.7 | 1.2 | 0.4 | 0.1 | 0.36 | 0.22 | 3.9 |
| | | 3889 | 1.3 | — | 0.6 | — | 0.40 | — | — |
| | 10.2 | 5016 | 3.6 | — | 0.3 | — | 0.27 | — | — |
| | | 3889 | 1.0 | — | 0.5 | — | 0.30 | — | — |

*Discharge conditions: p = 2.5 atm, C = 0.05 μf, U = 2.5 kv.
**The line widths were determined with an accuracy of 0.25 to 0.4 A, depending on the instrumental slit of the arrangement.

As is evident from the table, the values of the concentration determined from the halfwidth and from the shift of the lines are much closer to one another when the nonstationary theory of Vainshtein and Sobel'man is used.

It is interesting to compare the values of the concentration obtained in the present investigation from a study of arc lines with the values calculated in reference 8 from the broadening and displacement of the hydrogen-like spark line, 4686 A, of helium (Table 3). As is evident from Tables 2 and 3, the divergence of the results obtained from arc and spark lines amounts to 200–300%. In the present state of the theory of line broadening and in

Table 3

| Inductance L of the discharge circuit (μh) | Time t (μsec) | Electron concentration N ($cm^{-3} \times 10^{-17}$) | | |
|---|---|---|---|---|
| | | λ 4686 A | λ 3889 A | |
| | | | From γ | From Δ |
| 0.18 | 0.45 | 3.5 | 3.6 | 1.2 |
| | 0.7 | 2.8 | 3.7 | — |
| 3.6 | 0.45 | 2.4 | 2.7 | 0.83 |
| | 0.7 | 1.8 | 2.8 | — |

view of certain simplifications used as a basis for the calculations (neglect of the statistical wings, etc.), divergences of this order are to be expected.

## CONCLUSIONS

1. It is shown that the emission of a spark discharge in helium ($p = 2.5$ atm, $U/L = 1.4 \times 10^{10}$ amp/sec) in the wavelength region 2500-5500 A is characterized in the early stages by a relatively strong continuous background, on which the strong HeII line at 4686 A and the HeII line at 3203 A stand out. The arc lines of helium appear later, approximately 0.3-0.5 μsec after the beginning of the discharge

2. It was established that the spark lines as well as the arc lines emitted in the discharge are greatly broadened and displaced because of the Stark effect. The observed asymmetries of the arc lines can be attributed to statistical wings due to the effect of ions.

3. An estimate was made of the electron concentrations in the plasma of the spark discharge for various discharge conditions and for various times after the beginning of the discharge. The values of the concentration obtained from measurements of the halfwidth and displacement of the HeI line at 3889 A, and also from a study of the profile of the HeII line at 4686 A, show better agreement with each other when the corrections given by the nonstationary theory of Vainshtein and Sobel'man are taken into account.

## REFERENCES


1. H. Wulff. Z. Physik **150**, 614 (1958).
2. M. A. Mazing and S. L. Mandel'shtam. Zhur. Eksptl. i Teoret. Fiz. **36**, 1329 (1959).
3. A. Kol'b. "Magnitnaya gidrodinamika." (Magneto-Hydrodynamics), Atomizdat., Moscow, 1958.
4. H. Fischer. J. Opt. Soc. Am. **47**, 981 (1957).
5. H. Fischer. Proceedings of the Conference on Extremely High Temperatures, New York, p. 11, 1958.
6. B. A. Ermakov and A. A. Mak. Pribory i Tekh. Ekspt., No. 3, 94 (1959).
7. M. P. Vanyukov, B. A. Ermakov, A. A. Mak, and V. P. Muratov. Vestnik Leningrad Gosudarst. Univ., Ser. Fiz. i Khim. No. 16, 25 (1959).
8. A. A. Mak. Zhur. Ekspti. i Teoret. Fiz. **37**, 1488 (1959).
9. Landolt-Bornstein. "Zahlenwerte and Funktionen," Band I, Teil I. Springer-Verlag, Berlin, 1950.
10. L. H. Aller. "Astrophysics," Vol. I, Ronald Press, New York, 1953.
11. A. Unsöld. Z. Astrophys. **23**, 75 (1944).
12. I. I. Sobel'man. Uspekhi Fiz. Nauk **54**, 551 (1954).
13. L. Minnhagen. Arkiv Mat., Astron., Fysik **A35**, 16 (1948).
14. C. W. Allen. "Astrophysical Quantities." Athlone Press, London, 1955.
15. L. A. Vainshtein and I. I. Sobel'man. Opt. and Spectr. (Eng. transl.) **6**, 279 (1959).


# ISOTOPE SHIFT IN THE SPECTRUM OF MOLYBDENUM

Yu. P. Dontsov

Received 30 July 1959

It is established that the volume effect in the isotope shift in the spectrum of molybdenum is considerably greater than the mass effect. A sharp deviation from equidistance is observed in the positions of the isotopic components of the spectral lines. Correlations are noted between these anomalies in the isotope shift and changes in the square of the amplitude of the zero point vibrations of the nuclear quadrupole moment. Calculations of the "quadrupole" isotope shift using the formula derived for deformed nuclei lead to results which are too small.

## EXPERIMENTAL

The experimental technique and the method for reduction of the data have been described in detail in our paper on the investigation of isotope shift in the zirconium spectrum.[1] The technique used in the present work differs only in that the isotopic spectra were excited in separate discharge tubes with a hollow cathode cooled by liquid nitrogen. A schematic diagram of the discharge tube used is shown in the Figure. Before the isotope to be studied was introduced into the cathode cavity, the walls of the cavity were oxidized by maintaining a discharge in air at a pressure of 1-3 mm Hg for a few minutes. This procedure gave a significant decrease in the intensity of spectral lines of elements present in the cathode material. After the oxidation process 10-15 mg of molybdenum oxide were introduced into the cathode cavity and the tube was again connected to the vacuum apparatus. The walls of the discharge tube and the oxide introduced into it were carefully outgassed. The tube was then filled with

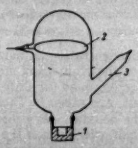


Diagrammatic sketch of the discharge tube: 1—Kovar cathode, 2—molybdenum wire anode, 3—side-tube for pumping out and sealing off the discharge tube.

spectroscopically pure argon at a pressure of about 0.5 mm Hg, and afterwards sealed off from the vacuum apparatus. The research was carried out with discharge tubes prepared by the method just described, each tube containing one of the enriched samples of the even-even isotopes of Mo,[2] the compositions of which are given in Table 1.

Table 1

| Sample | Isotopic composition (%) | | | | | | |
|---|---|---|---|---|---|---|---|
| | $Mo^{92}$ | $Mo^{94}$ | $Mo^{96}$ | $Mo^{98}$ | $Mo^{97}$ | $Mo^{95}$ | $Mo^{100}$ |
| $Mo^{92}$ . . . . | 94.7 | 1.5 | 0.9 | 1.0 | 0.6 | 1.0 | 0.2 |
| $Mo^{94}$ . . . . | 1.8 | 91.2 | 2.1 | 1.4 | 1.1 | 2.4 | 0.1 |
| $Mo^{96}$ . . . . | — | 0.2 | 5.6 | 87.0 | 2.0 | 2.8 | 0.6 |
| $Mo^{98}$ . . . . | — | — | 0.2 | 0.8 | 6.5 | 91.4 | 1.1 |
| $Mo^{100}$ . . . . | 1.7 | 3.3 | 5.4 | 6.1 | 4.8 | 11.8 | 66.8 |

The spectra were photographed in the region from 4500 to 6400 A on Kodak II-F plates with exposure times from 5 to 30 min. Spectra of each isotope were obtained with a Fabry-Perot interferometer ($R \sim 90\%$) with plate spacings of 10, 15, and 20 mm. Several spectrograms were obtained for each value of the spacing. The results of a series of measurements were used to determine average values of the shifts and root-mean-square experimental errors.

## RESULTS OF THE MEASUREMENTS

The magnitude of the isotope shift in the spectrum of molybdenum is less than the width of the spectral lines. Consequently, for a determination of the true shift, it is necessary to make allowance for the fact that the line profile of the main isotope of the line has the profiles of other isotopes present in the sample superimposed on it. As in the previous investigation[1] the correction was carried out analytically with the assumption that the line shapes were purely Doppler. Using the isotopic compositions of the samples given in Table 1, expressions were worked out, with an accuracy compatible with the experimental errors, for changing from the observed values of the isotope shift ($\Delta\nu_{obs.}$) to their true values ($\Delta\nu_{true}$):

$$\Delta\nu_{true\,(94-92)} = 1.06\ \Delta\nu_{obs.\,(94-92)},$$
$$\Delta\nu_{true\,(96-94)} = 1.07\ \Delta\nu_{obs.\,(96-94)},$$
$$\Delta\nu_{true\,(98-96)} = 1.05\ \Delta\nu_{obs.\,(98-96)},$$
$$\Delta\nu_{true\,(100-98)} = 1.36\ \Delta\nu_{obs.\,(100-98)}$$
$$+0.16\ \Delta\nu_{obs.\,(98-96)} + 0.07\ \Delta\nu_{obs.\,(96-94)}.$$

The true values of the shifts calculated according to these formulas are given in Table 2. In the first column of the table are given the wavelengths of the lines studied, in the second their assignments, and in the remaining columns the magnitudes of the isotope shifts between adjacent pairs of isotopes along with the root-mean-square errors of the measurements. The positive direction of the shift was taken as the direction of the isotope shift due to the volume effect.

From the results given in Table 2 it is seen that the sign of the isotope shift for 18 lines is the same as the sign for the volume effect, and for only two lines is the shift in the opposite direction. The magnitude of the shift is determined by the type of transition, as follows from the theory of the volume effect. The maximum shift is observed for lines which correspond to the transition of two 5s electrons; for lines corresponding to the transition of a single 5s electron the shift is substantially smaller. These facts indicate that the volume effect predominates over the mass effect in the isotope shift in the spectrum of molybdenum. It should also be noted that for all lines involving the transition of 5s electrons a marked deviation from equidistance in the positions of the isotope components is observed.

Table 2

| Wavelength (A) | Assignment | Shift, $\Delta\nu(cm^{-1}\times10^2)$ | | | |
|---|---|---|---|---|---|
| | | $\Delta\nu_{(94-92)}$ | $\Delta\nu_{(96-94)}$ | $\Delta\nu_{(98-96)}$ | $\Delta\nu_{(100-98)}$ |
| 6424.37 | $4d^55s^2\,^5D_4 - 4d^45s5p\,^5P_3^0$ | 3.0±2 | 7.1±3 | 2.7±1 | 5.2±5 |
| 6030.66 | $4d^55s^2\,^5D_4 - 4d^55p\,^5P_3^0$ | 25.9±1.0 | 19.3±1.0 | 11.9±1.0 | 35.5±2.8 |
| 5928.88 | $4d^55p\,^5P_3^0 - 4d^55d\,^5D_4$ | −4.3±3 | −1.3±3 | −3.8±2 | −1.4±3 |
| 5888.33 | $4d^55s^2\,^5D_3 - 4d^55p\,^5P_2^0$ | 26.5±1.3 | 17.7±1.2 | 13.1±1.2 | 32.5±2.8 |
| 5858.27 | $4d^55s^2\,^5D_2 - 4d^55p\,^5P_1^0$ | 26.4±0.8 | 14.2±0.6 | 12.7±0.8 | 34.8±1.2 |
| 5791.85 | $4d^55s^2\,^5D_3 - 4d^55p\,^5P_1^0$ | 25.0±0.8 | 17.8±0.7 | 11.9±0.5 | 33.9±2.1 |
| 5751.40 | $4d^55s^2\,^5D_4 - 4d^55p\,^5P_3^0$ | 25.4±1.0 | 18.1±0.9 | 11.9±0.7 | 34.7±2.1 |
| 5722.73 | $4d^55s^2\,^5D_3 - 4d^55p\,^5P_2^0$ | 27.1±1.3 | 19.5±2.0 | 11.8±2.2 | 34.3±3.1 |
| 5689.14 | $4d^55s^2\,^5D_1 - 4d^55p\,^5P_1^0$ | 25.3±1.3 | 17.6±1.2 | 12.3±1.2 | 29.6±2.8 |
| 5650.13 | $4d^55s^2\,^5D_1 - 4d^55p\,^5P_2^0$ | 25.5±1.3 | 17.9±2.0 | 12.6±2.2 | 31.7±3.1 |
| 5632.47 | $4d^55s^2\,^5D_0 - 4d^55p\,^5P_1^0$ | 26.3±1.3 | 18.4±1.2 | 12.9±1.2 | 32.0±2.8 |
| 5570.45 | $4d^55s\,^5S_2 - 4d^55p\,^5P_3^0$ | 7.6±0.4 | 5.5±0.4 | 3.2±0.5 | 9.3±0.7 |
| 5533.05 | $4d^55s\,^5S_2 - 4d^55p\,^5P_2^0$ | 8.1±0.6 | 6.1±0.8 | 3.7±0.5 | 9.8±0.9 |
| 5506.40 | $4d^55s\,^5S_2 - 4d^55p\,^5P_1^0$ | 7.9±0.7 | 6.4±0.7 | 4.4±0.4 | 10.9±1.2 |
| 5473.37 | $4d^55s\,^5D_4 - 4d^45s5p\,^5D_4^0$ | 3.6±1.5 | 4.2±1.5 | 2.6±2.0 | 7.4±5.0 |
| 5380.56 | $4d^55p^2\,^5P_3^0 - 4d^55d\,^7D_4$ | −3.1±2.0 | −2.2±1.5 | −4.3±3.0 | 1.3±3.0 |
| 5050.88 | $4d^55s\,^5D_4 - 1_4^0$ | 9.2±1.5 | 6.1±1.5 | 2.5±1.0 | 10.9±1.9 |
| 4662.76 | $4d^55s^2\,^5D_4 - 4d^45s5p^2\,^5P_3^0$ | 11.8±1.0 | 10.1±1.5 | 6.6±1.0 | 14.9±1.4 |
| 4628.47 | $4d^55s^2\,^5D_3 - 4d^45s5p^2\,^5P_2^0$ | 12.7±1.5 | 10.4±1.1 | 5.9±0.9 | 14.1±1.0 |
| 4576.50 | $4d^55s^2\,^5D_2 - 4d^45s5p^2\,^5P_1^0$ | 12.9±1.7 | 9.8±0.8 | 6.8±1.2 | 14.4±1.5 |

For a determination of the magnitude of volume effect it is necessary to eliminate the mass effect from the observed values of the shift. A calculation of the mass shift for many-electron atoms has been made by Gol'dman.[3] Using the formulas derived by him we have made an estimate of the mass shift in the energy terms for the $4d^45s^2$ and $4d^55s$ configurations. It was found that the difference between the shifts of these terms for $\Delta A = 2$ is equal to $\Delta\mu_m^* = 0.7\times10^{-3}$ cm$^{-1}$. On the other hand, on the basis of the measured values of the isotope shifts for the lines $4d^45s^2 - 4d^55p$ and $4d^55S - 4d^55p$, it is possible to obtain the difference of the total shifts of the above-mentioned levels; from these it is easy to determine the volume part of the isotope shift. In fact, if the mutual screening of the electrons is neglected, the difference between the isotope shifts $\delta T$ of the $4d^45s^2$ and $4d^55s$ levels and the mass shift subtracted is equal to the volume shift for one 5s electron, that is, $\beta\delta T_{5s}$, where the value of $\beta$ is ~1.

*Translator's note: Should probably be $\nu$.

Values of the volume isotope shift $\beta\delta T_{5s}$ determined by this procedure for the four pairs of molybdenum isotopes are given in Table 3. In this table are also given the mean values of the shifts of the spectral lines for the two types of electronic transitions and the differences of

Table 3

| Transition | Shift, $\Delta\nu(cm^{-1}\times10^2)$ | | | |
|---|---|---|---|---|
| | $Mo^{92}-Mo^{94}$ | $Mo^{94}-Mo^{96}$ | $Mo^{96}-Mo^{98}$ | $Mo^{98}-Mo^{100}$ |
| $4d^55s^2\,^5D - 4d^55p\,^5P$ . . . . . | 25.9±0.4 | 18.4±0.4 | 12.3±0.5 | 33.2±0.9 |
| $4d^55s\,^5S - 4d^55p\,^5P$ . . . . . | 7.9±0.4 | 6.0±0.4 | 3.8±0.3 | 10.0±0.8 |
| $4d^55s^2\,^5D - 4d^55s\,^5S$ . . . . . | 18.0±0.8 | 12.4±0.8 | 8.5±0.8 | 23.2±1.7 |
| $\beta\delta T_{5s}$ . . . . . | 17.3 | 11.7 | 7.8 | 22.5 |

The true values of the shifts calculated according to these formulas are given in Table 2. In the first column of the table are given the wavelengths of the lines studied, in the second their assignments, and in the remaining columns the magnitudes of the isotope shifts between adjacent pairs of isotopes along with the root-mean-square errors of the measurements. The positive direction of the shift was taken as the direction of the isotope shift due to the volume effect.

From the results given in Table 2 it is seen that the sign of the isotope shift for 18 lines is the same as the sign for the volume effect, and for only two lines is the shift in the opposite direction. The magnitude of the shift is determined by the type of transition, as follows from the theory of the volume effect. The maximum shift is observed for lines which correspond to the transition of two 5s electrons; for lines corresponding to the transition of a single 5s electron the shift is substantially smaller. These facts indicate that the volume effect predominates over the mass effect in the isotope shift in the

the shifts of the levels with $4d^45s^2$ and $4d^55s$ configurations.

It is concluded from a comparison of the values of $\beta\delta T_{2_1}$ for different pairs of isotopes that "anomalies" in the volume isotope shift are present in the spectrum of molybdenum. The largest values of the shift occur for the two extreme pairs of isotopes, where two neutrons are added to 50 and 56 neutrons; that is, the $d_{5/2}$ and $g_{7/2}$ neutron shells, respectively, are beginning to be occupied.

## DISCUSSION OF THE RESULTS

At the present time it is customary to explain "anomalies" in the isotope shift, like those which have been observed in the spectra of zirconium and molybdenum, in terms of the change in the statistical deformation of the isotopic nuclei,[1-4] as has been done in the case of the rare earths and the transition elements. However, the investigation of the excited levels of nuclei indicates that nuclei with a neutron number $N < 90$ and $116 < N > 134$ are spherical.[7] It is therefore impossible to explain the "anomalies" in the isotope shift discussed above by a change in the statistical deformation of the nucleus. It is known[7] that in spherical nuclei there exist collective vibrational motions, as a consequence of which a varying quadrupole moment with the vibrational amplitude $Q_k$ arises. The presence of these vibrations leads to a change in the quantity $\langle r^2\rho\rangle$, which in turn brings about a change in the isotope shift. If we assume as a first approximation that the averaging of the charge density in a deformed nucleus, as developed by Wilets et al.,[8] is valid also for the case of the zero-point vibrations of $Q_k$, the ratio of the "quadrupole" isotope shift to the "volume" shift should be determined by the same expression as for deformed nuclei, that is,

$$\frac{\delta T_{Q_2}}{\delta T_R} = \frac{\delta T_{\text{exptl.}}}{\delta T_R} - 0.75 = \frac{5}{24}\,\frac{(2_2+3)\,A}{Z^2R_0^4}\,\frac{\delta\left(Q_2^0\right)}{\delta A}, \qquad (1)$$

where $\delta(Q_2^0)$ is the difference between the squares of the amplitudes of the zero-point vibrations of the quadrupole moments of the two isotopes, A the atomic weight, Z the nuclear charge, $R_0$ is the radius of the nucleus and $\rho = \sqrt{1 - Z^2\alpha^2}$. Recently it has been shown[9] that the radius of the nucleus depends on the mass number in a more complex manner than $R_0 \sim A^{1/3}$, namely,

$$R_0 = (1.21\,A^{1/3} + 2.24A^{-1/3} - 6.614A^{-1}) \cdot 10^{-13}\ \text{cm}. \qquad (2)$$

In this case the right-hand side of Eq. (1) must be multiplied by the factor $[(3A/R_0)(dr_0/dA)]^{-1}$, which for A = 96 is equal to 1.15. Thus, we have

$$\frac{\delta T_{Q_2}}{\delta T_R} = \frac{\delta T_{\text{exptl.}}}{\delta T_R} - 0.87. \qquad (3)$$

To determine $\delta T_R$ the well-known expression

$$\delta T_R = \frac{Z_0^2}{n_{\text{eff.}}^3}\,\frac{dn_{\text{eff.}}}{dn}\,\frac{4\,(2+1)\,R_\infty}{(2_2+1)\,(2_2+3)\,l^2(2_2+1)}\left(\frac{2ZR_0}{a_0}\right)^{2\rho}\frac{dA}{A}. \qquad (4)$$

was used. This formula gives $\delta T_R = 12.3 \times 10^{-3}\ \text{cm}^{-1}$ for the case of molybdenum, and taking the relation (2) into account we have $\delta T_R = 10.7 \times 10^{-3}\ \text{cm}^{-1}$.

For the calculation of the ratio $\delta T_{Q_k}/\delta T_R$ it is necessary to know the value of $Q_k^0$ for the even-even isotopes in question. These quantities in the first place are directly related to the probability of electric quadrupole transitions from the ground state of the nucleus to the first excited state,

$$Q_2^0 = \frac{1}{5}\,B(E2,\ 0 \to 2). \qquad (5)$$

Table 4

| | Isotope pair | | | |
|---|---|---|---|---|
| | $Mo^{96}$—$Mo^{92}$ | $Mo^{96}$—$Mo^{94}$ | $Mo^{96}$—$Mo^{97}$ | $Mo^{96}$—$Mo^{98}$ |
| $\left(\frac{\delta T_{Q_2}}{\delta T_R}\right)_{\text{exptl.}}$ | 0.74 | 0.22 | —0.14 | 1.03 |
| $\left(\frac{\delta T_{Q_2}}{\delta T_R}\right)_{\text{theor.}}$ | 0.018 | 0.007 | 0.000 | 0.015 |
| $\frac{\delta T_{Q_2}}{\delta T_{Q_2}\,(96-94)}$ | 3.3 | 1.0 | —0.6 | 4.7 |
| $\frac{\delta B\,(E2)}{\delta B\,(E2)\,(96-94)}$ | 2.8 | 1.0 | 0.0 | 2.2 |
| $\frac{\delta\left(\frac{1}{E_1}\right)}{\delta\left(\frac{1}{E_1}\right)_{(96-94)}}$ | 3.2 | 1.0 | —0.1 | 4.0 |
| Neutron shell being filled | $d_{5/2}$ | $d_{5/2}$ | $d_{5/2}$ | $g_{7/2}$ |

Secondly, from the investigation of Belyaev[10] it follows that the value of $Q_k^0$ is inversely proportional to the value of the energy of the first excited vibrational state:

$$Q_2^0 \sim K\,\frac{1}{E}. \qquad (6)$$

where the coefficient K, as shown by Belyaev, is weakly dependent on the number of neutrons in the nucleus. Thus, using formulas (1) and (3)-(5) it is possible to calculate the ratio $\delta T_{Q_k}/\delta T_R$ and compare it with the experimental value of $(\delta T_{\text{exptl.}}/\delta T_R) - 0.87$. Table 4 gives the experimental and theoretical values of $\delta T_{Q_k}/\delta T_R$, obtained by the method described above, for the four pairs of isotopes. The table also gives the relative values of the "quadrupole" shift, of the change of the quadrupole transition probabilities, and of the change in the reciprocal of the energy of the first excited state of the nuclei. The unit is taken as the change of these quantities between the isotopes $Mo^{94}$ and $Mo^{96}$. In the last row of the table are given the configurations of the neutron shells which are in the process of being filled.

It is seen from the table that there is a definite correlation between the change of isotope shift and the change in the square of the amplitude of the zero-point vibrations of the quadrupole moment. However, a quantitative agreement between the experimental and calculated values of $\delta T_{Q_k}/\delta T_R$ is not indicated; the calculated values of the shift are approximately fifty times smaller than those observed. It should also be noted that the maximum "quadrupole" isotope shift and the greatest change in the amplitude of the zero-point vibrations of the quadrupole moment are observed in the case for which the added pair of neutrons begins to fill up a new shell.

On the basis of the above considerations the conclusion can be drawn that "anomalies" in the isotope shift in the spectra of elements, the atomic nuclei of which have no statistical deformation, are probably related to the change in the amplitude of the zero-point vibrations of the quadrupole moment of the nucleus. However, it must be emphasized that the calculation of the quadrupole isotope shift by means of formula (1) leads to results which are too low. This can be explained by the fact that a change in $Q_k^0$ apparently leads to a considerably greater change in the magnitude of $\langle r^2\rho\rangle$ than an equal change in $Q_2^0$ in the case of deformed nuclei. On the other hand, the discrepancy which has been shown can be taken as an indication of the fact that certain other effects have not been taken into account here, as for example, a nonuniform variation of the radius of the nucleus dependent on the shell structure.

In conclusion the author considers it his pleasant duty to express his thanks to A. R. Striganov for his in-

terest in this investigation, to S. T. Belyaev, V. I. Kogan, L. A. Korostyleva, and N. M. Yashin for their participation in the discussion of the work and for their valuable comments, and also to V. S. Zolotarev and B. A. Alekseev for their kindness in furnishing the separated isotopes.

REFERENCES

1. Yu. P. Dontsov. Opt. i Spektr. 6, 1 (1959).
2. V. S. Zolotarev. "Poluchenie izotopov." (Production of Isotopes), Izd. Akad. Nauk SSSR, Moscow, 1958.
3. I. I. Gol'dman. Zhur. Eksptl. i Teoret. Fiz. 24, 177 (1953).
4. H. Kopferman, L. Krüger, and A. Steudel. Ann. Physik 20, 258 (1957).
5. J. Blaise. Ann. phys. 3, 11, 1019 (1958).
6. G. Breit. Revs. Modern Phys. 30, 507 (1958).
7. K. Alder, A. Bohr, T. Huus, B. Mottelson, and A. Winther. Revs. Modern Phys. 28, 432 (1956); "Deformatsiya atomnykh yader." (Deformation of Atomic Nuclei), Izd. Inostrannoi Lit., Moscow, 1958.
8. L. Wilets, D. L. Hill, and K. W. Ford. Phys. Rev. 91, 1488 (1953).
9. L. Elton. Nuclear Phys. 5, 173 (1957).
10. S. T. Belyaev. Kgl. Danske Videnskab. Selskab., Mat.-Fys. Medd. 31, No. 11 (1959).

# ISOTOPIC BAND SHIFTS IN THE ELECTRONIC-VIBRATIONAL SPECTRA OF SOME DIATOMIC MOLECULES

R. R. Shvangiradze, K. A. Oganezov, and B. Ya. Chikhladze

Received 14 July 1959

The isotopic band shifts in the electronic-vibrational spectra of molecules of $N_2$, $N_2^+$, CO, and $CO^+$ enriched in the isotopes $N^{15}$ and $C^{13}$ have been measured. The experimental data have been compared with the results obtained from elementary theory, taking into account the change in the reduced mass of the molecule. The vibrational constants $\omega$ and $\omega x$ of the isotopic molecules have been determined. A method is proposed for an easily-seen graphical representation of the dependence of the isotopic shifts on the values of the vibrational quantum numbers.

## INTRODUCTION

The study of the spectra of isotopic molecules offers considerable interest both for molecular spectroscopy and for other branches of physics and physical chemistry. A knowledge of isotope effects is especially helpful toward a correct interpretation of naturally complicated molecular spectra and toward the clarification of details of molecular structure.

For detailed study of the spectra of isotopic molecules, substances markedly enriched in rare isotopes are indispensable; these are not always easy to obtain, which naturally limits the number of works devoted to the given question.[1-6] Deuterium-labeled molecules are an exception, and so most of the investigations have been devoted to a comparison of the spectra of hydrides and deuterides.

In the present work we present the results of our first systematic investigations with respect to the study of our first systematic investigations with respect to the study of isotope effects in the gross structure of the electronic-vibrational spectra of the simple molecules $N_2$, $N_2^+$, CO, and $CO^+$, markedly enriched in the rare isotopes $N^{15}$ and $C^{13}$.

## EXPERIMENTAL PROCEDURE

The isotopic shifts were measured on the band heads of the second positive system of the $N_2$ molecule, the first negative system of the $N_2^+$ molecule, the fourth positive system of CO, and the first negative system of $CO^+$. In all the cases investigated, with the exception of $N_2$, the lower electronic states of the molecules appeared normal. The spectra were photographed with the help of ISP-51 spectrographs with UF-84 and UF-85 cameras in the visible and ISP-22 in the ultraviolet regions. The measurement of the wavelengths of the band heads and of the isotopic shifts was carried out with the help of an IZA-2 comparator or directly on the spectrum projector.

The spectra of the molecules $N^{14}N^{15}$, $N_2^{15}$, $(N^{14}N^{15})^+$, $(N_2^{15})^+$, $C^{13}O$, and $(C^{13}O)^+$, formed in a discharge from gaseous $NH_3$, NO, $CH_4$, and $CO_2$ and enriched in the isotopes $N^{15}$ and $C^{13}$ in quantities from 15 to 90%, were excited in a hollow cathode or a Geissler tube in the stationary regime (without the addition of a foreign gas as working substance). The discharge was supplied from a rectifier designed for 1500 volts and 1 amp.

The second positive system of $N_2$ and the first negative system of $N_2^+$ were easily obtained in a hot hollow cathode, or in one cooled by water, at a pressure of ~1 mm Hg of ammonia or nitric oxide. In order to obtain a "clean" spectrum in the absence of gas circulation, it was necessary to work at low current densities (50 $ma/cm^2$). Under these conditions, the spectra of NO, NH, and Al (the cathode material) were practically absent.

The fourth positive system of CO was excited in a Geissler tube with a central capillary, 5 cm long and 4 mm in diameter, in a $CO_2$ atmosphere. The optimal conditions in this case were the following: gas pressure 0.3-0.4 mm Hg and a low current density. Weakening of the intense $CO^+$ bands superimposed on this system was achieved by producing in the discharge tube a flow of the gas under study. In our case this was accomplished by freezing out the $CO_2$ with liquid air in tubes attached to the discharge tube on both sides through capillary valves.

The first negative system of $CO^+$ was easily obtained in a hollow cathode in a $CO_2$ atmosphere at low pressures. The CO and $CO^+$ band systems were also excited in an atmosphere of methane with an admixture of oxygen. However, in this case an intense continuous hydrogen emission was superimposed on them, which made the decipherment of the spectrograms more difficult.

The isotopic shifts

$$\Delta\nu' = \nu(N^{14}N^{15}) - \nu(N_2^{14}) \qquad \Delta\nu'' = \nu(N_2^{15}) - \nu(N_2^{14})$$

Table 1. Isotopic Band Shifts in the Second Positive System of $N_2$ ($cm^{-1}$)

| v′—v″ | Wave numbers of the band heads of $N_2^{14}$ | $\Delta\nu^{I}_{exptl.}$ | $\Delta\nu^{II}_{exptl.}$ | $\Delta\nu^{I}_{theor.}$ | $\Delta\nu^{II}_{theor.}$ |
|---|---|---|---|---|---|
| 0—0 | 29655.3 | (—2.7) | (—5.5) | —2.5 | —5.1 |
| 0—1 | 27952.5 | 28.5 | 57.4 | 28.3 | 57.1 |
| 0—2 | 26276.3 | 54.5 | 108.8 | 55.7 | 112.4 |
| 0—3 | 24629.3 | 81.6 | 163.6 | 82.1 | 165.6 |
| 0—4 | 23018.3 | 105.5 | 211.6 | 107.2 | 216.4 |
| 1—0 | 31452.5 | —35.3 | —69.3 | —33.0 | —65.9 |
| 1—1 | 29942.2 | (—6.8) | (—13.3) | — 7.0 | —14.0 |
| 1—2 | 28270.2 | 21.6 | 43.2 | 22.7 | 46.5 |
| 1—3 | 26622.6 | 47.9 | 96.0 | 49.1 | 99.7 |
| 1—4 | 25005.0 | 73.4 | 147.2 | 74.3 | 150.5 |
| 2—0 | 33587.5 | —64.2 | —129.2 | —63.8 | —128.8 |
| 2—1 | 31883.4 | —36.6 | —73.0 | —35.5 | —71.7 |
| 2—2 | 30213.7 | (—9.6) | —19.0 | —10.1 | —20.4 |
| 2—3 | 28560.9 | 18.1 | 35.9 | 18.3 | 36.8 |
| 2—4 | 26944.7 | 41.8 | 83.8 | 43.4 | 87.7 |
| 2—5 | 25356 | 68.3 | 137.0 | 67.3 | 135.9 |
| 3—1 | 33753.1 | —63.7 | —127.0 | —63.0 | —129.0 |
| 3—2 | 32080.8 | —38.1 | —76.0 | —36.5 | —73.7 |
| 3—3 | 30431.6 | (—11.5) | (—22.5) | —11.7 | —24.0 |
| 3—4 | 27227.9 | 37.1 | 74.4 | 38.9 | 78.5 |
| 3—7 | 24139.5 | 87.7 | 176.1 | 82.1 | 166.0 |
| 3—8 | 22637.5 | 108.1 | 216.5 | 101.2 | 205.0 |
| 4—2 | 33853.7 | —60.7 | —121.1 | —62.1 | —125.6 |
| 4—3 | 32214.1 | —33.7 | —67.3 | —35.3 | —72.2 |
| 4—4 | 30591.8 | (—11.5) | (—24.0) | —11.7 | —24.8 |
| 4—6 | 27453.3 | 36.1 | 72.4 | 35.6 | 71.9 |
| 4—8 | 24416.4 | 86.7 | 1737 | 75.6 | 153.0 |

Table 2. Isotopic Band Shifts in the First Negative System of $N_2^+$ ($cm^{-1}$)

| v′—v″ | Wave numbers of the band heads of $(N_2^{14})^+$ | $\Delta\nu^{I}_{exptl.}$ | $\Delta\nu^{II}_{exptl.}$ | $\Delta\nu^{I}_{theor.}$ | $\Delta\nu^{II}_{theor.}$ |
|---|---|---|---|---|---|
| 0—0 | 25541.4 | (—1.7) | (—3.3) | —1.8 | —3.5 |
| 0—1 | 23370.8 | 35.5 | 71.2 | 36.1 | 72.9 |
| 0—2 | 21232.0 | 69.6 | 141.1 | 71.2 | 143.6 |
| 1—0 | 27910.4 | —38.9 | —77.7 | —39.3 | —78.4 |
| 1—1 | 25739.3 | (—4.5) | (—9.0) | —4.7 | —9.4 |
| 1—2 | 23599.7 | 30.9 | 62.5 | 31.9 | 64.4 |
| 1—3 | 21493.8 | 64.9 | 130.6 | 65.9 | 133.0 |
| 2—1 | 28052.9 | —40.9 | —81.6 | —40.5 | —81.8 |
| 2—2 | 25915.4 | (—6.7) | (—13.0) | (—6.9) | —13.6 |
| 2—3 | 23810.1 | 28.7 | 57.4 | 28.5 | 57.2 |
| 2—4 | 21737.2 | 61.2 | 122.1 | 61.4 | 124.0 |
| 3—2 | 28171.4 | —42.0 | —81.5 | —41.0 | —82.8 |
| 3—3 | 26067.4 | (—8.0) | (—15.5) | —8.2 | —16.3 |
| 3—4 | 23954.8 | 56.0 | 115.9 | 57.7 | 116.5 |
| 3—5 | 22140.4 | 55.0 | 110.3 | 54.8 | 110.6 |

measured on the band heads of the second positive system of nitrogen are presented in the third and fourth columns of Table 1. In the analogous columns of Table 2 are given the values of the isotopic shifts of the band heads of the first negative system of the ion $N_2^+$, that is,

$$\Delta\nu^{I} = \nu(N^{14}N^{15})^+ - \nu(N_2^{14})^+$$

and

$$\Delta\nu^{II} = \nu(N_2^{15}) - \nu(N_2^{14}).$$

Values found graphically (see below) are given in parentheses. The magnitudes of the isotopic band shifts of the first negative system of $CO^+$ and the fourth positive system of CO are presented in Tables 3 and 4 respectively:

$$\Delta\nu^{I} = \nu(C^{13}O)^+ - \nu(C^{12}O)^+$$

and

$$\Delta\nu^{I} = \nu(C^{13}O) - \nu(C^{12}O).$$

The maximum experimental error amounts to 2 $cm^{-1}$.

On the ISP-51 spectrograph with UF-84 and UF-85 cameras, the isotopic structure in the rotational lines of the $N_2^+$ bands is well resolved. Figure 1a shows the microphotometer tracing of the O – O band of the first negative system of $N_2^+$ obtained using natural nitrogen, and Fig. 1b shows that obtained using nitrogen enriched to 15% in the isotope $N^{15}$. As can be seen from the figure,

Table 3. Isotopic Band Shifts in the First Negative System of $CO^+$ ($cm^{-1}$)

| v′—v″ | Wave numbers of the $(C^{13}O)^+$ band | $\Delta\nu^{I}_{exptl.}$ | $\Delta\nu^{I}_{theor.}$ | v′—v″ | Wave numbers of the $(C^{13}O)^+$ band | $\Delta\nu^{I}_{exptl.}$ | $\Delta\nu^{I}_{theor.}$ |
|---|---|---|---|---|---|---|---|
| 0—0 | 45655.7 | (4.5) | 5.5 | 2—3 | 42498.9 | 74.2 | 74.1 |
| 0—1 | 43475.6 | 49.8 | 52.8 | 2—4 | 40405.5 | 117.6 | 118.4 |
| 0—2 | 41320.8 | 98.2 | 99.7 | 2—5 | 38346.4 | 158.0 | 161.5 |
| 0—3 | 39202.6 | 141.9 | 145.3 | 2—6 | 36316.3 | 201.7 | 203.2 |
| 0—4 | 37111.6 | 193.2 | 189.8 | 3—3 | 44699.7 | (44.5) | 43.3 |
| 1—1 | 45146.4 | (18.0) | 17.3 | 3—4 | 41980.5 | 85.5 | 86.0 |
| 1—2 | 42996.9 | 62.0 | 63.0 | 3—5 | 39917.2 | 129.5 | 129.1 |
| 1—3 | 40871.8 | 110.9 | 108.7 | 3—6 | 37894.4 | 166.0 | 168.8 |
| 1—4 | 38780.7 | 151.0 | 153.0 | 3—7 | 35989.2 | 207.3 | 211.2 |
| 2—2 | 44624.4 | (30.0) | 29.9 | 4—7 | 37414.9 | 180.3 | 181.0 |

Table 4. Isotopic Band Shifts in the Fourth Positive System of CO ($cm^{-1}$)

| v′—v″ | Wave numbers of the band heads of $C^{13}O$ | $\Delta\nu^{I}_{exptl.}$ | $\Delta\nu^{I}_{theor.}$ | v′—v″ | Wave numbers of the band heads of $C^{13}O$ | $\Delta\nu^{I}_{exptl.}$ | $\Delta\nu^{I}_{theor.}$ |
|---|---|---|---|---|---|---|---|
| 5—13 | 46002.2 | 381.2 | 379.6 | 7—16 | 43251.8 | 425.2 | 425.8 |
| 6—14 | 45510.1 | 386.5 | 387.4 | 8—17 | 42761.6 | 434.2 | 433.3 |
| 7—15 | 45002.1 | 396.5 | 395.4 | 5—17 | 42425.8 | 445.7 | 443.9 |
| 7—13 | 44661.3 | 411.8 | 406.2 | 5—18 | 42260.8 | 442.3 | 442.2 |
| 8—16 | 44487.4 | 410.6 | 411.7 | 8—18 | 41650.8 | 463.1 | 461.8 |
| 5—14 | 44198.3 | 112.2 | 112.4 | 7—17 | 41525.4 | 451.7 | 455.3 |
| 6—15 | 43731.4 | 418.1 | 418.9 | 9—19 | 40588.8 | 467.7 | 468.4 |

additional lines belonging to the molecule $N^{14}N^{15}$ appear in the second case.

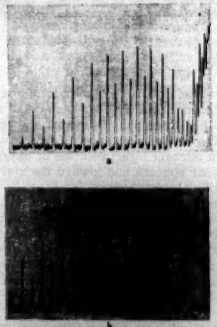

Fig. 1. Microphotometer tracings of the O – O band of the $N_2^+$ molecule, obtained using natural nitrogen (a) and nitrogen containing 15% $N^{15}$ (b).

## DISCUSSION OF RESULTS

The elementary theory of isotopic band shifts in the electronic-vibrational spectra of diatomic molecules (if we neglect the effect of isotopy on the electronic transitions) leads to the well-known relation[7]

$$\Delta\nu = \nu' - \nu = \omega'_e\left(v' + \frac{1}{2}\right)(\rho - 1) - \omega'_e x'_e\left(v' + \frac{1}{2}\right)^2(\rho^2 - 1)$$
$$- \left\{\left(\omega''_e v'' + \frac{1}{2}\right)(\rho - 1) - \omega''_e x''_e\left(v'' + \frac{1}{2}\right)^2(\rho^2 - 1)\right\}, \qquad (1)$$

where $\omega_e$ and $\omega_e x_e$ are the familiar vibrational constants, v is the vibrational quantum number, and $\rho$ is the re-

duced mass of the molecule. Singly-primed letters refer to the upper electronic state, doubly-primed letters to the lower.

This formula is strictly observed for the zero lines and gives a good approximation for the band heads, since the isotopic effect in the rotational terms is negligibly small compared to that in the vibrational terms. Comparison of the experimental values of the isotopic shifts with those calculated from the formula makes it possible to verify the accuracy of the identification of the bands.

The values found with the help of formula (1) for the isotopic band shifts for the molecules $N_2$ and $N_2^+$ are presented in the fifth and sixth columns of Tables 1 and 2, and for $CO^+$ and CO in the fourth column of Tables 3 and 4, respectively. In the computations, we used the values of $\omega_e$ and $\omega_e x_e$ found from the spectra, as listed in Table 5, for the upper and lower electronic states of the systems under consideration.

Table 5. Vibrational Constants and Zero-Point Energies $\varepsilon_0$ of Isotopic Molecules ($cm^{-1}$)

| Molecule | Electronic state | $\omega_e$ | $\omega_e x_e$ | $\omega_e y_e$ | $\varepsilon_0$ |
|---|---|---|---|---|---|
| $N_2^{14}$ | $C^3\Pi_u$ | 2052.7 | 26.24 | —1.013 | 1019.6 |
| | $B^3\Pi_g$ | 1726.9 | 11.31 | —0.44 | 860.6 |
| $N^{14}N^{15}$ | $C^3\Pi_u$ | 2018.3 | 25.37 | —0.96 | 1002.9 |
| | $B^3\Pi_g$ | 1697.9 | 10.93 | —0.42 | 846.3 |
| $N_2^{15}$ | $C^3\Pi_u$ | 1983.3 | 24.49 | —0.91 | 985.6 |
| | $B^3\Pi_g$ | 1668.5 | 10.55 | —0.396 | 831.7 |
| $(N_2^{14})^+$ | $B^2\Sigma_u^+$ | 2424.8 | 27.90 | — | 1205.4 |
| | $X^2\Sigma_g^+$ | 2203.0 | 16.09 | — | 1097.5 |
| $(N^{14}N^{15})^+$ | $B^2\Sigma_u^+$ | 2384.1 | 26.97 | — | 1185.3 |
| | $X^2\Sigma_g^+$ | 2166.1 | 15.55 | — | 1079.1 |
| $(N_2^{15})^+$ | $B^2\Sigma_u^+$ | 2342.8 | 26.04 | — | 1164.9 |
| | $X^2\Sigma_g^+$ | 2128.4 | 15.02 | — | 1060.5 |
| $(C^{13}O)^+$ | $B^2\Sigma^+$ | 1720.8 | 24.52 | — | 854.3 |
| | $X^2\Sigma^+$ | 2206.7 | 14.83 | — | 1101.2 |
| $(C^{13}O)^+$ | $B^2\Sigma^+$ | 1682.4 | 23.44 | — | 835.4 |
| | $X^2\Sigma^+$ | 2160.5 | 14.17 | — | 1076.7 |
| $C^{13}O$ | $A^1\Pi$ | 1514.7 | 17.18 | — | 753.0 |
| | $X^1\Sigma^+$ | 2168.9 | 13.30 | 0.012 | 1081.1 |
| $C^{13}O$ | $A^1\Pi$ | 1480.9 | 16.13 | — | 736.4 |
| | $X^1\Sigma^+$ | 2120.6 | 12.72 | 0.011 | 1057.1 |

For highly anharmonic states, such as the electronic states of the second positive system, cubic terms with the second anharmonicity coefficient $\omega_e y_e$ were taken into account. However, even with this allowance, a marked discrepancy is observed between the experimental and calculated values of the wave numbers of the bands, especially for values of $v'$ and $v''$ greater than five. With the exception of the bands just mentioned, there is observed in all cases a generally satisfactory agreement between the experimental and the theoretical values of the isotopic shifts (Tables 1-4).

Comparing the values of $\omega_e$ and $\omega_e x_e$ obtained by us with those known from the literature, we may note the following. In the case of the molecules $N_2^{14}$ and $(N_2^{14})^+$, marked differences from the corresponding quantities presented in reference 8 are observed. Inasmuch as our data give a better description of the position of the bands in the spectrum, we consider them more reliable. In the case of the molecule $(C^{14}O)^+$,* the agreement with the

*Translator's note: $(C^{13}O)^+$?

data of reference 8 is entirely satisfactory. The values of the constants for the molecule $C^{13}O$ were taken by us from reference 9, inasmuch as the empirical formula proposed in that work for the wave numbers gives a good description of the fourth positive system of the molecule in question.

The vibrational constants obtained by us for the $x^1\Sigma^+$ ground state of the $C^{13}O$ molecule are in good agreement with those found from the infrared spectrum.[3] For the other molecules with rare isotopes, and also for the $A^1\pi$ state of the $C^{13}O$ molecule, these quantities have been obtained for the first time by us, on the basis of an analysis of the vibrational structure of the corresponding systems of the electronic-vibrational spectra.

In Fig. 2 is presented, in the form of nomograms, the dependence of the magnitude of the isotopic shifts for the bands of $N_2$ and $CO^+$ on the values of $v'$ and $v''$.

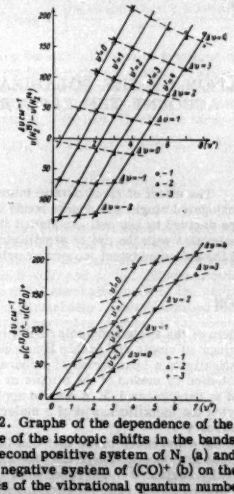


Fig. 2. Graphs of the dependence of the magnitude of the isotopic shifts in the bands of the second positive system of $N_2$ (a) and the first negative system of $(CO)^+$ (b) on the values of the vibrational quantum numbers $v'$ and $v''$. Symbols for the points on the graphs: 1—experimental, 2—theoretical, 3—graphical.

From the figure it can be seen that, when the values of $v'$ and $v''$ are not very large (and when $v'$ is constant), the isotopic shift changes practically linearly with $v''$. These constant-$v'$ straight lines (solid lines on the graph) cut off segments on the horizontal axis (for corresponding values of $v''$) which are proportional to the magnitudes of the isotopic shifts of bands with $\Delta v = 0$. The determination of the latter directly from the spectrograms is quite difficult in view of their small magnitude and the mutual overlapping of the bands. The values found in this way are entered in Tables 1-4 in parentheses, and are represented in Fig. 2 by crosses.

The variation of the isotopic shifts in bands with $\Delta v$ = const. is shown in the figures by dotted lines. It is easy to see that, with an increase of $v'$ or $v''$, the isotopic shift of bands with $\Delta v$ = const. increases when the system is degraded toward the red ($N_2$ and $N_2^+$) and falls off when it is degraded toward the violet (CO and $CO^+$).

It is well known that the ratio of the statistical weights of adjacent rotational levels of diatomic molecules with identical atoms equals $(I + 1)/I$, where I is the value of the nuclear spin. Analysis of the alternation of intensities in the resolved fine structure of the bands of the first negative system of the molecules $N_2^{14}$ and $N_2^{15}$ confirms that the spin of the $N^{14}$ nucleus equals unity while that of the $N^{15}$ nucleus equals one-half.

REFERENCES

1. A. H. Nielsen. Phys. Rev. 53, 983 (1938).
2. R. T. Lagemann, A. H. Nielsen, and F. P. Dickey. Phys. Rev. 72, 284 (1947).
3. R. W. Wood and G. H. Dieke. J. Chem. Phys. 8, 351 (1940).
4. W. Gordy, J. W. Simons, and A. G. Smith. Phys. Rev. 72, 344 (1947).
5. F. A. Jenkins and D. E. Wooldridge. Phys. Rev. 53, 137 (1938).
6. A. A. Mal'tsev, E. N. Moskvitina, and V. M. Tatevskii. Mater. X soveshch. po spektr. (Data of the Tenth Conference on Spectroscopy) 1, 465 (1957).
7. G. Herzberg. "Spektry i stroenie dvukhatomnykh molekul." (Spectra and Structure of Diatomic Molecules), Inostrannoi Lit., Moscow, 1949.
8. Landolt-Bornstein. "Tabellen Zahlenwerte und Funktionen," Vol. 1, 1951.
9. D. N. Read. Phys. Rev. 48, 571 (1934).

# CALCULATION OF THE POLARIZABILITY OF CONJUGATED MOLECULES TAKING INTO ACCOUNT THE ELECTROSTATIC INTERACTION OF $\pi$-ELECTRONS

T. K. Rebane

Received 20 July 1959

The effect of electrostatic interaction of $\pi$-electrons on the polarizability of molecules with conjugated single and double bonds is considered. Appropriate equations of perturbation theory are derived by the self-consistent field method. The theory is applied to ethylene and benzene molecules with the use of simplifying assumptions, taken from the semiempirical modification of the self-consistent molecular orbital method.

## INTRODUCTION

The problem of the $\pi$-electron polarizability of molecules with conjugated single and double bonds has been treated theoretically by a long series of authors. This problem was studied by means of the simple molecular orbital method in references 1-3. A second approach based on applying the metallic model of a molecule was used in references 4-9.

In spite of the differences in the methods that were used, the electrostatic interaction of the valence electron was generally neglected in the references cited above. On the other hand, it follows from simple physical considerations that displacements of the electronic charge induced by an externally applied homogeneous electric field cause supplementary (nonhomogeneous) electric fields inside the molecule. As a result, the "effective" field acting on the separate electrons in the molecule differs from the externally applied field, in that it is smaller in magnitude than the latter. This circumstance should lead to a decrease of the electronic polarizability of the molecule as compared to the value calculated without taking into account the interaction of the electrons.

If the usual separation of the electronic cloud of conjugated molecules into the mobile $\pi$-electrons and the electrons of the molecular core is made, then the effect of the interaction of the electrons on the polarizability of conjugated molecules can be mentally divided into the following basic factors: (1) the effect of the mutual repulsion of $\pi$-electrons on the $\pi$-electron polarizability of the molecule; (2) the effect of the mutual repulsion of molecular core electrons on the polarizability of the electronic core; (3) the effect of the mutual repulsion of the $\pi$-electrons and the core electrons on the polarizability of the $\pi$-electrons; (4) the effect of the interaction of these same electrons on the polarizability of the core electrons. In what follows, we shall limit outselves to a consideration of only the first of the indicated factors. The contribution to the phenomenon under consideration from the second factor is probably not very great (this follows in particular from the applicability of the additive valence-optical scheme to saturated molecules having only $\sigma$ bonds). The contributions of the last two factors( which in general can turn out to be large) will not be considered in detail by us.

In the next section, a brief account is presented of the calculation of second approximation corrections to the ground state energy of multielectron systems by the self-consistent field method. In the third section the theory is applied to the calculation of $\pi$-electron polarizability of the singly conjugated molecules ethylene and benzene.

## FUNDAMENTAL EQUATIONS OF PERTURBATION THEORY IN THE SELF-CONSISTENT FIELD METHOD

Self-consistent single electron functions of a system of 2N electrons are determined from the well known self-consistent field equation

$$H_{self.}\,\psi_i = (T+V)\psi_i + \sum_{k=1}^{N}\left[2\int \frac{\psi_k^*(r')\,\psi_k(r')\,d\tau'}{|r-r'|}\,\psi_i(r) - \int \frac{\psi_k^*(r')\,\psi_i(r')\,d\tau'}{|r-r'|}\,\psi_k(r)\right] = \varepsilon_i\psi_i. \qquad (1)$$

where T and V are the single electron kinetic and potential energy operators. The first N functions $\psi_i (i \leq N)$ which satisfy the system (1) and the corresponding N smallest values of the parameters $\varepsilon_i$ enter into the expression for the approximate wave function of the ground state of the system which has the form

$$\Psi = [(2N)!]^{-\frac{1}{2}}\,det\,[\psi_1\alpha;\ \psi_1\beta;\ \ldots\ \psi_N\alpha;\ \psi_N\beta]. \qquad (2)$$

The single electron wave functions $\psi_p$, which satisfy the system (1) for $p > N$, correspond to the excited single electron states which are unoccupied in the molecular ground state. Along with the multielectron wave function of the ground state $\Psi$ (2), let us consider the following multielectron function:

$$\Psi_{i\to p} = |2(2N)!|^{-\frac{1}{2}} \{ det\,[\psi_1\alpha;\ \ldots\ \psi_{i-1}\beta;\ \psi_p\alpha;\ \psi_i\beta;\ \psi_{i+1}\alpha;\ \ldots;\ \psi_N\beta] + det\,[\psi_1\alpha;\ \ldots\ \psi_{i-1}\beta;\ \psi_i\alpha;\ \psi_p\beta;\ \psi_{i+1}\alpha;\ \ldots\ \psi_N\beta] \}. \quad (3)$$

The function $\Psi_{i\to p}$ corresponds to a singlet singly excited state of a multielectron system in which the electron of the single electron state $\psi_i$ ($i \leq N$) is transferred to the excited state $\psi_p$ ($p > N$).

Consider the excitation of a multielectron system described by the operator

$$U = \sum_{k=1}^{2N} U(r_k). \quad (4)$$

Since the operator U does not act on spin reversals, and because of its single electron character does not have any matrix elements to couple the ground state of the multielectron system with states in which two or more electrons are excited, the normalization of the excited wave function $\tilde{\Psi}$ of the ground state of a multielectron system can be represented in the form

$$\tilde{\Psi} = \Big(1 + \sum_{\substack{k\leq N\\ p>N}} d_{kp}^2\Big)^{-\frac{1}{2}} \Big(\Psi + \sum_{\substack{i\leq N\\ p>N}} d_{ip}\Psi_{i\to p}\Big). \quad (5)$$

The requirement that the average value of the energy of a multielectron system calculated from the function $\tilde{\Psi}$ be a minimum, yields the following equation to which the coefficients $d_{ip}$ must conform:

$$(E_{ip} - E_0)\, d_{ip} + \sum_{\substack{k\leq N\\ q>N}} \langle i\to p\,|H|\,k\to q\rangle d_{kq} + \langle 0\,|U|\,i\to p\rangle = 0$$
$$(i = 1,\ 2\ \ldots,\ N);\ (p = N+1,\ N+2,\ \ldots). \quad (6)$$

The prime on the summation sign indicates that terms with k = i and q = p are excluded from the summation. The second approximation correction to the energy yields the equation

$$E^{(2)} = \sum_{\substack{i\leq N\\ p>N}} \langle 0\,|U|\,i\to p\rangle d_{ip}. \quad (7)$$

The following notation was introduced:

$$E_0 = \int \Psi^* H \Psi\, (d\tau);\quad E_{ip} = \int \Psi^*_{i\to p} H \Psi_{i\to p}\, (d\tau);\quad \langle i\to p\,|H|\,k\to q\rangle = \int \Psi^*_{i\to p} H \Psi_{k\to q}\, (d\tau);\quad \langle 0\,|U|\,i\to p\rangle = \int \Psi^* U \Psi_{i\to p}\, (d\tau);$$
$$(d\tau) = d\tau_1 d\tau_2 \ldots d\tau_{2N} dx_1 dx_2 \ldots dx_{2N}, \quad (8)$$

i.e., integration over $d\tau$ includes summation over spin reversals; H is the unperturbed total energy operator of the multielectron system.

In order to find the second order corrections to the ground state energy of multielectron systems, the (generally speaking, infinite) system of Eqs. (6) must be solved, and then Eq. (7) is used. The difference between Eqs. (6) obtained by us from the usual equations of perturbation theory which fall out of accurate multielectron wave functions $\Phi_i$ satisfying the equation

$$H\Phi_i = E_i\Phi_i, \quad (9)$$

consists of the presence of nondiagonal matrix elements $\langle i\to p\,|H|\,k\to q\rangle$. In fact, in the accurate wave functions of multielectron systems the nondiagonal matrix elements

$$\int \Phi_i^* H \Phi_k\, (d\tau)$$

vanish. Therefore, if in Eq. (6) the nondiagonal matrix elements $\langle i\to p\,|H|\,k\to q\rangle$ are left out, then our expressions take the form of the usual equations of perturbation theory

$$E^{(2)} = \sum_{k\neq 0} \frac{\left|\int \Phi_0^* U \Phi_k\, (d\tau)\right|^2}{E_0 - E_k}. \quad (10)$$

Introduce the following symbols for matrix elements calculated from one-electron self-consistent wave functions

$$|i\,|U|\,p| = \int \psi_i^* U \psi_p\, d\tau, \quad (11)$$

$$|ik|pq| = \int \frac{\psi_i^*(r)\,\psi_k^*(r')\,\psi_p(r)\,\psi_q(r')\, d\tau\, d\tau'}{|r - r'|}. \quad (12)$$

By using the explicit form of functions (2) and (3), we transform from matrix elements calculated with multielectron functions to matrix elements calculated with single electron functions. By taking into account Eqs. (1), we transform Eqs. (6) and (7) into the form

$$\sum_{\substack{k\leq N\\ q>N}} \{(\varepsilon_p - \varepsilon_i)\,\delta_{pq}\delta_{ik} + 2\,[pk\,|\,iq] - [pk\,|\,qi]\}\, d_{kq} + \sqrt{2}\,[i\,|U|\,p] = 0, \quad (13)$$

$$E^{(2)} = \sqrt{2} \sum_{\substack{i\leq N\\ p>N}} [i\,|U|\,p]\, d_{ip}. \quad (14)$$

Equations (14) and (13) allow one to calculate second order corrections to the ground state energy of a multielectron system if the self-consistent one-electron wave functions $\psi_i$ ($i \leq N$) and $\psi_p$ ($p > N$) are known. These equations are natural generalizations of the corresponding equations of perturbation theory obtained for systems of noninteracting particles. Indeed, if the electron repulsion integrals $[pk\,|\,iq]$ and $[pk\,|\,qi]$ are neglected in Eq. (13), then Eq. (14) gives the usual second order correction to the ground state energy of a system of noninteracting particles

$$E^{(2)} = 2 \sum_{\substack{i\leq N\\ p>N}} \frac{|[i|U|p]|^2}{\varepsilon_i - \varepsilon_p}. \quad (15)$$

The presence of electron repulsion integrals in Eqs. (13) takes into account the additional electric field existing in the molecule when its electronic cloud is polarized by an external electric field.

## THE POLARIZABILITY OF CONJUGATED π-ELECTRONS IN UNSATURATED HYDROCARBONS ACCORDING TO A SEMIEMPIRICAL VARIATION OF THE SELF-CONSISTENT MOLECULAR ORBITAL METHOD

Consider now the case in which approximate self-consistent single electron functions for π-electrons are constructed in the form of linear combinations of a finite number of orthogonal single-electron atomic functions

$$\psi_i = \sum_{\mu=1}^{2N} c_{i\mu}\chi_\mu. \quad (16)$$

Here $\chi_\mu$ is the $p_z$-function of the $\mu$-th carbon atom. In this approximation, the self-consistent field equations (1) assume the form

$$\sum_{\nu=1}^{2N} F_{\mu\nu} c_{i\nu} = \varepsilon_i c_{i\mu} \quad (i,\ \mu = 1,\ 2,\ \ldots,\ 2N), \quad (17)$$

where $F_{\mu\nu}$ is the matrix element of the effective single electron energy operator calculated with single electron wave functions, i.e.,

$$F_{\mu\nu} = \int \chi_\mu^* H_{eff}\, \chi_\nu\, d\tau. \quad (18)$$

In the series of papers by Pariser, Parr, and

Pople[10-12] it was shown that in calculating the π-electron structure of selected hydrocarbons by the self-consistent molecular orbital method, matrix elements $F_{\mu\nu}$ which have the following form are used:

$$F_{\mu\mu} = \text{const}; \quad F_{\mu\nu} = \beta_{\mu\nu}\eta_{\mu\nu} - \frac{1}{2}P_{\mu\nu}\gamma_{\mu\nu}, \tag{19}$$

where $\eta_{\mu\nu} = 1$ for neighboring atoms $\mu$ and $\nu$; $\eta_{\mu\nu} = 0$ for atoms $\mu$ and $\nu$ which are not neighbors. The self-consistent character of the matrix F resides in the fact that it depends on the order of π-bonds between the atoms $\mu$ and $\nu$.

$$P_{\mu\nu} = 2\sum_{i=1}^{N} c_{i\mu}^{*}c_{i\nu}, \tag{20}$$

determined by the form of the solution of the system of equations (17). As a result of Eq. (19), the following assumption about the form of the electrostatic interaction integrals for electrons is used:

$$\int \frac{\chi_\mu^{*}(\tau)\,\chi_\nu^{*}(\tau')\,\chi_\rho(\tau)\,\chi_\sigma(\tau')\,d\tau\,d\tau'}{|r-r'|} = \gamma_{\mu\rho}\delta_{\mu\rho}\delta_{\nu\sigma}. \tag{21}$$

The dependence of the quantities $\beta_{\mu\nu}$ and $\gamma_{\mu\nu}$ on the distance between the atoms $\mu$ and $\nu$ is given in reference 11.

In the approximation being considered here, Eqs. (13) and (14) take the form

$$\sum_{k<l;\ k>N}\left\{(\varepsilon_p-\varepsilon_k)\,b_{pq}\,b_{kl} + \sum_{\mu,\nu=1}^{2N}\left[2c_{p\mu}^{*}c_{k\nu}^{*}c_{l\mu}c_{q\nu} - c_{p\mu}^{*}c_{k\nu}^{*}c_{l\nu}c_{q\mu}\right]\gamma_{\mu\nu}\right\}d_{kl} + \sqrt{2}\sum_{\mu,\nu=1}^{2N}c_{q\mu}^{*}c_{p\nu}\,(\mu\,|U|\,\nu) = 0 \tag{22}$$

$$E^{(2)} = \sqrt{2}\sum_{k<N}\sum_{q>N}\sum_{\mu,\nu=1}^{2N}c_{q\mu}^{*}c_{p\nu}\,(\mu\,|U|\,\nu)\,d_{kp}. \tag{23}$$

In these equations, the following notation was used:

$$(\mu\,|U|\,\nu) = \int \chi_\mu^{*}U\chi_\nu\,d\tau. \tag{24}$$

In the particular case when the perturbation is caused by a homogeneous electric field E parallel to the face of the molecule (U = Ex), we have (using the assumption that the atomic wave functions χ belonging to the different atoms $\mu$ and $\nu$ are orthogonal)

$$(\mu\,|U|\,\nu) = Ex_\mu\delta_{\mu\nu}. \tag{25}$$

If the self-consistent π-electron molecular orbitals satisfying Eq. (16) are known, then the polarizability of the π-electrons in unsaturated hydrocarbon molecules including their interactions are determined from Eqs. (24) and (25).

Consider some examples.

Ethylene: The self-consistent molecular orbitals of the π-electrons are completely determined by symmetry properties

$$\psi_1 = 2^{-\frac{1}{2}}(\chi_1+\chi_2); \quad \psi_2 = 2^{-\frac{1}{2}}(\chi_1-\chi_2). \tag{26}$$

The order of the π-bonds $C_1 - C_2$ is equal to $p_{12} = 1$, and the energies of the respective molecular orbital are equal to

$$\varepsilon_1 = -\varepsilon_2 = \beta_{12} - \frac{\gamma_{12}}{2}. \tag{27}$$

The matrix element of the dipole transition is equal $[1\,|x|\,2] = l/2$ (l is the bond length C=C). The system of equation (22) reduces to a single equation for which i = 1 and p = 2. By determining $d_{12}$ from this equation and using (23), we obtain the following expression for the π-electron polarizability of ethylene along the C=C bond

$$a_x = \frac{e^2l^2}{-2\beta_{12} + \frac{1}{2}(\gamma_{11}-\gamma_{12})} = 23.1 \text{ atomic units} \tag{28}$$

In the above the following numerical values were used; l = 1.33 A, $\beta_{12} = -2.92$ ev, $\gamma_{11} = 10.53$, and $\gamma_{12} = 7.38$ ev; the atomic unit of polarizability is equal to $1.48 \times 10^{-25}$ $cm^3$.

If in (28) we neglect the electron repulsion integrals, we obtain

$$a_x^{(0)} = -\frac{e^2l^2}{2\beta_{12}} = 29.3 \text{ atomic units} \tag{29}$$

The ratio of the quantities (29) and (28) is 1.27. Thus, neglecting the interaction of π-electrons increases the π-electron polarizability of ethylene along the C=C bond by 27%.

Benzene: Just as in the case of ethylene, the self-consistent molecular orbitals are completely determined by the symmetry of the molecule:

$$\left.\begin{aligned}
&\psi_1 = \frac{1}{\sqrt{6}}(\chi_1+\chi_2+\chi_3+\chi_4+\chi_5+\chi_6); \quad \varepsilon_1 = 2\beta - \frac{2}{3}\gamma_{12} - \frac{\gamma_{14}}{6};\\
&\psi_2 = \frac{1}{2\sqrt{3}}(2\chi_1+\chi_2-\chi_3-2\chi_4-\chi_5+\chi_6); \quad \varepsilon_2 = \beta - \frac{1}{2}\gamma_{12} - \frac{\gamma_{14}}{6};\\
&\psi_3 = \frac{1}{2}(-\chi_2-\chi_3+\chi_5+\chi_6); \quad \varepsilon_3 = \varepsilon_2;\\
&\psi_4 = \frac{1}{2}(-\chi_2+\chi_3-\chi_5+\chi_6); \quad \varepsilon_4 = -\varepsilon_2;\\
&\psi_5 = \frac{1}{2\sqrt{3}}(-2\chi_1+\chi_2+\chi_3-2\chi_4+\chi_5+\chi_6); \quad \varepsilon_5 = -\varepsilon_2;\\
&\psi_6 = \frac{1}{\sqrt{6}}(-\chi_1+\chi_2+\chi_3+\chi_4-\chi_5+\chi_6); \quad \varepsilon_6 = -\varepsilon_1.
\end{aligned}\right\} \tag{30}$$

The order of the π-bonds are respectively:

$$p_{1,2} = \frac{2}{3}; \quad p_{1,3} = 0; \quad p_{1,4} = -\frac{1}{3}.$$

By assuming, for definiteness, that the electric field is directed parallel to the line C=C, we find that only the following matrix elements for dipole transitions differ from zero:

$$[2\,|x|\,5] = -[3\,|x|\,4] = \frac{l}{2} \quad (l - \text{bond length C = C}).$$

The system of equation (22) in the case under consideration has the form:

$$\left.\begin{aligned}
Ad_{25} + Bd_{34} + \frac{1}{\sqrt{2}}lE = 0,\\
Bd_{25} + Ad_{34} - \frac{1}{\sqrt{2}}lE = 0,
\end{aligned}\right\} \tag{31}$$

where

$$A = -2\beta_{12} + \frac{\gamma_{11}}{4} - \frac{\gamma_{12}}{12} + \frac{\gamma_{13}}{4} - \frac{5\gamma_{14}}{12};$$

$$B = \frac{\gamma_{11}}{2} - \frac{3\gamma_{12}}{4} + \frac{11\gamma_{13}}{12} - \frac{\gamma_{14}}{4}.$$

By substituting the solution of the system of equation (32)

$$d_{25} = -d_{34} = \frac{lE}{\sqrt{2}\,(B-A)}$$

into Eq. (23), we obtain for the second approximation correction to the energy of π-electrons in benzene, the expression

$$E^{(2)} = \frac{e^2l^2E^2}{A-B} = \frac{e^2l^2E^2}{-2\beta_{12} + \frac{1}{6}(\gamma_{11}-\gamma_{14}) + \frac{2}{3}(\gamma_{12}-\gamma_{13})} \quad (32)$$

By using the numerical values $l = 1.39$ A, $\beta_{12} = -2.39$ ev, $\gamma_{11} = 10.53$ ev, $\gamma_{12} = 7.30$ ev, $\gamma_{13} = 5.46$ ev, and $\gamma_{14} = 4.90$ ev we find for the polarizability of the $\pi$-electrons in benzene in the plane of the ring: $a_\pi = 54.0$ atomic units. If the repulsion integrals of the $\pi$-electrons are neglected in Eq. (32), we obtain $a_\pi^{(0)} = 78.3$ atomic units. The ratio $a_\pi^{(0)}/a_\pi$ amounts to 1.45. Thus, neglect of the interaction of $\pi$-electrons increases the theoretical $\pi$-electron polarizability of the benzene molecule by 45%. Apart from this considerable decrease with respect to $a_\pi^{(0)}$, however, the quantity $a_\pi$ still exceeds the probable value of $\pi$-electron polarizability of benzene in the plane of the ring, which amounts to about 40 atomic units.[3] The higher theoretical value of $a_\pi$ can be caused by either inaccuracies in the numerical parameters of the Pariser, Parr, and Pople method or by neglecting the interaction of $\pi$- and $\sigma$-electrons.

## CONCLUSIONS

The examples which were considered above showed that the electrostac interaction of $\pi$-electrons lowers the $\pi$-electron polarizability of conjugated molecules by a considerable amount. There is considerable interest in investigating this effect in the case of large conjugated molecules. This requires, however, rather involved calculations associated with calculations of self-consistent molecular orbitals.

As was already noted in the introduction, the polarizability of conjugated molecules can also be lowered because of the interaction of $\pi$-electrons with molecular core electrons. According to an approximate calculation,[3] the $\pi$-electron and $\sigma$-electron polarizabilities of benzene in the plane of the ring are approximately equal. Therefore, it can be assumed that the polarization of the $\sigma$-electron core affects the polarizability of the $\pi$-electrons to as great a degree as the mutual interaction of the $\pi$-electrons. The polarization of the $\pi$-electrons, in turn, screens the $\sigma$-bonds from the external field to a certain degree, which ought to result in a lowering of the polarizability of $\sigma$-bonds in conjugated molecules as compared to aliphatic compounds (such a screening, although it was strongly exaggerated, was taken into account in reference 13 during a calculation of molecular refraction in aromatic compounds by applying classical electrostatic methods). The indicated problems require further investigation.

In conclusion we note that the equations of perturbation theory for the self-consistent field method which were introduced in the second part can be applied to a wide circle of problems; it is not limited to the specific simplifying assumptions of the semi-empirical method of molecular orbitals used in the third part.

## REFERENCES


1. P. L. Davies. Trans. Faraday Soc. **48**, 789 (1952).
2. N. V. Cohan, C. A. Coulson, and J. B. Jamiesson. Trans. Faraday Soc. **53**, 582 (1957).
3. H. Bolton. Trans. Faraday Soc. **53**, 582 (1957).
4. M. V. Vol'kenshtein and S. M. Yazykova. Doklady Akad. Nauk SSSR **104**, 834 (1955).
5. M. N. Adamov and I. S. Milevskaya. Doklady Akad. Nauk SSSR **109**, 57 (1956).
6. M. N. Adamov and I. S. Milevskaya. Opt. i Spektr. **2**, 399 (1957).
7. M. N. Adamov. Zhur. Fiz. Khim. **32**, 2087 (1958).
8. M. N. Adamov and B. I. Orlov. Vestnik Leningrad. Gosudarst. Univ., Ser. Fiz. i. Khim. No. 22, 182 (1958).
9. M. A. Kovner. Opt. i Spektr. **2**, 304 (1957).
10. R. Pariser and R. G. Parr. J. Chem. Phys. **21**, 466 (1953).
11. R. Pariser and R. G. Parr. J. Chem. Phys. **21**, 767 (1953).
12. J. A. Pople. Trans. Faraday Soc. **49**, 1375 (1953).
13. J. Schuyer, L. Blom, and D. W. Krevelen. Trans. Faraday Soc. **49**, 1391 (1953).


# FREQUENCIES AND INTENSITIES IN THE INFRARED SPECTRUM OF BROMOFORM

N. E. Gaponova, M. P. Lisitsa, and Yu. P. Tsyashchenko

Received 29 June 1959

The results of quantitative studies of the absorption spectrum of $CHBr_3$ in the region 460-11700 $cm^{-1}$ are described. The integrated absorption and the halfwidth have been computed for the fundamental vibrations, and also for the isolated and weakly overlapping absorption bands which correspond to overtones and combination frequencies. The overshelming majority of the bands have been identified. The degree of polarity of the bonds has been set up as the basis of an explanation of the intensity values for the fundamental vibrations and overtones. A comparison of the spectra of $CHBr_3$ and $CHCl_3$ has been carried out.

## INTRODUCTION

The halogen substitution products of methane have always offered considerable interest for molecular spectroscopy; however, few works have been devoted to a quantitative investigation of their infrared spectra. As far as bromoform is concerned, up to the present the literature contains no sufficiently complete data on even the presence of fundamental overtones and combination frequencies. Sporadic data are contained in references 1-7, and in reference 8 are presented the results of more complete investigations, but only with a qualitative estimation of the intensities. The first quantitative result was obtained by Chulanovskii and Burgova,[9] who determined the absorption coefficient of the band corresponding to the fundamental frequency $\nu_1$. The aim of the present work was to fill in the existing gap.

## ACCURACY AND RESULTS OF THE MEASUREMENTS

The procedure described earlier[10, 11] was used in this work. The positions of the band maxima and the absorption coefficients were determined with the previous

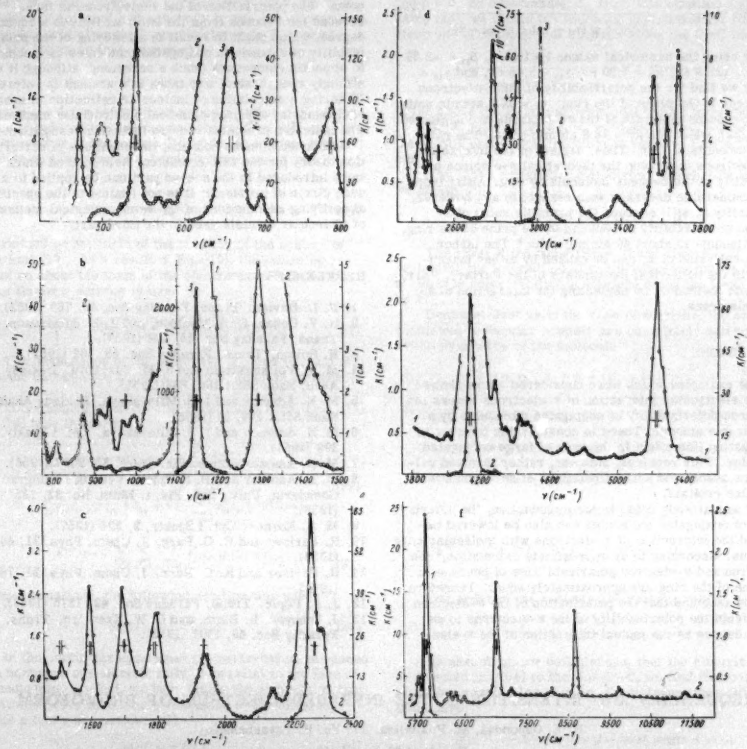

Fig. 1. Absorption spectrum of bromoform in the region 450-11700 $cm^{-1}$. Left-hand scale corresponds to curve 1, right-hand scale to curve 2, middle scale to curve 3.

accuracy. The bromoform absorption curve obtained is presented in sectional form in Fig. 1. The interpretation, symmetry, absorption coefficients at the maximum ($K_{max}$), halfwidths ($\Gamma$), and integrated absorption values (S) of the bands discovered are presented in the Table. For comparison, the data of references 4 and 8 are presented there also.

The quantities S and $\Gamma$ were found only for isolated bands and those easily separable into symmetrical components. In computing the values of S in the region 5000-11000 $cm^{-1}$, the area of the curve was measured starting from the continuous featureless background which was probably brought about by losses produced by reflection of the radiation from the walls of the long cells (the cross section of the cell was less than the cross section of the light beam emerging from the window of the illuminator).

The values of the frequencies of the fundamental vibrations which were used to establish the frequencies of the combination tones and overtones were derived from the Raman spectrum.[13] In computing the frequencies corresponding to the combinations $n\nu_1 + \nu_k$ and $n\nu_1 + \nu_j + \nu_k$ ($n = 2, 3, 4, \ldots$), the frequencies of the overtones and of some combination tones were taken from experiment in order to roughly take into account the anharmonicity correction ($n\nu_2$, $n\nu_3$, $n\nu_4$, $n\nu_5$, $n\nu_6$, and $\nu_1 + \nu_4$ from our own measurements, and $2\nu_1$, $2\nu_1 + \nu_4$ from reference 4, in which they were more exactly determined).

In the vibrational spectrum of a molecule with the symmetry $C_{3v}$, almost all the transitions are allowed by the selection rules (combinations of the fundamental levels with sub-levels of symmetry type $A_2$ constitute an exception); in connection with this, we did not succeed in unequivocally identifying some 10 bands. For these cases, the most probable identifications are indicated in the Table (they are joined by braces). Furthermore, starting from the generally accepted rules, some of the bands found cannot be identified at all, for example, the band $\nu$ 2282 $cm^{-1}$, located in the region of the short wavelength

**Identification and Spectral Characteristics of the Bands in the Infrared Absorption Spectrum of Bromoform**

| No. | Identification | Symmetry | Calculated frequencies* ($cm^{-1}$) | Experimental frequencies ($cm^{-1}$) | $K_{max}$ ($cm^{-1}$) | Integrated absorption S ($cm^{-2}$) | Half-width ($cm^{-1}$) | Frequencies according to refs. 4, 8 ($cm^{-1}$) |
|---|---|---|---|---|---|---|---|---|
| 1 | $\nu_6$ | $E$ | 153.8 | — | — | — | — | 154** |
| 2 | $\nu_9$ | $A_1$ | 222.3 | — | — | — | — | 222** |
| 3 | $2\nu_6$ | $A_1 + E$ | 307.6 | — | — | — | — | 300**? |
| 4 | $\nu_6 + \nu_9$ | $E$ | 376 | — | — | — | — | 380 |
| 5 | $\nu_5 - \nu_6$ | $E$ | 385 | — | — | — | — | 389 |
| 6 | $2\nu_9$ | $A_1$ | 444 | — | — | — | — | 435 |
| 7 | $\nu_5 + \nu_6 - \nu_9$ | $E$ | 470 | 473 | 10.5 | 90 | 7.5 | — |
| 8 | $\nu_5 - \nu_9$ | $A_1 + A_2 + E$ | 503 | 498 | 9.5 | — | — | 501 |
| 9 | $\nu_3$ | $A_1$ | 538.6 | 539 | 145 | 1600 | 9 | 541 |
| 10 | ? | — | — | 567 | 18 | — | — | — |
| 11 | $2\nu_9 + \nu_6$ | $E$ | 589 | 580 | 16 | — | — | — |
| | $\nu_5 + \nu_6 - \nu_9$ | $A_1 + A_2 + E$ | 587 | | | | | |
| 12 | $\nu_5$ | $E$ | 656 | 655 | 4200 | 130000 | 28 | 668 |
| 13 | $\nu_5 + \nu_9$ | $E$ | 692 | 693 | 690 (570 ***) | 7000 | 10 | 694? |
| 14 | $\nu_2 + \nu_6$ | $A_2$ | 761 | 778 | 11.6 | 270 | 19 | 762 |
| 15 | $\nu_5 + \nu_9$ | $A_1 + A_2 + E$ | 810 | 811 | 7.7 | 160 | 16 | — |
| 16 | $\nu_5 + \nu_5$ | $E$ | 878 | 875 | 14.3 | 440 | 24 | 873 |
| 17 | $\nu_5 + \nu_5 - \nu_9$ | $E$ | 914 | 913 | 1.5 | — | — | — |
| 18 | $2\nu_9 - \nu_6$ | $E$ | 923 | 938 | 1.8 | — | — | — |
| 19 | $\nu_5 + \nu_5 - \nu_6$ | $E$ | 972 | 969 | 1.3 | — | — | — |
| 20 | $\nu_1 - \nu_6$ | $A_1 + A_2 + E$ | 988 | 995 | 1.4 | — | — | — |
| 21 | $\nu_5 + \nu_5 - \nu_6$ | $A_1 + A_2 + E$ | 1040 | 1043 | 2.4 | — | — | — |
| 22 | $2\nu_9$ | $A_1$ | 1077 | 1078 | 7 | — | — | 1078 |
| 23 | $\nu_4$ | $E$ | 1142 | 1145 | 2200 | 33000 | 12 | 1142 |
| 24 | $\nu_5 + \nu_9$ | $E$ | 1195 | 1191 | 42 | — | — | 1188 |
| 25 | $2\nu_5$ | $A_1 + E$ | 1312 | 1291 | 50 | 2200 | 36 | 1295 |
| | $\nu_4 + \nu_9$ | $A_1 + A_2 + E$ | 1296 | | | | | |
| 26 | $\nu_5 + \nu_5 + \nu_9$ | $E$ | 1417 | 1420 | 2.8 (1.6) | 95 | 48 | — |
| 27 | $2\nu_5 + \nu_9$ | $A_1 + E$ | 1513 | 1515 | 1.1 | 60 | 45 | 1493? |
| | $\nu_5 + \nu_5 + \nu_6$ | $A_1 + A_2 + E$ | 1518 | | | | | |
| 28 | $3\nu_9$ | $A_1$ | 1616 | 1588 | 2.5 | 80 | 22 | 1597? |
| 29 | $\nu_3 + \nu_4$ | $E$ | 1681 | 1698 | 2.5 | 120 | 28 | — |
| 30 | $\nu_5 + \nu_4$ | $A_1 + A_2 + E$ | 1798 | 1797 | 2.0 | 130 | 50 | — |
| 31 | $3\nu_5$ | $A_1$ | 1968 | 1940 | 1.2 | 100 | 65 | — |
| | $\nu_4 + \nu_5 + \nu_9$ | $A_1 + A_2 + 3E$ | 1952 | | | | | |
| 32 | $\nu_1 + \nu_5 - \nu_6$ | $E$ | 2103 | 2105 | 0.15 | — | — | — |
| | $2\nu_5 - \nu_6$ | $A_1 + A_2 + 2E$ | 2107 | | | | | |
| 33 | $\nu_{10}$ | $A_1$ | 2154 | 1144 | 0.60 | 24 | — | — |
| 34 | $2\nu_9 + \nu_4$ | $E$ | 2219 | 2198 | 0.80 | 11 | — | — |
| 35 | $2\nu_4$ | $A_1 + E$ | 2284 | 2291 | 63 | 1600 | 19 | 2257 |
| 36 | ? | — | — | 2282 | 28 (23) | 1100 | 38 | — |
| 37 | $2\nu_9 + \nu_5$ | $A_1 + A_2 + 2E$ | 2433 | 2445 | 1.1 | 60 | 37 | — |
| 38 | $2\nu_5 + \nu_5$ | $A_1 + E$ | 2483 | 2484 | 1.2 (1.0) | 25 | 17 | — |
| | $\nu_5 - \nu_6$ | $A_1$ | 2484 | | | | | |
| 39 | $4\nu_9$ | $A_1 + 2E$ | 2624 | 2581 | 0.26 | — | — | — |
| | $\nu_5 + \nu_5 - \nu_5$ | $E$ | 2589 | | | | | |
| 40 | $\nu_1 - \nu_4$ | $E$ | 2800 | 2796 | 2.2 | 70 | 23 | — |
| | $2\nu_4 + \nu_5$ | $A_1 + E$ | 2800 | | | | | |
| 41 | $\nu_1 - \nu_5$ | $E$ | 2869 | 2865 | 1.2 | — | — | — |
| 42 | $\nu_4 + \nu_5 - \nu_9$ | $E$ | 2955 | 2945 | 8 | — | — | — |
| 43 | $\nu_1$ | $A_1$ | 3023 | 3020 | 660 | 15000 | — | 3040 |
| 44 | $\nu_1 + \nu_9$ | $A_1$ | 3245 | 3248 | 0.55 | — | — | — |
| 45 | $\nu_1 + \nu_9 + \nu_6$ | $E$ | 3399 | 3383 | 1.3 | — | — | — |
| | $3\nu_4$ | $A_1 + A_2 + E$ | 3426 | | | | | |
| 46 | $\nu_1 + \nu_5$ | $A_1$ | 3561 | 3555 | 7 | 280 | 35 | — |
| 47 | $\nu_1 + \nu_5 - \nu_9$ | $E$ | 3602 | 3621 | 5.2 | 150 | 33 | — |
| 48 | $\nu_1 + \nu_5$ | $E$ | 3679 | 3672 | 8.3 | 340 | 30 | — |
| 49 | $\nu_1 + \nu_5 - \nu_6$ | $A_1 + A_2 + E$ | 3986 | 4000 | 0.5 | — | — | — |
| 50 | $\nu_1 + \nu_4$ | $E$ | 4165 | 4140 | 62 | 3300 | 38 | 4202 |
| 51 | $\nu_1 + \nu_4 + \nu_9$ | $A_1 + A_2 + E$ | 4294 | 4278 | 1.1 | — | — | — |
| 52 | $\nu_1 + \nu_4 + \nu_5$ | $E$ | 4362 | 4345 | 0.5 | — | — | — |
| 53 | ? | ? | — | 4417 | 0.7 | — | — | — |
| 54 | $4\nu_4$ | $A_1 + 2E$ | 4568 | 4470 | 0.6 | — | — | — |
| 55 | $\nu_1 + \nu_4 + \nu_5$ | $E$ | 4680 | 4687 | 0.4 | — | — | — |
| 56 | $\nu_1 + \nu_4 + \nu_5$ | $A_1 + A_2 + E$ | 4796 | 4800 | 0.3 | — | — | — |
| 57 | ? | ? | — | 4980 | 0.25 | — | — | — |
| 58 | $2\nu_4 + \nu_1$ | $A_1 + E$ | 5284 | 5220 | 2.3 | 150 | — | — |
| 59 | ? | ? | — | 5265 | 1.4 | | | |
| 60 | $2\nu_5 + \nu_9$ | $A_1$ | 5364 | 5340 | 0.35 | — | — | — |
| 61 | $2\nu_5 - \nu_6$ | $E$ | 5749 | 5765 | 0.50 | 16.5 | — | — |
| 62 | $2\nu_5$ | $A_1$ | 6046 | 5890 | 24 | 1700 | 55 | 5902? |
| 63 | $2\nu_5 + \nu_9$ | $A_1$ | 6125 | — | — | — | — | 6134 |
| 64 | ? | ? | — | 6240 | 0.3 | 10.0 | 66 | 6300 |
| 65 | $2\nu_5 + \nu_5$ | $A_1$ | 6441 | 6350 | 0.28 | 12 | 80 | 6439 |
| 66 | $2\nu_5 + \nu_5$ | $E$ | 6560 | 6490 | 0.24 | 7.0 | 68 | 6550 |
| 67 | ? | ? | — | — | — | — | — | 6790 |
| 68 | ? | ? | — | — | — | — | — | 6870 |
| 69 | $2\nu_5 + \nu_4$ | $E$ | 7045 | 7000 | 1.6 | 100 | 68 | 7023 |
| 70 | $2\nu_5 + \nu_4 + \nu_9$ | $E$ | 7245 | 7230 | 0.34 | 7.0 | 50 | — |
| 71 | $2\nu_5 + 2\nu_9$ | $A_1 + E$ | 8151 | 8125 | 0.36 | 7.0 | 70 | — |
| 72 | $3\nu_5$ | $A_1$ | 9069 | 9080 | 1.3 | 70 | 80 | — |
| 73 | $3\nu_5 + \nu_4$ | $E$ | 9622 | 9740 | 0.3 | 8.5 | 100 | — |
| 74 | $4\nu_5$ | $A_1$ | 12002 | 11930 | 0.25 | 6.5 | 110 | — |

*With the exception of frequencies of the normal vibrations, the values of the calculated frequencies are given which were derived from the Raman spectrum.[12]

**Frequencies determined from the Raman spectrum.

***Values of the absorption coefficient at the maximum after graphical separation of overlapping bands are given in parentheses.

†Data taken from reference 4.

edge of the overtone $2\nu_4$. It might be supposed that it is produced by an impurity; however, a similar satellite is observed for the same overtone in the spectrum of chloroform. The nature of the band referred to is still unclarified.

## DISCUSSION OF RESULTS

In a well-known approximation, the fundamental frequencies $\nu_2$, $\nu_3$, $\nu_5$, and $\nu_6$ of the bromoform molecule may be considered to be produced by vibrations in the $CBr_3$ group: $\nu_2$ and $\nu_5$ by the valence vibrations of the C—Br bonds, and $\nu_3$ and $\nu_6$ by the deformation vibrations of the BrCBr angles. The frequencies $\nu_1$ and $\nu_4$ belong respectively to the valence and deformation vibrations of the C—H bond. The form of the latter is highly characteristic, since in such vibrations the changes in the natural coordinates of the $CBr_3$ group are very small in comparison with the change in the length of the C—H bond and its deviation from the $C_3$ axis.[13]

We cannot judge the intensities of the vibrations $\nu_2$ and $\nu_6$, since they lie in a region inaccessible to the apparatus at our disposal.

As for the remaining four vibrations, whose integrated absorption we succeeded in determining, the difference in their intensities may be explained by the degree of polarity of the bonds. It is well known that the C—Br bond is substantially more nearly ionic than the C—H bond.[14] Consequently, the integrated absorption in the band of the degenerate valence vibration $\nu_5$ is far greater than the integrated intensity in the bands corresponding to the vibrations $\nu_1$ and $\nu_4$ ($\nu_1$ in particular). In the external deformation vibration $\nu_4$ the axial symmetry is lost, and the "repulsion" of the valence electron of the hydrogen atom by the electron clouds of one or two of the C—Br bonds (and consequently its localization on the hydrogen atom) is apparently greater than in the case of the totally symmetrical valence vibration $\nu_1$. This must diminish the homeopolarity of the C—H bond and lead to an increase in the intensity of the vibration $\nu_4$ in comparison with the vibration $\nu_1$. Actually, the measurements have shown that the absorption in the band of the vibration $\nu_4$ is twice as great as in the band of the vibration $\nu_1$. However, the fact that the totally symmetrical valence vibration $\nu_2$ of the C—Br bonds is less intense than the vibrations $\nu_1$ and $\nu_4$ contradicts the assumed scheme. This is probably explained by the significantly smaller change in the lengths of the C—Br bonds (and consequently in the dipole moment as well) in the case of the vibration $\nu_2$ in comparison with the change in the length of the C—H bond in the case of the vibration $\nu_1$.

A similar picture of the intensity distribution over the fundamental bands is also observed in the spectrum of chloroform.[11] Indeed, in this case it is more marked, inasmuch as the C—Cl bond is more polar than the C—Br bond.[14] For the same reason, the integrated absorption in the bands of each of the vibrations $\nu_2$ and $\nu_5$ in $CHBr_3$ is far less than in $CHCl_3$.

Let us consider the intensities of the overtones and some combination tones. In the ideal case of purely ionic bonds, apart from the interaction of the latter, the dipole moment of the molecule in a first approximation may be written in the form

$$P = \sum_i \mu_i = \sum_i e_i r_i, \qquad (1)$$

and one of its projections as

$$p^{(x)} = \sum_i e_i r_i^{(x)}, \qquad (2)$$

where $\mu_i$ is the dipole moment of the i-th bond, $r_i$ its length, and $e_i$ the effective charge. In the general case, there are linear relationships[13, 14] of the type

$$r_i^{(\nu)} = \sum_k A_{ik} q_k. \qquad (2a)$$

where the summation is carried out over all the natural coordinates $q_k$ of the molecule, and

$$q_k = \sum_i B_i Q_i. \qquad (3)$$

Here $Q_i$ is the normal coordinate corresponding to the i-th fundamental vibration, $A_{ik}$ and $B_i$ are numerical coefficients expressed in terms of the equilibrium molecular constants.

From (1)-(3) it follows that

$$\frac{\partial P^{(\nu)}}{\partial Q_i} = \sum_i e_i \frac{\partial r_i^{(\nu)}}{\partial Q_i} = \sum_i e_i \sum_k \frac{\partial r_i^{(\nu)}}{\partial q_k} \cdot \frac{\partial q_k}{\partial Q_i}$$

$$= \sum_i e_i \sum_k A_{ik} B_k = C \sum_i e_i. \qquad (4)$$

Hence it follows that $\partial^2 P / \partial Q_i^2 = 0$, as well as the derivatives of higher order. This means that in the case under consideration there is no electro-optical anharmonicity. Such a case, naturally, is not fully realized in actuality, since the bonds do interact and always possess a significant fraction of homeopolarity. Nevertheless, one may expect, qualitatively, that the overtones of the fundamental vibrations in which changes in the bonds of more ionic character predominate will be relatively less intense, since the intensities of the overtones are determined principally by the electro-optical anharmonicity.

The assumption stated here is actually confirmed by analysis of the spectra of chloroform and bromoform. It appears that the intensities of the absorption bands corresponding to different overtones of the vibration $\nu_1$ decrease significantly more slowly, on going from the first overtone to overtones of higher order, than in the series of overtones of the vibration $\nu_5$. Meanwhile, the band of the vibration $\nu_1$ is significantly less intense than the band of the vibration $\nu_5$. From a comparison of the observed and calculated frequency values (see Table) of the overtones referred to, it follows that the mechanical anharmonicity of the vibration $\nu_1$ is greater than that for the vibration $\nu_5$. Besides, it is difficult to suppose that the substantial difference in the character of the fall-off of the intensities of the overtones is produced only by the mechanical anharmonicity. The relative distribution of the integrated intensities in the series of overtones of the vibrations $\nu_1$ and $\nu_5$ of bromoform and chloroform is shown in Fig. 2. Data on the overtones of the vibration $\nu_3$ of carbon tetrachloride[15] are also presented here for purposes of comparison. For convenience of comparison, the integrated intensities of the fundamental vibrations are taken as unity. From the data of Fig. 2 it follows that the intensities of the overtones of the vibration $\nu_5$ of $CHCl_3$ decrease more rapidly than in the case of $CHBr_3$, since the C—Cl bond is more polar. The very abrupt fall in intensity in the series of overtones of the trebly degenerate vibration $\nu_3$ of carbon tetrachloride is produced, apparently, by the greater mutual polarization of the C—Cl bonds.

The absence from the literature of quantitative data on the intensities of fundamental vibrations and their overtones for bonds with a substantially different degree of ionic character does not permit us to consider the present question in greater detail.

In conclusion, let us pause briefly on the intensity distribution in the combination tones of bromoform, and

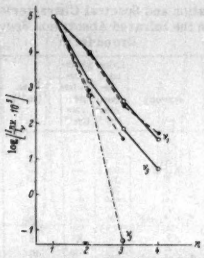


Fig. 2. Distribution of the relative intensities in series of the overtones of the vibrations $\nu_1$ and $\nu_5$ of chloroform (broken line) and bromoform (solid line) and the vibration $\nu_3$ of carbon tetrachloride (n—order of the overtone).

let us compare them with the intensities of the corresponding tones of chloroform. First of all, we must note the anomalously high intensity of the combination $\nu_2 + \nu_6$, whose absorption maximum lies at $\nu = 693$ cm$^{-1}$. The integrated absorption in the band of this vibration exceeds by almost an order of magnitude the same quantity for any other combination of the type $\nu_i + \nu_k$. This fact is easily explained if we admit the presence of Fermi resonance between the combination tone $\nu_2 + \nu_6$ and the fundamental vibration $\nu_4$. They have the same symmetry E and frequencies, for transitions between the unperturbed levels, which are relatively close ($\Delta\nu = 36$ cm$^{-1}$). With such an interval, one cannot expect a practically complete equalization of the intensities of the resonating vibrations or an additional separation of the frequencies produced exclusively by the resonance. Therefore, the intensities of the vibrations under consideration differ by almost an order of magnitude, and the additional separation (~2 cm$^{-1}$) does not exceed the limits of experimental error. According to theoretical prediction,[16] the liquid-vapor phase transition must lead to a diminution in the intensity of the higher-order vibration. Thus a final opinion on the presence of resonance between the corresponding levels must be expressed only after quantitative absorption measurements on gaseous $CHBr_3$.

With the exception of the vibration $\nu_2 + \nu_6$ considered above, the intensity distributions in the absorption bands of the first-order combination tones of $CHBr_3$ and $CHCl_3$ fundamentally coincide. Here we must point out the absence of a direct dependence between the intensities of the fundamental vibrations and of their combinations. For example, the most intense vibrations, $\nu_4$ and $\nu_5$, give the combination $\nu_4 + \nu_5$, the integrated absorption in the band of which proves in general to be weaker than in the case of other first-order combinations. As a rule, combination tones are most intense when they arise in consequence of combinations of a totally symmetrical and a doubly degenerate fundamental vibration, each of which is produced predominantly by a change of one and the same bonds or angles in the molecule. The combinations $\nu_3 + \nu_6$, $\nu_2 + \nu_5$, and especially $\nu_1 + \nu_4$, are such combination tones. The latter yields only to the combination $\nu_2 + \nu_6$ in regard to intensity.

## CONCLUSIONS

1. Comparison of the absorption spectra of $CHBr_3$ and $CHCl_3$ shows that the integrated absorption in the

bands of the fundamental vibrations depends on the degree of polarity of the bonds which determine the form of the vibration.

2. The decrease in the intensities in a series of overtones which are related to the vibration of certain bonds is more pronounced, the greater the ionic character of the bonds. This conclusion is confirmed by comparison of the intensities of the different-order overtones of the vibrations $\nu_1$ and $\nu_5$ in the case of chloroform and bromoform.

3. The anomalously high intensity of the combination vibration $\nu_2 + \nu_6$ is apparently explained by its participation in Fermi resonance (together with the fundamental vibration $\nu_3$).

REFERENCES


1. J. W. Ellis. Phys. Rev. **23**, 48 (1924).
2. A. Maione. Nuovo cimento **14**, 361 (1937).
3. G. Emschviller and J. Lecomte. J. phys. radium **8**, 130 (1937).
4. T. Yeou. Compt. Rend. Acad. Sci. **206**, 1371 (1938).
5. J. Lecomte. Compt. Rend. Acad. Sci. **196**, 1101 (1933).
6. P. Barschewitz and M. Parodi. J. phys. radium **10**, 143 (1939).
7. E. Plyler. J. Chem. Phys. **16**, 1008 (1949).
8. E. Plyler and W. Benedict. J. Research Natl. Bur. Standards **47**, 202 (1951).
9. V. M. Chulanovskii and M. P. Burgova. Opt. i Spektr. **2**, 330 (1957).
10. M. P. Lisitsa and V. N. Malinko. Pribory i Tekh. Eksp. No. 3, 52 (1957).
11. M. P. Lisitsa and Yu. P. Tsyashchenko. Opt. i Spektr. **5**, 605 (1959).
12. G. Herzberg. "Kolebatel'nye i vrashchatel'nye spektry mnogoatomnykh molekul." (Vibrational and Rotational Spectra of Polyatomic Molecules), Izd. Inostrannoi Lit., Moscow, 1949.
13. M. V. Vol'kenshtein, M. A. El'yashevich, and B. I. Stepanov. "Kolebaniya molekul," Vol. 1. (Molecular Vibrations), Gosudarst. Izd. Tekh.-Teoret. Lit., Moscow-Leningrad, 1949.
14. M. V. Vol'kenshtein, M. A. El'yashevich, and B. I. Stepanov. "Kolebaniya molekul," Vol. 2. (Molecular Vibrations), Gosudarst. Izd. Tekh.-Teoret. Lit., Moscow-Leningrad, 1949.
15. M. P. Lisitsa and V. N. Malinko. Opt. i Spektr. **4**, 455 (1958).
16. M. P. Lisitsa and V. L. Strizhevskii. Opt. i Spektr. **7**, 478 (1959).


# THE INDICATRIX OF THE RAMAN SCATTERING OF LIGHT

I. I. Kondilenko, P. A. Korotkov, and V. L. Strizhevskii

Received 29 July 1959

A derivation is given of a simple and descriptive conclusion of Placzek's formulas, determining the dependence of the Raman line intensity on the angle of observation $\varphi$ and the value of the degree of depolarization of the line $\rho$. The angular dependence of the intensity of the Raman lines of carbon tetrachloride, benzene, and chloroform are measured. The experimental data obtained are in satisfactory agreement with theory. The possibility of a new method of measurement of the degree of depolarization of a Raman line is shown.

We do not know of experimental investigations of the indicatrix of Raman scattering other than that given in reference 1. Theoretically, the question of the angular dependence of the intensity of Raman scattering has already been examined by Placzek in 1935.[2] However, the calculations of Placzek are extremely complicated, and a formula defining the angular dependence in a simpler manner is needed. For the frequent case of scattering through the angle $\pi/2$ the value of the intensity (by an analogous method) has been already obtained.[3]

## I. THEORY OF THE INDICATRIX OF RAMAN SCATTERING

We examine first the case where the exciting light appears naturally. We assume that this exciting light is emitted along a direction forming an angle $\varphi$ with the direction of observation, chosen as the X axis in the space-fixed coordinate system XYZ (Fig. 1).

Without limiting the generality it is possible to consider the direction of the incident light to be located in the XY plane (OM in Fig. 1). For a calculation of the Raman intensity it is necessary to determine the dipole moment of the corresponding intramolecular transition. This is conveniently done in the system of coordinates $\xi$, $\eta$, $\zeta$, for axes which coincide with the principal directions

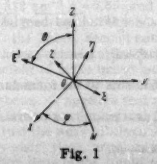


Fig. 1

of the polarizability tensor, which establishes the proportionality between the electric dipole moment and the intensity of the electric field of the light wave.[3] If the principal values of this tensor are indicated by $\alpha_\xi$, $\alpha_\eta$, $\alpha_\zeta$, then the components of the dipole moment are determined by the relationships

$$P_\xi = \alpha_\xi E_\xi, \quad P_\eta = \alpha_\eta E_\eta, \quad P_\zeta = \alpha_\zeta E_\zeta, \tag{1}$$

where $E_\xi$, $E_\eta$, $E_\zeta$ are the components of the electric vector of the monochromatic light wave in the vicinity of the molecule $E_0 e^{i\omega t}$ along the axes $\xi$, $\eta$, $\zeta$, connected with the components of the underlying XYZ coordinate system by the transformations

$$\left.\begin{aligned} E_\xi &= E_x \cos(\xi, X) + E_y \cos(\xi, Y) + E_z \cos(\xi, Z), \\ E_\eta &= E_x \cos(\eta, X) + E_y \cos(\eta, Y) + E_z \cos(\eta, Z), \\ E_\zeta &= E_x \cos(\zeta, X) + E_y \cos(\zeta, Y) + E_z \cos(\zeta, Z). \end{aligned}\right\} \tag{2}$$

Radiation in the direction of the X axis is determined by the components $P_Y$ and $P_Z$. The latter are expressed in $P_\xi$, $P_\eta$, $P_\zeta$ (1) by the following scheme

$$\left.\begin{aligned} P_y &= P_\xi \cos(Y, \xi) + P_\eta \cos(Y, \eta) + P_\zeta \cos(Y, \zeta), \\ P_z &= P_\xi \cos(Z, \xi) + P_\eta \cos(Z, \eta) + P_\zeta \cos(Z, \zeta). \end{aligned}\right\} \quad (3)$$

The light intensity scattered by one molecule, and polarized along the Y and Z axes, is proportional to $\overline{P_{0y}^2}$ and $\overline{P_{0z}^2}$ —the squares of the y-th and z-th components of the amplitude $P_0$ of the dipole moment averaged over all possible directions of the vector E. If it is assumed that we are concerned with molecules freely rotating in space, then for a determination of the total intensity $I_y$ and $I_z$ of the light scattered by all the molecules and polarized along the Y and Z axes respectively, we must still average overall orientations of the system $\xi\eta\zeta$ relative to XYZ. It is not difficult to establish that

$$\left.\begin{aligned} \overline{E_x^2} &= \tfrac{1}{2} E^2 \sin^2\gamma, \quad \overline{E_y^2} = \tfrac{1}{2} E^2 \cos^2\gamma, \quad \overline{E_z^2} = \tfrac{1}{2} E^2, \\ \overline{E_x E_y} &= -\tfrac{1}{2} E^2 \sin\gamma\cos\gamma, \quad \overline{E_y E_z} = \overline{E_x E_z^*} = 0 \end{aligned}\right\} \quad (4)$$

(The average in (4) is carried out over all possible orientations of the vector E.)

Using (1)-(4) we obtain

$$\left.\begin{aligned} I_y &\sim I_0 \left\{ [\,]_{yx}^2 \sin^2\gamma + [\,]_{yy}^2 \cos^2\gamma + [\,]_{yz}^2 - 2[\,]_{yx}[\,]_{yy} \sin\gamma\cos\gamma \right\}, \\ I_z &\sim I_0 \left\{ [\,]_{zx}^2 \sin^2\gamma + [\,]_{zy}^2 \cos^2\gamma + [\,]_{zz}^2 - 2[\,]_{zx}[\,]_{zy} \sin\gamma\cos\gamma \right\}. \end{aligned}\right\} \quad (5)$$

Here $I_0$ is the intensity of the incident light,

$$[\,]_{yx} = \alpha_\xi \cos(Y, \xi)\cos(X, \xi) + \alpha_\eta \cos(Y, \eta)\cos(X, \eta) + \alpha_\zeta \cos(Y, \zeta)\cos(X, \zeta) \quad (6)$$

and similarly for the other combinations of the indices XYZ. The average in (5) is carried out over all orientations $\xi\eta\zeta$ relative to XYZ. The latter is not difficult to do using the expressions for the cosines of the angles between the two sets of axes, well known from courses in mechanics. The averaging gives

$$\left.\begin{aligned} &\overline{[\,]_{yx}^2} = \overline{[\,]_{yz}^2} = \overline{[\,]_{zx}^2} = \overline{[\,]_{zy}^2} = \tfrac{1}{15}(A - B); \\ &\overline{[\,]_{yy}^2} = \overline{[\,]_{zz}^2} = \tfrac{1}{15}(3A + 2B); \quad \overline{[\,]_{yx}[\,]_{yy}} = \overline{[\,]_{zx}[\,]_{zy}} = 0; \end{aligned}\right\} \quad (7)$$

$$A = \alpha_\zeta^2 + \alpha_\eta^2 + \alpha_\xi^2; \quad B = \alpha_\xi\alpha_\eta + \alpha_\eta\alpha_\xi + \alpha_\zeta\alpha_\zeta. \quad (8)$$

Substituting (7) in (5) leads to the formulas

$$\left.\begin{aligned} I_y &\sim I_0 \left[ \frac{2}{15}(A - B) + \frac{1}{15}(2A + 3B)\cos^2\gamma \right], \\ I_z &\sim I_0 \frac{1}{15}(4A + B). \end{aligned}\right\} \quad (9)$$

Naturally, $I_z$ does not depend on the angle $\varphi$. The total intensity is

$$I = I_y + I_z \sim I_0 \frac{1}{15}(6A - B)\left[ 1 + \frac{2A + 3B}{6A - B}\cos^2\gamma \right]. \quad (10)$$

In place of the two unknown quantities, A and B, it is possible to introduce the observed experimental total Raman intensity and the degree of depolarization for

$$\varphi = \frac{\pi}{2}, \quad I\left(\frac{\pi}{2}\right) \text{ and } \rho = \frac{I_y\left(\frac{\pi}{2}\right)}{I_z\left(\frac{\pi}{2}\right)}.$$

With the aid of these quantities (10) is written in the form

$$I = I\left(\frac{\pi}{2}\right)\left(1 + \frac{1 - \rho}{1 + \rho}\cos^2\gamma\right). \quad (11)$$

We will now examine the case where the incident light is linearly polarized. In this case the Raman intensity does not depend on the angle $\varphi$, but does depend on the angle $\theta$ between the direction of observation and the electric vector E', which we take as lying in the XZ plane (Fig. 1). Completely analogous to the preceding, we find with the aid of formulas (1)-(3)

$$\left.\begin{aligned} I_y &\sim I_0 \tfrac{1}{15}(A - B), \\ I_z &\sim I_0 \left[ \tfrac{1}{15}(3A + 2B) - \tfrac{1}{15}(2A + 3B)\cos^2\theta \right], \\ I &= I_y + I_z. \end{aligned}\right\} \quad (12)$$

Introducing the intensity and the degree of depolarization for

$$\theta = \frac{\pi}{2}, \quad I\left(\frac{\pi}{2}\right) \text{ and } \rho' = \frac{I_y\left(\frac{\pi}{2}\right)}{I_z\left(\frac{\pi}{2}\right)},$$

we transform I to the form

$$I(\theta) = I\left(\frac{\pi}{2}\right)\left(1 - \frac{1 - \rho'}{1 + \rho'}\cos^2\theta\right). \quad (13)$$

Formulas (11) and (13) solve the stated problem.

If we take the approximation of polarizability theory, in place of the polarizability tensor $\alpha$, we must examine the tensor

$$\left(\frac{\partial\alpha}{\partial Q_i}\right)_0 (Q_i)_{v_i \pm 1,\, v_i};$$

where $(Q_i)_{v_i \pm 1,\, v_i}$ are the matrix elements of the respective normal coordinate $Q_i$ between the final and initial vibrational states with the quantum numbers $v_i \pm 1$, $v_i$.[3] Then the quantities A and B are substituted by $A'(Q_i)_{v_i \pm 1, v_i}$ and $B'(Q_i)_{v_i \pm 1, v_i}$, where A' and B' are expressed by the principal values of the tensor $(\partial\alpha/\partial Q_i)_0$ analogously to (8). It is easy to see that the terms in $\cos^2\varphi$ and $\cos^2\theta$ in (11) and (13), defining the gngular dependence, will not contain the quantities $(Q_i)_{v_i \pm 1, v_i}$. Therefore, the temperature dependence of the indicatrixes $I(\varphi)$ and $I(\theta)$ is the same as the temperature dependence $I(\pi/2)$ examined in reference 3; the form of the angular dependence does not depend on temperature in the approximation under study.

## 2. EXPERIMENTAL INVESTIGATIONS

The measurement of the Raman line intensities for different angles of observation $\varphi$ were made with the aid of the apparatus schematically indicated in Fig. 2.

The cell with the liquid under investigation K was illuminated by two vertically located mercury lamps PRK-4 (in the figure they are denoted by $L_1$ and $L_2$). Each

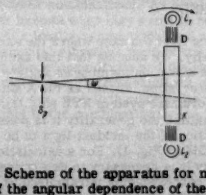


Fig. 2. Scheme of the apparatus for measurement of the angular dependence of the Raman spectra.

lamp was enclosed in a metal casing with a rectangular opening oriented towards the cell K. In order to cool the light sources they were inserted in glass cooling jackets of a general construction, through which water was passed continuously during the investigation. The mercury lamps were operated with alternating current from a ferro-resonance stabilizer SN-350. Between the lamps and the cell K were placed diaphragms D, consisting of a system of parallel metal plates. These diaphragms rendered the exciting light parallel with a maximum spread of the beam of the order of 1 deg. The scattered light fell on the entrance slit of a photoelectric spectrometer DFS-4. The lamps, diaphragms, and cell K were joined together and could be rotated about a vertical axis in the direction indicated in the figure by the arrow. The rotation and measurement of the angle of rotation was made with a special goniometer devised for our purposes. Simple graphical calculations showed that with such a rotation the volume of the scattering liquid, expressed by the aperture angle of the collimator objective, practically does not change. Accordingly, for the chosen experimental conditions, a change of the Raman intensity can be related only to the assumed angular dependence.

It must be noted that in the interpretation of the photoelectric records of lines with different values of depolarization a change of the reflection coefficient at the exit of the scattered light from the cell at the glass-air boundary was taken into consideration. The calculation was carried out by Fresnel's formula for the particular angle of incidence and refractive index of the glass. The intensity loss of the S-component was 8% (for the angle $\varphi = 50°$), and the corresponding addition to the P-component not greater than 2-3%.

It is possible to neglect the polarizing effect of the apparatus since the P-component of the light coming from the cell depends only slightly on the angle, and for this component, in particular, in the given case the light vector is perpendicular to the jaws of the entrance slit, and accordingly, to the rulings of the diffraction grating. As far as the S-component is concerned the spectrometer in this case does not introduce distortions, as has been shown in special investigations. We note also that for each compound the experiments were repeated not less than ten times, and the mean error of measurement was 3%.

The results of the investigations are given in the Table.* The width of the entrance and exit slits of the photoelectric spectrometer were chosen so as to guarantee recording of the integrated intensity of the spectral lines. We also considered the spectral sensitivity of the phototube in a manner which has been described earlier by us.[4,5] Therefore, the data in the Table are given in comparable relative units. One hundredth of the intensity of the 313 $cm^{-1}$ Raman line of $CCl_4$ was taken as unit intensity.

*Student S. Baranov took part in the measurements.

The measurements were carried out for three values of the angle of observation: 90, 50, and 40°. As follows from the Table (data for two angles only are presented here), the value of the intensity calculated by Placzek's formula for the angle $\varphi = 50°$ agrees sufficiently well with the experimentally obtained data. It was shown that in the case of the depolarized lines (217 $cm^{-1}$, 313 $cm^{-1}$ of $CCl_4$, 261 $cm^{-1}$ of $CHCl_3$) the intensity depends weakly on the angle of observation. On the contrary, the intensity of the polarized lines changes significantly for a rotation of the cell through the same angle (667 $cm^{-1}$, 366 $cm^{-1}$ of $CHCl_3$, 992 $cm^{-1}$ of benzene). For example, the intensity of the 217 $cm^{-1}$ line of $CCl_4$, having a degree of depolarization $\rho = 0.93$, increases only by 4%, at the same time that the strongly polarized 459 $cm^{-1}$ line grows in intensity by 37.5% with a change in the angle of observation $\varphi$ from 90° to 50°.

| Compound | $\Delta\nu$ ($cm^{-1}$) | $\rho$ (ref. 6) | $I\left(\frac{\pi}{2}\right)$ | $I$ (50°) experimental | $I$ (50°) theoretical | Increase of I (%) |
|---|---|---|---|---|---|---|
| $CCl_4$ | 217 | 0.93 | 90.5 | 94.2 | 90.5 | 4 |
| | 313 | 0.88 | 100 | 112 | 103 | 12 |
| | 459 | 0.07 | 109 | 150 | 149 | 37.5 |
| $CHCl_3$ | 261 | 0.88 | 87 | 98 | 90.5 | 12 |
| | 366 | 0.34 | 56 | 71.6 | 70 | 28 |
| | 667 | 0.05 | 56 | 74 | 79.6 | 32 |
| $C_6H_6$ | 992 | 0.09 | 172.5 | 215 | 230 | 25 |
| | 3062 | 0.34 | 115 | 134 | 137.9 | 16.5 |

A graphic picture of the change of the relative intensity in the Raman spectrum of $CCl_4$ with a rotation of the apparatus is given in Fig. 3. Here, evidently, there is a significant strengthening of the 459 $cm^{-1}$ line, a lesser effect on the 313 $cm^{-1}$ line, and the 217 $cm^{-1}$ line remains practically without change.

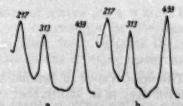


Fig. 3. The Raman spectra of carbon tetrachloride for angles of observation (a)—$\varphi = \pi/2$, and (b)—$\varphi = 50°$.

By taking the ratio of intensities $I(\varphi)/I(\pi/2)$ measured experimentally for the two angles of observation $\varphi$ and $\pi/2$, the Placzek formula (11) presented earlier permits a determination of the degree of depolarization $\rho$ of the Raman line, corresponding to the customary way of observation at an angle $\varphi = \pi/2$.

After slightly rewriting (11) we obtain

$$\rho = \frac{1 - Q_\varphi + \cos^2\varphi}{Q_\varphi - 1 + \cos^2\varphi},$$

where $Q_\varphi = I(\varphi)/I(\pi/2)$.

A computation produced with the last formula showed that the degree of depolarization of the Raman lines of $CCl_4$ has the following values: in the case $\nu = 217$ $cm^{-1}$ $\rho = 0.86$, for $\nu = 313$ $cm^{-1}$ $\rho = 0.58$, and for $\nu = 459$ $cm^{-1}$ $\rho = 0.04$, which in general corresponds to the known literature data (cf. the Table, second column).

Of course the experimental material obtained by us is still not sufficient to make broad generalizations. But for the objects investigated the validity of Placzek's formula has been shown. It appears that a substantial deviation of the indicatrix from spherical form is once more confirmed, and that the act of Raman scattering of light occurs in a very short time, which is significantly less than the relaxation time of the liquid molecules. In the opposite case, i.e., if the moment of absorption of the first photon were separated from the moment of emission of the scattered photon by a long interval of time, attaining many hundreds of periods of the light wave, we would expect Lummel's law to be obeyed since it holds in the case of common photoluminescence.

It is of interest to measure the complete indicatrix of the scattering and to verify the experimental data of reference 1, where the angular dependence was investigated for one of the water lines and one of the benzene lines (the vibrations of the O—H and C—H bonds, respectively). The authors of this work observed in particular an asymmetry of the indicatrix—$I(\varphi) \neq I(\pi - \varphi)$—in contradiction to formula (11). In addition, their experimental data in all the interval of values of the scattering angle do not fit into Placzek's formula (11), in

contrast with our results for the very same conditions of measurement. In the authors' opinion it is necessary to make further investigations for the purpose of a more complete and closer study of the question.

REFERENCES

1. G. I. Pokrowski and E. A. Gordon. Ann phys. 4, 488 (1930).
2. G. Placzek. "Releevskoe Rasseyanie i Raman Effekt." (Rayleigh Scattering and Raman Effect), ONTI, 1935.
3. M. V. Vol'kenshtein, M. A. El'yashevish, and B. I. Stepanov. "Kolebaniya Molekul," Vol. 2, Chap. 18. (Molecular Vibrations), Gosudarst. Izd. Tekh.-Teoret. Lit., Moscow, 1949.
4. I. I. Kondilenko and I. L. Babich. Mater. X Vsesoyuz. Soveshchanie po Spektr., Vol. 1, (Proceedings of the Tenth All-Union Conference on Spectroscopy), Izd. L'vovsk. Univ., 1957.
5. I. I. Kondilenko. Nauk Zapiski, Kliv. Derzhav. Univ. 18, 3 (1959): Sbornik Fiz. Fakul'tetu, No. 10, Kiev.
6. D. H. Rank, R. J. Pfister, and Grimm. J. Opt. Soc. Am. 33, No. 1, 1943.

# THE ANTI-STOKES COMPONENT OF THE RAMAN SPECTRUM FOR HYDROGEN-BONDED COMPOUNDS

L. N. Ovander

Received 14 July 1959

The appearance of Raman spectra in compounds, containing a hydrogen bond, is examined theoretically. It is shown that the structure of the anti-Stokes component should be similar to the structure of the Stokes component.

The hydrogen bond presents a well-known appearance, and its mechanism has been relatively well studied.[1,2] The singularities connected with the presence of a hydrogen bond, and appearing in infrared absorption spectra and in Raman spectra, consist of a broadening of the spectral line corresponding to the vibration of the O—H bond and to a decrease of the frequency of this line. The spectral structure of the infrared line and of the red component in the Raman spectra has been studied.[1] However, works on the structure of the anti-Stokes component in the Raman spectra are unknown to us. In the present work one of the possible theoretical methods of finding this structure is presented.

## CHOICE OF THE MODEL

As a model for the description of the properties of the hydrogen bond a one-dimensional model is used, investigated earlier in references 1 and 2. It presents a quantum mechanical system, consisting of three nuclei characterized by the radius vectors $R_1$, $R_2$, and $R_3$. The energy operator of the above-described systems can be written in the form

$$H = T(\tau) + T(q_1) + T(q_2) + V(\tau, q_1, q_2). \qquad (1)$$

where $\tau$ indicates the totality of the electronic coordinates, $T(\tau)$ is the kinetic energy of the electrons

$$T(q_1) = -\frac{\hbar^2}{2\mu_1}\cdot\frac{\partial^2}{\partial q_1^2}, \quad q_1 = \Delta(R_1 - R_2),$$

$$T(q_2) = -\frac{\hbar^2}{2\mu_2}\cdot\frac{\partial^2}{\partial q_2^2}, \quad q_2 = \Delta(R_1 - R_3),$$

$$\frac{1}{\mu_1} = \frac{1}{m} + \frac{1}{M_1}, \quad \frac{1}{\mu_2} = \frac{1}{M_1 + m} + \frac{1}{M_2}.$$

Here m is the mass of the proton, $M_1$ the mass of nucleus 1, $M_2$ the mass of nucleus 3.*

*Translator's note: I believe this should be "nucleus 2."

The wave function of the operator (1) in the adiabatic approximation can be written as

$$\Phi_{sxp} = \Psi_s(\tau, q_1, q_2)\Psi_x^r(q_1, q_2)\Psi_p^{r'}(q_2), \qquad (2)$$

(error in Russian original)

where $\psi_s$ is the electronic wave function, $\psi_x^r$ the wave function corresponding to the vibrational coordinate $q_0$ (O—H bond), and $\psi_p^{r'}$ the wave function corresponding to the vibrational coordinate $q_2$ (the bond H...X, where X is the symbol of the element, participating in the formation of the hydrogen bond). The energy levels of the system in the adiabatic approximation can be written in the form

$$E_{sxp} = E_s + E_x^{(r)} + E_p^{(r',s)}. \qquad (3)$$

In the following the lowest state will be denoted by the index 0. As a result of violation of the adiabatic condition transitions are possible between the levels (3), in which the radiation field does not participate. The matrix elements of these radiationless transitions we will designate by $K_{xp}^{r'r}$.

## ESTABLISHMENT AND SOLUTION OF THE DIFFERENTIAL EQUATIONS

For the investigation of the scattering we took the method used analogously in reference 4. The red satellite of the Raman spectrum is obtained there as the result of a successive combination of transitions. The original state of the system, described in the preceding paragraph, is characterized by the quantum numbers r = s = 0, the radiation field contains an arbitrary collection of quanta $\{n\lambda\}$. The original state we will designate, for the sake of brevity, by the letter a.

From the original state the system goes under the influence of the radiation into the state $r \neq 0$, s', p'. Simultaneously, from the radiation field a quantum $\lambda$ vanishes, or there appears a quantum $\sigma$. These first intermediate states we will designate by the letters $b\lambda$, $b\sigma$, respectively. From the first intermediate states the system goes over into second intermediate states, for which r = 0, s = 1, p'' = p. After the irradiation with this transition it either obtains a quantum $\sigma$, or loses a quantum $\lambda$. It should be noted that transitions into states with

$p'' \neq p$ are also possible, but, as was shown in reference 5, such transitions occur with relatively small probability and in the present work will not be examined. The second intermediate state we will denote by $c\lambda\sigma$.

From the state $c\lambda\sigma$ there are possible radiationless transitions into states $r = 0$, $s = 0$, $p'''$, without the radiation field for this transition undergoing any change. These states we will denote by $d\lambda\sigma$.

The differential equations for the probability amplitude of residence of the system in the above-described states can be written in the form

$$\left.\begin{aligned}
-i\dot{b}_a &= \sum_\lambda H^a_{b\lambda} b_{b\lambda} e^{i(\omega_{b\lambda}-\omega_a)t} + \sum_\sigma H^a_{b\sigma} b_{b\sigma} e^{i(\omega_{b\lambda}-\omega_a)t},\\
-i\dot{b}_{b\lambda} &= H^{b\lambda}_a b_a e^{i(\omega_a-\omega_{b\lambda})t} + \sum_\sigma H^{b\lambda}_{c\lambda\sigma} b_{c\lambda\sigma} e^{i(\omega_{c\lambda\sigma}-\omega_{b\lambda})t},\\
-i\dot{b}_{b\sigma} &= H^{b\sigma}_a b_a e^{i(\omega_a-\omega_{b\sigma})t} + \sum_\lambda H^{b\sigma}_{c\lambda\sigma} b_{c\lambda\sigma} e^{i(\omega_{c\lambda\sigma}-\omega_{b\sigma})t},\\
-i\dot{b}_{c\lambda\sigma} &= H^{c\lambda\sigma}_{b\lambda} b_{b\lambda} e^{i(\omega_{b\lambda}-\omega_{c\lambda\sigma})t} + H^{c\lambda\sigma}_{b\sigma} b_{b\sigma} e^{i(\omega_{b\sigma}-\omega_{c\lambda\sigma})t} +\\
&\quad + \sum_{p'} K^{c\lambda\sigma}_{d\lambda\sigma} b_{d\lambda\sigma} e^{i(\omega_{d\lambda\sigma}-\omega_{c\lambda\sigma})t},\\
-i\dot{b}_{d\lambda\sigma} &= K^{d\lambda\sigma}_{c\lambda\sigma} b_{c\lambda\sigma} e^{i(\omega_{c\lambda\sigma}-\omega_{d\lambda\sigma})t}.
\end{aligned}\right\} \quad (4)$$

Here H is the interaction operator of the system with the radiation, and K the operator of the radiationless transitions.

The system of equations (4) are to be solved taking account of the initial conditions: $b_a(0) = 1$, $b_{b\lambda}(0) = b_{b\sigma}(0) = b_{c\lambda\sigma}(0) = b_{d\lambda\sigma}(0) = 0$. A method derived from that used in reference 4 was chosen for its solution.

To obtain the contour of the scattering spectral line for the transition $s = 0$, $p \to s = 1$, p, it is necessary to sum the expression for $bd\lambda\sigma(\infty)$ over $\lambda$ and $p''$. The summation was replaced by an integration over $\nu_\lambda$ and $p''$, in which the expression within the integral is multiplied by the density of the states. Assuming that the incident radiation is far from an absorption band, we find that the form of the Raman spectrum for the transition 0, $p \to 1$, p is defined by the formula

$$f^{(1)}_p(\omega_s) = \frac{\text{const}}{\frac{\gamma_p^2}{4} + [\omega_{\lambda_1} - \omega_s - \Omega^{1p}_{0p}]^2}, \quad (5)$$

where $\omega_{\lambda_1}$ is the center of the incident radiation spectrum, $\omega_s$ is the frequency of the scattered light,

$$\gamma_p = \frac{2\pi}{\hbar}\int |K^{d\lambda\sigma}_{a\lambda\sigma}|^2 \rho(\Omega) d\Omega. \quad (6)$$

$\rho(\Omega)$ is the density of states for the bond H ... X, and the magnitude of $1/\gamma_p$ represents the lifetime of the system in the state 1, p. Then, from formula (6) it follows that the spectral width of the exciting spectrum should be significantly less than $\gamma_p$. For obtaining the Raman spectrum, observed experimentally, it is necessary to average (5) over all levels p. This will be done in the following paragraph.

For the examination of the anti-Stokes component it is necessary to solve a system of equations similar to (4), but taking account only of intermediate states of one kind. These equations can be written in the form

$$\left.\begin{aligned}
-i\dot{b}_a &= \sum_\lambda H^a_{b\lambda} b_{b\lambda} e^{i(\omega_{b\lambda}-\omega_a)t} + \sum_\sigma H^a_{b\sigma} b_{b\sigma} e^{i(\omega_{b\sigma}-\omega_a)t} + \sum_{p'} K^{1p}_{dp'} b_d e^{i(\omega_d-\omega_a)t},\\
-i\dot{b}_{b\lambda} &= H^{b\lambda}_a b_a e^{i(\omega_a-\omega_{b\lambda})t} + \sum_\sigma H^{b\lambda}_{c\lambda\sigma} b_{c\lambda\sigma} e^{i(\omega_{c\lambda\sigma}-\omega_{b\lambda})t},\\
-i\dot{b}_{b\sigma} &= H^{b\sigma}_a b_a e^{i(\omega_a-\omega_{b\sigma})t} + \sum_\lambda H^{b\sigma}_{c\lambda\sigma} b_{c\lambda\sigma} e^{i(\omega_{c\lambda\sigma}-\omega_{b\sigma})t},\\
-i\dot{b}_{c\lambda\sigma} &= H^{c\lambda\sigma}_{b\lambda} b_{b\lambda} e^{i(\omega_{b\lambda}-\omega_{c\lambda\sigma})t} + H^{c\lambda\sigma}_{b\sigma} b_{b\sigma} e^{i(\omega_{b\sigma}-\omega_{c\lambda\sigma})t},\\
-i\dot{b}_d &= K^{1p}_{dp'} b_{dp'} e^{i(\omega_a-\omega_d)t}.
\end{aligned}\right\} \quad (7)$$

Here for the initial state it is assumed that the system exists in the state $s = 1$, p, and the radiation field contains a collection of quanta $\{n\lambda\}$. The intermediate states $b\lambda$, $b\sigma$ represent the following: the system exists in the state $r \neq 0$, s, p, with a quantum $\sigma$ vanishing from or a quantum $\lambda$ appearing in the radiation field. In the transition to the final state $0\lambda\sigma$ there appears in the radiation field a quantum $\sigma$ or there disappears therefrom a quantum $\lambda$, and the system goes into the state $s = 0$, p. A radiationless transition to the state d ($s = 0$, p) can occur from the initial state, independent of the particular states of the system.

The system of equations produced above is solved accurately by the very same method as the system (4). The spectral form of the Raman line for the transition $1, p \to 0$, p is then defined by the formula

$$f^{(2)}_p(\omega s) = \frac{\text{const}}{\frac{\gamma_p^2}{4} + [\omega_{\lambda_1} - \omega_s + \Omega^{1p}_{0p}]^2}, \quad (8)$$

where the symbols are the same as in formula (5).

## DISCUSSION OF THE RESULTS

To obtain the structure of the Stokes and anti-Stokes components in the Raman spectra it is necessary to average expressions (5) and (8) over all vibrational levels p. In these expressions only $\gamma_p$ and $\Omega^{1p}_{0p}$ depend on p. All remaining quantities depend weakly on p, so that it is possible simply to neglect this dependence.

We will evaluate the dependence of $\gamma_p$ on p, determined by the matrix elements

$$K^{1p}_{0p} = \int \Psi^{*10}_p \Psi^{e*}_1 \left[T_{(n)} \Psi^0_0 - \frac{\hbar^2}{\mu_q}\frac{\partial}{\partial q_1}\Psi^0_0 \frac{\partial}{\partial q_1}\right] \Psi^{00}_p d\tau(q_1)\, d\tau(q_2), \quad (9)$$

the magnitude of which is related to how strongly $\psi^0_0$ changes with a change of $q_2$.

The potential energy of the system O—H ... X in the ground electronic state can be represented in the form

$$V = V_0(q_1) + V_1(q_1, q_2),$$

where $V_1$ is small by comparison with $V_0$. $V_1$ decreases with an increase in $q_2$, therefore $\psi^0_0 = \overline{\psi}^0_0 + U^0_0$, where $\overline{\psi}^0_0$ is the unperturbed wave function, not depending on $q_2$; $U^0_0$ is an addition, depending on $q_2$ and decreasing as $q_2$ increases.

Accordingly, the matrix element (9) can be written in the form

$$K^{1p}_{0p} = \int \Psi^{10}_p R \Psi^{00}_p d\tau(q_2), \quad (10)$$

where R is a quantity which decreases with an increase of $q_2$. We will denote the region where R has a substantial

value by $\xi$. Further, considering that

$$\Psi_p^{00} \sim \frac{1}{\sqrt{V}},$$

and

$$\Psi_p^{10} \sim \begin{cases} \frac{1}{\sqrt{V}} & \text{for a dissociative state} \\ \frac{1}{\sqrt{\xi}} & \text{for a nondissociative state,} \end{cases}$$

we obtain

$$K \sim \begin{cases} \frac{\xi}{\sqrt{\xi V}} & \text{for a dissociative state} \\ \frac{\xi}{V} & \text{for a nondissociative state.} \end{cases}$$

Thus, $\gamma_{p_1} \gg \gamma_{p_2}$, where $p_1$ is a nondissociative and $p_2$ a dissociative state.

We will examine the spectral structure of the red and violet components. We average (5) over the states p. The complete intensity can be written in the form

$$I_{(\omega_0)}^{(R)} = \frac{\sum_p I_p^{(1)}(\omega_0) \exp\left\{-\frac{E_p}{kT}\right\}}{\sum_p \exp\left\{-\frac{E_p}{kT}\right\}}. \qquad (11)$$

From the summation it is possible to transform to the integral

$$\sum_p \to \int \rho_0(E)\, dE. \qquad (12)$$

where $\rho_0$ is the density of levels being studied in the function through $E_p$. The anti-Stokes component is obtained in an analogous fashion

$$I_{(\omega_0)}^{(V)} = \frac{\int I^2(\omega_0) \exp\left\{-\frac{E}{kT}\right\} \rho_1(E)\, dE}{\int \exp\left\{-\frac{E}{kT}\right\} \rho_1(E)\, dE}, \qquad (13)$$

where $\rho_1$ is the density of levels corresponding to the excited state of the O—H bond. Evidently, in the zeroth approximation[2] it is possible to consider that $\rho_0(E - \hbar\Omega_{01}) = \rho(E)$.

Thus, the structures of the Raman spectra for both components coincide in the zeroth approximation.

Proceeding from formulas (11) and (13) it is possible to show that with an increase of temperature a narrowing of the line occurs. Specifically, with an elevation of the temperature there is an increase of the role of the levels with large $E_p$, and to large $E_p$ correspond small values of $\gamma_p$, i.e., the spectral curve sharpens. The phenomenon of narrowing of the spectral curve with an elevation of the temperature was not explained in reference 2. (There, for high temperatures an extremely sloping curve was obtained.)

In conclusion, the author thanks I. I. Kondilenko, who drew the author's attention to the question examined in the paper.

REFERENCES

1. B. I. Stepanov. Zhur. Fiz. Khim. **20**, 987 (1946).
2. M. V. Vol'kenshtein, M. A. Elyashevich, and B. I. Stepanov, "Kolebaniya Molekul," (Molecular Vibrations), Moscow, Leningrad, 1949.
3. M. Born and J. R. Oppenheimer. Ann. Physik **84**, 457 (1927).
4. V. Weisskopf. Ann. Physik **89**, 23 (1931).
5. N. D. Sokolov. Uspekhi Fiz. Nauk **57**, 205 (1955).

# INFRARED SPECTRA OF CHLOROPHYLL AND ITS ANALOGUES

A. N. Sidorov and A. N. Terenin

Received 10 July 1959

The infrared absorption spectra obtained were of pheophytin, chlorophyll, Zn-, Ni-, and Cu-pheophytin, both in solid films and in solutions of $CCl_4$, and of mixtures of pyridine + $CCl_4$. Introduction of a metal atom into the pheophytin molecule leads to significant changes in its spectra, showing that this atom influences not only the nearest atoms, with which it is directly bound, but even the peripheral groups of atoms of the pigment molecule. The conclusion is drawn that during the formation of a complex with chlorophyll the pyridine molecule attaches itself directly to the central magnesium atom. The influence of pyridine, transmitted through the magnesium atom to the entire chlorophyll molecule, results in stabilization of the keto form of its cyclopentanone ring. For formation of a complex of chlorophyll with water the central metal atom in the pigment molecule is not necessary. However, a metal atom, particularly magnesium, activates the pigment molecule with respect to formation of complexes with water as is shown by the stability of the complexes formed.

At the present time spectroscopic methods, chiefly in the visible region, have enabled a wealth of experimental material to be accumulated describing the qualities of chlorophyll and its analogues. It was discovered, in particular, that in dry pure hydrocarbons (benzene, heptane, isooctane, chlorobenzene, carbon tetrachloride) chlorophyll fluoresces very weakly. Introduction of traces of water, alcohols, or amines into the solution results in a significant strengthening of the fluorescence. This result is explained by the occurrence of molecular complexes of chlorophyll with the added substances.[1-4]

It is well known that chlorophyll is a mixture of chlorophyll a and chlorophyll b. The structural formula of chlorophyll a is presented in Fig. 1. Chlorophyll b differs from chlorophyll a in that at atom $C_3$ instead of the $-CH_3$ group there is a $-C\overset{H}{\underset{O}{<}}$ group. The characteristic peculiarities of the molecular structure of chlorophyll are the following:

1. The presence of a porphyrin ring of conjugated bonds, inside of which is located the central magnesium

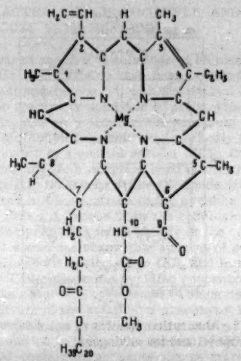

Fig. 1. Structural formula of the chlorophyll a molecule.

atom joined to the nitrogen atoms of the pyrrole nuclei. In Fig. 1 the porphyrin rings of conjugated bonds are shown by heavy lines.

2. The atoms $C_9$ and $C_{10}$ with the carbon atoms of the porphyrin ring form a cyclopentanone ring capable of tautomeric transformation according to the scheme in Fig. 2.

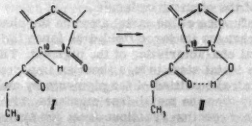

Fig. 2. Tautomeric transformation of the cyclopentanone ring of the chlorophyll molecule. I—keto form; II—enol form with intramolecular hydrogen bonds.

3. Atoms $C_3$ and $C_4$ are bound to each other by a "partially isolated" double bond, which is only partially linked to the porphyrin ring of conjugated bonds.

4. There is an $HC=CH_2$ vinyl group attached to the $C_3$ atom.

Pheophytin has the same structural formula as chlorophyll, but the central magnesium atom has been replaced by two hydrogen atoms forming NH imine groups with the nitrogen atoms of the pyrrole nuclei of the molecule. Methylchlorophyllide differs from chlorophyll in that instead of a phytol radical $C_{20}H_{39}$, its molecule has a $CH_3$ methyl group.

Various points of view have been expressed concerning the ability of an addend molecule to join with a chlorophyll molecule in the formation of a chlorophyll-addend complex. According to one of these viewpoints, put forth by Livingston, Watson, and McCardle,[3] the addend molecule attaches itself to the cyclopentanone ring located in the keto form of the chlorophyll molecule. In particular, the amine molecule attaches itself with the help of a hydrogen bond by means of its own nitrogen atom to a labile H atom of the cyclopentanone ring located at the $C_{10}$ atom. According to the point of view of Evstigneev, Gavrilova, and Krasnovskii[1] the addend molecule is attached directly to the central magnesium atom of the chlorophyll molecule. As support for this conclusion they cite the fact that an increase in fluorescence is not observed in solutions of pheophytin, the molecules of which have a cyclopentanone ring but no central magnesium atom, while fluorescence is observed in solutions of magnesium phthalocyanine in the structure of which there is a cyclopentanone ring. After studying the indicated effect in a series of compounds (Ca-, Mg-, and Zn- derivatives of dimethyl ether of mesoporphyrin, Mg-tetraphenylchlorin, Zn- and Ca-pheophytins, and also the corresponding metal-free pigments), Livingston rejected his original interpretation.[4] However, some investigators continue to support it.[5] Franck explains the low intensity of the fluorescence of chlorophyll in hydrocarbons by the great probability of a nonradiative transition between the singlet and metastable triplet states. In his opinion water molecules attach themselves to two nitrogen atoms of the pyrrole nuclei of chlorophyll, which leads to a decrease in the probability of a nonradiative transition and thus to an increase in the intensity of fluorescence.[6]

Thus as the present time there is no generally accepted point of view as to the nature of the interaction of a chlorophyll molecule with addend molecules. Infrared spectroscopy provides a good possibility for clarification of the nature of this interaction. Infrared spectra of chlorophyll, ethyl chlorophyllide, and pheophytin were first obtained as early as 1933 by Stair and Coblentz.[7] In 1953 Weigl and Livingston on the basis of a comparison of the infrared spectra of chlorophyll a, chlorophyll b, pheophytin a, bacteriochlorophyll, and allomerized chlorophyll[8] made an attempt to interpret the different absorption bands of these pigments. Holt and Jacobs[9] investigated the dependence on solvents of the infrared absorption spectra of chlorophyll and its derivatives. Except for the above-mentioned works, we have no information about investigations of chlorophyll and its analogues by infrared spectroscopy. In this paper it was with the aim of clarifying the influence of the central metal atom on the chlorophyll molecule and of studying the nature of the intermolecular forces in complexes of chlorophyll with addends that we investigated the infrared spectra of pheophytin, chlorophyll, methylchlorophyllide, and analogues of chlorophyll, with various central metal atoms (Met-pheophytins).

## EXPERIMENTAL PROCEDURE

Chlorophyll, pheophytin, and methylchlorophyllide, composed of a mixture of a and b components, were prepared in the laboratory of the photobiochemical institute of the Biochemical Academy of Science of the USSR. The a components made up 80–90% of the contents of these pigments; therefore the conclusions drawn in this work from the corresponding investigation hold with respect to chlorophyll a. The Met-pheophytins (Met-Zn, Cu, Ni) were prepared by us according to Zalesky's method:[10] 7–10 mg of pheophytin and 50–70 mg of an acetate salt of the given metal were dissolved in glacial acetic acid after which the solutions of pheophytin and the salt were stirred together and heated in a boiling water bath for 1.5 to 2.0 hr. After cooling, the resulting pigment was extracted from the acid by ethyl ether and the extract was repeatedly washed with water to remove the acid and excess salt. The ether solutions were then dried and the pigments were stored in carefully polished containers under refrigeration. Measurements of the absorption spectra of Met-pheophytins in the visible region showed that the pigments obtained were free from impurities of metal-free pheophytin. Two principal absorp-

tion maxima of the ether solution of pheophytin were located at 666 and 417 mμ. The corresponding maxima of Zn-pheophytin were located at 651 and 425 mμ, Cu-pheophytin at 646 and 414 mμ, and Ni-pheophytin at 643 and 425 mμ.

The spectroscopic measurements of the solutions of chlorophyll and its analogues were taken in air. Some control measurements of the spectra of the solutions were made under vacuum conditions. In this case a known quantity of pigment was placed in the vacuum cell; then, after evacuation of the cell, the solvent in the cell was distilled off by a special branch of the vacuum system. The concentration of pigments in the solutions for spectra recorded in the 700-3800 $cm^{-1}$ region was about 0.1 mole/liter. The cells used were of uniform thickness equal to 0.1 mm. In the 1800-3800 $cm^{-1}$ region dilute solutions of pigments in $CCl_4$ were also studied (concentrations of the order of $10^{-2}$ mole/liter, layers 10-30 mm thick).

The measurements of the absorption spectra were made on a double beam infrared UR-10 spectrophotometer (Karl Zeiss, Jena) with NaCl and LiF prisms.

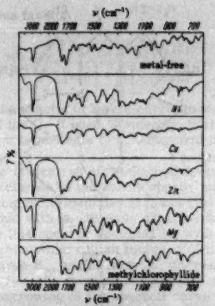


Fig. 3. Absorption spectra of solid films of chlorophyll and its analogues.

## THE INFLUENCE OF THE CENTRAL METAL ATOM ON THE CHLOROPHYLL MOLECULE

Figure 3 shows the spectra of pheophytin, chlorophyll, methylchlorophyllide, and Met-pheophytins which were obtained in solid films by drying ether solutions of the pigments on plates of sylvite. Although previously we had had no hope of interpreting most of the infrared absorption bands of chlorophyll, by referring to the spectra in Fig. 3 it is possible to draw the following definite conclusions.

In the first place, introduction of a metal atom into the pheophytin molecule leads to a significant change in the spectrum of the pigment. This result represents the presence of a change in the entire system of molecular bonds. In particular, there is a change in the position of the absorption band in the region of the stretching vibrations of the double bonds. Secondly, atoms of various metals, upon introduction into the pheophytin molecule, influence it differently, indicating variations in the pheophytin spectra corresponding to variations in the metals. In particular, there are such variations in the position of the absorption band in the region of double bonds (Fig. 3 and Table). Since the central metal atom influences the position of the absorption band of the double bonds in the Met-pheophytin molecules, it becomes evident that not only does this atom exert influence on the nearest atoms with which it is directly bound, but also, through the system of conjugated bonds, it influences the peripheral groups of atoms of the pigment molecule.

The influence of the metal atom on the pheophytin molecule changes its force field; this force field defines the spectral characteristics of the pigment. The influence of the metal atom brings about an important change in the chemical qualities of the pigments by making them more active than the metal-free pigments, with respect to oxidation-reduction reactions (see, for example, references 11 and 12).

Position of Absorption Bands of Chlorophyll and its Analogues in the Region of the Characteristic Frequencies of Double Bond Vibrations (in $cm^{-1}$)

| Compound | State | Interpretation | | | | | | |
|---|---|---|---|---|---|---|---|---|
| | | C=O at $C_9$ and $C_{10}$ | Not established | Keto group C=O | Aldehyde C=O | C=O···H | Enol C=C | Pyridine in complex with pigment |
| Pheophytin | Solid layer | 1738 | — | 1703 | 1669 b | — | 1620 n.r. | — |
| | In $CCl_4$ | 1740 | — | 1710 | 1669 | — | 1620 n.r. | — |
| | In $CCl_4$ + pyridine* | 1737 | — | 1708 | 1668 | — | 1620 n.r. | — |
| Chlorophyll | Solid layer | 1737 b | — | 1700 | | 1665 + | 1611 | — |
| | In $CCl_4$ | 1740 | — | 1701 | | 1665 | 1611 | — |
| | In $CCl_4$ + pyridine* | 1739 + | — | 1688 + | 1670 n.r. | — | — | 1596 |
| Methylchlorophyllide | Solid layer | 1734 | — | 1695 | | 1665 + | 1611 | — |
| | In $CCl_4$ | 1737 | — | 1700 | | 1663 | 1611 | — |
| | In $CCl_4$ + pyridine* | 1735 + | — | 1693 + | 1670 n.r. | — | — | 1595 |
| Zn-pheophytin | Solid layer | 1738 | — | 1707 | 1670 n.r. | — | 1615 | — |
| | In $CCl_4$ | 1740 | — | 1707 | 1672 | 1642 weak | 1616 | — |
| | In $CCl_4$ + pyridine* | 1737 b | — | 1707 | 1668 | | 1608 — | 1595 |
| Cu-pheophytin | Solid layer | 1736 | — | 1712 n.r. | 1671 | 1642 | 1601 | — |
| | In $CCl_4$ | 1740 | — | 1712 n.r. | 1671 | 1642 | 1601 | — |
| | In $CCl_4$ + pyridine* | 1740 n.r. | 1730 | 1710 n.r. | 1669 | 1638 | — | 1596 |
| Ni-pheophytin | Solid layer | 1740 n.r. | 1730 | 1710 n.r. | 1670 | 1650 n.r. | 1615 | — |
| | In $CCl_4$ | 1740 | — | 1710 n.r. | 1670 | 1650 n.r. | 1615 | — |
| | In $CCl_4$ + pyridine* | 1740 n.r. | 1730 | 1710 n.r. | 1667 | — | 1615 — | 1596 |

*The pyridine concentration in the $CCl_4$ mixture was about 10% by volume.

Notation: n.r. – the band was found in coincidence with another band and was not resolved; in comparison with the corresponding band in a solution of $CCl_4$; b – the band was broadened, (+) – the intensity of the band was increased, (–) – the intensity of the band was decreased.

## THE INTERACTION OF CHLOROPHYLL AND ITS ANALOGUES WITH PYRIDINE

The infrared spectra of solutions of chlorophyll a and pheophytin a in pyridine have been investigated previously by Holt and Jacobs.[9] It was discovered by them that while the spectra of solutions of pheophytin in $CCl_4$ and in pyridine are very similar, the spectrum of a solution of chlorophyll in pyridine is markedly different from its spectrum in a neutral solvent ($CCl_4$, $CS_2$). Inasmuch as a new intense absorption band in the region of the characteristic frequency of the OH bonds (at 3400 $cm^{-1}$) was discovered in the spectrum of the pyridine solution of chlorophyll, Holt and Jacobs drew the conclusion that chlorophyll in pyridine is found chiefly in the enolic form.

Figure 4 shows the absorption spectra of solutions of chlorophyll and its analogues in $CCl_4$ and in mixtures of pyridine + $CCl_4$ (where the pyridine concentration in the mixture is about 10% by volume). Comparison shows that the spectrum of the solution of pheophytin in a pyridine + $CCl_4$ mixture is practically identical to the spectrum of its solution in $CCl_4$. The spectra of $CCl_4$ solutions of metal-containing pigments change markedly upon addition of pyridine to the solution. Let us now consider these changes in the spectrum in the region of double bond vibrations (Fig. 4 and Table).

The addition of pyriding to a solution of chlorophyll in $CCl_4$ leads to the following changes. A new absorption band appears at 1596 $cm^{-1}$ while the bands at 1611 and 1665 $cm^{-1}$ vanish. In place of the band at 1665 $cm^{-1}$ there remains a weak band at 1670 $cm^{-1}$ which apparently can be related to the absorption of the C=O aldehyde group of chlorophyll b.[9] Moreover there is an increase in intensity of the absorption bands at 1701 and 1740 $cm^{-1}$, the first of which corresponds to the vibrations of the C=O keto group of the cyclopentanone ring and the second to the vibrations of the ether groups C=O at atoms $C_7$ and $C_{10}$.[8,9]

The increase in intensity of the absorption lines of the keto group of the cyclopentanone ring does not agree with Holt and Jacobs' conclusion that chlorophyll in pyridine is found chiefly in the enolic form. For clarification of the question of the tautomeric transformation of chlorophyll, the absorption band at 1611 $cm^{-1}$ is interesting.

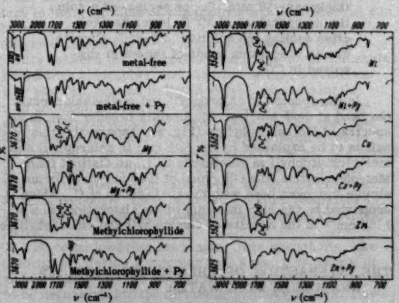


Fig. 4. Absorption spectra of chlorophyll and its analogues in solutions of $CCl_4$ and mixtures of $CCl_4$ and pyridine. Pigment concentration about 0.1 mole/liter. Concentration of pyridine in mixtures—about 10% by volume. Thickness of the absorbing layer—0.1 mm.

Holt and Jacobs ascribe to this band the vibrations of the C=C conjugated bonds of the porphyrin ring of the chlorophyll molecule. Such an interpretation seems to us to have little basis since this band disappears in the presence of pyridine and it is difficult to suppose that the vibrations of the C=C conjugated bonds of the porphyrin ring would be disrupted in the presence of pyridine to the extent that the corresponding absorption line would disappear. Furthermore, Falk and Willis,[13] while measuring the infrared spectra of over twenty porphyrins, showed that the absorption band at about 1611 $cm^{-1}$ is observed only in those porphyrins whose molecules have a cyclopentanone ring. Falk and Willis ascribe the 1611 $cm^{-1}$ band to vibrations of a C=C vinyl group. However, the absence of vinyl and semi-isolated C=C groups in the structure of bacteriochlorophyll, which according to Holt and Jacobs' data also has an absorption band at 1611 $cm^{-1}$, shows that this band cannot be ascribed to vinyl or to semi-isolated C=C bonds. Inasmuch as the band at 1611 $cm^{-1}$ is found in the region of the characteristic frequency of the C=C bonds it is possible to assume that this band corresponds to the C=C bond of the cyclopentanone ring in its enolic form. If such a supposition is true then the absence of the absorption band at 1611 $cm^{-1}$ and the increase in intensity of the band of the keto group of the cyclopentanone ring of the chlorophyll molecule in the presence of pyridine show that pyridine stabilizes the keto form of chlorophyll, and not the enolic form, as is assumed by Holt and Jacobs. The 3400 $cm^{-1}$ absorption band discovered by these investigators in the spectrum of a pyridine solution of chlorophyll, and ascribed by them to the vibrations of the OH groups of the enolic form of the pigment, apparently belongs to traces of water which pyridine can rapidly absorb from the atmosphere. When the spectrum of the pyridine solution of chlorophyll was measured by us under vacuum conditions using carefully dried pyridine and chlorophyll, this band was not found.

The absorption band at 1665 $cm^{-1}$, according to Holt and Jacobs' interpretation,[9] corresponds to the vibrations of the C=O group at atom $C_{10}$, being disturbed by the intramolecular hydrogen bonds with the OH group of the enol form of the cyclopentanone ring (Fig. 2). Such an interpretation is in complete agreement with the conclusions about the stabilization of the chlorophyll keto form in the presence of pyridine. Since in the presence of pyridine there exists for all practical purposes only the keto form, the band at 1665 $cm^{-1}$ must be absent and this absence is actually noted. The disappearance of the absorption band at 1665 $cm^{-1}$ upon formation of molecular complexes of chlorophyll-pyridine is accompanied by an increase in the intensity of the 1740 $cm^{-1}$ band, corresponding to vibrations of a C=O group not bound by hydrogen bonds.

Judging from the change in intensity of the absorption band of the keto group of the cyclopentanone ring upon formation of a chlorophyll-pyridine complex, 20-30% of the chlorophyll molecules in the $CCl_4$ solution are found in enol form. This estimate, which is a good one under the assumption that the intensity of the absorption bands of the keto group changes only at the expense of a change in the quantity of the absorbing group, is supported by the fact that the intensity of the band at 1740 $cm^{-1}$ upon formation of a chlorophyll-pyridine complex increases only 10-15%, i.e., a factor of two less than the intensity of the keto group band. This result is to be expected because the 1740 $cm^{-1}$ band corresponds to the vibrations of two types of carbonylic groups: ether C=O groups at atom $C_7$ which the tautomeric transformations of chlorophyll do not effect, and ether groups at $C_{10}$, some of which are disturbed by hydrogen bonds with the enolic OH groups and give a band at 1665 $cm^{-1}$.[8,9]

The new absorption band at 1596 $cm^{-1}$, observed in the spectra of the solution of chlorophyll in the mixture of pyridine + $CCl_4$, belongs to the absorption of the pyridine molecule forming the complex with the chlorophyll molecule. The corresponding band of liquid pyridine is located at 1581 $cm^{-1}$. Confirmation of such an interpretation lies in the following facts. In the first place, the absorption band around 1595–1596 $cm^{-1}$ appears in the presence of pyridine in the spectra of all metal-containing analogues of chlorophyll. (This band does not appear in the spectra of pheophytin in the presence of pyridine.) In the second place, just as when pyridine interacts with chlorophyll, the 1581 $cm^{-1}$ absorption band of pyridine is shifted in the direction of higher frequency upon interaction of pyridine with donor protons; for example, with water[14] or upon interaction with halides of metals, with which the pyridine molecule forms a coordination bond by means of the free electron pair of its own nitrogen atom.[15] The increase in the frequency of the 1581 $cm^{-1}$ absorption band upon reaction with chlorophyll allows us to assume that in this case the reaction is accomplished by means of the free electron pair of the nitrogen atom of pyridine. Moreover, since pyridine, according to spectral data, does not interact with pheophytin but does form a complex with magnesium phthalocyanine,[16] it is possible to draw the conclusion that the pyridine molecule attaches itself first of all to the pigment's central metal molecule, which like the metal atom in halides[15] possesses electronophilic properties. The influence of the pyridine molecule, which is joined to chlorophyll at the metal atom, is distributed over the entire chlorophyll molecule by way of the conjugated bonds and serves to stabilize the keto form of chlorophyll.

The spectrum of the solution of chlorophyll in a mixture of pyridine + $CCl_4$, with the concentrations stated in the captions to Fig. 4, completely coincides (with the exception of the absorption bands of the solvents) with the spectrum of the solution of chlorophyll in pyridine.

The spectral changes of methylchlorophyllide on reaction with pyridine are the same as the spectral changes of chlorophyll (Table and Fig. 4).

The spectra of Met-pheophytins differ from the spectra of chlorophyll and chlorophyllide primarily in that the intensity of the absorption bands corresponding to the vibrations of the ether C=O group at atom $C_{10}$, which are disturbed by the hydrogen bonds with the OH group of the enol form, is weak in comparison with the corresponding bands of chlorophyll and chlorophyllide. Upon contact of the pigment with pyridine this band vanishes in the case of Zn- and Ni-pheophytins and is only a little diminished in the case of Cu-pheophytin. In addition, in the spectra of Cu- and Ni-pheophytins there appears a new absorption band at 1730 $cm^{-1}$ which can be related to the vibrations of the C=O bonds. It is curious that this band is observed in the spectrum of solid films of Ni-pheophytin. On the basis of the data we have it is difficult to offer any explanation of this band.

Let us consider now the spectrum region of the stretching vibrations of the OH groups (3100–3800 $cm^{-1}$). In this region, the spectra of dilute solutions of chlorophyll and its analogues in $CCl_4$ were measured (concentrations were on the order of $10^{-3}$ moles/liter, layer thickness was 10 mm). The spectra of these solutions with water impurities is displayed in Fig. 5. In the absence of water, the spectra agree with the upper series of spectrograms shown in this drawing if we do not consider the absorption lines of the water dissolved in the $CCl_4$ and those of the water linked to the chlorophyll (cf. below). In the spectra of solutions of pheophytin and Met-pheophytins in $CCl_4$ both in the dilute (Fig. 5) and in the concentrated (Fig. 4) solutions a weak narrow absorption band at 3525 $cm^{-1}$ is observed. Since this band is shifted up to 2600 $cm^{-1}$ upon addition of heavy water to the solution there is no doubt that it belongs to the vibrations of some OH groups. It is unlikely that this band corresponds to absorption by the water molecule joined to the pibment, since upon addition to the pigment solution of a mixture of $H_2O + D_2O$ (in a ratio of 1:1) the position of this band in the spectrum does not change. For water molecules under these conditions isotopic shift would be expected. Furthermore, the intensity of the band at 3525 $cm^{-1}$ does not decrease upon recording the spectrum in a vacuum using dried $CCl_4$ and pigment (the experiment was performed with a dilute solution of Ni-pheophytin). We assume that the band at 3525 $cm^{-1}$ corresponds to the vibration of the OH groups of the enol form of the pigment. This supposition is supported by the fact that the intensity of the 3525 $cm^{-1}$ band decreases upon addition of pyridine to the solutions, which helps to stabilize the keto form of the pigment. The OH band of the enol form of pheophytin upon addition of pyridine remains practically unchanged. This result is in complete agreement with the fact that in the region of 700–1800 $cm^{-1}$, upon contact of pheophytin with pyridine no changes in the spectrum of the pigment are observed, which shows that pyridine does not influence the tautomeric transformation of phoephytin.

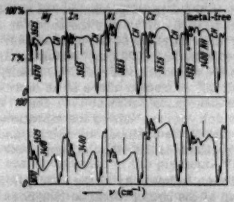


Fig. 5. Absorption spectra of chlorophyll and its analogues in $CCl_4$ in the presence of water (one drop per 6 ml solution). Pigment concentration—5–10 mg per 6 ml. Layer thickness—10 mm. Upper series—at a solution temperature of 30°C, lower series—after cooling the solution to 3–8°C. Circles denote absorption bands of the water dissolved in $CCl_4$.

In the spectra of chlorophyll and methylchlorophyll the band at 3525 $cm^{-1}$ is significantly broader than in the spectra of Met-pheophytins (Fig. 5). Apparently, this result is to be explained by the fact that in chlorophyll and methylchlorophyll in solution in $CCl_4$, as distinct from Met-pheophytins, the OH group of the enol form forms a simple hydrogen bond with the C=O group at $C_{10}$ which is supported by the high intensity of the absorption band at 1665 $cm^{-1}$ in the spectra of chlorophyll and chlorophyllide.

## THE INTERACTION OF CHLOROPHYLL AND ITS ANALOGUES WITH WATER

In the spectra of solid films of chlorophyll and its metal-containing analogues there is a broad absorption band at 3400 $cm^{-1}$, located in the region of the characteristic frequency of vibration of OH bonds, which have been disturbed by hydrogen bonds (Fig. 3). Such an absorption band is observed in the spectra of concentrated solutions of metal-containing pigments (Fig. 4). Careful measure-

ments show that this band is asymmetrical and, further, that its profile is similar to the profile of the absorption band of liquid water. The asymmetry of the band at 3400 $cm^{-1}$ reflects the presence in its structure of at least two components: the more intense component is the high frequency one and the less intense the low frequency one. The presence of a structure similar to the structure of the absorption band of liquid water enables us to interpret the 3400 $cm^{-1}$ band as the absorption band of water molecules linked to chlorophyll.

The absorption band at 3400 $cm^{-1}$ in the spectra of dilute solutions of pigments in $CCl_4$ is less intense than in spectra of solid films and concentrated solutions. In the spectra of dilute Cu- and Ni- pheophytin samples this band is almost completely absent (Fig. 5). This fact is apparently explained by the large interaction energy of the pigment molecule with the attached water molecules. This energy, judging by the intensity of the 3400 $cm^{-1}$ band, successively decreases for chlorophyll, Zn-, Ni-, and Cu-pheophytin. Lowering the temperature of the solution leads to an increase in the quantity of water molecules reacting with the pigment. Thus, if water is added to the pigment and the solution is cooled to 3-8°C, the intensity of the 3400 $cm^{-1}$ bands increases sharply for all pigments (Fig. 5). At this temperature the absorption band of the attached water molecules is found even in the spectra of solutions of metal free pheophytin (at 3350 $cm^{-1}$), for which at room temperature it can be observed neither in the spectra of solid films nor in the spectra of solutions. Upon raising the temperature of the solution to room temperature the intensity of the 3400 $cm^{-1}$ band again decreases.

Addition of heavy water to the solution of pigment in $CCl_4$ leads to a decrease in the intensity of the 3400 $cm^{-1}$ band and the formation of an absorption band corresponding to the region of vibration of the OD bonds.

The absorption band of water linked to chlorophyll has the profile typical of an absorption band of a hydroxyl-containing molecule which has the hydrogen atom of the hydroxyl forming an OH ... X type hydrogen bond. This enables us to assume that upon interaction with chlorophyll and its analogues the water molecule attaches itself by means of its own hydrogen atoms, forming a hydrogen bond with some sort of electronegative center. Such centers in the molecules of chlorophyll and its analogues can be either the nitrogen atoms of the pyrrole nuclei or the oxygen atoms of the C=O groups. Because of the similarity between the absorption band of the water molecule joined with chlorophyll and the band of liquid water we may say that, just as in liquid water, upon interaction with chlorophyll both hydrogen atoms of a water molecule are connected by hydrogen bonds. In this case the place where the water molecules attach themselves is most likely at the two nitrogen atoms of the pyrrole nuclei of the pigment. Such a supposition is supported by the fact that the absorption band of the water molecule which is simultaneously linked with two pyridine molecules in a $CCl_4$ solution has an absorption band like that of liquid water.[14]

Since on lowering the temperature pheophytin, like chlorophyll, forms a complex with a water molecule, it should follow that the central metal atom does not appear to be necessary for the formation of this complex. However, it is evident that the metal atom, particularly magnesium, activates the pigment molecule with respect to the formation of complexes with water, as is apparent in the stability of the complexes formed. This stability can be estimated on the basis of the intensity of the absorption bands of the attached water.

The 3400 $cm^{-1}$ absorption band of water molecules attached to the pigment in a $CCl_4$ solution is changed by addition of pyridine to the solution. The high frequency component of this band decreases, and consequently the low frequency component stands out more distinctly. The entire band is somewhat broadened and its center of weight is shifted in the direction of lower frequency. This shift attests the strong protonization of the H atoms of the water molecule attached to the pigment in the presence of pyridine.

In conclusion, we compare the chlorophyll and analogue spectra obtained from solid films of pigment and from both concentrated and dilute $CCl_4$ solutions. The spectra of the solid films and concentrated solutions (Figs. 3, 4, and Table) do not differ significantly from each other in the 700-3100 $cm^{-1}$ region. Some differences can be observed in the 3100-3800 $cm^{-1}$ region. For solutions of Met-pheophytins in $CCl_4$ in this region a band appears at 3525 $cm^{-1}$ which is absent from the spectra of the solid films. The intensity of this band corresponding to the vibration of OH groups of the enol forms of the pigment increases in proportion to the dilution of the solution. This fact which supports the interpretation of the 3525 $cm^{-1}$ band bears out that in the solid state the OH groups of the enol form are disturbed by the intermolecular interactions, as a consequence of which the narrow band at 3525 $cm^{-1}$ is broadened and shifted in the direction of lower frequency. As the solution is diluted this interaction diminishes. Moreover, in the case of chlorophyll and methylchlorophyllide it is possible to observe a weak absorption band at 3670 $cm^{-1}$. Upon addition of heavy water to the solution, this band remains unchanged.

REFERENCES

1. V. B. Evstigneev, V. A. Gavrilova, and A. A. Krasnovskii. Doklady Akad. Nauk SSSR 66, 1133 (1949); Ibid. 70, 261 (1950).
2. A. N. Terenin. "Fotokhimiya khlorofilla i fotosintez." (Photochemistry of Chlorophyll and Photosynthesis), Izd. Akad. Nauk SSSR, Moscow, 1951.
3. R. Livingston, W. F. Watson, and J. F. McCardle. J. Am. Chem. Soc. 71, 1542 (1949).
4. R. Livingston and S. Weil. Nature, 170, 750 (1952).
5. R. S. Becker and M. Kasha. "The Luminescence of Biological Systems," Washington, 1955.
6. J. Franck. Proc. Natl. Acad. Sci. 44, 941 (1958).
7. R. Stair and W. W. Coblentz. J. Research Natl. Bur. Standards 11, 703 (1933).
8. J. W. Weigl and R. Livingston. J. Am. Chem. Soc. 75, 2173 (1953).
9. A. S. Holt and E. E. Jacobs. Plant Physiol. 30, 553 (1955).
10. J. Zalesky. Z. Physiol. Chem. 43, 11 (1904).
11. E. Rabinovich. "Fotosintez," Vol. I. (Photosynthesis), Izd. Inostrannoi Lit., Moscow, 1951.
12. A. A. Krasnovskii. Zhur. Fiz. Khim 30, 968 (1956).
13. J. E. Falk and J. B. Willis. Australian J. Sci. Res. A4, 579 (1951).
14. A. N. Sidorov. Opt. i Spektr. 8, 51 (1960).
15. V. N. Filomonov, D. S. Bystrov, and A. N. Terenin. Opt. i Spektr. 3, 480 (1957).
16. A. N. Sidorov and A. N. Terenin. Doklady Akad. Nauk SSSR 104, 575 (1955);
A. N. Terenin and A. N. Sidorov. Proc. Colloquium Spectroscopicum Intern. VI, London, 1957, p. 573.

# STUDY OF INFRARED ABSORPTION SPECTRA OF DICYCLIC HYDROCARBONS

S. V. Markova, P. A. Bazhulin, A. F. Plate, V. I. Stanko

Received 16 July 1959

The absorption spectra of five- and six-membered dicyclic hydrocarbons were investigated in the region from 3 to 24 $\mu$. The additive properties of the absorption coefficients of the most intense lines of the spectra of these compounds were studied.

The absorption spectra in the infrared region are widely used at the present time to solve various scientific and practical problems. In addition to the frequencies, the absorption coefficients of the bands are also of importance. These values can provide a source of information about the molecular structure. A quantitative molecular spectral analysis is also based on measurements of absorption coefficients.

The present work is dedicated to a study of the additive properties of the absorption coefficients for certain of the most intense characteristic bands in the spectra of dicyclic compounds. The investigated hydrocarbons contain two five-membered or two six-membered rings in the molecule. The choice of molecules studied allowed us to observe the dependence of the absorption coefficients of the bands on the number of absorbing groups located both in the ring and in the connective chain. The majority of the compounds investigated were first synthesized in the catalytic synthesis laboratory of the N. D. Zelinsky Institute of Organic Chemistry and have been described by Stanko and Plate.[1] The data obtained in this work supplement the results obtained from the Raman spectra of these same substances[2,3] and have much importance in the theory of the intensity of infrared spectra.

## EXPERIMENTAL METHOD

All measurements were carried out on a double-beam spectrometer which consisted of a standard monochromator IKS-11 and an automatic attachment which had been developed in our laboratory.[4] The resolution of the equipment can be characterized by the following parameters: for a time constant of the equipment of about one second, and for noise with a mean quadratic value of about 2% on all scales, the slit width in the 10 $\mu$ region was 0.12 mm (~2 $cm^{-1}$ on the spectrum). Special cells which had been developed and used in our laboratory long ago were used for the work. In the region of 3 $\mu$ the substances were examined in solution ($CCl_4$) in which the volume concentration was 1%. In the remaining regions of the spectrum the pure compounds were studied without the use of a solvent. The path length was selected from a calculation of the minimum error in the value of the absorption coefficient (from 0.005 to 0.25 mm in different regions of the spectrum). The cell thickness was measured from the interference pattern obtained during recording of the signal from the empty cell. The measurement error of cell width was usually 3-5%, but in the most unfavorable cases of very thin cells ~10%. In order to avoid any possible difference in the cell path length on clamping, the recording of each line was carried out 3 or 4 times, and each time the cell was recharged and reclamped.

On each spectrogram, in addition to the absorption band of the substance, lines of 100% transmission and lines of 100% absorption were indicated. In order to eliminate the influence of scattered light and also in order to compute the reflection at the liquid NaCl boundary, a cell with the substance being investigated was also placed in the comparison beam. The width of this cell was significantly smaller than that which was located in the sample beam. In order to take into account the amount of scattered light in the long wavelength region of the spectrum the line of 100% absorption for $\lambda > 10$ $\mu$ was recorded using a plate of $CaF_2$, and the absorption band using a filter (ground plate of KBr). In other cases, special recordings of the line with a narrow slit under conditions possibly closer to the optimum were carried out in order to study the additive properties of certain characteristic frequencies.[5] It was also shown possible to exclude the effect of the slits.

The spectrograms obtained were analyzed in the following manner. First a correction for slit width was introduced. Since the slit width used for recording the different lines was about 0.25 of the observed line widths, then the corresponding correction was introduced graphically (by the method of Rayleigh, improved by Rautian[6]). The final value of the integral coefficient of absorption was obtained from the equation

$$\int_{\nu_1}^{\nu_2} \ln \frac{I_0}{I}\, d\nu = cdK_{\infty}.$$

This integral was taken within certain finite limits of integration in the frequency range from $\nu_1$ to $\nu_2$. The theoretical quantity $K_{\infty}$ requires infinite limits of integration. In those cases when the investigated bands were not overlapped very strongly and it was possible to separate them, the requisite corrections were introduced for the wings. The method of introducing such corrections, which take into account the form of the bands and real limits of integration, was developed and described by Sushchinsky.[7] The mean error in the measurement of absorption coefficients was ~8%.

In Table 1 the frequencies of all the compounds we studied are shown. The accuracy of measurements of frequencies in the region of 3000 $cm^{-1}$ was 2 $cm^{-1}$, in the 1400 $cm^{-1}$ region, 2-3 $cm^{-1}$, and in the 800 $cm^{-1}$ region and below, 1 $cm^{-1}$. Also presented in Table 1 are the literature data for five- and six-membered naphthalenes[7-11] and paraffins.[12,13] Besides these, the investigation of the dependence of the absorption coefficients on the length of the connective chain allowed us, in a number of cases, to attribute frequencies to the vibrations of different structural groups in the molecule.

For illustrative purposes, in Fig. 1 are presented the spectrum of dicyclohexyl in the region from 700 to to 1500 $cm^{-1}$. Data taken from the literature were used for the assignment of frequencies to the five- and six-membered naphthalenes,[7-11] and to paraffins.[12,13] The investigation of the dependence of the absorption coefficients on length of the connective chain also allowed us to assign frequencies more precisely to vibrations of different structural groups in the molecule.

Table 1*

| | | | | | | | | | |
|---|---|---|---|---|---|---|---|---|---|
| | | $-CH_2-$ | | $-(CH_2)_3-$ | | $-(CH_2)_4-$ | | $-(CH_2)_5-$ | |
| ν | I | ν | I | ν | I | ν | I | ν | I |
| | | 449 | v.w. | 439 | v.w. | 448 | v.w. | | |
| 497 | w. | 497 | v.w. | 465 | w. | 488 | v.w. | | |
| 573 | av. | 567 | s. | 486 | v.w. | 553 | av. | 557 | av. |
| 596 | av. | 618 | v.w. | 544 | s. | 650 | v.w. | 653 | v.w. |
| | | | | 563 | av. | | | | |
| 634 | v.w. | | | 657 | v.w. | 736 | w. | 728 | av. |
| | | | | 757 | v.w. | | | 781 | v.w. |
| 781 | v.w. | 781 | v.w. | 781 | v.w. | | | 779 | v.w. |
| 828 | v.w. | 837 | v.w. | | | 830 | v.w. | 844 | v.w. |
| | | | | 850 | v.w. | | | | |
| 895 | av. | 893 | av. | 895 | av. | 895 | av. | 896 | av. |
| 928 | av. | 937 | w. | 937 | av. | 924 | av. | 940 | av. |
| | | 975 | w. | | | | | | |
| | | | | 1014 | v.w. | 1005 | w. | | |
| 1029 | w. | 1028 | v.w. | | | | | 1022 | v.w. |
| 1109 | v.w. | | | | | | | | |
| 1186 | w. | 1185 | w. | | | | | | |
| | | | | 1189 | v.w. | | | | |
| | | | | 1233 | v.w. | 1235 | v.w. | 1219 | v.w. |
| | | 1236 | v.w. | | | | | | |
| 1260 | w. | 1271 | av. | | | | | 1263 | v.w. |
| 1290 | av. | | | | | 1306 | w. | 1307 | av. |
| | | 1309 | av. | 1312 | av. | 1318 | w. | | |
| 1331 | av. | 1337 | av. | 1328 | w. | 1342 | av. | | |
| 1365 | w. | 1350 | w. | 1356 | w. | 1350 | av. | 1347 | av. |
| | | 1378 | v.w. | | | 1371 | w. | 1374 | w. |
| 1448 | v.s. | 1445 | v.s. | 1447 | v.s. | 1446 | v.s. | 1448 | v.s. |
| 1470 | av. | 1456 | s. | 1455 | s. | 1455 | v.s. | 1458 | v.s. |
| | | 1468 | av. | 1469 | av. | 1468 | av. | 1468 | av. |
| 2867 | v.s. | 2863 | v.s. | 2863 | v.s. | 2865 | v.s. | 2860 | v.s. |
| 2911 | s. | 2918 | s. | 2911 | s. | 2918 | s. | 2919 | s. |
| 2953 | v.s. | 2948 | v.s. | 2944 | v.s. | 2949 | v.s. | 2944 | v.s. |

| | | | | | | | | | |
|---|---|---|---|---|---|---|---|---|---|
| $-(CH_2)_6-$ | | $-\underset{CH_3}{\underset{\vert}{C}}H-$ | | $-\underset{CH_3}{\underset{\vert}{C}}H-CH_2-$ | | | | $-CH_2-$ | |
| ν | I | ν | I | ν | I | ν | I | ν | I |
| 440 | v.w. | | | 443 | w. | 431 | av. | | |
| | | 513 | av. | 485 | v.w. | | | | |
| 559 | av. | 566 | w. | 506 | w. | | | 444 | v.w. |
| 654 | v.w. | 613 | v.w. | 549 | av. | 458 | av. | 461 | av. |
| 724 | av. | | | 639 | v.w. | | | | |
| 755 | v.w. | | | | | 514 | s. | 551 | av. |
| 771 | v.w. | 774 | w. | 775 | v.w. | 600 | s. | 578 | s. |
| 816 | v.w. | 818 | v.w. | 829 | v.w. | 622 | av. | 611 | v.w. |
| 844 | v.w. | 844 | v.w. | | | 656 | v.w. | | |
| | | 856 | av. | 860 | v.w. | 767 | v.w. | 767 | v.w. |
| 895 | av. | 886 | s. | 894 | av. | 787 | v.w. | 787 | v.w. |
| 935 | av. | 907 | av. | | | 799 | v.w. | 821 | v.w. |
| | | 940 | s. | 940 | av. | 845 | s. | 845 | av. |
| | | 976 | av. | 970 | v.w. | 862 | w. | | |
| | | | | | | 872 | w. | 874 | w. |
| | | | | | | 882 | av. | 884 | av. |
| 1025 | v.w. | 1035 | av. | 1028 | v.w. | 888 | av. | 889 | av. |
| | | | | | | 896 | av. | | |
| | | | | | | 917 | v.w. | 910 | w. |
| | | | | | | 930 | v.w. | 930 | av. |
| | | | | | | 956 | w. | 954 | v.w. |
| | | 1136 | v.w. | 1131 | w. | 994 | av. | 975 | av. |
| | | | | | | 998 | av. | | |
| | | 1176 | av. | 1174 | av. | 1028 | w. | | |
| | | | | | | 1030 | w. | 1031 | w. |
| | | | | | | 1042 | v.w. | | |
| 1230 | v.w. | | | 1241 | v.w. | | | 1070 | w. |
| | | | | | | 1106 | v.w. | 1105 | w. |
| | | 1275 | w. | | | 1138 | v.w. | 1139 | w. |
| 1304 | av | 1301 | av. | 1306 | w. | 1171 | w. | 1171 | w. |
| | | 1321 | av. | 1327 | w. | 1206 | w. | 1210 | w. |
| | | | | | | | | 1237 | w. |
| 1343 | w. | 1353 | av. | 1350 | av. | 1253 | av. | | |
| 1371 | w. | 1385 | v.s. | 1385 | s. | 1266 | av. | 1260 | av. |
| | | | | | | 1281 | w. | 1277 | av. |
| | | | | | | 1290 | w. | 1295 | v.w. |
| | | | | | | | | 1300 | v.w. |
| | | | | | | 1307 | w. | 1336 | av. |
| | | | | | | 1348 | av. | 1350 | av. |
| | | | | | | 1365 | w. | | |
| 1448 | v.s. | 1443 | v.s. | 1446 | v.s. | 1442 | v.s. | 1444 | v.s. |
| 1461 | v.s. | 1455 | v.s. | 1455 | v.s. | 1457 | s. | 1457 | s. |
| 1476 | s. | 1470 | av. | 1470 | s. | | | | |
| 2861 | v.s. | 2867 | v.s. | 2869 | v.s. | 2851 | v.s. | 2850 | v.s. |
| 2924 | v.s. | 2913 | s. | 2913 | s. | 2904 | s. | 2905 | s. |
| 2946 | v.s. | 2949 | v.s. | 2950 | v.s. | 2923 | v.s. | 2923 | v.s. |

| | | | | | | | | | |
|---|---|---|---|---|---|---|---|---|---|
| | | $-CH_2-$ | | $-(CH_2)_4-$ | | | | | |
| ν | I | ν | I | ν | I | ν | I | ν | I |
| | | | | | | | | | |
| | | 444 | v.w. | 444 | v.w. | | | | |
| 458 | av. | 461 | av. | 473 | av. | | | | |
| | | | | 497 | w. | | | | |
| 514 | s. | 551 | av. | 533 | v.w. | | | | |
| 600 | s. | 578 | s. | 549 | s. | | | | |
| 622 | av. | 611 | v.w. | 584 | w. | | | | |
| 656 | v.w. | | | 612 | w. | | | | |
| 767 | v.w. | 767 | v.w. | 741 | w. | | | | |
| 787 | v.w. | 787 | v.w. | 767 | w. | | | | |
| 799 | v.w. | 821 | v.w. | 811 | v.w. | | | | |
| 845 | s. | 845 | av. | 841 | av. | | | | |
| 862 | w. | | | | | | | | |
| 872 | w. | 874 | w. | | | | | | |
| 882 | av. | 884 | av. | | | | | | |
| 888 | av. | 889 | av. | 889 | s. | | | | |
| 896 | av. | | | | | | | | |
| 917 | v.w. | 910 | w. | | | | | | |
| 930 | v.w. | 930 | av. | | | | | | |
| 956 | w. | 954 | v.w. | 962 | av. | | | | |
| 994 | av. | 975 | av. | | | | | | |
| 998 | av. | | | 992 | v.w. | | | | |
| 1028 | w. | | | | | | | | |
| 1030 | w. | 1031 | w. | 1030 | w. | | | | |
| 1042 | v.w. | | | | | | | | |
| | | 1070 | w. | 1080 | v.w. | | | | |
| 1106 | v.w. | 1105 | w. | | | | | | |
| 1138 | v.w. | 1139 | w. | | | | | | |
| 1171 | w. | 1171 | w. | 1190 | v.w. | | | | |
| 1206 | w. | 1210 | w. | 1215 | v.w. | | | | |
| | | 1237 | w. | | | | | | |
| 1253 | av. | | | 1257 | av. | | | | |
| 1266 | av. | 1260 | av. | 1265 | av. | | | | |
| 1281 | w. | 1277 | av. | 1272 | av. | | | | |
| 1290 | w. | 1295 | v.w. | | | | | | |
| | | 1300 | v.w. | | | | | | |
| 1307 | w. | 1336 | av. | | | | | | |
| 1348 | av. | 1350 | av. | 1345 | av. | | | | |
| 1365 | w. | | | 1360 | w. | | | | |
| 1442 | v.s. | 1444 | v.s. | 1440 | v.s. | | | | |
| 1457 | s. | 1457 | s. | 1455 | s. | | | | |
| 2851 | v.s. | 2850 | v.s. | 2851 | v.s. | | | | |
| 2904 | s. | 2905 | s. | 2907 | s. | | | | |
| 2923 | v.s. | 2923 | v.s. | 2925 | v.s. | | | | |

*Frequencies ν are given in $cm^{-1}$; intensities I are given here in the pentabal scale: v.w.–very weak; w.–weak; av.–average intensity; s–strong v.s.–very strong.

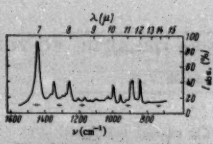


Fig. 1. The absorption spectrum of dicyclohexane in the region from 700 to 1500 $cm^{-1}$ (slit width is shown on the spectrum).

## MEASUREMENTS OF THE ABSORPTION COEFFICIENTS

For certain bands the dependence of the integral absorption coefficient and of the coefficient of absorption at the maximum on the number of absorbing groups in the molecule was studied.

The band at ~730 $cm^{-1}$ was observed only for substances containing $CH_2$ groups in the connective chain. Its frequency diminished monotonic with an increase of chain length from 757 $cm^{-1}$ (for a molecule with two $CH_2$ groups) to 726 $cm^{-1}$ (for a molecule with five such groups). This procedure agrees well with the behavior of the frequency of the same bands for n-paraffins.[14]

In Table 2 the absorption coefficients of the band at ~730 $cm^{-1}$ for five-membered dicyclic hydrocarbons are presented.

Table 2

| Substance | ν (cm⁻¹) | $K_0 \cdot 10^{-4}$ ($cm^2$/mole) | $K_m \cdot 10^{-4}$ (cm/mole) |
|---|---|---|---|
| 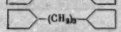 | 757 | 0.8 | 24 |
| 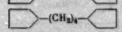 | 737 | 1.5 | 31 |
| 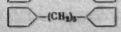 | 729 | 2.0 | 38 |
| 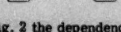 | 726 | 2.8 | 53 |

In Fig. 2 the dependence of the integral absorption coefficient on the number of paraffin $CH_2$ groups in the molecule is shown. Here also the corresponding coefficients for mono-substituted five-membered naphthenes and n-paraffins are presented. As is seen from the figure, the value of the absorption coefficient is directly proportional to the number of absorbing groups. Also, it is possible to consider that the numerical values of the absorption coefficients for all three types of compounds are approximately identical. The coefficients of absorption at the maximum show the same dependence on the number of absorbing groups.

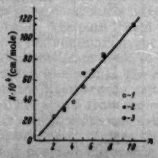


Fig. 2. The dependence of integral absorption coefficient of the band ~730 $cm^{-1}$ of various compounds on the number of linear $CH_2$ groups in the molecule (n). 1—dicyclanes, 2—mono-substituted, five-membered naphthalenes, 3—n-paraffins.

We compared our results with literature data for the absorption coefficients of the bands at ~730 $cm^{-1}$ in paraffins.[15–17] For comparison we selected n-nonane and n-heptane. The results which are presented in Table 3 are computed on the basis of a single $CH_2$ group.

Table 3

| Characteristics | Substance | | | | | | |
|---|---|---|---|---|---|---|---|
| | n-nonane | | | n-heptane | | | |
| | data, ref. 15 | data, ref. 16 | our data | data, ref. 17 | data, ref. 15 | data, ref. 16 | our data |
| $K_0 \cdot 10^{-4}$ ($cm^2$/mole) | 0.6 | 0.8 | 0.54 | 0.64 | 0.6 | 0.6 | 0.61 |
| $K_m \cdot 10^{-4}$ (cm/mole) | 12.2 | — | 12.2 | — | 12.2 | — | 13.0 |

As is seen from the tables, good agreement was observed of our data with those taken from the literature (for which, it should be noted, the investigations were performed on equipment of different makes and with different characteristics). It would seem apparent that the calculation of apparatus distortions of the equipment used and the introduction of corresponding corrections makes it possible to use the numerical data obtained in other laboratories.

Bands in the 1450 $cm^{-1}$ region are caused by $\alpha$-vibrations of the $CH_2$ groups located in the ring and in the connective chain. For five-membered dicyclanes they consist of three components which overlap one another. In Table 4 the results of measurements of absorption coefficients at the maximum are presented for the two most intense components.

Table 4

| Substance | ν(cm⁻¹) | $K_0 \cdot 10^{-4}$ ($cm^2$/mole) | ν(cm⁻¹) | $K_m \cdot 10^{-4}$ (cm/mole) |
|---|---|---|---|---|
| | 1448 | 8.3 | | |
| 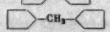 | 1445 | 10 | 1456 | 3.1 |
| 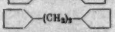 | 1447 | 12 | 1458 | 3.8 |
| 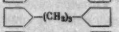 | 1446 | 12 | 1455 | 7.3 |
| 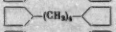 | 1448 | 12 | 1458 | 8.5 |
| 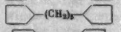 | 1448 | 12 | 1461 | 8.8 |
| 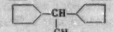 | 1443 | 10 | 1455 | 7.2 |
| 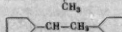 | 1446 | 11 | 1455 | 7.7 |
| 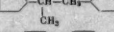 | 1442 | 23 | 1457 | 4.0 |
| | 1444 | 27 | 1457 | 5.1 |
| 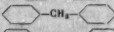 | 1440 | 25 | 1455 | 6.2 |

The absorption coefficient for the band at ~1456 $cm^{-1}$, as is seen from the table, increases almost linearly with the chain length of the molecule. It is possible to consider that the fundamental contribution to this band is introduced by vibrations of the $CH_2$ groups located in the chain. The presence in the molecule of a $CH_2$ group strongly intensifies the absorption coefficient of this band. Conversely, the absorption coefficient of the band at ~1447 $cm^{-1}$ does not depend either on the connective chain length or on any groups it contains. Therefore, we attribute this band to vibrations of the $CH_2$ groups located in the ring.

In Table 4 the corresponding absorption coefficients of the six-membered dicyclanes are also presented. It is

interesting to note that the absorption coefficient of the band at ~1442 $cm^{-1}$ is significantly larger than the corresponding coefficient of the five-membered ones. However, the change of absorption with increase of chain length in a molecule for the six-membered dicyclanes is the same as for the five-membered one.

## VALENCE VIBRATIONS OF C–H IN THE 3000 $cm^{-1}$ REGION

For five-membered dicyclanes in this region there are three bands: ~2947, ~2915, and ~2863 $cm^{-1}$, which are shown in Fig. 3. From this figure it is seen that the high and low frequency bands scarcely change during transition from one compound to another, while the absorption of the middle one strongly intensifies with an increase in the connective chain length of the molecule. The corresponding absorption coefficients, obtained by graphically separating the bands and calculated for the entire molecule, are presented in Table 5.

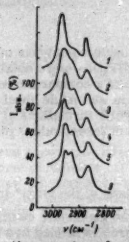


Fig. 3. Absorption spectra of various compounds in the regions ~3000 $cm^{-1}$. Curve 1—dicyclopenane; curve 2—dicyclopentylmethane; curve 3—1, 2-dicyclopentylethane; curve 4—1, 3-dicyclopentylpropane; curve 5—1, 4-dicyclopentylbutane; curve 6—1, 5-dicyclopentylpentane. For convenience of comparison the spectra are shifted vertically.

From Table 5 it is seen that the absorption coefficients of the bands at ~2947 and ~2863 $cm^{-1}$ actually remain constant for a given series of compounds. Therefore it is possible to consider that, in principle, this absorption is explained by vibrations of CH-bonds located in the rings. The band ~2915 $cm^{-1}$, judging from the dependence of its absorption coefficient on chain length, can be attributed to vibrations of CH-bonds of the chain.

Table 5*

| Substance | $\nu$ ($cm^{-1}$) | $K_\nu \cdot 10^{-4}$ ($cm^2$/mole) | $K_{max} \cdot 10^{-4}$ (cm/mole) | $\nu$ ($cm^{-1}$) | $K_\nu \cdot 10^{-4}$ ($cm^2$/mole) | $K_{max} \cdot 10^{-4}$ (cm/mole) | $\nu$ ($cm^{-1}$) | $K_\nu \cdot 10^{-4}$ ($cm^2$/mole) | $K_{max} \cdot 10^{-4}$ (cm/mole) |
|---|---|---|---|---|---|---|---|---|---|
| | 2953 | 120 | 5000 | 2911 | 35 | 2867 | 55 | 2000 | |
| | 2948 | 110 | 4600 | 2918 | 55 | 2863 | 50 | 2200 | |
| | 2944 | 120 | 5500 | 2911 | 70 | 2863 | 55 | 2400 | |
| | 2949 | 110 | 5300 | 2918 | 85 | 2865 | 55 | 2400 | |
| | 2944 | 120 | 5600 | 2919 | 100 | 2850 | 60 | 2600 | |
| | 2946 | 130 | — | 2924 | 120 | 2861 | 70 | — | |

*Because of the strong overlapping of the bands we were not able to evaluate the integral coefficients of absorption of the ~2915 $cm^{-1}$ band, nor of all bands for 1,5-dicyclopentylpentanes.

The established regularity of change in value of the absorption coefficient with the length of the connective chain is also satisfied for the six-membered dicyclanes. It is only necessary to note that all bands of the six-membered dicyclanes are somewhat shifted in the direction of lower frequencies in comparison with corresponding bands of five-membered ones.

The 845 $cm^{-1}$ band of the six-membered dicyclanes in the Raman spectra, as for the six-membered naphthenes, is strong and polarized. In reference 9 it was attributed to vibrations of the substituent radical relative to the ring. Our measurements of frequencies, intensity, and degree of polarization of this line in the Raman spectrum of the six-membered dicyclanes are presented in Table 6. They show similarity of all parameters of the line for dicyclanes and corresponding mono-substituted six-membered naphthenes, in which the value $I_\rho$ increases in proportion to the number of rings in the molecule.

The measurements in the infrared region showed that this frequency is developed sufficiently well in the infrared spectrum. The results of the infrared measurements are presented also in Table 6. From the table it is seen that for dicyclic hydrocarbons in the infrared spectra the integral absorption coefficient at this frequency maintains a constant value. In comparison with the six-membered naphthenes, an almost twofold enhancement of intensity is observed, as in the Raman spectra. It is interesting to notice that both the value of the absorption coefficient in the infrared spectrum and the intensity of this line in the Raman spectrum depend very slightly on the length of the connective chain. Thus, if this line is explained by vibrations of the radical relative to the ring, then a basic role must be played by the C—C bond immediately abutting the ring. For this it is necessary to take into account the existence of an interaction between this bond of the chain and the bonds of the ring.

Table 6

| Substance | Raman* | | | Infrared absorption | | |
|---|---|---|---|---|---|---|
| | $\Delta\nu$ ($cm^{-1}$) | $I_\rho$ | $\rho$ ** | $\nu$ ($cm^{-1}$) | $K_\nu \cdot 10^{-4}$ ($cm^2$/mole) | $K_{max} \cdot 10^{-4}$ (cm/mole) |
| | 847 | 84 | 0.11 | 845 | 6.0 | 31 |
| | 842 | 90 | 0.12 | 845 | 5.5 | 30 |
| | 842 | 78 | 0.15 | 841 | 5.0 | 35 |
| 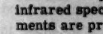 | 844 | 44 | 0.19 | 845 | 2.5 | 15 |

*The data were taken from Ref. 3 and computed for one molecule.
**The amount of depolarization of these lines was measured on apparatus described in ref. 2.

In conclusion it is necessary to note that the obtained experimental results can be also used for the solution of analytical problems. As is seen from Table 1, the frequencies which characterized the individual compounds lie in the region 600–400 $cm^{-1}$.

## REFERENCES

1. V. I. Stanko and A. F. Plate. Izvest. Akad. Nauk SSSR, Ser. Khim. **23**, 124 (1959);
A. F. Plate and V. I. Stanko. Izvest. Akad. Nauk SSSR, Ser. Khim. **22**, 1472 (1958); Doklady Akad. Nauk SSSR **114**, 339 (1957).
2. S. V. Markova, P. A. Bazhulin, V. I. Stanko, and A. F. Plate. Izvest. Akad. Nauk SSSR, Ser. Khim. **23**, (1959).
3. G. V. Peregudov, S. V. Markova, P. A. Bazhulin, A. F. Plate, and E. M. Terenteva. Izvest. Akad. Nauk SSSR, Ser. Khim. **21**, 37 (1957).

4. V. I. Malyshev, M. N. Markov, and A. A. Shubin. Doklady Akad. Nauk SSSR 86, 273 (1952).
5. G. G. Petrash and S. G. Rautian. Proc. Tenth Inter. Conf. on Spectroscopy, 1, 102, 107 (1957).
6. S. G. Rautian. Kand. Diss., Fiz. Inst., Akad. Nauk SSSR Moscow, 1957.
7. M. M. Sushchinsky. Dokt. Diss., Fiz. Inst., Akad. Nauk SSSR, Moscow, 1957.
8. F. A. Miller and R. G. Inskeep. J. Chem. Phys. 18, 1519 (1950);
H. Tschamier and H. Voeter. Monatsh. Chem. 83, 302, 1228 (1952).
9. P. S. Lebedev. Opt. i Spektr. 6, 154, 329 (1959).
10. H. Tschamler. J. Chem. Phys. 22, 1845 (1954).
11. G. A. Aleksandrov. Opt. i Spektr. 5, 128 (1958).
12. C. G. Pimental and H. A. Klemperer. J. Chem. Phys. 23, 376 (1955).
13. H. Voetter and H. Tschamler. Sitzber. Abt. II B162, 134 (1953).
14. S. H. Hastings, A. T. Watson, R. B. Williams, and J. A. Anderson. Anal. Chem. 24, 612 (1952).
15. H. Luther and G. Czewony. Z. physik. Chem. 6, 286 (1956).
16. H. L. McMurry and V. Thornton. Anal. Chem. 24, 318 (1952).
17. R. N. Jones. Spectrochim. Acta 9, 235 (1957).

# INFRARED ABSORPTION SPECTRA OF HYDROXYFLUOROBORIC COMPLEXES OF POTASSIUM AND SODIUM

M. V. Aknmanova and G. E. Kurilchikova

Received 15 July 1959

The infrared absorption spectra (1600-700 $cm^{-1}$) of hydroxyfluoroboric complexes of potassium and sodium—$K_2B_3O_3F_5$, $K_2B_3O_3F_4OH$, $Na_2B_3O_3F_5$, $KBF_3OH$, and $NaBF_3OH$—were obtained. A qualitative interpretation of the spectra was carried out on the basis of a comparison with spectra of boric and fluroboric compounds studied earlier. A conclusion was made about the existence in the complexes $K_2B_3O_3F_5$, $K_2B_3O_3F_4OH$, and $Na_2B_3O_3F_5$ of cyclic formations of the type of a borate ring. The change of the spectra of the complexes with different values of pH of the aqueous solutions was studied.

The hydroxyfluoroboric complexes of potassium and sodium ($K_2B_3O_3F_5$, $K_2B_3O_3F_4OH$, $Na_2B_3O_3F_5$, $KBF_3OH$, and $NaBF_3OH$) are among a number of compounds seldom investigated in spite of the great interest in these compounds in chemistry and geochemistry. The data obtained about the infrared absorption spectra of these compounds have been lacking until the present time and have great importance for the study of their structure and properties.

Riss[1] assumed the presence in complexes $K_2B_3O_3F_5$, $K_2B_3O_3F_4OH$, and $Na_2B_3O_3F_5$ of a borate ring and cited some structural formulas for the anions of these compounds.

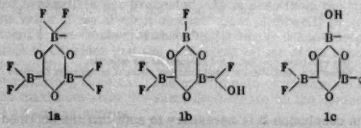

1a 1b 1c

The presence of a six-membered boron-oxygen ring is confirmed by the study of electron diffraction[2] and Raman spectra[3] on a number of substitution products of hydrogen in $H_3B_3O_3$. According to electron diffraction measurements the borate ring has a flat structure with the following geometric parameters: r = 1.39 A* and the B-O-B angle = 112°.

*This same value of r (1.38 A) is found in potassium metaborate $K_3B_3O_6$.[3]

The complexes $K_2B_3O_3F_5$, $K_2B_3O_3F_4OH$, and $Na_2B_3O_3F_5$ are addition compounds of fluoride ions and hydroxyl ions to atoms of boron in the borate ring. It is assumed that the structural units of the crystalline lattice of these complexes are anionic groupings of $(B_3O_3F_5)^{=}$ (1a) or $(B_3O_3F_4OH)^{=}$ (1b and 1c). In the first case all six fluoride ions are not in the plane of the ring;* in the case of substitution of fluoride ions by a hydroxyl, one fluoride ion or hydroxyl ion is in the plane of the ring. The compounds $KBF_3OH$ and $NaBF_3OH$ are related to hydroxytrifluoroborates—salts of the monohydrate of boron trifluoride—and their structure is determined by the anion $(BF_3OH)^{-}$, which in its configuration is like the $BF_4^-$ ion.

*This follows from the geometric configuration of the bonds: an atom of boron is bonded in a given case with two atoms of oxygen and two atoms of fluorine, the bonds are accomplished by the s- and p-electrons.

The infrared absorption spectra of the substances presented above were determined by vibrations of the anionic groups. In this work the absorption spectra of the compounds enumerated above in the region 1600-700 $cm^{-1}$ were investigated and also changes of these spectra with changes of pH in the aqueous solutions. The experiments on the infrared absorption spectra gave a more precise structure and explanation of the stability of hydroxyfluoroboric complexes, which relates to the geochemically important question of the transfer of boron by alkaline solutions containing fluorine.[4]

The potassium and sodium complexes which were subjected to investigation were obtained with the help of the method developed by Riss:[1] the compounds were precipitated from aqueous solutions which contained a calculated amount of $KHF_2$ or $NaHF_2$ and $H_3BO_3$, crystallized or salted out by ethyl alcohol.

In all cases the spectra were obtained for the solid substance. The samples were suspended in isobutyl alcohol (size of the particles <5$\mu$) and then were deposited on a plate of KBr. The thickness of the layer was determined in mg/$cm^2$ by weighing the plate with the deposited sample (uniformity of the deposit was checked with a microscope). The suspension in isobutyl alcohol did not have any effect on the spectrum of the compounds studied.

This was proved experimentally by comparison with spectra of samples obtained by simple dusting. The measurement of spectra was carried out with the help of spectrometer IKS-11 with a NaCl prism and a photoelectric optical amplifier.

The infrared absorption spectra obtained are presented in Figs. 1 and 2; the frequencies of the absorption bands (in $cm^{-1}$) are shown in Tables 1 and 2. Analysis of the presented data permitted the following conclusions: (1) the spectra of $K_2B_3O_3F_5$ and $K_2B_3O_3F_4OH$ within the limits of the accuracy of the measurements agree with each other; (2) the spectra of $KBF_3OH$ and $NaBF_3OH$ also appear to be identical; (3) the spectrum of $Na_2B_3O_3F_5$ is different from the spectra of $K_2B_3O_3F_5$ and $K_2B_3O_3F_4OH$.

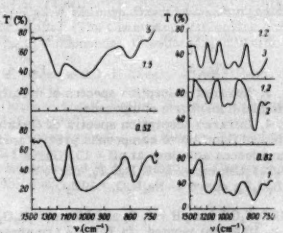


Fig. 1. Infrared absorption spectra of hydroxyfluoroboric complexes (a) and hydroxytrifluoroborates (b). Curve 1—$K_2B_3O_3F_4OH$; curve 2—$K_2B_3O_3F_5$; curve 3—$Na_2B_3O_3F_5$; curve 4—$KBF_3OH$; curve 5—$NaBF_3OH$. The sample thickness (in $mg/cm^2$) is shown on each graph.

In the interpretation of the spectral data the question of basic interest to us was about the cyclic structure of the compounds $K_2B_3O_3F_5$, $K_2B_3O_3F_4OH$, and $Na_2B_3O_3F_5$, since the presence of a boroxyl ring in these compounds was assumed on the basis of only a few purely chemical data.[1]

In the joining of six atoms of fluorine to a boroxyl ring the anion has $D_{3h}$ symmetry. Triply-substituted benzenes, for example, $C_6(CH_3)_3H_3$, trimethylborazoles $B_3N_3(CH_3)_3H_3$, trimethylboraxoles $B_3N_3(CH_3)_3$, and others, the Raman spectra of which have been studied,[2] and also

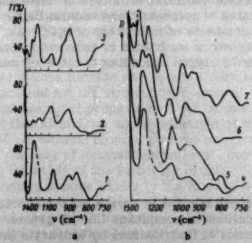


Fig. 2. Infrared absorption spectra of $K_2B_3O_3F_4OH$ (a) and $K_2B_3O_3F_5$ (b) at different values of pH. Values of pH: Curve 1—5; curve 2—8; curve 3—10; curve 4—7; curve 5—8; curve 6—9; curve 7—10.

Table 1

| Compound | ν (cm⁻¹) | | | | | | | | |
|---|---|---|---|---|---|---|---|---|---|
| $K_2B_3O_3F_4OH$ | 1470 | — | 1170 | — | 980 | 930 | — | 800 | 750 |
| $K_2B_3O_3F_5$ | 1480 | — | 1150 | — | 980 | 920 | — | 790 | 750 |
| $Na_2B_3O_3F_5$ | — | 1270 | — | 1060 | — | 950 | 880 | 780 | — |
| $KBF_3OH$ | — | — | 1180 | — | 1000 | — | — | 790 | 750 |
| $NaBF_3OH$ | — | — | 1180 | — | 1000 | — | — | 800 | 750 |

cyanuric acid, the infrared spectrum of which has been qualitatively interpreted[3] have this same symmetry. The reduction of symmetry from $D_{3h}$ to $C_{2v}$ (in our case during substitution in the ring of fluoride ions by hydroxyls) can lead to the appearance in the spectrum of the complexes of additional bands and intensitifcation in the existing bands. An anion of hydroxytrifluoroborates $(BF_3OH)^-$ has the symmetry of an unsymmetrical tetrahedron, $C_{3v}$.

Table 2

| pH | $K_2B_3O_3F_4OH$ ν (cm⁻¹) | | | | | | | | | |
|---|---|---|---|---|---|---|---|---|---|---|
| 5 | 1480 | — | — | 1180 | 1000 | — | 890 | 790 | 750 | |
| 8 | — | 1415 | 1300 | 1180 | 1000 | — | 860—830 | 790 | 750 | |
| 10 | 1510 | 1400 | 1320 | 1160 | 1010 | 950 | 835 | 815 | 750 | |
| pH | $K_2B_3O_3F_5$ ν (cm⁻¹) | | | | | | | | | |
| 7 | 1430 | — | — | 1150 | 990 | — | 800 | 850 | — | 800 | 760 |
| 8 | 1490 | — | — | 1105 | 995 | 940 | — | — | 830 | 790 | — |
| 9 | 1430 | 1360 | 1270 | 1110 | 1000 | 920 | — | — | 825 | — | — |
| 10 | 1460 | 1400 | 1290 | 1160 | 1010 | 940 | 910 | 870 | — | 825 | 760 |

In Table 3 the characteristic vibrational frequencies of the benzene ring in benzene, mono-, di-, and tri-substituted benzenes,[3,4] a ring of $C_3N_3$ in the molecule of cyanuric acid,[3] and also borazole and boroxate rings in several compounds[3] are presented for comparison.

Table 3

| Substance | ν (cm⁻¹) | | | | | |
|---|---|---|---|---|---|---|
| Benzene $C_6H_6$ | 1585+1485 | — | 1037 | 992 * | — | |
| Toluene* $C_6H_5CH_3$ | 1585 | — | 1030 | 1004 | 786 | |
| Xylene* $C_6H_4(CH_3)_2$ | 1600 | 170 | — | 995 | — | |
| Pyridine* $C_5H_5N$ | 1581 | 217 | 1030 | 990 | — | |
| Trimethylbenzene* $C_6H_3(CH_3)_3$ | — | 280 | — | 977 | — | |
| Cyanuric acid $C_3H_3O_3N_3$ | 1470 | — | 1050 | 853 | 765 ** | 807 |
| Trigethyltoraxene* $B_3N_3(CH_3)_3H_3$ | 1451 1335 | 236 | 111 | 940 | — | |
| Trimethylborax* $B_3O_3(CH_3)_3$ | 1450 1312 | — | 1155 | 908 | 807 | |
| Trichloroboroxax $B_3O_3Cl_3$ | — | — | 1037 | — | 807 | |
| Trimethoxyborax $B_3O_3(OCH_3)_3$ | — | 1286 | — | 849 | 804 | |

*Data from the Raman spectra.

**Interpreted in reference 5 as the frequency at which atoms move out of the plane.

Editor's note: The formulas for toluene, xylene, and pyridine are given incorrectly in the Russian original.

In Fig. 3 our experimental data are compared with frequencies and relative intensities of absorption bands in the spectra of certain boron and fluoroboron compounds studied earlier. In Table 4 the literature data about the characteristic vibrations in the range 1600-700 $cm^{-1}$ possible in the compounds studied by us are summarized. In Tables 3 and 4 data are also presented for the Raman spectra since certain vibrations can become active in the infrared as a result of relaxing the selection rules (in our case, for example, during the substitution in the fluoroboroxyl ring of two fluoride ions by a hydroxyl ion). A qualitative interpretation of the spectra of the compounds studied by us is presented in Table 5.

On the basis of the analysis of the presented data, it is possible to draw the conclusion that the spectra of complexes of $K_2B_3O_3F_5$, $K_2B_3O_3F_4OH$, and $Na_2B_3O_3F_5$ contain bands characteristic of a cyclic formation of the type of the boroxyl ring (1450, 1280, 1150, 990, and 800 $cm^{-1}$),

Table 4

| $\nu$ (cm$^{-1}$) | Characteristics vibrations |
|---|---|
| 1400-1500 | 1. Stretching vibrations B-OH in a planar triangle (symmetry $D_{3h}$; for example, boric acid.[3]<br>2. Stretching vibrations B-F in a planar triangle ($D_{3h}$; $BF_3$[3]).<br>3. Stretching vibrations of the ring (benzene, substituted benzene, cyanuric acid, borazene and boronyl compounds[4,5,6]). |
| 1300-1350 | Stretching vibrations B-O (boron-organic compounds[7]) |
| 1250 | Stretching symmetric vibrations of the ring (substituted benzenes, borazyls and borazenes[5,6]). |
| 1150 | 1. Bending vibrations B-OH (boric acid[3]).<br>2. Vibrations of the ring (trimethylborax[2]). |
| 1100-1050 | Stretching vibrations of anions $BF_4^-$ (symmetry $T_d$; examples, $KBF_4$ and $NaBF_4$[10]). |
| 1050-1000 | Vibrations of the ring (benzene, substituted benzenes, trichloroborazole at 1037 cm$^{-1}$ [5,6]). |
| 960-900 | Stretching vibrations B-F in planar triangle ($D_{3h}$; 895 cm$^{-1}$ for $BF_3$[10]). |
| 800-750 | 1. Stretching vibrations B-F of anion $BF_4^-$ ($T_d$; 779 cm$^{-1}$ for $NaBF_4$ and 771 cm$^{-1}$ for $KBF_4$[10]).<br>2. Stretching symmetric vibrations of the ring (trimethylborax at 804 cm$^{-1}$[2]).<br>3. Bending vibrations of different groups coming out of the plane of the ring (853, 807, 765 cm$^{-1}$ in the spectrum of cyanuric acid). |

although in the complete spectra there are few peculiarities. The similarity of the spectra of $K_2B_2O_3F_2$ and $K_2B_3O_3F_4OH$ is proven by the presence in these compounds of a common (for their anions) group $(B_3O_3F_4OH)^{=}$. Since the spectrum of $Na_2B_2O_3F_2$ is substantially different from the spectra of $K_2B_2O_3F_2$ and $K_2B_3O_3F_4OH$, it is possible to assume that the spectrum of the first compound is determined in principle by vibrations of the fluoroboroxyl ring $(B_2O_3F_2)^{=}$. The broad absorption bands in the spectra of $KBF_4OH$ and $NaBF_4OH$ (with a maximum at 1000 cm$^{-1}$) can be connected with the formation of hydrogen bonds in the compounds or the appearance of associated anionic groups.

As was shown above, the study of the stability of hydroxyfluoroboric complexes in an aqueous medium is of great interest (particularly for problems of geochemistry). We studied the spectra of compounds precipitated by salting out with ethyl alcohol or crystallized on reduction of temperature from aqueous solution of complexes at pH = 5, 7, 8, 9, and 10. A pH of 5 is close to the natural pH of the complexes. In Figs. 2(a) and 2(b) the spectra of com-

Table 5

| $K_2B_3O_3F_4OH$ | | $K_2B_2O_3F_2$ | | $Na_2B_2O_3F_2$ | | $KBF_4OH$ | | $NaBF_4OH$ | |
|---|---|---|---|---|---|---|---|---|---|
| $\nu$ (cm$^{-1}$) | Assignment | $\nu$ (cm$^{-1}$) | Assignment | $\nu$ (cm$^{-1}$) | Assignment | $\nu$ (cm$^{-1}$) | Assignment | $\nu$ (cm$^{-1}$) | Assignment |
| 1470 | B—OH, B—F (symmetry $D_{3h}$) | 1480 | $\nu$B—OH?, $\nu$B—F?, Vibrations of the ring during reduction of symmetry | | | | | | |
| | | | | 1270 | Vibration of the ring | | | | |
| 1170 | Vibration of the ring $\delta$B-OH | 1150 | Vibration of the ring | 1090 | $\nu$B—F | 1180 | $\delta$B—OH | 1100 | $\delta$B—OH |
| 980 | Vibration of the ring | | | | | 1000 | Hydrogen bond | 1000 | Hydrogen bond |
| 930 | Inter-anionic interaction* | 930 | Vibration of the ring | 950 | Inter-anionic interaction | | | | |
| | | 920 | Inter-anionic interaction* | | | | | | |
| | | | | 880 | | | | | |
| 800 ** | B—F, vibration of the ring | 790 | $\nu$B—F | 780 | $\nu$B—F, vibration of the ring | 790 ** | $\nu$B—F | 800 ** | $\nu$B—F |
| 750 | ? | 750 | ? | | | 740 | ? | 750 | ? |

*With molecular (inter-anionic) interaction, all the 980-920 cm$^{-1}$ bands can be connected.

**Two bands in the 800-700 cm$^{-1}$ region in the spectra of $K_2B_3O_3F_4OH$, $K_2B_2O_3F_2$, $KBF_4OH$, and $NaBF_4OH$ together with one in the spectrum of $Na_2B_2O_3F_2$ can arise on replacement of fluoride ions by hydroxyl ion as a result of removing degeneracy for the vibrations.

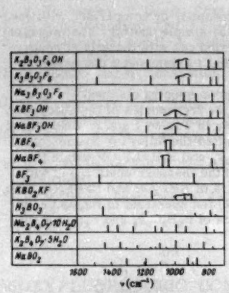


Fig. 3

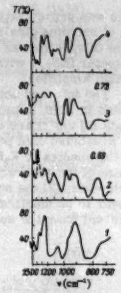


Fig. 4

Fig. 3. Infrared absorption spectra of certain boric and fluoroboric compounds.
Fig. 4. Infrared absorption spectra of certain boric and fluoroboric compounds precipitated from aqueous solutions at pH = 10. Curve 1—$K_2B_3O_3F_4OH$; curve 2—$K_2B_2O_3F_2$; curve 3—$Na_2B_2O_3F_2$; curve 4—$Na_2B_4O_7 \cdot 10H_2O$.[8]

plexes $K_2B_3O_3F_4OH$ for pH = 5, 8, and 10 and $K_2B_2O_3F_2$ for pH = 7, 8, 9, 10 are presented. In Table 2 are presented the corresponding frequencies (in cm$^{-1}$). As is seen from the data, the spectrum of $K_2B_3O_3F_4OH$ precipitated from a solution of pH equal to 5, preserves the spectral characteristics of the original complex. For values of pH of 8-10 there is observed the appearance in the spectra of $K_2B_3O_3F_4$, $K_2B_3O_3F_4OH$, and $Na_2B_2O_3F_2$ of an absorption band similar in position and intensity. For example, in Fig. 4 are presented the spectra of the three above-mentioned compounds, precipitated from aqueous solution at pH = 10. In Table 6 are shown the corresponding values of the frequencies of absorption bands (in cm$^{-1}$).

Analysis of the data allowed us to draw the conclusion that the spectra of complexes at increasing values of pH is very similar to those for metaborates and tetraborates of K, Na, and Mg, measured by Miller et al.[9] The frequencies of absorption bands for several of these compounds are also presented in Table 6. In Fig. 4, the spectrum of borax[8] is shown. On the basis of the similarity of the spectra of the investigated compounds with the spectra of metaborates of potassium and sodium, it is possible to assume a similar structure of these substances. In metaborates of potassium and sodium Bauer et al.[2] assumed the existence of a flat ring of $B_3O_6^{=}$; i.e., the boroxyl ring where each atom of boron was bonded with three atoms of oxygen according to the diagram:

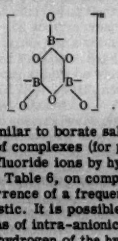


Compounds similar to borate salts can arise in aqueous solutions of complexes (for pH greater than 7) by replacement of fluoride ions by hydroxyls in the appropriate rings. In Table 6, on comparing values of frequencies, the occurrence of a frequency close to 1000 cm$^{-1}$ is characteristic. It is possible that this band is caused by vibrations of intra-anionic groups which are bonded across the hydrogen of the hydroxyl. The dis-

Table 6

| Compound | pH | ν(cm⁻¹) | | | | | | | | | | |
|---|---|---|---|---|---|---|---|---|---|---|---|---|
| $K_3B_3O_3F_6OH$ . . | 10 | 1510 | 1400 | 1320 | — | 1160 | — | 1010 | 950 | — | 835 | 750 |
| $K_3B_3O_3F_6$ . . . . | 10 | 1460 | 1420 | 1290 | — | 1160 | — | 1010 | 940 | 870 | 825 | 760 |
| $Na_3B_3O_3F_6$ . . . | 10 | 1520 | 1430 | 1330 | — | 1160 | — | 1010 | 950 | 880 | 830 | 750 |
| $K_2B_4O_7 \cdot 5H_2O$ . | — | — | 1440 | 1345 | 1245 | 1155 | 1100 | 1000 | 920 | — | 835 | 780 |
| $Na_2B_4O_7 \cdot 10H_2O$ . | — | — | 1420 | 1360 | 1270 | 1130 | 1090 | 1000 | 945 | — | 825 | 775 |
| $NaBO_2$ . . . . . | — | — | — | 1310 | — | 1175 | — | — | 930 | 895 | — | — |
| $Mg(BO_2)_2 \cdot 8H_2O$ . | — | — | 1420 | 1370 | 1220 | 1140 | — | 1020 | 955 | 890 | 835 | 800 |

placement of the band at 800 $cm^{-1}$ to 830 $cm^{-1}$ in the spectra of compounds obtained from alkaline solutions and in the spectra of borates, in comparison with the spectra of the original compounds, is perhaps connected with the displacement of bonds B—F by B—O and B—OH. The additional narrow and broad bands which appear in this spectra can be attributed to vibrations of the more or less stable intramolecular groups (type of borate chains as in polyborate compounds).

In conclusion the authors express gratitude to E. E. Vainshtein and V. L. Barsukov for suggesting the topic of the present work and for constant interest in it.

## REFERENCES

1. I. G. Riss. "Khimiya Ftora i Ego Neorganicheskikh Soedinenii." (The Chemistry of Fluorine and its Organic Compounds), Gosudarst. Izd. Khim. Lit., Moscow, 1956.
2. S. H. Bauer and J. I. Beach. J. Am. Chem. Soc. **63** 1394 (1941).
3. J. Goubeau and H. Keller. Z. anorg. u. allgem Chem. **272**, 313 (1953).
4. V. L. Barsukov and A. P. Egorov. Geokhimiya, No. 8, 673 (1957).
5. R. Newman and P. M. Badger. J. Chem. Soc. **74**, 3545 (1952).
6. M. V. Volkenshtein, M. A. Elyashevich, and B. I. Stepanov. "Kolebaniya Molekul." (Molecular Vibrations), Gosudarst. Izd. Tekh.-Teoret. Lit., Moscow, 1949.
7. L. J. Bellamy, W. Gerrard, M. F. Lampert, and P. L. Williams. J. Chem. Soc. **78**, 2412 (1958).
8. F. A. Miller and C. H. Wilkens. Anal. Chem. **24**, 1253 (1952).
9. D. E. Bethell and N. Sheppard. Trans. Faraday Soc. **51**, 9 (1955).
10. G. L. Cote and O. Tomson. Proc. Roy. Soc. **A210**, 217 (1955).

# VIBRATIONAL SPECTRA OF THE MODIFICATIONS OF GERMANIUM DIOXIDE

V. V. Obukhov-Denisov, N. N. Sobolev, and V. P. Cheremisinov

Received 11 June 1959

The vibrational spectra of the vitreous and crystalline modifications of germanium dioxide were investigated. Basically, the spectra of the soluble and vitreous modifications differ little from one another; this might be a consequence of similarity of structure. At the same time, the insoluble form of $GeO_2$ has a completely different vibrational spectrum. This indicates the structure of the latter form to be different from the structure of the other modifications of $GeO_2$, which is in agreement with x-ray data.

A comparison of the vibrational spectra of the soluble modification of $GeO_2$ and low temperature $\alpha$-quartz is made, and a compilation of the frequencies of the vibrational spectrum of the soluble modification of $GeO_2$ is given, arranged according to the type of vibration.

## INTRODUCTION

The present work is devoted to an investigation of the vibrational spectra of the vitreous and crystalline modifications of germanium dioxide.

In our first paper, which was devoted to an investigation of $GeO_2$,[1] and also in reference 2, the great similarity of the vibrational spectra of fused (vitreous) germanium and silicon dioxide was noted. Other authors have also pointed out the similarity of several other physical and chemical properties of the oxides mentioned.[2] Because of this similarity an investigation of the modifications of germanium dioxide with the aid of vibrational spectra is not only of independent interest, but also contributes to the study of the structure of $SiO_2$.

Germanium dioxide exists in the form of several modifications—two crystalline (soluble and insoluble) and one vitreous. According to physico-chemical[4] and x-ray data, germanium dioxide obtained by crystallization from aqueous solutions has a crystal lattice analogous to the structure of low temperature $\alpha$-quartz. X-ray analysis has shown that crystalline $GeO_2$ obtained by another method (devitrification of fused $GeO_2$) has the same crystal structure. This crystalline modification is partially soluble in water and therefore is called the soluble modification of $GeO_2$.

The second crystalline modification of $GeO_2$ was discovered by Müller and Blank.[7] They called it the insoluble modification, since it is practically insoluble in water. This form is obtained from the soluble modification by a hydrothermal method. X-ray data indicate that it has the rutile crystalline lattice.

Besides the structural differences indicated, the two modifications have completely different physical and chemical properties. This is illustrated by Table 1,[9] which also gives data on the properties of the vitreous modification of $GeO_2$, obtained by rapid cooling of the melted soluble modification.

## EXPERIMENTAL PART

Vitreous germanium dioxide was first obtained in 1926 in a platinum crucible with the aid of a high frequency furnace.[3] The authors of the work noted that the production of vitreous germanium dioxide in the form of a clear homogeneous product without impurities or reduction phenomena was very difficult.

Table 1. Physical and Chemical Characteristics of the Modifications of Germanium Dioxide

| Characteristic | Modification | | |
|---|---|---|---|
| | Insoluble tetragonal | Soluble hexagonal | Vitreous amorphous |
| Crystal structure | Rutile | α-quartz | — |
| Density (gm/cm³) at 25° C | 6.239 | 4.228 | 3.637 |
| Refractive index $n_0$ | 1.99 | 1.695 | — |
| Refractive index $n_E$ | 2.05—2.10 | 1.735 | 1.607 |
| Inversion point | 1033° ± 10° | 1033° ± 10° | — |
| Melting point | 1086° ± 5° C | 1116° ± 4° C | — |
| Solubility (in 100 gm of $H_2O$) | Insoluble | 0.453 (25° C) | 0.5184 (30° C) |
| Effect of hydrofluoric acid | Does not react | Reacts and gives $H_2GeF_6$ | |
| Effect of hydrochloric acid | Does not react | Reacts and gives $GeCl_4$ | |
| Effect of sodium hydroxide at 100° C | Dissolves very slowly | Dissolves very rapidly | |

We constructed a special high temperature furnace with six Silit resistors arranged vertically around the periphery for the production of the vitreous form from germanium dioxide. The temperature of the furnace was controlled by means of an optical pyrometer. White crystalline powder of the soluble modification of germanium dioxide with a very small impurity content ($SiO_2$ < 0.0004%) served as the starting material. As a consequence of the high shrinkage and intense vaporization of germanium dioxide it was necessary to perform a series of successive fusions in order to obtain a sample of the required dimensions. A platinum test tube was used as a crucible. It was necessary to slit this tube to extract the sample. Although germanium dioxide is a fairly liquid mass at its boiling point (~1400°C), intense vaporization made it impossible to keep the melt at this temperature for any length of time. The specimens which were obtained therefore contained a few gas bubbles. The samples prepared in this way were later annealed at a cooling rate of ~0.2 deg/min. Three samples were obtained in all—two in the form of bars 10 × 10 × 20 mm and one in the form of a cylinder, 16 mm in diameter and 60 mm long. The samples were completely adequate for obtaining Raman spectra.

The white finely divided crystalline germanium dioxide powder produced domestically consists mainly of the soluble modification, with a slight admixture of the insoluble. We obtained the pure soluble modification by crystallization from an aqueous solution of the commercial germanium dioxide powder. The insoluble crystalline modification was obtained by a hydrothermal method.[10] The transformation of one modification to the other was accomplished by means of the catalytic effect of steam.

The procedure for obtaining this modification was as follows: 10 gm of the soluble modification of $GeO_2$ and 10 gm of distilled water were placed in a platinum crucible with a tightly fitting lid, which was set in a stainless steel bomb with a hermetically sealed screw plug. The bomb was kept in a furnace at 480°C for 120 hr, and then rapidly cooled to room temperature. The resulting product was purified of iron oxides in a steam bath of a 6N aqueous solution of hydrochloric acid. The residue obtained was rinsed with hot distilled water and baked at 400°C for 12 hr. No appreciable loss in weight was observed upon washing with HCl which attested to the complete transformation of the soluble modification into the insoluble. Besides a check of the solubility of the samples, an identification of the various modifications of $GeO_2$ was also made by determining their indices of refraction. Measured values of the refractive indices of all the modifications agreed well with the tabulated data.

Investigations of the Raman spectra of the crystalline modifications of $GeO_2$ were carried out by one of the methods for investigating powders—by passage of the exciting line through a layer of the material. For the soluble modification, the thickness of the layer (0.5 mm) was chosen empirically. Various layer-thicknesses—0.25, 0.5, and 1 mm—were used for the insoluble form of $GeO_2$. Spectra of the vitreous modification were obtained by the usual method.

Investigation of the Raman spectra was performed photographically by means of an ISP-51 spectrograph with the medium size camera (f = 270 mm). A low pressure mercury lamp, combined with filters for isolating the exciting line (405 or 435 mμ) served as the light source.

The spectra were photographed on Agfa Raman plates. Exposures for the investigation of powders lasted 60-100 hr; for the investigation of vitreous $GeO_2$ they lasted 20-30 hr.

The infrared absorption spectra in the region of 2.5-37μ were recorded with the aid of a split-beam spectrophotometer developed at the Physical Institute of the Academy of Sciences.[11] The powders were mulled in paraffin oil. We also made use of the data on the vibrational spectra of the soluble and vitreous modifications of $GeO_2$ in the region of 2.5-24 μ, obtained earlier by Sidorov.

## RESULTS OF THE INVESTIGATION

The results obtained in the present work are given in Table 2. It is necessary to point out that because of the strong influence of the scattered background of the exciting line, the determination of weak Raman lines of powders in the low frequency region was difficult.

Table 2. Vibrational Spectra of Different Modifications of $GeO_2$ (Frequencies in $cm^{-1}$)

| Soluble modification | | Vitreous modification | | Insoluble modification | |
|---|---|---|---|---|---|
| Raman spectrum | Infrared spectrum | Raman spectrum | Infrared spectrum | Raman spectrum | Infrared spectrum |
| | | 193 (vw) | | Spectrum not observed | |
| | | 250 (vw) | 295 (s) | | |
| | 333 (s) | 315 (i) | 315 (s) | | |
| 340 (i) | 343 (s) | 342 (i) | 334 (s) | | |
| 408 (i) | | 373—401 (vs) | | | 407 (vs) |
| 440 (s) | | | | | |
| 508 (i) | 515 (i) | 520—615 (i) | 564 (s) | | |
| 560 (w) | 551 (i) | | | | |
| | 587 (i) | | | | |
| 640 (w) | | | | | 606 (i) |
| | | | | | 709 (vs) |
| 888 (vw) | 872 (vs) | 825—894 (w) | 888 (vs) | | |
| 959 (vw) | 955 (i) | 935—973 (w) | 966 (s) | | 945 (w) |

Scale of line intensities: vw – very weak, w – weak, i – intermediate, s – strong, vs – very strong.

The infrared absorption spectra of the various modifications between 2.5 and 37 μ are shown in Figs. 1-3 (asterisks mark the absorption bands of paraffin oil). The data on the infrared absorption spectrum of the soluble modification of $GeO_2$ agree well with reference 13, although the agreement in the case of the insoluble modification is not as good.

It is evident from the tables and the spectra shown in the figures that the vibrational spectrum of the vitreous modification of $GeO_2$ is quite different from the vibrational spectra of the other modifications. A unique feature of this insoluble modification of $GeO_2$ was its complete lack of any Raman spectrum. It should be noted that the Raman lines of vitreous $GeO_2$ are considerably broader than the lines of the soluble modification; there is even a merging of close lines into one broad band (for example, the lines at 515, 551, and 587 $cm^{-1}$, present in the spectrum of the soluble modification, upon transformation to the vitreous form combine into one band with a maximum at 564 $cm^{-1}$). Another characteristic feature of the Raman spectrum of vitreous $GeO_2$ is the presence

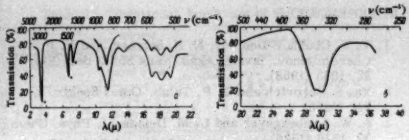

Fig. 1. Infrared absorption spectrum of the soluble modification of $GeO_2$ between 2 and 37 μ.

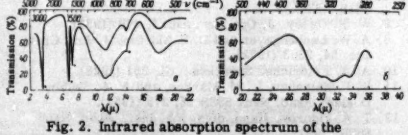

Fig. 2. Infrared absorption spectrum of the vitreous modification of $GeO_2$ between 2 and 37 μ.

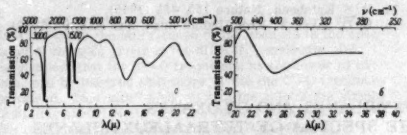

Fig. 3. Infrared absorption spectrum of the insoluble modification of $GeO_2$ between 2 and 37 μ.

of a continuous spectrum adjacent to the exciting line λ = 4358 A and extending approximately 600 $cm^{-1}$.

## DISCUSSION OF THE RESULTS

In a previous paper[1] we gave a preliminary discussion of the experimental Raman spectra of the vitreous modification of $GeO_2$. The data obtained on the vibrational spectra of all the modifications of germanium dioxide make it possible to draw more complete conclusions.

First of all, it should be noted that there is fairly good agreement between the positions of the lines in the vibrational spectra of the soluble and vitreous modifications of $GeO_2$. This experimental fact attests to the result that the vitreous modification, in spite of being a different state of agregation (amorphous) than the crystalline (soluble) modification, has a space lattice of the same type as the soluble form, i.e., it consists of cells of hexagonal form.

The variation in intensity and broadening of the lines, and the appearance of a continuous spectrum are apparently connected with the nonperiodic lattice of the glass, which leads to a certain distortion of the crystalline unit cell. But this distortion is not so great as to substantially change the type of symmetry and, together with it, the vibrational spectrum of the material. The vibrational spectrum of the insoluble modification differs strongly from the spectra of the other forms of $GeO_2$, which indicates the presence of another crystalline structure. Actually, x-ray data confirm the hypothesis that the insoluble modification has a crystalline structure (tetragonal) different from the structures of the other forms of $GeO_2$. The absence of a Raman spectrum is the characteristic feature of this form of $GeO_2$, although the possibility is not excluded that this apparent absence is due to the faintness of lines characteristic of the powder method. The absence of a Raman spectrum indicates that the insoluble modification is apparently characterized to a large extent by ionic bonds.

The hypothesis proposed in reference 1 concerning the similarity of the structures of vitreous $SiO_2$ and $GeO_2$ is confirmed, since vitreous $GeO_2$, as shown above, has the same hexagonal structure as vitreous $SiO_2$.

Therefore, it is of interest to compare the vibrational spectra of soluble $GeO_2$ and low temperature α-quartz. The results of such a comparison are given in Table 3.

Table 3. Comparison of the Vibrational Spectra of Crystalline Germanium and Silicon Dioxide (Frequencies in $cm^{-1}$)

| Low temperature α-quartz $SiO_2$ | | Soluble modification of $GeO_2$ | | |
|---|---|---|---|---|
| Raman spectrum | Infrared spectrum | Raman spectrum | Infrared spectrum | Type of vibration |
| | 374 (i) | | 333 (s) | B |
| 395 (5) | 397 (i) | 340 (i) | 343 (s) | E |
| 404 (5) | | 408 (i) | | A |
| 467 (10) | | 440 (s) | | A |
| 696 (4) | 696 (w) | 508 (i) | 515 (i) | E |
| | 780 (i) | | 587 (i) | B |
| 794—805 (5) | 801 (i) | 560 (w) | 551 (i) | E |
| | | 640 (w) | | A |
| 1065 (4) | 1091 (vs) | 898 (vw) | 872 (vs) | E |
| 1160 (7) | 1178 (s) | 959 (vw) | 955 (i) | E |

Scale of line intensities: first column – scale of thirty; remaining columns: vw very weak, w – weak, i – intermediate, s – strong, vs – very strong.

The infrared absorption spectrum of α-quartz is taken from reference 3, and the Raman spectrum from reference 14 (for estimating the line intensities in the latter case we used a scale of thirty.)

In comparing these spectra, account was taken of the fact that the data on the Raman spectrum of α-quartz are more complete, since they were obtained using the mercury line λ = 2537 A for excitation of the spectrum, and the samples were single crystals. The spectrum of crystalline $GeO_2$, on the other hand, was investigated by the powder method with the lines λ = 4358 and 4047 A for excitation. This, of course, did not permit one to expose all the details of the Raman spectra.

Saksena[15] carried out a fairly complete analysis of the vibrational spectrum of low temperature α-quartz. Since the soluble modification has the same unit cell as α-quartz (consisting of three $GeO_2$ groups), it is possible to carry out the same analysis of the vibrational spectrum for this modification of germanium dioxide. The selection rules for the hexagonal cell of the type described above requires the occurrence of 24 fundamental modes of which 4 are totally symmetrical vibrations of type A, active only in the Raman spectrum, 4 are vibrations of type B, active only in the infrared absorption spectrum, and 8 are doubly degenerate vibrations of type E, active in both spectra. On the basis of the comparison of the Raman and infrared absorption spectra, a compilation of the frequencies according to type of vibration is given in Table 3.

It should be noted that this compilation of frequencies cannot be considered complete, since the infrared spectrum was not investigated below 300 $cm^{-1}$; and it was difficult to obtain the corresponding part of the Raman spectrum because of the strong influence of the background of the exciting line.

## CONCLUSION

Investigation of the vibrational spectra of the modifications of germanium dioxide shows that the vitreous

modification has the same hexagonal structure as the soluble crystalline form. At the same time, the sharp difference between the vibrational spectrum of the insoluble modification of $GeO_2$ and the spectra of the other modifications indicates that this crystalline form has another structure. Actually, it is known from x-ray data that the insoluble modification possesses a tetragonal structure. The absence of a Raman spectrum leads to the conclusion that the bonds in this crystalline form of $GeO_2$ are apparently largely ionic.

The hypothesis concerning the similarity of the crystalline structures of vitreous germanium and silicon dioxides, expressed in connection with a comparison of the Raman spectra of these materials,[1] is confirmed. On the basis of an analysis of the Raman spectra and infrared absorption of the soluble modification, a compilation of the frequencies according to the type of vibration is given.

In conclusion, let us note that since the structure of soluble germanium dioxide is analogous to the structure of $\alpha$-quartz, which possesses a large piezoeffect and is widely used in radio engineering, it is possible to expect that the soluble modification will also be useful for radio engineering applications. From this viewpoint one must consider the production of a single crystal of the soluble modification of germanium dioxide as a very essential task.

REFERENCES

1. V. V. Obukhov-Denisov, N. N. Sobolev, and V. P. Cheremisinov. Izvest. Akad. Nauk SSSR, Ser. Fiz. **22**, 1083 (1958).
2. Ya. S. Bobovich and T. P. Tulub. Opt. i Spektr. **5**, 210 (1958).
3. A. W. Laubengayer and L. M. Dennis. J. Phys. Chem. **30**, 1510 (1926).
4. V. M. Goldschmidt. Naturwiss. **14**, 295 (1926).
5. W. H. Zachariasen. Z. Krist. **67**, 226 (1928).
6. J. H. Müller. Proc. Am. Phil. Soc. **65**, 183 (1926).
7. J. H. Müller and H. R. Blank. J. Am. Chem. Soc. **46**, 2338 (1924).
8. W. P. Davey. J. Opt. Soc. Am. **5**, 479 (1921).
9. A. W. Laubengayer and D. S. Morton. J. Am. Chem. Soc. **54**, 2303 (1932).
10. A. A. Fridrichs. Sprechsaal **61**, 261 (1928).
11. V. I. Malyshev, L. M. Markov, and A. A. Shubin. Doklady Akad. Nauk SSSR **86**, 273 (1952).
12. T. A. Sidorov. Kand. diss. Fiz. Inst., Akad. Nauk SSSR, 1957.
13. E. R. Lippincott. J. Res. Natl. Bur. Standards **61**, 61 (1958).
14. R. S. Krishnan. Nature **155**, 452 (1945).
15. B. D. Saksena. Proc. Indian Acad. Sci. **A12**, 93 (1940).

# VIBRATIONAL SPECTRA OF ALKOXYSILANES AND SILOXANES
## II. VIBRATIONS OF THE $SiO_4$ GROUPS IN THE SPECTRA OF TETRAALKOXYSILANES

A. N. Lazarev

Received 6 July 1959

The vibrational spectra of four tetra-n-alkoxysilanes have been studied. The valence vibrations of the skeleton—in particular, of the $SiO_4$ groups—are discussed.

The similarity in the structure of the esters of orthosilicic acid and its salts—the silicates—has repeatedly attracted the attention of investigators. The idea of using the spectra of esters of orthosilicic acid for the interpretation of the spectra of the silicates was first expressed by Weiler and Signer, who were investigating the Raman spectra of tetramethoxysilane and the polymethoxysiloxanes.[1] These authors endeavored to interpret the spectrum of quartz on the basis of the data which they obtained. Recently we have carried out a detailed investigation of the vibrational spectra of polyalkoxysiloxanes for the purpose of studying the changes which take place in the spectrum on "polymerization" of the $SiO_4$ groups into a chain.[2-4]

In an attempt to make use of the analogy between the spectra of the esters of orthosilicic acid and of the silicates, the first problem which arises is the separation of the frequencies of the $SiO_4$ group in the spectra of molecules of the type $Si(OR)_4$. However, the preliminary identification proposed in our first communications for the vibrations of the "isolated" $SiO_4$ group in the spectra of tetraalkoxysilanes[5,6] had a number of defects. The obtaining of more complete experimental data on the one hand, and the calculations of the vibrational spectrum of $Si(OCH_3)_4$ carried out by Iguchi[7,8] on the other, permit us to return to this question and to give a more reliable frequency assignment.

As we have already pointed out,[5] the fundamental causes of the change in the vibrations of the $SiO_4$ group on going from the isolated $[SiO_4]^{4-}$ ion to the $Si(OCH_3)_4$ molecule are the interaction of the Si—O and C—O bonds and the fact that the symmetry of the whole molecule is lower than $T_d$. Judging from the data of electron diffraction studies[9] and dipole moment measurements,[10] the tetramethoxysilane molecule $Si(OCH_3)_4$ has the symmetry $V_d$ (Fig. 1), the tetrahedral form of the $SiO_4$ group remaining undistorted. The lowering of the symmetry from $T_d$ (the isolated $SiO_4$ tetrahedron) to $V_d$ leads to breakdown of the degenerate symmetry types of the group $T_d$:

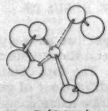

Fig. 1. The $Si(OCH_3)_4$ molecule.

$$\begin{array}{cc} T_d & V_d \\ \hline F_2 & \rightarrow B_2, \\ & \searrow E; \\ E & \rightarrow B_1, \\ & \searrow A_1; \\ A_1 & \rightarrow A_1. \end{array}$$

Therefore, to the four normal vibrations of the $SiO_4$ group ($2F_2$, E, $A_1$), there must correspond, generally speaking, seven vibrations in the $Si(OCH_3)_4$ spectrum ($2B_2$, 2E, $B_1$, $2A_1$). The magnitude of the splitting, however, may not be large.

Table 1. Vibrational Spectrum of $Si(OCH_3)_4$

| Raman spectrum (liquid) | | | Infrared spectrum | | Assignment | | | |
|---|---|---|---|---|---|---|---|---|
| | | | Liquid | Gas | Symmetry of the vibration | | | |
| Frequency ($cm^{-1}$) | Intensity | Polarization ($\rho$) | Frequency ($cm^{-1}$) and intensity | Frequency ($cm^{-1}$) | $T_d$ $SiO_4$ | $T_d$ $SiO_4$ | Calculated frequency | Description of the vibration |
| 221 | 0.5 d | — | — | — | — | $E$? | — | OSiO deformation |
| 312 | 1 | — | — | — | — | $F_2$? | — | |
| 412 | 1 vd | 3.80 | <418 s | <418 | — | — | — | SiOC deformation |
| 458 | ? | — | — | — | — | — | — | |
| 505 | ? | — | — | — | — | — | — | |
| 640 | 10 sh | 0.03 | 639 w | — | $A_1$ | $A_1$ | 665 | Si-O symmetrical valence |
| 844 | 3 d | 0.80 | 825 s | 832 | $B_2$ | $F_2$ | 825 | Si-O antisymmetrical valence |
| | | | 838 s | 847 | $E$ | | 899 | |
| 1082 | 5 | | | | $A_1$ | — | 1145 | |
| | | 0.20* | 1093 vs | 1108 | $E$ | — | 1146 | C-O valence |
| 1111 | 4 | | | 1141 | $B_2$ | — | 1142 | |
| 1186 | 4 d | 0.32 | 1190 s | 1197 | | | | CH, internal and external deformation |
| 1463 | 8 | 0.80 | 1469 m | 1474 | | | | |
| 1476 | 2 | | | | | | | |

*In the polarization measurements with photoelectric recording, we did not succeed in resolving the lines 1082 and 1111 $cm^{-1}$. We may suppose that the narrower and more intense line, 1082 $cm^{-1}$, is polarized.

Symbols: d – diffuse, vd – very diffuse, sh – sharp, w – weak, m – medium, s – strong, vs – very strong.

The interaction of the vibrations of the Si—O and C—O bonds is the other cause of the changes in the spectrum of the $SiO_4$ group in the $Si(OCH_3)_4$ molecule. We may expect that the Si—O frequency, as the lower of the two, will be lowered still more, while the C—O frequency is raised. This may be shown with the help of the simple triatomic model Si—O—C. The results of investigation of the spectra of molecules of the type $R_3Si—O—CH_3$ [11, 12] lead to the same conclusion. Thus, in the $Si(OCH_3)_4$ spectrum we may expect not only splitting, but also lowering of the frequencies of the $SiO_4$ group.

The lowering of the frequency must apparently be more pronounced for the totally symmetrical valence vibration (breathing) of the $SiO_4$ tetrahedron than for the antisymmetrical valence vibration. This is related to the fact that in the breathing vibration the amplitudes of the O atoms are greater and the interaction of the Si—O and C—O vibrations is stronger.*

*We do not touch here upon those differences in the frequencies of the $SiO_4$ group in the $Si(OCH_3)_4$ molecule and in the $[SiO_4]^{4-}$ ion which result from the different values of the dynamic coefficients $k_{Si-O}$ for the Si—O(—C) and $Si—O^-$ bonds, inasmuch as in the present case the frequency changes brought about by kinematic interaction are more substantial.

Table 2. Vibrational Spectrum of $Si(OC_2H_5)_4$ (in the Liquid Phase)

| Raman spectrum | | | Infrared spectrum, frequency ($cm^{-1}$) and intensity | Assignment |
|---|---|---|---|---|
| Frequency ($cm^{-1}$) | Intensity | Polarization ($\rho$) | | |
| 232 | 0 d | — | — | OSiO, SiOC, and CCO deformation |
| 300 | 1 d | — | — | |
| 328 | | | | |
| 424 | 0 d | — | — | |
| 498 | ? | — | 478 m | |
| 656 | 6 sh | 0.05 | 656 w | $SiO_4$ valence, symmetrical |
| 782 | 3 d | 0.62 | 789 s | $SiO_4$ valence, antisymmetrical |
| 822 | | | 809 m | |
| 939 | 3 | 0.53 | — | C-C valence |
| 974 | 1 | — | 962 s | |
| 1096 | 8 d | 0.27 | 1080 vs | C-O valence |
| | | | 1102 vs | |
| 1173 | 4.5 | 0.15 | 1163 m | CH, and CH, internal and external deformation |
| 1205 | 2 | 0.74 | — | |
| 1302 | 4.5 sh | 0.77 | 1291 m | |
| 1365 | 2 sh | — | 1391 m | |
| 1441 | 10 | 0.83 | 1441 w | |
| 1456 | | | 1456 w | |
| 1489 | 2 sh | — | 1482 w | |

Table 3. Vibrational Spectra of Tetrapropoxy- and Tetrabutoxysilanes (in the Liquid Phase)

| $Si(OC_3H_{7-n})_4$ | | | $Si(OC_4H_{9-n})_4$ | | |
|---|---|---|---|---|---|
| Raman spectrum | | Infrared spectrum (frequency and intensity) | Raman spectrum | | Infrared spectrum (frequency and intensity) |
| Frequency ($cm^{-1}$) | Intensity | | Frequency ($cm^{-1}$) | Intensity | |
| 232 | ? | — | — | — | — |
| 266 | 0 d | — | ~240 | 0 vd | — |
| 289 | | | | | |
| 399 | 0 d | | | | |
| 423 | | | | | |
| 504 | 0 d | <418 | ~417 | 0 d | <418 |
| 666 | 2 sh | 500 m | ~513 | 0 sh | 526 m |
| | | 666 w | 668 | 1 sh | 670 w |
| | | 743 m | 740 | 0 vd | 723 w |
| 786 | 0 d | ~774 w | 812 | 2 sh | 799 m |
| | | 847 s | 832 | 4 sh | ~840 w |
| 875 | 4 d | 877 m | 886 | 1 vd | 901 m |
| 893 | 1 d | 899 m | ~908 | | 952 w |
| | | 913 w | 960 | 0 d | 972 w |
| | | | 983 | | 985 m |
| 1026 | 5 d | 1015 s | 1043 | 4 vd | 1006 w |
| 1066 | 4 vd | 1082 vs | 1066 | 2 d | 1038 s |
| 1113 | | 1099 vs | 1114 | 3 d | 1080 vs |
| 1154 | 0 d | 1148 s | 1153 | 0 vd | 1111 s |
| | | | 1209 | 0 sh | 1144 m |
| 1255 | 1 d | 1256 w | 1237 | 0 sh | 1228 w |
| 1278 | 4 d | | 1267 | 0 sh | 1259 w |
| 1302 | 2 d | 1258 w | 1300 | 8 sh | 1295 w |
| 1363 | 0 d | — | 1391 | 1 vd | — |
| 1436 | 1 d | — | 1438 | 1 d | — |
| 1450 | 8 sh | — | 1458 | 7 d | — |
| 1476 | 2 d | — | 1490 | 3 sh | — |

We have investigated the vibrational spectra of four tetra-n-alkoxysilanes. The frequencies, intensities, and polarizations of the lines in the Raman spectra are presented in Tables 1-3 (the CH valence frequencies are not included in the tables).

Figure 2 gives the curves for the infrared absorption spectra in the region 800-420 $cm^{-1}$.* In the investigation of the Raman spectra, we used both photographic (glass spectrographs with linear dispersion of about 25 and 18 A/mm in the region $\lambda$ = 4358 A) and photoelectric

*Absorption spectra in the region 1300-700 $cm^{-1}$ were presented by us earlier.[8]

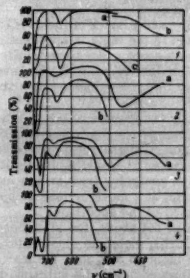


Fig. 2. Absorption spectra of tetraalkoxysilanes in the region 800-420 $cm^{-1}$ (d—thickness of the absorbing layer (mm); C—concentration of a solution in $CCl_4$, (%)). 1—$Si(OCH_3)_4$: curve a—d = 0.03; curve b—d = 0.015, C = 20; curve c—d = 0.17. 2—$Si(OC_2H_5)_4$: curve a—d = 0.015; curve b—d = 0.1. 3—$Si(OC_3H_{7-n})_4$: curve a—d = 0.015; curve b—d = 0.1. 4—$Si(OC_4H_{9-n})_4$: curve a—d = 0.015; curve b—d = 0.1.

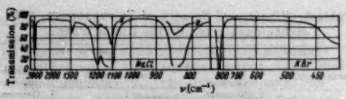


Fig. 3. Absorption spectrum of gaseous tetramethoxysilane $Si(OCH_3)_4$; thickness of the absorbing layer, 120 mm; pressure, 15 mm Hg; curve a—the same at a pressure of 3 mm Hg.

(for the polarization measurements[3]) recording. The infrared spectra were studied with the help of an ISP 14b spectrometer (f = 315 mm) with NaCl and KBr prisms, and a vacuum spectrometer (f = 800 mm) with an NaCl prism. All the substances were studied in the liquid phase, both in the pure form and in solutions in $CS_2$ and $CCl_4$. Solvent absorption has been eliminated from the curves presented in the figures. The absorption spectrum of tetramethoxysilane vapor was also taken (Fig. 3).

The frequency assignment in the $Si(OCH_3)_4$ spectrum (assuming the symmetry $V_d$) is given in Table 1. Here are also presented, for comparison with the experimental data, the values for the frequencies of the "skeletal" vibrations of this molecule as calculated by Iguchi.[7,8] In the model used by Iguchi, the $CH_3$ groups are considered as point masses, and the force field of the molecule is characterized by a simple quadratic potential function with five force constants (two valence constants: Si—O and C—O, two deformation constants: SiOC and OSiO, and one nonbonded interaction, O...O); therefore, the calculations are approximate and correspond only qualitatively with the experimental data. The discrepancies are particularly significant in the values of the calculated and observed frequencies of the C—O valence vibrations. This may be explained (aside from a not altogether fortunate choice of the force constant $k_{C-O}$) by the failure of Iguchi's model to take into account the interaction of the C—O vibrations with the $CH_3$ deformation vibrations. It is possible that the partial polarization observed in the experiment for the 1186 $cm^{-1}$ line, which is ascribed to the $CH_3$ external deformation vibration, is a consequence of this interaction.

The frequency assignment of the Si—O valence vibrations presented in the table is apparently not subject to doubt, especially since it does not conflict with the conclusions of a number of authors who have identified the frequencies of the $SiO_4$ group through study of the spectral transition $SiCl_4 \rightarrow Si(CH_3)_4$.[11,12]

The frequency assignment in the region of the deformation vibrations of the "skeleton" is less reliable. The absence of data on the absorption spectrum and the approximate character of Iguchi's calculations, which makes their use in assigning frequencies more difficult, prevent any attempt at a more or less complete interpretation of this region of the spectrum.

As was pointed out above, the vibrations of the $SiO_4$ group in the $Si(OCH_3)_4$ molecule must differ from the vibrations of the isolated $SiO_4$ ion. We may expect a lowering of the frequencies and a splitting of the degenerate vibrations. As can be seen, at least judging from the valence vibrations, the splitting is not large. As for the frequency shift, comparison of the frequencies of the $SiO_4$ group in the $Si(OCH_3)_4$ spectrum with the frequencies of the "isolated" (but probably hydrated, even if only partially so) $SiO_4$ ion (the Raman spectrum of an aqueous solution of sodium silicate[14])—777 and 935 $cm^{-1}$—confirms the supposition of their lowering in the tetramethoxysilane spectrum. In this connection, as was also supposed, the frequency of the symmetrical vibration is lowered by 17.5%, while the frequency of the antisymmetrical vibration is lowered by only 11%.

The transition from $Si(OCH_3)_4$ to the other tetra-n-alkoxysilanes leads to complication of the spectrum, principally on account of the frequencies of the C—C valence vibrations.

Table 2 gives a frequency assignment in the $Si(OC_2H_5)_4$ spectrum. In the $Si(OC_3H_7\text{-}n)_4$ and $Si(OC_4H_9\text{-}n)_4$ spectra (Table 3), one can identify only the frequencies of the symmetrical Si—O vibration, which increase along with the lengthening of the organic radicals, and the intense C—O absorption bands in the neighborhood of 1090-1100 $cm^{-1}$.

## REFERENCES

1. R. Signer and J. Weiler. Helv. Chim. Acta, **16**, 115 (1933).
2. A. N.Lazarev. Opt. i Spektr. **4**, 805 (1958).
3. A. N. Lazarev, T. P. Tulub, and Ya. S. Bobovich. Opt. i Spektr. **4**, 417 (1958).
4. A. N. Lazarev and M. G. Voronkov. Sb. Khimiya i prakticheskoe primenenie kremneorganicheskikh soedinenii. (Collection, Chemistry and Practical Application of Silicon-Organic Compounds), Pt. 3, p. 52. Tsentral. Byuro Tekh. Informatsii (Central Bureau of Technical Information), Leningrad, 1958.
5. A. N. Lazarev. Mat. X. Vsesoyuz. Soveshchaniya po Spektroskopii, 1. Molekulyarnaya Spektroskopiya (Data from the Tenth All-Union Conference on Spectroscopy, 1. Molecular Spectroscopy), pp. 440, 1957.
6. A. N. Lazarev and M. G. Voronkov. Opt. i Spektr. **4**, 180 (1958).
7. K. Iguchi. Result Repts., Electrical Communication Laboratory, Tokyo, No. 320, 1953.
8. K. Iguchi. J. phys. radium **16**, 401 (1955).
9. K. Jamasaki, A. Kotera, M. Jokoi, and J. Ueda. J. Chem. Phys. **18**, 1414 (1950).
10. B. A. Arbuzov and T. G. Shavsha. Doklady Akad. Nauk **68**, 859 (1949); Ibid. **79**, 599 (1951).
11. V. A. Stuart, C. Lalau, and H. Breederveld. Rec. trav. chim. **74**, 747 (1955);
H. Murata, K. Kawai, and M. Jokoi. J. Chem. Soc. Japan, Pure Chem. Sec. **77**, 893 (1956);
H. Murata and K. Kawai. J. Chem. Soc. Japan, Pure Chem. Sec. **77**, 1543 (1956).
12. M. O. Bulanin, B. N. Dolgov, G. A. Speranskaya, and N. P. Kharitonov. Zhur. Fiz. Khim **31**, 1321 (1957).
13. J. Goubeau and H. Behr. Z. anorg. u. allgem. Chem. **272**, 2 (1953).
14. D. Fortnum and J. O. Edwards. J. Inorg. & Nuclear Chem. **2**, 264 (1956).

# INVESTIGATION OF THE ABSORPTION SPECTRA OF ZINC SULFIDE CRYSTALS

E. F. Gross, L. G. Suslina, and K. F. Komarovskikh

Received 13 August 1959

We have investigated the polarization of the line spectrum of ZnS in the absorption region of the hexagonal monocrystalline modification at 4.2°K. We observed a slight shifting of the position of the absorption lines, associated with mechanical strain in the crystals.

The absorption spectra of films of hexagonal ZnS sublimed in vacuum were studied and compared with the spectra of monocrystalline samples of ZnS.

As was found by Piper, Johnson, and Marple[1] and by us,[2] the long wavelength edge of the characteristic absorption band of monocrystalline zinc sulfide has a complex structure and consists of a series of lines and absorption "steps." The present work comprises an investigation of the polarization of the line structure of the absorption region of monocrystalline ZnS, and also a study of the absorption spectra of sublimed polycrystalline films of zinc sulfide.

## POLARIZATION OF THE LINE STRUCTURE OF THE ABSORPTION EDGE OF MONOCRYSTALLINE ZnS

In studying the polarization of ZnS spectra we used single crystals of zinc sulfide, prepared in our laboratory by subliming zinc sulfide powder in a neutral gas atmosphere.[3] The crystals obtained are the hexagonal modification of ZnS, in which the sixfold axis ("c" axis) lies in the face of the crystal and is directed along the grooves which are usually oriented perpendicular to the long side of the crystalline platelet. The crystals of ZnS are usually obtained in the form of colorless transparent plates of various thicknesses—from a fraction of a micron to several hundred microns. This permitted an investigation of the shape and polarization of the absorption spectrum with progressively deeper penetration into the short wavelength region.

To prevent the deformation caused by mounting the sample from affecting the absorption spectrum,[3] the crystals of ZnS were attached to the sample holder at only one end. The other end of the sample remained unfastened, and the absorption spectra were determined only for this free part of the crystal.

The investigation was carried out at low temperature (77° and 4.2°K) in polarized and natural ultraviolet light. Absorption spectra were recorded photographically with the help of a Q-12 quartz spectrograph with a linear dispersion of 25 A in the 3200 A region.

In the investigation of the absorption of single crystals of ZnS it was observed that the line structure of the absorption edge was polarized.

When normal light fell on the monocrystalline plate oriented in such a way that the "c" axis was horizontal (perpendicular to the axis of the spectrograph), the absorption spectra of sufficiently thick crystals (thickness d of the order of 10 $\mu$ or greater) showed only a sharp absorption edge. The position of this edge depended on the thickness of the crystal, and on whether the electrical vector of the incident light was perpendicular or parallel to the "c" axis. For a thickness of $d \gtrsim 10$ $\mu$ and at a temperature of 4.2°K, the absorption edge for light with $E \perp c$ occurs at 3227 A (Fig. 1,a) and with $E \parallel c$ at 3197 A (Fig. 1,b). With oblique incidence of light on a $\approx 10$ $\mu$ crystalline plate, rotated about the vertical axis in such a way that E and c are nonparallel and, while remaining perpendicular to the axis of the spectrograph, form an angle between themselves. The spectrum contained a sharp absorption line at 3205 A, with a width of ≈10 A. The intensity of this line increases with increasing $\angle Ec$ (Fig. 1,c,d).

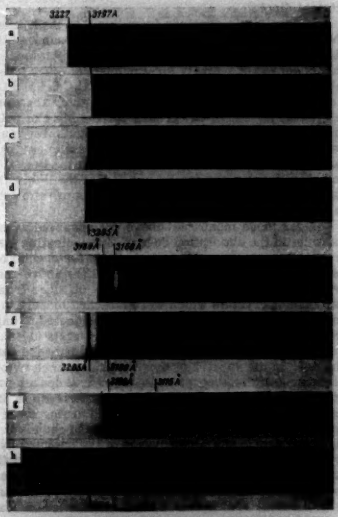


Fig. 1. Absorption spectra of single crystals of ZnS in polarized light at 4.2°K, with varying orientations and sample thicknesses. Orientation of the c axis of the crystal with respect to the electrical field E of the light wave. Sample thickness (in microns): a—$E \perp c$, 10; b—$E \parallel c$, 10; c—$\angle Ec \approx 10°$, 10; d—$\angle Ec \approx 20°$, 10; e—$E \parallel c$, 1; f—$\angle Ec \approx 30°$, 1; g—$E \parallel c$, 0.1; h—$E \perp c$, 0.1.

For crystals ≈1 $\mu$ thick, the spectrum obtained with $E \perp c$ again shows only the long wavelength absorption edge, while in the spectrum with $E \parallel c$ (Fig. 1,e) and with $\angle Ec \neq 0$ (Fig. 1,f) there is also an intense line at 3180 A ($\Delta\lambda \approx 20$ A) and the edge of a weaker continuous absorption at 3160 A. In contrast to 3205 A, which is observed only for $\angle Ec \neq 0$, the line at 3180 A also appears with

normal incidence of the light on the crystal ($E \parallel c$) and does not change appreciably in intensity with oblique incidence, i.e., with increasing $\angle Ec$ (Fig. 1,e,f).

In the spectra of crystals $\approx 0.1\ \mu$ thick it is possible to observe structure in the absorption edge down to 3000 A. The spectrum of the beam for which $E \perp c$ not only shows the line at 3205 A, but also shows a line $\approx 10$ A wide at 3180 A and a new and more diffuse line at 3115 A (Fig. 1,h). In the spectrum of light with $E \parallel c$, lines can be seen at 3180 A and 3115 A (Fig. 1,g); in this state of polarization the latter is more intense and broader ($\Delta\lambda \approx 20$ A).

An analysis of the above described spectra, observed in polarized light with samples of various thicknesses, shows that the line 3205 A is totally polarized, so that electrical vector is oriented perpendicular to the optical axis of the crystal ($E \perp c$); in other words, this line corresponds to absorption by a planar electrical oscillator. The line at 3180 A is unpolarized (or not appreciably polarized), while the line 3115 A is strongly polarized for $E \parallel c$ (the absorption oscillator resembles a linear electrical dipole).

It is possible to conclude from this that the nature of the polarization of the spectrum corresponding to the fundamental absorption edge of hexagonal ZnS is analogous to that observed previously for a number of other uniaxial crystals (tetragonal $HgI_2$,[4] hexagonal CdS[5] and CdSe,[6] and others), having discrete structure in their absorption edge. A comparison of our results for the state of polarization of the lines of zinc sulfide with other investigators[1] shows agreement for 3205 A, but in contrast to our results, the authors of reference 1 infer that the line 3180 A is completely polarized for $E \perp c$, and that the line with the shortest wavelength (3107 A, according to reference 1) is completely polarized for $E \parallel c$.

Besides those mentioned above, we observed several phenomena in the absorption edge of ZnS indicating a significant influence of mechanical strain in the crystal on the structure of the absorption edge. All the above-mentioned positions of absorption lines were obtained from the spectra of crystals which were attached loosely to the quartz sample holder and were not subjected to any appreciable stress. In the case of thin crystals ($d \approx 0.1\ \mu$) there was occasional "adhesion" of samples to the sample holder. In the spectra of these crystals there is a displacement of the absorption lines towards longer wavelengths (Table 1), and simultaneously an increase in diffuseness (for 3205 A). Apparently this is analogous to the effect which was observed in crystals of cadmium sulfide[5] and ascribed to deformation of the samples by the sample holder as a result of the difference in coefficients of thermal expansion of sample holder and crystal when the sample was cooled. This direction of band shift (toward the red) agrees with that observed on heating zinc sulfide, and corresponds with the fact that the coefficient of thermal expansion of ZnS exceeds that of quartz. Hence, upon cooling the sample, the "adhesion" of the crystal to the sample holder causes it to be stretched in a plane by the sample holder, i.e., the interatomic distance increases as in the case of heating.

It should be noted that the absorption spectra of several unstressed crystals are displaced as a whole by 1-2 A in the opposite direction to that indicated in Table 1. This is probably explainable by internal strain arising from the growth of the crystals, and associated with nonequilibrium temperature distribution as a result of the conditions of crystal growth.[3] These slight displacements are observed even within a single group of crystals prepared simultaneously. It is possible that the differences in the positions of the spectral lines in individual crystals is associated with differences in the way in which they were fastened to the support, which in turn caused differences in the degree of stress created at the "free" ends of the crystals. Apparently, the observed effects are the cause of some of the discrepancies between our results and the data of others[1] (at 4.2°K these discrepancies amount to about 1-5 A).

Table 1. Location of Absorption Lines in the Spectrum of Crystalline ZnS (A)

| Experimental conditions | Temperature (°K) | | | | | |
|---|---|---|---|---|---|---|
| | 4.2 | | | 77 | | |
| "Free" (unstressed) crystals | 3205 | 3180 | 3115 | 3214 | 3190 | 3120 |
| Crystals "adhering" to sample holder | 3217 | 3192 | 3120 | 3220 | 3197 | 3126 |

Note: Sample thickness 0.1 $\mu$.

## ABSORPTION SPECTRA OF SUBLIMED POLYCRYSTALLINE FILMS OF ZnS

We have also investigated the absorption spectra of thin vacuum-sublimed films of zinc sulfide. The use of polycrystalline films of any desired thickness makes it possible to reach the region of the fundamental absorption of ZnS. It is consequently possible to hope that a comparison of these results with absorption spectra of single crystals will permit various conclusions concerning the structure of superimposed layers and the influence of the sample holder on the absorption spectrum.

The investigation of the absorption spectrum of polycrystalline films of ZnS has been the subject of many studies.[7-9] Shalimova obtained some narrow absorption maxima, (3340, 3130, and 2840 A) in the fundamental absorption edge of sublimed films of ZnS prepared by different methods. In the opinion of the author, these were due to the cubic modification of ZnS.[7] Arapova[8] similarly observed a discrete structure in the absorption edge of sublimed films of ZnS.

Our polycrystalline films of ZnS were ordinarily obtained in quartz tubes by the sublimation of "scintillator" grade ZnS powder under continuous pumping. The vaporization temperature of the powder was 800-1100°C, and the temperature of the sample holder 600-700°C. On the lower parts of the walls of the apparatus we obtained transparent films showing colored interference patterns, while the upper parts were coated with a thick white deposit. Several films were prepared in evacuated sealed tubes, and some by heating zinc mirrors, which had previously been degassed in vacuum, with sulfur vapor. In all cases we obtained films which were stable in air and were characterized by identical spectra. The absorption spectra obtained for the films were recorded at 77 and 4.2°K with the help of an ISP-22 spectrograph with a dispersion of 18 A/mm in the 3200 A region.

In the absorption spectra of thin transparent films we obtained transmission bands on the short wavelength side (down to wavelengths shorter than 2800 A). At 4.2° K, absorption lines with maxima at 3212 A ($\Delta\lambda \approx 10$ A), 3190 A ($\Delta\lambda \approx 10$ A) and a wider, more diffuse line at 3128 A ($\Delta\lambda \approx 20$A)(Fig. 2,a) can be resolved along the long wavelength edge of the fundamental absorption band. The spectra of several films show a weaker line at 3271 A ($\Delta\lambda \approx 20$ A)(Fig. 2,b) on the long wavelength side of the absorption maxima. This line is only very slightly displaced on heating the crystal from 4.2° to 77°K. The positions of the absorption lines at 4.2° and 77°K are given in Table 2.

Comparison of the data of Tables 1 and 2 shows that the positions and widths of the absorption lines of films are very similar to those of single crystals of ZnS "adhering" to the sample holder. This fact makes it pos-

Fig. 2. Absorption spectra of thin polycrystalline films of ZnS. a—Spectrum of the majority of films; b—spectrum of a few films.

sible to assume that under the conditions described for the preparation, the films of ZnS were obtained in the hexagonal modification. Furthermore, one can conclude that in the case of films tightly attached to the sample holder, stresses must arise as a result of cooling.

Taking into account the reproducibility of the discrete line structure occurring in the spectra of both the single crystals and the films (3212, 3190, and 3128 A), it can be assumed that these lines are associated with the fundamental lattice (exciton excitation). It is also possible that the observed change in the line 3271 A is associated with dislocations in the lattice (e.g., with the excitation of the so-called impurity exciton in the dislocation region).

It is interesting to note that Arkhangel'skaya and Feofilov,[9] in studying the spectra of powdered samples of ZnS, found luminescence at 319 mμ and 321 mμ, which apparently correspond to the absorption lines which we found at 3190 and 3214 A.

Table 2. Positions of Absorption Lines in the Spectra of Sublimed Films of ZnS at 77° and 4.2°K (A)

| 77°K | 4.2°K |
|---|---|
| 3273 | 3271 |
| 3222 | 3212 |
| 3200 | 3190 |
| 3138 | 3128 |

REFERENCES

1. W. W. Piper, P. D. Johnson, and D. T. F. Marple. Phys. and Chem. Solids **8**, 457 (1959).
2. E. F. Gross and L. G. Suslina. Opt. i Spektr. **6**, 115 (1959).
3. E. F. Gross and B. S. Razbirin. Zhur. Tekh. Fiz. **27**, 9, 2173 (1957).
4. E. F. Gross and A. A. Kaplyanskii. Zhur. Tekh. Fiz. **25**, 2, 2061 (1955).
5. E. F. Gross and M. A. Yakobson. Zhur. Tekh. Fiz. **25**, 364 (1955); Doklady Akad. Nauk SSSR 102, 485 (1955).
6. E. F. Gross and V. V. Sobolev. Zhur. Tekh. Fiz. **26**, 1622 (1956).
7. K. V. Shalimova. Doklady Akad. Nauk SSSR **80**, 4, 587 (1951).
8. E. Ya. Arapova. Doklady na VII Konf. po Lyuminests. (Report of the Seventh Conference on Luminescence), Moscow, 1958.
9. V. A. Arkhangel'skaya and P. P. Feofilov. Opt. i Spektr. 1, 107 (1957).

## THE LUMINESCENCE SPECTRA OF DIAMONDS

G. O. Gomon

Received 3 July 1959

A study was made of the luminescence spectra of a series of diamonds from domestic deposits. It was found that the variety in luminescence color and intensity was caused by a change in the absolute and relative intensities of the blue and yellow-green components of the spectrum. The structure of the blue component remained the same in different diamonds, but appreciable variations were observed in the yellow-green band.

We have made a study of the luminescence spectra of a large number of diamonds from domestic deposits. The luminescence of the diamonds was excited by the light of an SVDSH-250 quartz mercury lamp after passage through a UFS-3 light filter. The luminescence spectra of the diamonds were photographed by means of an ISP-51 spectrograph. The focal lengths of the cameras were 270 and 800 mm. The Figure shows the luminescence spectra of different diamonds (a–j) obtained when the samples were cooled down to 80°K.

The luminescence spectra of diamonds of the type shown in Fig. a were first described in detail by Nyar[1] and those of the type shown in Fig. b, by Mani.[2] Dyer and Matthews[3] recently reported on luminescence spectra of diamonds of the type shown in Fig. c.

Figure a shows the spectrum of a diamond with the commonest type of blue luminescence. At room temperature this spectrum consists of the 4156 A line and 4 or 5 equidistant bands on the red side. The weak continuous background extends almost to 6300 A. When the sample is cooled down to 80°K, the bands become sharper. Their maxima are somewhat displaced toward the blue, and are located at approximately 4270, 4380, 4515, and 4640 A. (The spacing between them is of the order of 0.080 ev.) The spectrum also shows several narrow lines at approximately 4210, 4228, 4324, 4336, 4349, 4360, 4379, and 4396 A. At 90°K, the principal line at ≈4156 A is also displaced and is found at ≈4152 A. In spectra photographed at high dispersion it is seen that in some samples this line becomes a doublet.

Figure b shows a diamond luminescence spectrum which, in addition to the blue system of bands, also contains a yellow-green system adjoining a narrow line at 5033 A, the maxima of the bands being at approximately 5120, 5216, 5290, 5370, and 5470 A. The spacing between neighboring bands in the yellow-green component of the luminescence spectrum of diamonds is about 0.040 ev.

It is known that the luminescent intensity of a series of diamond samples excited by 365 mμ radiation may vary over a very wide range (3–4 orders of magnitude), while the color may vary from blue to yellow-green. However, in spite of the considerable variation in the

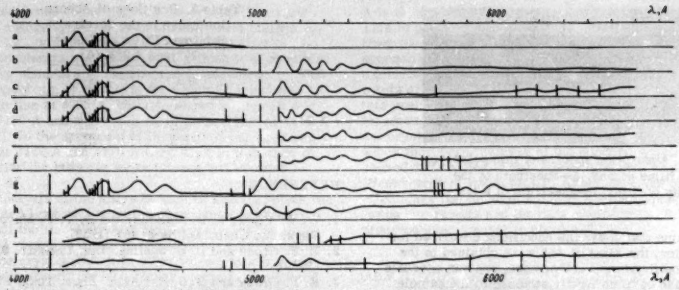


Luminescence spectra of diamonds at 80°K (schematic).

intensity and color of luminescence of individual samples, it has been assumed that the luminescence spectrum of diamonds contains two bands—blue and yellow-green. (See Fig. b.) All variations in the intensity and color of individual samples were ascribed to a variation in the absolute and relative intensities of the blue and yellow-green systems of bands.

In the luminescence spectra of certain diamonds from domestic deposits we found a third system of bands (See Fig. c) with maxima at approximately 6095, 6180, 6260, 6350, and 6445 A. The spacing between neighboring bands amounts to 0.030 ev. We should presumably ascribe certain differences in the positions of the bands between our results and the data given in reference 3 to inaccuracy in the determination of $\lambda$ in the low dispersion region of the spectrograph.

The spectra shown in Figs. a, b, and c adequately represent the diversity in the structure of the luminescence spectra of diamonds from all of the various deposits as reported so far in the literature.

A systematic study of a large number of luminescent spectra of domestic diamonds has led to the following conclusion: The diversity in the intensity and color of luminescence of these diamonds is usually caused by a variation in the absolute and relative intensities of the blue and yellow-green components of the spectrum of the type shown in Fig. d, and not of the type shown in Fig. b.

The structure of the blue component of the luminescence spectrum shown in Fig. d is analogous to the structure of the blue band in the spectra (see Figs. a, b, and c). On the other hand, the yellow-green component not only contains the narrow line 5033 A, but also has an equally narrow and intense line at ≈5108 A, while the intensity of the broader bands at approximately 5115, 5165, 5230, 5298, 5370, 5475, and 5600 A alternates regularly. This led us to assume that in this case there are two systems of bands: one (5115, 5230 A, etc.) adjoins the 5033 A line, the other (5165, 5295 A, etc.) accompanies the narrow line at 5107 A. The spacing between neighboring bands in the two systems is approximately equal and amounts to about 0.030–0.040 ev.

In studying the effect of irradiation by electrons, neutrons, $\gamma$-rays, and subsequent heat treatment on the luminescence of diamonds, Dyer and Matthews[3] found that a system of emission bands appears in the spectrum near 5032 A after such a treatment. This system of bands is analogous to the known yellow-green band in the luminescence spectrum of nonirradiated diamonds. In contrast to the natural system, the system of bands near 5032 A appearing as a result of irradiation followed by heating is also accompanied by a line at 4960 A. In this connection it is interesting to point out that the luminescence spectra of certain diamonds (see Figs. c and d) showed very narrow and intense lines at 4890 and 4960 A, in addition to the previously mentioned lines at 5033 and 5108 A.

The blue radiation component and the 4152 A line are considered characteristic of the luminescence spectra of diamonds. Thus, according to the Raman theory,[4,5] a line at 4152 A, even though very weak, must of necessity appear in the luminescence spectrum of every diamond. The results of our experiments do not agree with this conclusion. Figure e shows a luminescence spectrum of diamond which contains only the yellow-green component (strongly overexposed). In this spectrum it is impossible to find a line near 4152 A, no matter how long the exposures are made. The structure of the yellow-green band is also similar to that shown in Fig. d. It should be noted that the various characteristics of this radiation (duration, temperature extinction, etc.) differ fundamentally from the characteristics of the luminescence of diamonds whose spectra contain a blue component, no matter how weak.

Diamonds with a purely yellow luminescence (spectrum of the type shown in Fig. e) are extremely rare. We found only 5 such samples, 4 of them coming from the Urals. Their luminescence spectra are identical. The luminescence spectrum of one of the samples from Yakutsk (see Fig. f) also contains a group of narrow lines at approximately at 5700, 5720, 5782, 5815, and 5860 A.

The yellow-green component of the luminescence spectrum of diamond (see Fig. g) consists of a narrow line at 4960 A and a group of bands with maxima at 5040, 5120, 5218, 5294, 5370, and 5476 A. (The spacing between neighboring bands is equal to 0.040 ev.) In addition to this series, there are narrow lines at approximately 4907, 4984, 5750, 5764, 5805, and 5850 A and broader weak bands at 5882 and 6000 A.

The 4890 A line is the principal line in the yellow-green component of the spectrum. (See Fig. h.) As seen in the Figure, there are two wider bands near this line at ≈4970 and 5055 A, with a spacing equal to 0.040 ev. There is also an intense line at 5235 A and two bands at ≈5280 and 5380 A.

In the yellow-green component of the luminescence spectrum of one of the diamonds we found lines with the wavelengths 5190, 5235, 5270, 5320, 5360, 5463?, 5570, 5750, 5850, and 6030 A. (See Fig. i.) In another we found lines at 4878, 4907, 4960, 5033, 5463, 5900, 6120, 6217, and 6340 A and wider bands at ≈5120 and 5218 A. (See Fig. j.)

Our data show that the structure of the blue component is the same for all spectra (except e and f) and that it is only the intensity of this band which varies from sample to sample.

Differences in the structure of the yellow-green band in the luminescence spectra of diamonds can be observed only when the samples are cooled (Figs. a-j). At room temperature the yellow-green component consists of a continuous band between 500 and 680 mμ.

The nature of diamond luminescence is not yet clear. According to one opinion, the luminescence of diamonds is caused by the presence in the crystalline lattice of superstoichiometric atoms or impurity atoms. Raman and his coworkers,[4,5] however, consider luminescence an inherent property of the crystal lattice of the diamond. One of the basic arguments of Raman's supporters is the identity of the fluorescent spectra of diamonds from different locations.

Our data show the following: Only the blue component, which contains a regular alternating pattern of bands relative to the narrow line 4152 A, remains unchanged in the luminescence spectra of different diamonds. When the samples are cooled, a fine structure is resolved in certain bands (narrow lines at 4324, 4336, 4349, 4360, 4379, and 4396 A, with a spacing equal to 0.008-0.010 ev).

In the yellow-green band, we observed considerable variations in both the position of the principal narrow line and in the actual structure of the long wavelength component of the luminescence spectrum of different diamonds. This probably indicates a great sensitivity on the part of the luminescence centers responsible for the luminescence centers responsible for the yellow-green component to impurities or other defects of the diamond lattice.

REFERENCES

1. P. G. N. Nayar. Proc. Indian Acad. Sci **A13**, 483 (1941); Ibid. **A14**, 1 (1941); Ibid. **A15**, 310 (1942).
2. A. Mani. Proc. Indian Acad. Sci. **A19**, 231 (1944); Ibid. **A20**, 155 (1944).
3. H. B. Dyer and I. G. Matthews. Proc. Roy Soc. **243**, 1234 (1958).
4. Proc. Indian Acad. Sci. **A19**, No. 5 (1944).
5. Proc. Indian Acad. Sci. **A24**, No. 1 (1946).

# THE MECHANISM OF SCINTILLATIONS IN ORGANIC SUBSTANCES

I. M. Rozman

Received 30 July 1959

A brief summary is given of the theory proposed for explaining the relationship of the specific scintillation value to the ionizing capacity of a particle. A method of investigation is proposed, which considers the local density of activations and, particularly, the presence of "isolated" activations in the over-all path of heavy particles, and the presence of "accumulations" of activated molecules in the path of a high-speed electron.

The problem of the absolute luminescence yield should be considered a fundamental problem of the theory of the radioluminescence of organic substances. The accumulation of resulting experimental data irrefutably confirms the fact that quenching, in addition to photoluminescence, the extent of which depends on the density of excitation and ionization or on the density of activations, plays an essential role in the process of scintillation of organic substances. Moreover, the following regularities occur: (a) the scintillation* value, as a rule, is proportional to the fluorescence yield of a substance.[1-4] The specific scintillation value for high-speed electrons $s_0$ is related to the fluorescence quantum yield $\eta_f$ by the relation*

$$s_0 \approx \frac{1}{40}\eta_f \text{ (e.v.}^{-1}\text{)}, \quad (1)$$

i.e., for conversion of a molecule to the "fluorescent" state five times more energy on an average is consumed than for one activation;[5] (b) for slow heavy particles, the specific scintillation value s(E) is much less than $s_0$. The extent of quenching $s/s_0$ depends somewhat on the individual properties of the scintillators. As a matter of fact, the ratio $\alpha/\beta$* for all crystalling, liquid, and plastic scintillators measured lies within the limits of 0.07-0.15,[6,7] that is, the differences in quenching are not large in comparison with the magnitude of this quenching; (c) the average duration of the scintillations on excitation with $\alpha$-particles and high-speed electrons differs little.[8] Unfortunately, the available experimental data are not of high accuracy; however, it can be stated with confidence that if $\tau_\alpha$ (for $\alpha$-particles with energies of 5 Mev.) is less than $\tau_\beta$, by no more than a factor of two, then

$$\frac{\tau_\alpha}{\tau_\beta} \geqslant D_{\alpha\beta}.$$

According to the hypothesis of Kallmann and coworkers[9-10] a decrease in the luminescence yield of organic substances with an increase in the density of ac-

*By the scintillation value S we mean the number of luminescence photons emitted by a scintillating substance during the complete retardation in it of a charged particle (initial energy $E_0$). Externally or technically the scintillation value is less than S because of the partial absorption of photons within the scintillator. The quantity S can be presented in the form

$$S = \int_0^{E_0} s(E)\, dE$$

where s(E) is the specific scintillation value. Averaging the specific scintillation value, $\bar{s} = S/E_0$.

*They have in mind single-component scintillators. In mixed crystals and solutions $s_0$ depends on the efficiency of transfer of the energy of excitation from the major component to the luminescing component.

*The so-called $\alpha/\beta$ ratio is determined by the relationship

$$D_{\alpha\beta} = \frac{s_\alpha (E_\alpha = 5 \text{ m.e.v.})}{s_0}.$$

tivations was associated with quenching, due to the interaction of the excited molecules with one another. Wright[11] carried out a quantitative investigation for a bimolecular reaction. Moreover, for the concentration of excited molecules we have

$$\frac{dn}{dt} = -\lambda n - \delta n^2, \quad (n = n_0 \quad \text{at} \quad t = 0), \tag{2}$$

where $\lambda$ is the sum of the probabilities of the emission of a photon $k_\nu$ and of intramolecular quenching $k_q$, and $\delta$ is the rate constant of bimolecular quenching. If over a total volume V the density of excitation is uniform, the total number of excited molecules will equal

$$N(t) = \frac{N_0}{(1+Q)e^{\lambda t} - Q}, \tag{3}$$

and the scintillation value

$$S \equiv \int_0^\infty k_\nu N dt = \frac{k_\nu}{\lambda} N_0 \frac{\ln(1+Q)}{Q}, \tag{4}$$

where

$$Q = \frac{\delta}{\lambda} n_0 \text{ and } N_0 = n_0 V.$$

We consider a portion of the path l, for which a particle loses energy $\Delta E = l\,dE/dx$ and excites $N_0 = \omega\Delta E$ of the molecules, uniformly distributed along the volume of the path[11] $V = Al$. According to (4), the specific scintillation value equals

$$s(E) = \frac{k_\nu \omega}{\lambda} \frac{\ln(1+Q)}{Q}, \quad Q = \frac{\omega\delta}{\lambda A}\frac{dE}{dx}. \tag{5}$$

For high speed electrons $Q \ll 1$ and $s_0 = k_\nu(\omega/\lambda)$. On selection of the numerical value $\omega\delta/\lambda A = 0.02$ gm cm$^{-2}$/Mev, formula (5) agrees satisfactorily with experimental data for anthracene down to $dE/dx \approx 700$ Mev/gm cm$^{-2}$, which corresponds to an $\alpha$-particle energy of about 6 Mev and to a proton energy of about 0.2 Mev.[12] However, the theory considered, as was shown in reference 6, is contradicted by the foregoing requirements (points b and c).

As a matter of fact, averaging (3) along the path of a particle, we obtain for the average duration of scintillation

$$\tau_s \equiv \frac{\int_0^\infty tN dt}{\int_0^\infty N dt} = \frac{\tau_0 \bar{Q}}{\ln(1+\bar{Q})} \int_0^\infty \frac{t dt}{(1+\bar{Q})e^{\lambda t} - \bar{Q}},$$

where $\tau_0$ is the duration of the scintillations for $Q \ll 1$. Consequently, for heavy particles

$$\tau_s \leqslant \tau_0 \frac{\pi^2}{6\ln(1+\bar{Q})}.$$

For $\alpha$-particles (5 Mev.) we have

$$D_{\alpha\tau} = \frac{\ln(1+\bar{Q})}{\bar{Q}} = 0.1 \quad \text{or} \quad \bar{Q} = 35,$$

that is, $\tau_\alpha \leqslant 0.47\tau_0$, which apparently contradicts experiment. A still clearer contradiction occurs if one compares the time during which the first half of the scintillation photons is emitted[8]

$$T_{\frac{1}{2}} = \tau_0 \ln \frac{\bar{Q}}{1+\bar{Q}-\sqrt{1+\bar{Q}}}. \tag{6}$$

For $\bar{Q} = 35$, we obtain $T_{\frac{1}{2}}' = 0.16\tau_0$, in contrast to high-speed electrons* for which $T_{\frac{1}{2}}' = 0.69\tau_0$.

*It will be shown below that in the path of a high-speed electron there are regions with a very high activation density. Therefore, we do not accept the ordinarily employed transition to the limit $Q \to 0$ as a description of the scintillations of high-speed electrons. However, the calculation of the local activation density appears to be beyond the scope of the theory described.[11]

According to Birks' theory,[13] the relationship of the luminescence yield of organic substances to the specific loss of energy is determined by the quenching by the "affected molecules," forming during retardation of the exciting particle. In accordance with this, the specific scintillation value will equal

$$s(E) = \frac{s_0}{1 + B\frac{dE}{dx}},$$

and averaging the duration of scintillation

$$\tau_s = \tau_0 \frac{s(E)}{s_0},$$

which contradicts experiment. Thus, neither Birks' "monomolecular" theory,[13] nor Wright's "bimolecular" theory[11] satisfies the fundamental requirement of experiment: with an increase in the specific loss of energy of the exciting particles, a considerable decrease in luminescence yield occurs with a comparatively small (if any) change in the mean duration of the luminosity. The rate of the process of quenching with a high density of activations, exceeds by many times the rate of emission of photons by the excited molecules, i.e., it is much greater than the value $k_\nu$ ($k_\nu \leqslant 5 \cdot 10^8$ sec$^{-1}$). Complete quenching does not occur, either because the quenching process proceeds during a small interval of time ($\ll k_\nu^{-1}$), or because some of the activations do not fall under its influence. Since "bimolecular" quenching proved to be insufficiently rapid, it can be suggested, based on the hypothesis of quenching at the expense of interaction of the excited molecules, that the quenching is related to "collective" interaction and is of a higher order. Kallmann and Brucker[8] showed that $D_{\alpha\beta} \approx 0.1$ and $\tau_\alpha \approx \tau_\beta$ for a quenching reaction of the fifth order. In the author's opinion, this phenomenon is difficult to explain, especially with regard to the fact that a larger reaction rate constant is obtained.

We have not mentioned until now the emissionless migration of energy of excitation. If the coefficient of diffusion of "quanta of excitation" is large enough, this process can lead to the discharge of a large portion of the "quanta" beyond the limit of the path of the particle, and by the same token, change the conditions of quenching.[9,14] It could be suggested that, within the path, so rapid a process of quenching occurs, that the scintillation value is practically completely determined by the emission of photons due to the "discharging quanta" of excitation. In this case, fulfillment of the condition $\tau_\alpha \approx \tau_\beta$ is accomplished. However, as noted in reference 15, the coefficient of diffusion of the energy of excitation in organic monocrystals is 20 times greater than in plastic scintillators. At the same time, the values of their $\alpha$, $\beta$-ratios differ very little.

The radiationless quenching of the excited state of scintillator molecules can be caused by a local increase in the temperature in the path of the particle, with a high specific loss of energy. Galinin[15] made a quantitative investigation of the role of such quenching. The author[15] proceeded from the assumption that in the central part of the path ($r \leqslant R$), where the temperature drop exceeds a

certain value $\Delta T$, the fluorescence quantum yield is less by a factor of a hundred than the quantum yield at "ordinary" temperature $\eta_0$. In the peripheral part of the path ($r > R$) the quantum yield remains equal to $\eta_0$. The radius of quenching R is related to $\Delta T$, the heat capacity C, and the specific loss of energy dE/dx by the relationship

$$R^2 = \text{const} \cdot \frac{\frac{dE}{dx}}{C \cdot \Delta T}, \qquad (7)$$

i.e., with an increase of the dE/dx value, the radius of quenching increases and the specific scintillation value decreases. Moreover, the instantaneous quenching at $r \leq R$ and the complete absence of quenching at $r > R$ could have provided the independence of the duration of luminosity from the specific loss of energy.

The basic assumption of the theory[15] concerning the nature of the thermal quenching is justified for certain crystals: the luminescence yield depends little on the temperature down to the melting point, but the yield of the melt is many times smaller.[9, 16] In noncrystalline luminescing substances (polystyrene, polyvinyltoluene) the yield decreases smoothly with an increase in temperature.[16, 17] However, the theory of thermal quenching is also inadmissible for crystals, since from (7), in contradiction to experiment, it follows that the $\alpha$, $\beta$-ratio should depend on the individual properties of the scintillator (heat capacity, melting point) and especially on the temperature of the scintillator.*

*In Galanin's theory[15] the "instantaneous" source of heat is considered. The duration of the "thermal peak" is obtained as ~$10^{-11}$ sec. Consequently, the complete transfer of energy from the electrons to the atomic nucleus of the molecule (or to the lattice) should occur after a time of ~$10^{-12}$ sec. This possibility is not obvious (see, for example, an analogous problem for metals in reference 18.

A number of processes of quenching occur simultaneously[12] in the path of the ionizing particle: a local increase in temperature occurs and, consequently, the probability of intramolecular quenching increases; reaction of the activated molecules proceeds, which leads to emissionless deactivation which, generally speaking, can be accompanied by dissociations of the molecules or by other effects of radiation "disturbance." "Disturbed" molecules can also be formed directly by charged particles or by the secondary electrons accompanying them. On the strength of the Frank-Rabinowitch principle, it should be assumed that, together with these "stationary" disturbances of the particle, a large number of "temporary disturbances" are evoked, which during the time of its life ($10^{-11}$-$10^{-10}$ sec) can influence the kinetics of luminosity. The excited molecules are also disturbed by the action of electric fields of ions, some of which display a greater length of life. Unfortunately, these phenomena have not been studied so thoroughly that one can a priori assign the fundamental or major processes of quenching to different stages of scintillation. The failure of the above-mentioned theories* is explained not only by the fact that for the initial stage of scintillation they assume, possibly, an inadequate major process, but also by the fact that no complete spatial distribution of the activations was produced: the real distribution is replaced by the average value, proportional to the linear specific loss of energy dE/dx. It is true that in Galanin's theory[15] the change in the activation density with distance from the trajectory of the particle is considered, but the presence of secondary electrons was not considered. At the same time, it is known that the interpretation of much experimental data in radiation chemistry and biology was related to the assumption of effects produced by $\delta$-electrons.[22-24] From the field of luminescence the following example can be considered. The quantity dE/dx = 1000 Mev/cm (in anthracene) corresponds to an $\alpha$-particle energy of 5.2 Mev and a proton energy of 0.17 Mev. At these energies the specific scintillation values are equal to

$$s_\alpha = 0.18 s_0 \text{ and } s_p = 0.15 s_0.$$

This illustrates well the fact that, for identical values of dE/dx, the luminescence yield for $\alpha$-particles is greater than for protons.[25] The difference can be explained by the fact that the retardation of an $\alpha$-particle is accompanied by the appearance of faster $\delta$-electrons. In our example, the maximum energies of the $\delta$-electrons was equal to 2.9 kev for an $\alpha$-particle and 0.37 kev for a proton. The secondary electrons with energies from 0.37 to 2.9 kev "carry off" 23% of the total loss of energy of the $\alpha$-particle.[25]

The spatial distribution of the activations, with retardation of the charged particle in a condensed substance, is presented in the following form.[23] The "path" of a sufficiently fast electron consists of the individual excited and ionized molecules (atoms) and of a certain number of "accumulations" of activated molecules. These "accumulations" are produced by slow electrons ($T \leq 100$ ev), which due to elastic scattering cannot be freed from the positive ion and lose their energy in its vicinity. The fast $\delta$-electrons split up the paths. For slow heavy particles, the primary activations are arranged so densely that they, together with the "accumulations," caused by slow secondary electrons, comprise the total column. The $\delta$-electrons in this case also split up the paths. Thus, both for fast electrons, and for slow heavy particles, in the total "path" two regions can be distinguished: a region of high activation density of the "column" and "accumulations" and a region of practically isolated activations.

Classification of the path of fast electrons into "accumulations" and isolated activations enabled Kilin and the author[26] to show that, at the expense of bimolecular quenching in the "accumulations," they were able to explain the quantity of the energy yield (see reference 1) in satisfactory agreement with data on the kinetics of scintillation. For slow heavy particles the separate consideration of the fundamental path ("column") and of the paths of $\delta$-electrons is expedient. If it is assumed that the activations in the fundamental path are caused by the particles themselves and by slow secondary electrons ($T < T_0$), then the specific scintillation value can be written in the form

$$s(E) = (1 - f)\, s_1 + f s_2, \qquad (8)$$

where $f(E, T_0)$ is the fraction which comprises the total energy of the $\delta$-electrons with $T > T_0$ in the total loss of energy dE/dx, $s_1$ is the specific scintillation value for the fundamental path, and $s_2$ is the average specific scintillation value for $\delta$-electrons, i.e.,

$$f s_2 = \int_{T_0}^{T_m} n_1(E, T)\, S(T)\, dT. \qquad (9)$$

Here $n_1 dT$ is the number of $\delta$-electrons with energies from T to T + dT in the calculation per unit loss of energy of the primary particle, S(T) is the scintillation value for an electron of initial energy T, and $T_m$ is the

*Nothing was mentioned above concerning Birks' theory of "primary photons."[19, 20] Such photons cannot be observed in direct experiments.[21] Birks' theory is contradicted by many experimental data in radiation chemistry and luminescence.

maximum energy of δ-electrons. The proposed "classification" is possible in the case where electrons with $T < T_0$ are retarded within limits of the radius of action of the primary particle, but the electrons with $T > T_0$ barely lose energy within this region. Elastic scattering by atoms chiefly impedes the departure of slow electrons from the fundamental path. Since the cross section of elastic scattering $\sim T^{-2}$, then the transition region of energies in the vicinity of $T_0$ can prove to be sufficiently narrow. In fact, the evaluation of the lateral displacement of an electron at the expense of repeated scattering in the medium, consisting of an equal quantity of C and H atoms (1 gm/cm²), carried out by the method of reference 27, gives the following result: with electron energies of 110, 220, 440, and 1100 ev, the lateral displacement amounts to about 10, 20, 50, and 200 A, respectively, i.e., it rapidly increases with an increase in energy.

From (8) it follows that, even with momentary quenching in the fundamental path, the yield was different from zero, i.e.,

$$\varepsilon = f\sigma_3.$$

The assumption of practically complete quenching in the fundamental path (at the expense of the thermal wave, disturbing their electrical fields in the column) agrees qualitatively with many experimental facts ($\tau_\alpha \approx \tau_\beta$, $D_{\alpha\beta}$ = const. independently of the substance and the temperature[25, 17]), but is contradicted by other facts (by the increase in the α, β-ratio with an increase in the concentration of the luminescing substance in liquid* scintillators[7] and, especially, the considerably higher yield for protons than for α-particles with the same spectrum of secondary electrons[28]). For example, from data of reference 28 for anthracene $s_\alpha(0.4\ \text{Mev}) = 0.028\ s_0$ and $s_\beta(0.1\ \text{Mev}) = 0.12\ s_0$ is obtained. The difference consists in the specific loss of energy (3100 and 1200 Mev/cm). In any case, experiment required that the process of additional quenching with excitation by slow particles be very fast, but quenching would not be complete. In the proposed method of classification of the path into a fundamental path and a path of δ-electrons this requirement to a considerable extent was considered, since activations caused by δ-electrons do not come under the influence of processes in the fundamental path. The quantitative consideration of the method goes beyond the scope of the present report, and will be presented separately.

*Apparently, the reverse relationship[29, 30] occurs in plastic scintillators.

The author thanks S. F. Kilin for criticism and discussion of the manuscript.

REFERENCES

1. G. T. Wright. Proc. Phys. Soc. A68, 701 (1955).
2. Z. A. Chizhikova and M. D. Galanin. Zhur. Ekspti. i Teoret. Fiz. 30, 187 (1956).
3. M. Furst, H. Kallmann, and F. H. Brown. J. Chem. Phys. 26, 1321 (1957).
4. E. A. Andreeshchev and I. M. Rozman. Opt. i Spektr. 5, 39 (1958).
5. I. M. Rozman, E. A. Andreeshchev, and S. F. Kilin. Izvest. Akad. Nauk SSSR, Ser. Fiz. 23, 102 (1959).
6. H. Kallmann and G. J. Brucker. Phys. Rev. 108, 1122 (1957).
7. M. D. Galanin and Z. A. Chizhikova. Opt. i Spektr. 4, 196 (1958).
8. I. Broser, L. Horforth, H. Kallmann, and U. M. Matrius. Z. Naturforsch 3a, 6 (1948).
9. L. Herforth and H. Kallmann. Ann. Phys. 4, 231 (1949).
10. M. Furst and H. Kallmann. Phys. Rev. 85, 816 (1952).
11. G. T. Wright. Phys. Rev. 91, 1282 (1953).
12. F. D. Brooks. Progr. in Nuclear Phys. 5, 252 (1956).
13. J. B. Birks. Phys. Rev. 84, 364 (1951); Proc. Phys. Soc. A64, 874 (1951).
14. F. A. Black. Phil. Mag. 44, 263 (1953).
15. M. D. Galanin. Opt. i Spektr. 4, 758 (1958).
16. A. F. Kulakova and I. M. Rozman. Opt. i Spektr. 8, 140 (1960).
17. I. M. Rozman. Opt. i Spektr. 2, 480 (1957).
18. I. M. Lifshits, M. I. Kaganov, and L. V. Tanatarov. Atomnaya Energ. 6, 391 (1959).
19. Dzh. Birks. "Stsintillyatsionnye schetchiki." (Scintillation Counters), Izd. Inostrannoi Lit., Moscow, 1955.
20. J. B. Birks. Phys. Rev. 94, 1567 (1954).
21. L. O. Brown and N. Miller. Trans. Faraday Soc. 51, 1623 (1955).
22. W. M. Dale, L. H. Gray, and W. J. Meredith. Phil. Trans. Roy. Soc. A242, 33 (1949).
23. D. E. Lea. "Actions of Radiations on Living Cells." Cambridge Univ. Press, 1946.
24. R. A. Deering. Radiation Research 5, 238 (1956).
25. I. M. Rozman. Kand. diss. (Candidate)s Dissertation), Moscow, 1957.
26. S. F. Kilin and I. M. Rozman. Opt. i Spektr. 6, 65 (1959).
27. H. W. Lewis. Phys. Rev. 78, 526 (1950).
28. E. J. Zimmerman. Phys. Rev. 99, 1199 (1955).
29. R. K. Swank and W. L. Buck. Phys. Rev. 91, 926 (1953).

# EFFECT OF HIGH-TEMPERATURE ANNEALING ON THE LUMINESCENCE AND COLORATION OF X-RAYED QUARTZ CRYSTALS

M. N. D'yachenko

Received 26 January 1959

It is shown that high-temperature annealing of x-rayed quartz produces additional trapping levels and increases coloration and luminescence. The role of coloration by impurities and lattice defects in luminescence phenomena in crystals is explained.

## INTRODUCTION

Among the great variety of forms of natural single crystals of quartz some are found with a smoky or violet coloration. It has been shown that both the absorption band at 548 mμ in the spectrum of quartz x-rayed in a reducing medium and the band at 550 mμ in the spectrum of the natural violet α-quartz (amethyst) are explainable in terms of F-centers, that is, electrons located at oxygen vacancies (1, 2). This band is not observed in the spectra of smoky α-quartz crystallized in an oxidizing medium (smoky crystals of this type do not have oxygen vacancies in the lattice). Absorption bands in the spectra of smoky quartz are located at 425 mμ and 625 mμ. They disappear on heating to 400°K and reappear during x-irradiation.[1] The presence of bands at 380 and 480 mμ has also been noted.[3] It should be remarked that the observed paramagnetism of amethyst is due to the presence of $Fe^{3+}$ ions (F-centers).[4]

According to O'Brien,[5] the smoky coloration of x-rayed quartz is due to the presence of $Al^{3+}$ ions substituted for $Si^{4+}$ ions. This has been confirmed by an investigation of paramagnetic absorption spectra.[6] Charge compensation in this case is taken care of by means of the alkali ion impurities present. The presence of impurities in quartz crystals has been confirmed in references 7 and 8. A number of workers have investigated the luminescence and coloration,[8-12] as well as the optical and anisotropic absorption[5, 10, 11, 13-15] of fused and crystalline quartz.

We conclude that on the whole the results given in the literature on the luminescence of crystalline quartz in the visible region are quire inconsistent. The luminescence of quartz crystals in the ultraviolet has not been sufficiently investigated. It is obviously conceivable that impurity atoms and dislocations in the crystalline structure play a basic role in luminescence phenomena in quartz.

The problems considered in the present work are (1) investigation of the trapping levels in x-rayed quartz crystals by thermal de-excitation of the luminescence in the ultraviolet and visible regions; (2) study of the effect of high-temperature annealing and structural defects on electron and hole trapping levels; (3) explanation of the effect of the presence of impurities and artificial coloration on the trapping levels in quartz crystals.

## EXPERIMENTAL PART

In our experiments a photon counter sensitive to radiation in the 1800-4000 A region[16] is used to measure ultraviolet luminescence. Luminescence in the visible region of the spectrum is measured with the aid of a type FEU-19 photomultiplier.

Transparent single crystals of quartz of magmatic and thermal origin were used in the experiments. The heating was carried out at a constant rate of 2 deg/min. The sample was excited with 150 kv x-rays, using an anode current of 10 ma. The duration of the irradiation ranged from 30 min to 3 hr at room temperature, with a supplementary irradiation for 15 min at liquid nitrogen temperature.

## ULTRAVIOLET AND VISIBLE LUMINESCENCE OF X-RAYED QUARTZ CRYSTALS

Figure 1 gives curves for the thermal de-excitation of the ultraviolet luminescence of x-rayed quartz crystals, both unannealed and annealed at a temperature of 500°C for 3 hr. The additional maxima which appear in the luminescence spectra of the annealed samples as compared with the unannealed (control) sample are the result of a change in the lattice structure of the quartz. High-temperature annealing of the crystals causes the appearance of free vacancies in the quartz lattice and the introduction of impurities from the intercrystalline surfaces into the lattice. The formation of a solid substitutional solution is possible upon prolonged annealing at 500-800°C. During cooling and heating of the quartz to high temperatures, polymorphic transformations also take place. These may influence both the formation of lattice defects and the redistribution of impurities in the crystal.

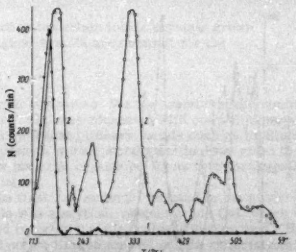


Fig. 1. Thermal de-excitation of the luminescence of x-rayed quartz crystals in the ultraviolet region. Curve 1, unannealed (control) specimen; curve 2, annealed at 500°C for 3 hr. Excitation: 30 min at 20°C and 15 min at −196°C.

Repeated experiments on the thermal de-excitation of a single crystal, carried out in connection with repeated x-irradiation, cooling and heating (77-600°K) show that under these conditions new emission maxima appear be-

tween 200 and 600°K. The increase in trapping levels in this case can be explained only in terms of lattice defects, since the impurity atoms deposited at grain boundaries obviously cannot form a solid solution with $SiO_2$ at these temperatures. Cooling and heating the crystals may also produce additional mechanical stresses and deformations in the quartz, affecting the trapping levels.

Figure 2 shows the results of an investigation of the thermal de-excitation of the ultraviolet luminescence of annealed quartz excited by $\beta$-particles (curve 1) and x-rays (curve 2) and apparently containing more natural impurities than occurred in other crystals. The low intensity of the luminescence in the 240-500°K region (curve 2) was due to three hour x-irradiation.

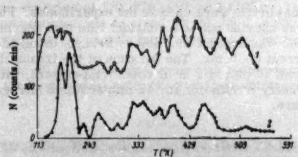


Fig. 2. Ultraviolet fluorescence of unannealed crystalline quartz for different means of excitation. Curve 1, continuous irradiation by $\beta$-particles of $Sr^{90}$; curve 2, x-irradiation for 3 hr at 20°C and 15 min at −196°C.

Figure 3 shows the effect of high-temperature annealing at 800°C for 10 hr on the luminescence of quartz. In the spectra of the control (unannealed) specimens, one peak in the luminescence is to be noted at 140°K and two weak peaks at 200 and 260°K. Unannealed x-rayed quartz crystals have only one or two luminescence maxima in the visible region at temperatures of 140-200°K. At higher temperatures, luminescence is either absent or very weak. On the whole, annealed x-rayed quartz crystals assume a more intense smoky coloration and luminesce more in the ultraviolet and visible regions than do unannealed crystals.

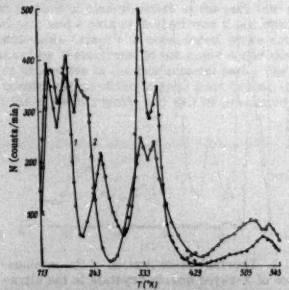


Fig. 3. Thermal de-excitation of the luminescence of x-rayed quartz crystals in the ultraviolet region after annealing at 800°C. Curves 1 and 2, different samples. Excitation: 30 min at 20°C and 15 min at −196°C.

The de-excitation of the luminescence of quartz crystals annealed at 600°C, x-rayed, and excited by $\beta$-particles, respectively is shown in Fig. 4. It is clear

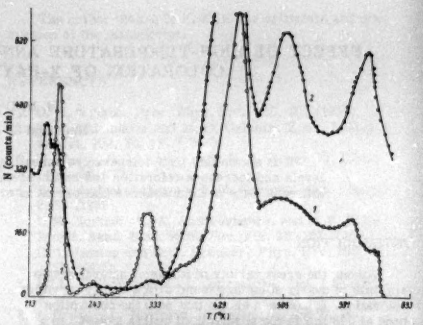


Fig. 4. Thermal de-excitation of excited quartz crystals in the visible region after annealing at 600°C for 3 hr. Curve 1, x-rayed for 30 min at 20°C and 15 min at −196°C; curve 2, irradiated during thermal de-excitation by $\beta$-particles of $Sr^{90}$ (ordinate scale multiplied by 4).

from the figure that the luminescence maxima have a significant width in the visible region. The maxima in the ultraviolet region are narrower and very numerous. The explanation is that the character of the thermal de-excitation curves in the visible region depends only on the properties of the electron levels, whereas in the ultraviolet region it depends on the occurrence of electron and hole levels.

The effect of the presence of coloration in annealed quartz crystals on luminescence and trapping levels is shown in Fig. 5. The difference between curves 1 and 2 results from the difference in the coloration times of the specimens (a more extended coloration time producing a more intense coloration). The intensity of the coloration and the duration of the excitation of the crystals in this experiment were twice as great in one case as in the other.

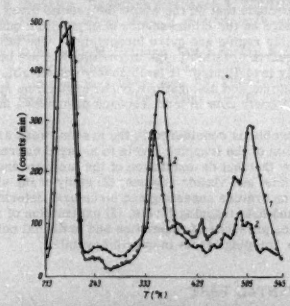


Fig. 5. Thermal de-excitation of the luminescence of x-rayed quartz crystals in the ultraviolet region in the presence of coloration. Curve 1, specimen annealed for 3 hr at 500°C, x-rayed for 30 min at 20°C and 15 min at −196°C; curve 2, same specimen x-rayed for 1 hr at 20°C and 15 min at −196°C.

This led to a decrease in the intensity of the luminescence peaks between 430 and 550°K (curve 2). Since the centers of artificial coloration are destroyed at 400°K, while the formation of the smoky coloration is impeded at lower temperatures, the presence of the latter is connected to some degree with the occurrence of luminescence at 300-400°K. This is confirmed by the fact that the height of the observed luminescence peaks in this temperature region is approximately proportional to the intensity of the coloration. It should be noted that the occurrence of coloration in quartz does not affect the intensity of luminescence between 113 and 240°K.

The decrease in the intensity of luminescence between 430 and 550°K is evidently connected with a decrease in the free (hole) vacancies as a result of their being filled by electrons during the prolonged x-irradiation process. Such transfers of electrons into low levels during x-irradiation are accompanied by fluorescence in the ultraviolet region of the spectrum. Special experiments which we conducted showed that annealed x-irradiated quartz has thermoluminescence bands with maxima at wavelengths of approximately 210, 230, and 300 mμ between 113 and 200°K and bands at 210 and 230 mμ in the 300-400 and 500-600°K ranges, caused by the transition of electrons into low levels of the crystal. The results which we have obtained for the luminescence spectra are in agreement with those given by absorption spectra.[15]

## CONCLUSIONS

High-temperature annealing of quartz produces new peaks of thermal de-excitation in the ultraviolet and visible regions, caused by the formation of thermal lattice defects (vacancies) and the redistribution of the impurities occurring in the crystal together with their transition into a solid solution as a result of isomorphic displacement.

Polymorphic transformations taking place in quartz lead to a reorganization of the crystalline structure (lattice) and may also produce lattice defects (vacancies) and a redistribution of impurities in the crystal.

All these causes lead to the production of new trapping levels in annealed x-irradiated quartz.

## REFERENCES

1. A. I. Cohen. J. Chem. Phys. **22**, 570 (1954).
2. R. Yokota. Phys. Rev. **91**, 1013 (1953).
3. L. Chentsova. Trudy Inst. Krist., Akad. Nauk SSSR **11**, 195 (1955).
4. M. Leela. Nature **172**, 464 (1953).
5. M. C. M. O'Brien. Proc. Roy. Soc. **A231**, 404 (1955).
6. I. Griffiths, J. Owen, and I. Ward. Nature **173**, 439 (1954).
7. V. Garino-Canina. Rev. opt. **34**, 365 (1955).
8. M. Lautout. Compt. Rend., **239**, 875 (1954).
9. V. Garino-Canina. C. R. Acad. Sci. **239**, 875 (1954).
10. M. Lautout. C. R. Acad. Sci. **238**, 2409 (1954).
11. P. Levy. J. Chem. Phys. **23**, 764 (1955).
12. L. Chentsova, B. Grechushnikov, and E. Batrak. Opt. i Spektr. **3**, 619 (1957).
13. E. Mitchell and E. Paige. Proc. Phys. Soc. **B67**, 262 (1954).
14. A. Cohen. J. Chem. Phys. **23**, 289 (1955).
15. E. Mitchell and E. Paige. Phil. Mag. **46**, 1353 (1955).
16. M. D'yachenko. J. Phys. (USSR) **3**, 479 (1940).

# LUMINESCENCE PROPERTIES OF CESIUM IODIDE CRYSTALS GROWN FROM A SUPERHEATED MELT

Yu. A. Tsirlin, V. I. Startsev, and L. M. Soifer

Received 13 July 1959

The kinetics of the production of luminescence properties in cesium iodide crystals grown from a superheated melt is investigated. A number of original results are obtained for the explanation of this phenomenon.

In a series of papers published in 1956-1959,[1-3] Knoepfel, Loepfe, and Stoll reported on the luminescence of single crystals of cesium iodide grown from a melt previously heated to 800-900°C. According to these authors, this luminescence cannot be ascribed to contamination (for example, by traces of thallium). The phenomenon described is of considerable interest from the practical point of view, since according to reference 3, crystals of cesium iodide grown from a superheated melt have a high quantum yield for $\alpha$-particles (9.3%).

An essential point in the explanation of the nature of the luminescence is the statement of the above-mentioned authors concerning the identity of the mechanisms of luminescence in CsI(Tl) crystals and in CsI crystals grown from a superheated melt.

The purpose of the present work is the investigation of the kinetics of the production of luminescence properties in CsI crystals grown from a superheated melt and the obtaining of original data to explain this phenomenon.

1. According to the results of a number of authors,[4-8] unactivated crystals of CsI have noticeable luminescence at room temperature. We surmised that the luminescence of "pure" CsI was connected with contamination of the crystal by traces of heavy metals such as thallium. Hence, in the present work special attention was given to obtaining raw material of such purity as to be practically nonscintillating.

The first raw material we used in the growing of crystals was analytical reagent grade CsI, which was purified twice by the chromatographic method.[9] However, we had only a limited amount of this material available, and were only able to grow a few crystals from it (1st series). The presence of thallium in these crystals was revealed by their absorption spectra (Fig. 1). A comparison of curve 1 of Fig. 2 for CsI(Tl) with a thallium concentration of 0.001% by weight (standard), determined by a chemical method, and curves 1-3 of Fig. 1 permits the estimation of the concentration of thallium in crystals grown from the raw material of this series. Crystal no. 1 (not superheated) has $2.3 \times 10^{-4}$% thallium, no. 3 (superheated for 10 min)* has $2.1 \times 10^{-4}$% and no. 14 (super-

*Translator's note: 15 min according to legend of Fig. 1.

heated for 5 hr) has $2.7 \times 10^{-3}$%. The concentration of thallium was determined optically, using the magnitude of the absorption at the very prominent long wavelength maximum located at about 299 mμ in the absorption spectrum. This method is sensitive down to $2 \times 10^{-4}$% thallium.

The application of zone refining (8 passes) enabled us to obtain raw material with a thallium content of $2 \times 10^{-3}$% (2nd series).* The absorption spectra of the crystals of the second series are similar to curve 3 of Fig. 1. An improvement of the chromatographic purification[7] gave a very pure sample: Cu, Ni, Mn, Co, and Fe were not present at all, according to the results of a chemical analysis (sensitivity $5 \times 10^{-6}$% by weight). Also, thallium was not observed in the absorption spectrum. However, crystals grown from this raw material gave scintillation of appreciable intensity under γ-irradiation.

*A more complete purification of the raw material than was accomplished in reference 8 permitted us to determine the variation of luminescence with concentration at low concentrations with greater accuracy. The curve of relative yield I(conc.) passes through zero and increases almost linearly to a maximum.

Fig. 1

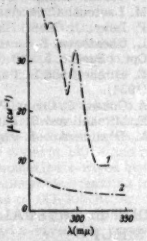


Fig. 2

Fig. 1. Absorption spectra of crystals of cesium iodide of the 1st series. Number of the crystalline specimen (time of superheating given in parentheses): curve 1, no. 1 (not superheated; curve 2, no. 3, (15 min);* curve 3, no. 14 (5 hr). Temperature of superheat of the melt 900°C.

*Translator's note: 10 min according to text.

Fig. 2. Absorption spectra of crystals of CsI(Tl) containing $10^{-3}$% thallium (curve 1) and CsI of the 3rd series (curve 2)(time of superheating, 4 hr).

In order to produce especially pure CsI, the raw material, after the improved chromatographic purification, was subjected to additional purification by repeated recrystallization. The upper part of the crystal, in which the impurities were concentrated, was removed, and a single crystal was again grown from the remaining part. We performed a series of four such recrystallizations. Single crystals grown from raw material purified in this manner (3rd series) did not give any scintillation under γ-irradiation (the amplitude of the photomultiplier pulse was less than 1-2% of the signal obtained in the case of CsI(Tl) crystals with the optimum concentration of thallium). The upper limit of the thallium concentration in the crystals of the third series may be estimated from the concentration curve of reference 8. An estimate made in this manner showed that the thallium content of the crystals of this series did not exceed $10^{-7}$% (Fig. 2).

Thus, on the basis of the experiments mentioned, we may state that the luminescence of unactivated CsI crystals which has been observed at room temperature by several authors[4-6] is connected with the presence of uncontrolled impurities. It must be emphasized that the scintillation method is thus the most sensitive method for the detection of thallium in CsI crystals.

2. We will now consider the results of a study of crystals grown from a superheated molt. The CsI crystals were grown by Stockbarger's method. The heating elements of the furnace were arranged so as to obtain a gradient of 60 deg/cm in the region of the diaphragm.

In view of the high purity requirements, particular attention was paid to the cleanness of the quartz ampoule in which the crystal growing was carried out. The ampoule was carefully washed with chromate solution, after which it was rinsed several times with distilled water and dried. After being filled with the starting material, it was evacuated to a pressure of 0.01 mm of mercury, heated at that pressure to 200°C in order to remove the moisture from the raw material, and then sealed off.

Before the growing of a crystal, the melt was subjected to superheating. For this the furnace was heated to 900°C, after which the ampoule was placed in it for a designated time. Then the current supply to the furnace was quickly lowered to a value at which crystal growth was initiated. The required value of the current was determined in preliminary experiments. The rate of growth was 3-5 mm/hr. After the crystal was grown, it and the furnace were cooled to room temperature over a period of 5 hr. The grown crystal had a diameter of 15 mm and a height of as much as 60 mm. Samples 15 mm in diameter and 15 mm high were cut from it and mounted like ordinary scintillation crystals.[9] The quantum yield was measured with the aid of a pulse-height analyzer, using an FEU-29 photomultiplier as detector. The ratio of the pulse height of the photopeak produced by $Cs^{137}$ γ-rays in the experimental crystal to the height produced in a standard 30 mm diam. by 15 mm crystal was taken as a measure of the relative quantum yield f of the CsI crystal.

3. The results obtained for crystals grown from the melts of all series are presented in Fig. 3, which shows the dependence of the relative quantum yield on the superheating time.

As has been mentioned above the absorption spectra of the crystals of the first series are given in Fig. 1. It is clear from this figure that with an increase in the time of superheating, the magnitude of the absorption μ (and hence the concentration of thallium) decreases sharply from a value of $2.3 \times 10^{-4}$% (without superheating, curve 1) to $3 \times 10^{-5}$% (5 hr of superheating, curve 3). From the shape of curves 2 and 3 of Fig. 3, it is clear that there is an optimal time of superheating (1-2 hr), after which the quantum yield begins to decrease.

It was noted in all three series that samples cut from different places in a crystal had different quantum efficiencies. Thus, for example, for three samples cut from a long crystal of the second series, the quantum yield increased as a function of the nearness to the upper part of the crystal, the values being 13.2%, 14.8%, and 18.7%, respectively. The values of the quantum yield which are plotted in Fig. 3 are average values for 2 or 3 samples cut from the given crystal.

4. Our experiments qualitatively confirm the results of reference 3 on the origin of the luminescence properties of CsI crystals grown from a superheated melt. How-

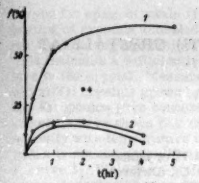


Fig. 3

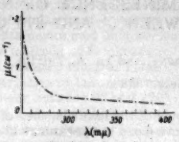


Fig. 4

Fig. 3. Dependence of the quantum yield of crystals of cesium iodide on the time of superheating. (The number adjacent to each curve is the number of the series.)
Fig. 4. Absorption spectrum of a cesium iodide crystal grown in the presence of silicon.

ever, the quantitative value of the quantum efficiency obtained in the present work is considerably smaller than that obtained by the authors of references 1-3.

The results which we have obtained also agree with the statement made in reference 3, excluding the hypothesis that the luminescence properties of unactivated CsI crystals might be ascribable to slight contamination of the crystals with thallium: it follows from the spectrogram of Fig. 1 that the increase in scintillation yield with superheating of the melt (series 1) is accompanied by a decrease in the amount of thallium in the single crystals. In the crystals of the second and third series the thallium content is less than $10^{-6}$ by weight. This excludes the possibility of luminescence by thallium activation. In connection with this, the dependence of the luminescence properties of CsI on the time of superheating of the melt (Fig. 3) seems to indicate a change in the composition of the melt as a result of reaction with the walls of the quartz ampoule. Actually it is difficult to suppose that a change in composition by means of evaporation within the free volume of the sealed-off ampoule would proceed as slowly as would follow from the curves of Fig. 3. In support of this it may also be noted that experiments on superheating a melt in vacuum for a short time did not lead to any speeding up of the process.

The hypothesis that the iodine vacancies play an essential role is also contradicted by the following facts: (1) the negative result of the experiments on superheating a melt for a short time in vacuum; (2) the absence of the decrease in quantum yield with time (aging) which was observed by the authors of reference 3 and which they ascribed to a disappearance of ionic vacancies (the quantum efficiency of the crystals we have grown has not changed over a period of 1.5 years); (3) the absence of any decrease in the quantum efficiency on annealing the crystals. According to the hypothesis of reference 3, an acceleration of the aging process would have been expected on annealing. Thus the hypothesis of the authors of reference 3, that the luminescence properties of cesium iodide have their origin in iodine vacancies, appears to us to involve contradictions.

The results obtained in the present work and in reference 3 on the investigation of the luminescence properties of crystals grown from a superheated melt may be explained in two ways—the combination of iodine with the material of the ampoule and the entrance of silicon into the melt as an activator. The difference in the results for the first series as compared to those for the second and third series may be related to an accidental difference in the quality of the quartz ampoules. Actually, while fragments of the ampoules of the second and third series did not differ in external appearance from new quartz tubing, the internal surface of the ampoule of the first series had a characteristic flaky structure and was easily disintegrated.

Of the two explanations given above, it appears to us that the second should be adopted. An indirect verification of this is given by an experiment of ours in which 0.7% by weight of silicon dioxide in the form of silica gel was added to the raw material before melting. The resulting crystal (with 2 hr of superheating) had a quantum yield of 32% (point 4 in Fig. 3). No traces of thallium were observed in the absorption spectrum of the crystal (Fig. 4).

It should also be noted that no lines which could be ascribed to activation by silicon were observed in the absorption spectrum. Evidently these absorption lines lie in a shorter wavelength region than the lowest wavelength passed by the ISP-22 spectrograph which we used.

The results given here, although they are not to be considered a refutation of the hypothesis given in reference 3, nevertheless place its basic theses in doubt. The correctness of the observations made above can be clarified by further experiments.

We with to express our thanks to N. S. Budnik and L. G. Maistrenko for their help in growing the crystals and in counting, and to A. N. Panova for obtaining the absorption spectra of the crystals.

REFERENCES

1. W. Beusch, H. Knoepfel, E. Lopfe, D. Maeder, and P. Stoll. Nuovo cimento **5**, 575 (1957).
2. H. Knoepfel, E. Loepfe, and P. Stoll. Helv. Phys. Acta **29**, 241 (1956).
3. H. Knoepfel, E. Loepfe, and P. Stoll. Helv. Phys. Acta **30**, 521 (1957).
4. B. Hahn and I. Rossel. Helv. Phys. Acta **26**, 803 (1953).
5. H. Enz and J. Rossel. Helv. Phys. Acta **31**, 25 (1958).
6. L. M. Schwab and K. Sockers. Angew. Chem. **50**, 546 (1937).
7. B. G. Distanov, L. Z. Kresal'naya, and N. S. Stepanova. Zhur. Priklad. Khim. (in press).
8. Yu. A. Tsirlin, S. N. Komnik, and L. M. Soifer. Opt. i Spektr. **6**, 422 (1959).
9. B. S. Alexandrov. Biul. I.R.E.A., No. 5, 52 (1958).

# TEMPERATURE DEPENDENCE OF THE LUMINESCENCE OF NaI(Tl) CRYSTALS AT TEMPERATURES BETWEEN 0° AND 270°C

V. I. Startsev, Z. B. Baturicheva, and Yu. A. Tsirlin

Received 17 July 1959

A study was made of the temperature dependence of the luminescence of NaI:Tl crystals under the action of γ-rays over a wide range of above-zero temperatures (0-270°C). Different methods (integral and pulsed) were used to determine the de-excitation time at different temperatures for the crystals investigated. The experimental data obtained were compared with theory and the results of other authors.

1. The temperature dependence of the luminescence intensity of NaI:Tl crystals has been studied by a number of authors both above and below 0°C.[1-4] However, the results obtained are highly contradictory, particularly above room temperature. This is explained first of all by experimental difficulties, such as the need to avoid heating the cathode of the photomultiplier—a precaution which was not observed by all authors. Furthermore, the experimental procedures were not identical. (It may easily be shown that the nature of the dependence of pulse height on temperature is strongly affected by the ratio between the smallest time constant $x = RC$ of the system and the de-excitation time $\tau$ of the scintillator.) This last fact was completely ignored by a number of authors. The behavior of the I(T) function is apparently also affected by the thallium content of the crystals and by the method of growing the crystal. In addition, one cannot exclude the possibility that moisture may reach the surface of the crystal during the experiment.

The purpose of this paper was to investigate the temperature dependence of the luminescence intensity of NaI(Tl) crystals under the action of γ-rays over a wider range of above-zero temperatures (0-270°C) than was covered in the articles cited above. A distinction had to be made here between two effects: the actual variation in the light yield I of NaI(Tl) crystals and the variation in the utilization of scintillation light caused by a variation in the de-excitation time.

2. The experiment was performed as follows: A NaI(Tl) crystal, 4, 13 mm in diameter and 13 mm high, was polished and then packed in a hermetically sealed container 6. (See Fig. 1.) The container with the crystal was placed in a massive copper block, 3, connected to a furnace by a metal rod. Temperature uniformity throughout the volume of the crystal was assured by the massive nature of the block and the thermal insulation (glass) of the crystal surface facing the photocathode. The temperature variations were found to be sufficiently slow so that the temperature difference between the surface and the center of the crystal did not exceed 2 deg. This was ascertained by preliminary experiments. The temperature of the crystal was measured at its surface by a copper-constantan thermocouple, 5. The FEU-29 photomultiplier, 9, whose photocathode was about 20 mm away from the surface of the crystal, was separated from the crystal by a plane-parallel glass plate, 7, which divided the experimental chamber into two parts. Air at room temperature was blown at the photomultiplier (through tubes, 8), and in particular at the photocathode to prevent heating up the photomultiplier. Temperature measurements at the surface of the photocathode showed that its temperature rose no more than 6 deg during an experiment. Special experiments carried out by illuminating the photomultiplier with a constant light source while heating the copper block have shown that, under the conditions of the experiment, the heating of the photocathode does not affect photomultiplier sensitivity.

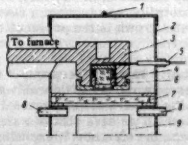


Fig. 1. Schematic of experimental arrangement.

We studied the scintillation of NaI(Tl) crystals under the action of γ-rays from $Cs^{137}$ (E = 661 kev). The radiation source was placed on the cover of the photomultiplier housing. Two methods were used in carrying out the experiments. In the first method (integral measurements), the dependence of the magnitude of the photomultiplier anode current on crystal temperature was studied by means of an M-91a microammeter having a capacity of 10 μf in parallel. This gave a time constant of RC = 4 sec. In the second method (pulsed), the pulses were taken off the preamplifier connected (through a cathode follower) to the anode of the photomultiplier, and were photographed with the help of a 25 I oscilloscope. At each temperature the measurements were carried out for several values of the time constant x of the photomultiplier anode. (The load resistance R was varied.) Since we did not have an oscilloscope of sufficiently high frequency, it was not possible to determine the de-excitation time from the steepness of the leading edge (rise) of the pulse on the oscilloscope screen. The de-excitation time was therefore extimated from the shape of the curve showing the dependence of pulse height on T and x. (It can be shown that the pulse height reproduced by the oscilloscope is distorted much less than the leading edge of the signal. For the oscilloscope used, the height distortion is negligible.)

3. We used NaI(Tl) crystals grown by the methods of Kiropoulos and Stockbarger; the Tl concentration ranged from 0.05 to 0.1% by weight.

The experiments were performed for different rates of heating as well as cooling (from 15 to 90 deg/hour). The first series of measurements with a given sample gave a certain disagreement between the heating and cooling curves. Thus, for a first rapid heating of certain NaI(Tl) crystals, integral measurements revealed the presence of noticeable thermoluminescence (Fig. 2, curve 1). An actual break in the heating curve was ob-

served for some crystals (Fig. 2, curve 2). Repeated heating of crystals annealed in the first experiments did not confirm any distinctions between heating and cooling. This indicates a sufficiently slow variation of temperature in the crystal. Measurements performed on a series of NaI(Tl) crystals grown by the methods of Stockbarger and Kiropoulos gave concordant results. Integral measurements have shown that the variation of luminescence intensity with temperature is linear between 0° and 270°, with a temperature coefficient of 0.12 ± 0.03%/deg (Fig. 2, curve 3). We did not notice any dependence of luminescence characteristics on thallium concentration in the indicated range of concentrations.

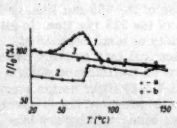

Fig. 2

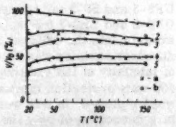

Fig. 3

Fig. 2. Temperature dependence of the luminescence intensity of NaI(Tl) crystals. Curves 1, 2—typical first heating curves, measured by the integral method. Curve 3—cooling and repeated heating curve (a—measurements by the integral method; b—measurements by the pulse method for x = 27 μsec).

Fig. 3. Temperature dependence of the pulse height at the output of a scintillation counter for NaI(Tl) crystals for different time constants (a—experimental points; b—calculated points).

4. The magnitude of the signal U at the output of a scintillation counter is determined (cf., for example, reference 5) by

$$V = V_0\Gamma, \qquad (1)$$

where $V_0$ is the magnitude of the signal for RC → ∞, while

$$\Gamma = \gamma^{\frac{1}{1-\gamma}}; \quad \gamma = \frac{x}{\tau}. \qquad (2)$$

The function V(T, x), determined from measurements made by the pulse method, is shown in Fig. 3.

In order to evaluate τ, the experimental curves $V(x)/V_0$ were plotted on semilogarithmic coordinates and compared with the curve Γ(γ) (Fig. 4).

The value of τ was determined from the amount by which it is necessary to shift the curve Γ(γ) to obtain the best fit with the experimental points. An analysis of the experimental results has shown that at room temperature the experimental results can be satisfactorily described by the theoretical curve only under the assumption that the fundamental component of the radiation (τ = 0.25 μsec) constitutes 90-95% of the entire signal, while the remaining 5-10% is due to the component with a de-excitation time of 0.7-1.2 μsec. The procedure we used unfortunately did not allow us to measure this component more accurately. The values of τ thus determined are shown in Fig. 5 as functions of the temperature. This function τ(T) makes it possible to explain the behavior of the V(T, x) curves for different values of x. The calculated curves $V_{calc}(T, x)$ found on the basis of the functions τ(T) and $V_0(T)$ from Eqs. (1) and (2) agree satisfactorily with the experimental data (Fig. 3).

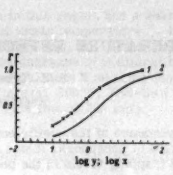

Fig. 4

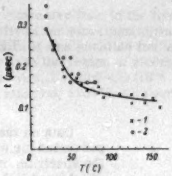

Fig. 5

Fig. 4. Calculation of the magnitude of the time constant (curve 1—experiment; curve 2—calculations).

Fig. 5. Temperature dependence of the de-excitation time of NaI(Tl) crystals. Curve 1—our data; curve 2—data from reference 7.

The absence of a noticeable slow component of luminescence (with τ in the range of $10^{-6}$-$10^{-3}$ sec) allows us to explain the good agreement between the data obtained by the pulse method with RC = 27 μsec and by integral measurements with RC = ∞ (more exactly for RC = 4 sec).

5. Our curves $V_{calc}(T, x)$ agree well with experimental data[3] for the function V(T) for x = 0.4 μsec. Our results for RC = ∞ agree for the range of 0-45°C with those of Kinard (x = 25 μsec)[3] and of Webb and Johansen.[2] It is not clear why our data disagree with the results of Meessen,[4] while it is difficult to make a comparison with the data of Solon et al.[1] Since their experiments do not make it possible to consider the effect by itself.

We commented above that we found no difference in the scintillation properties of NaI(Tl) crystals grown by methods of Stockbarger and Kiropoulos, respectively. The only experiment in which such a difference was found was described in reference 6. The authors[6] found that at low temperatures there is a difference in the light yield of crystals grown by the two methods, the difference decreasing with increasing temperature. We should note, however, that in reference 6 a study was made of luminescence under the action of α-particles. The dependence of de-excitation time on temperature which we found for the 20-80°C region agrees within the limits of experimental error with the data of Plyavin'.[7] We are not aware of any data in the literature for the higher temperature range.

REFERENCES

1. L. R. Solon, I. E. McLaughlin, and H. Blatz. Nucleonics 12, 50 (1954).
2. L. A. Webb and R. F. Johanson. Phys. Rev. 98, 234 (1955).
3. F. E. Kinard. Nucleonics 15, 92 (1957).
4. A. Meessen. J. phys. radium 19, 437 (1958).
5. R. K. Swank. Ann. Rev. Nuclear Sci. 4, 111 (1954).
6. E. Mateosian, M. McKeown, and C. O. Muehlhause. Phys. Rev. 101, 967 (1956).
7. I. K. Plyavin'. Opt. i Spektr. 2, 384 (1957).

# TEMPERATURE EFFECT ON INFRARED QUENCHING

K. S. K. Rebane and E. Sakarinen

Received 8 July 1959

Data on the dependence of the coefficient of infrared quenching $\mu(T)$ on temperature are presented for a series of phosphors. It was shown that the nonmonotony of $\mu(T)$ is explained by the spectrum of the trapping levels in the phosphors and luminosity action of temperature and of infrared light.

## INTRODUCTION

According to contemporary ideas, the primary step in both temperature and infrared quenching in a group of phosphors of the ZnS type is the elimination of holes trapped by ions of the activator.[1-4] * It is of great interest

*It is necessary to emphasize that the value of quenching itself is determined by the ratio of the average lifetime of all electrons to the average lifetime of all holes.

therefore to study the interactions between these two forms of quenching. At the present time, data about the interaction between temperature and infrared quenching is very slight. In reference 5, the dependence on temperature in all regions of temperature quenching was studied for certain phosphors. The dependence of infrared quenching on temperature in the region of temperature quenching was studied on a sample of one phosphor in reference 6. The purpose of the present work is the study of this dependence in more detail on a large number of different samples and under different experimental conditions.

## SAMPLES INVESTIGATED AND THE EXPERIMENTAL METHOD

All the samples investigated in this work are presented in the Table. Phosphors 1-7 were prepared by us in the usual method of annealing in quartz test tubes in an atmosphere of air. Phosphors with a large percentage of copper ($10^{-3}$ and $10^{-2}$ gm/gm) were washed after annealing with a solution of NaCl in order to remove the free $Cu_xS$. Phosphors 8 and 9 were prepared in the A. A. Bundel laboratory.

| No. in sequence | Phosphor (amount of Cu and Fe, in gm/gm) | Temperature of annealing (°C) | Time of annealing (min) |
|---|---|---|---|
| 1 | ZnS-Cu($10^{-3}$)NaCl (2%) | 1100 | 30 |
| 2 | ZnS Cu($10^{-4}$)NaCl (2%) | 1100 | 30 |
| 3 | ZnS Cu($10^{-5}$)NaCl (2%) | 1100 | 30 |
| 4 | ZnS Cu($10^{-5}$)NaCl (2%) | 1100 | 30 |
| 5 | ZnS-Cu($10^{-4}$)NaCl (2%) | 550 | 15 |
| 6 | ZnS-Cu($10^{-4}$)NaCl (2%) | 900 | 30 |
| 7 | ZnS-Cu($10^{-2}$)NaCl (2%) | 1000 | 15 |
| 8 | ZnS-Cu($3 \cdot 10^{-5}$)ZnO (3%) NaCl (2%) | 900 | 30 |
| 9 | ZnS-Cu($3 \cdot 10^{-5}$)Fe($10^{-3}$)NaCl (5%)(without oxygen) | 950 | 30 |

In order to carry out the measurements, powder was embedded into a depression in the metallic body of an electric furnace and was covered by a quartz plate. The curves of the temperature dependence of the intensity of phosphorescence were taken during slow heating of the phosphor up to full quenching and then during slow cooling down to room temperature. Control experiments showed that the curves obtained in such a manner agree with curves measured under conditions of complete temperature equilibrium over the cycle. Excitation sources were mercury-quartz lamps PRK-2 or PRK-7 with filters UFS-3 and SS-9 for the isolation of the 365 mμ line, and UFS-2 and ZhS-3 for isolation of the 313 mμ line. In all experiments the original intensity of luminescence of different samples was made identical by a suitable choice of intensity of the exciting light. In the infrared study a 400 watt projection lamp with a KS-19 filter as the source was employed. In this work we investigated the temperature quenching of only the green bands which were isolated with the help of filters SZS-18 and ZhS-18. The intensity of luminescence was recorded with the help of a photoelectric multipier FEU-17.

For the extent of infrared quenching $\mu$ the usual ratio was taken

$$\mu = \frac{I_0 - I}{I_0}, \qquad (1)$$

where $I_0$ and I are the intensities of phosphor luminescence before and after exposure to quenching infrared radiation, respectively.

## EXPERIMENTAL RESULTS

For the phosphors studied by us, as in the work of Yastrebov,[1] "hysteresis" of temperature quenching was observed. On cooling, the intensity of luminescence did not return to its original value, but remained 2 to 3 times smaller. A restoration of intensity occurred after prolonged storage in the dark.. In addition, the curve of the temperature quenching on cooling was different from the curve on heating in that during cooling there appeared or increased a maximum on the curve of temperature quenching but the onset of temperature quenching shifted toward higher temperatures. The character of the dependence of $\mu(T)$ does not depend essentially on whether it was measured on heating or on cooling. It should be noted only that on cooling the values of $\mu(T)$ somewhat exceed those on heating. This is explained, probably, by the smaller intensity of luminescence on cooling.

The majority of the phosphors studied by us were noticeably thermally quenched even at room temperature. For the phosphor ZnS-Cu ($10^{-4}$ gm/gm) with 313 and 365 mμ excitation and for phosphor ZnS-Cu ($10^{-5}$ gm/gm) with 365 mμ excitation after exposure to infrared light the dependence of the intensity of luminescence on temperature changes: a maximum appears on the curves of temperature quenching but the onset of temperature quenching shifts toward higher temperature. This agrees with the results obtained earlier by Litvinova.[6] The well-known dependence of the character of temperature quenching curves on the wavelength of the excitation light[7] was not observed for our phorphors.

The temperature quenching curves and corresponding curves of $\mu(T)$ are presented in the Figures (only the curves obtained on heating are shown). In the Figures it is possible to distinguish three basic regions of change in $\mu(T)$: (1) a section of decreasing values of $\mu$ with in-

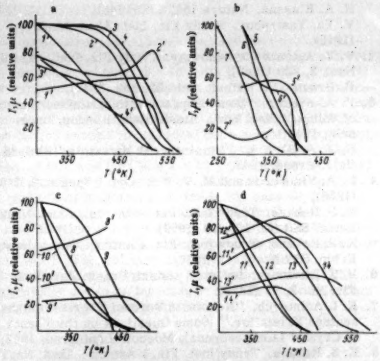


Curves of the dependence of the intensity of luminescence I (curves 1-14) and the function $\mu$ (curves 1-14) on temperature for various phosphors at various conditions of excitation. Phosphor (concentration of Cu and Fe in gm/gm) and wavelength of the excitation light (m$\mu$): 1, 1′—ZnS-Cu ($10^{-3}$), 313; 2, 2′—ZnS-Cu ($10^{-5}$), 365; 3, 3′—ZnS-Cu ($10^{-4}$), 313; 4, 4′—ZnS-Cu ($10^{-4}$), 365; 5, 5′—ZnS-Cu ($10^{-3}$), 313; 6, 6′—ZnS-Cu ($10^{-3}$), 365; 7, 7′—ZnS-Cu ($10^{-3}$), 313; 8, 8′—ZnS-Cu ($10^{-3}$), 313, annealing temperature, $T_{ann.}$ = 1000°C; 9, 9′—ZnS-ZnO(3%) Cu ($3 \cdot 10^{-3}$), 313; 10, 10′—ZnS-Cu ($3 \cdot 10^{-3}$) Fe, 313; 11, 11′—ZnS-Cu ($10^{-4}$), 313, $T_{ann.}$ = 550°C; 12, 12′—ZnS-Cu ($10^{-4}$), 365, $T_{ann.}$ = 550°C; 13, 13′—ZnS-Cu ($10^{-4}$), 313, $T_{ann.}$ = 900°C; 14, 14′—ZnS-Cu ($10^{-4}$), 365, $T_{ann.}$ = 900°C.

creasing temperature in the region of the onset of temperature quenching at lower temperatures; (2) a section of increasing $\mu$ with increasing temperature in the region of temperature quenching, and (3) a section of rapid decrease of the value of $\mu$ with increasing temperature in the region of strong temperature quenching. The indicated regions appear most clearly in the case of the phosphor ZnS-Cu ($10^{-4}$ gm/gm) with the 365 m$\mu$ excitation line. We note that the first type of $\mu$(T) dependence occurs only for certain of our phosphors, since for the majority of them the measurements began only in the region of temperature quenching. In this region the most frequently observed effect is the increase of the value of $\mu$ with an increase of temperature. The only exception is the phosphor ZnS-Cu ($10^{-4}$ gm/gm) for which $\mu$ always decreases with an increase of temperature. In the case of phosphors ZnS-Cu ($10^{-5}$ gm/gm) and ZnS-Cu ($10^{-3}$ gm/gm) with the excitation line at 313 m$\mu$ an increase is observed, but with the 365 m$\mu$ excitation line a decrease in the value of $\mu$ occurs for an increase of temperature in the same temperature region. The increase of $\mu$(T) ceases in the temperature region near 100 or 150-200°C. Only for the phosphor ZnS-Cu ($10^{-3}$ gm/gm) is a maximum of $\mu$(T) found at high temperature.

The last (third) region of change of $\mu$(T) is sometimes found at such high temperatures that it is difficult to carry out measurements accurately on the intensity of radiation because of the large degree of quenching. Nevertheless, in the Figures it is seen that the decrease of $\mu$ in this region has a sharper character than in the first (at lower temperatures). In spite of the aforementioned difficulties, for certain phosphors it was possible to show the decrease of $\mu$ almost to zero in the region of strong temperature quenching (see ZnS-Cu, Fe; ZnS-Cu ($10^{-4}$ gm/gm), 900°C; ZnS-Cu ($10^{-4}$ gm/gm), 1100°C with excitation line at 365 m$\mu$).

## DISCUSSION OF RESULTS

In the work of Litvinova,[9] the decrease of magnitude of $\mu$(T) with an increase of temperature is explained by the fact that the time of residence of electrons at trapping levels is decreased and the most probable of the nonradiating recombinations of free holes is with electrons localized in trapping levels. For the samples studied in the present work, it is seen that the dependence of $\mu$(T) is more complicated. Therefore the assumptions made in reference 6 do not explain the behavior of $\mu$(T) in all temperature intervals.

Both temperature and infrared quenchings of the outer type; i.e., the nonradiating transition occurs outside the luminescence center. On the basis of a band model, the intensity of luminescence I is given by*

*We took into account only the luminescence which is explained by electron processes; the luminescence explained by hole processes[9] we consider very weak.

$$I = \beta n N^-,$$

where $\beta$ is the probability of a radiating transition, n is the number of ionization centers of the luminescence, and $N^-$ is the number of electrons in the conduction band. The equilibrium values n and $N^-$ depend on the spectrum of the trapping levels and on the luminosity action both of the excitation light (LAEL) and of infrared light (LAIRL). Besides, n and $N^-$ depend also on the luminosity action of temperature. The spectrum of the trapping levels is determined by the number of separate levels, by the luminosity action, and by the probability of recombination in these levels. The luminosity action in the general case can be presented in the form:

$$W_i = W_i(T) + W_i(E) + W_i(I_{IR}), \qquad (2)$$

where i is the level index, and $W_i$(T), $W_i$(E), and $W_i(I_{IR})$ are, respectively, the luminosity action of temperature, of exciting light with intensity E, and of infrared light with intensity $I_{IR}$.

In the region of decreasing values of $\mu$(T) it is necessary to achieve the condition $dI/dT > dI_0/dT$ (see Eq. 1). From the experiment it follows that in this region $I_0$ does not change or changes very slowly, and I rapidly increases with an increase of temperature. This growth can be explained both by the effect mentioned by Litvinova and by the fact that the effective cross section for nonradiating recombination in the deep levels is smaller than in the shallow ones. For phosphors of certain other types a similar effect has been discovered and investigated by a number of authors.[9]

The region of increasing $\mu$(T) is possible if the condition $dI/dT < dI_0/dT$ holds. As was shown by our measurements, this region agrees quite well with the temperature region in which the destruction of trapping levels occurs, which explains the sensitivity of phosphor to red and infrared light.[10] * It may be thought that on exposure

*For phosphors ZnS-Cu ($10^{-3}$ gm/gm) and ZnS-Cu ($10^{-4}$ gm/gm) the existence of such levels was shown by Talvist, a student at the Tartusky State University.

to infrared light the intensity is determined by LAIRL,

which is not dependent on temperature. If the action of infrared light is small, then the thermal elimination of electrons from these levels can cause a decrease of nonradiating recombinations on them and also in a certain manner retard the temperature quenching, explained by the decrease of n since $N^-$ increased.

In the latter region the change of value of $\mu(T)$ evidently satisfies the condition $W_t(T) > W_t(E) + W_t(I_{IR})$ and with an increase of temperature the share of LAEL and LAIRL becomes unimportant in connection with the temperature quenchings. This circumstance causes the drop of $\mu(T)$ to zero. From this, one gets some idea why at high intensity of infrared light the onset of temperature quenching shifts to higher temperatures and a decrease of intensity of infrared light reduces the value of $\mu$ practically to zero at lower temperatures.

From what has been stated above it is evident that the nonmonotonic character of the function $\mu(T)$ in every case is determined by the luminosity action and the spectrum of the trapping levels. In future it will be necessary to carry out a parallel study of the behavior of $\mu(T)$ and the state of the spectrum of the trapping levels.

In conclusion we take the opportunity to express gratitude to Ch. B. Lushchik for interest in the work and discussions about it.

REFERENCES

1. M. Schon. Z. Phys. **119**, 463 (1942);
H. A. Klasens. Nature **158**, 306 (1946);
V. Ya. Yastrebov. Trudy Fiz. Inst. Akad. Nauk **3**, (1946).
2. V. V. Antonov-Romanovsky. Trudy Fiz. Inst. Akad. Nauk **2**, 220 (1942);
P. Brauer. Z. Naturforsch. **21**, 238 (1947).
3. F. A. Kruger. "Some Aspects of the Luminescence of Solids." New York, Amsterdam, London, Brussels, 1948;
G. F. J. Garlick. "Luminescent Materials." Oxford Univ. Press, 1949.
4. L. A. Vinokurov and M. V. Fok. Opt. i Spektr. **2**, 248 (1956);
K. S. Rebane. Trudy Inst. Fiz. i Astron., Akad. Nauk Eston. SSR No. 10, 209 (1959).
5. K. S. Rebane. Trudy Inst. Fiz. i Astron., Akad. Nauk Eston. SSR No. 4, 81 (1956).
6. P. S. Litvinova. Izvest. Vysshikh Ucheb. Zavedeni Fiz. No. 2, 73 (1958).
7. E. I. Adinovich. "Nekotorie Voproci Teorii Luminestsentsee Kristallov." (Some Questions on the Theory of Crystal Luminescence), Moscow-Leningrad, 1951.
8. K. S. Rebane. Trudy Inst. Fiz. i Astron., Akad. Nauk Eston. SSR No. 8, 105 (1958).
9. V. V. Antonov-Romanovsky, V. L. Levshin, Z. L. Morgenshtern, and Z. A. Trapeznikova. Izvest. Akad. Nauk SSSR **13**, 75 (1949);
Ch. B. Lushchik and F. N. Zaitov. Trudy Inst. Fiz. i Astron., Akad. Nauk Eston. SSR No. 7, 276 (1958).
10. K. S. Rebane. Opt. i Spektr. **4**, 211 (1958).

# THE PROPERTIES OF ZnS:Mn, Ni, Cl PHOSPHORS UNDER CATHODE RAY EXCITATION

A. I. Blazhevich, A. G. Zavrazhin, and A. V. Lavrov

Received 11 July 1959

A study is made of the influence of the addition of Ni on the luminescence of ZnS:Mn phosphors, and on the behavior of their decay curves at different chlorine concentrations. It is shown that an increase in the Ni concentration brings about a decrease in the hyperbolic decay component and the predominance of the exponential component.

It has been shown[1,2] that the addition of chlorine plays an essential role in the formation of capture levels in ZnS:Mn phosphors and in the formation of a hyperbolic component in the afterglow. Since there is a clear division of the decay curve into exponential and hyperbolic components, we may assume that the luminescence kinetics of this phosphor are determined by at least two competing processes. We can also investigate the effect of different additions on these processes.

Since the ZnS:Mn phosphor has a system of capture levels which is similar, in general, to that of other zinc sulfide phosphors, the results of an investigation of the inertial properties of ZnS:Mn may be of importance for the whole class of sulfides.

In this work we investigated the effect on luminescence of adding Ni at the instant of excitation, and on the behavior of the decay curves of ZnS:Mn phosphors prepared with different chloride concentrations.

## EXPERIMENTAL PART

Apparatus. All measurements were performed with the high voltage apparatus for the study of cathodoluminors described in reference 2. The brightness at the instant of excitation was measured by means of an FEUI-B photomultiplier with an antimony-cesium photocathode.

The measurement of the decay curves was performed with the same photomultiplier, whose signal was fed through a short cable into the input of an ENO-1 oscilloscope. The calibrated variation in the sensitivity of the photomultiplier permitted intensity measurements over a range of four orders of magnitude, starting with the brightness level at excitation.

In all experiments, excitation was accomplished by means of an electron beam with a density of $1 \times 10^{-4}$ amp/cm$^2$ and a voltage of 40 kv. We also performed control experiments in which the density was varied from $1 \times 10^{-7}$ to $1 \times 10^{-9}$ amp/cm$^2$ and the voltage from 10 to 50 kv. All of the results observed under the regular experimental conditions are qualitatively completely repeatable for all modes of excitation of the phosphors.

Preparation of samples. All phosphor samples were prepared by firing in argon at 900°C for 30 min. Mn was introduced into the mixture as the sulfate (reagent grade) at a concentration of $3 \times 10^{-3}$ gm/gm and Ni as the nitrate (reagent grade) at concentrations of $1 \times 10^{-7}$ to $1 \times 10^{-4}$ gm/gm.

## EXPERIMENTAL RESULTS

In the first experiments we used zinc sulfide activated with Mn ($3 \times 10^{-3}$ gm/gm) and containing (according to our analysis) about $2 \times 10^{-5}$ gm Cl/gm ZnS. When Ni is introduced into such a phosphor (the activator concentration being kept constant), the decay curves show characteristic peculiarities (Fig. 1). The increase in Ni concentration results in a gradual decrease of the hyperbolic and predominance of the exponential decay component. This is followed (at $C_{Ni} = 1 \times 10^{-4}$ gm/gm) by an almost pure exponential decay over a range of four orders of magnitude of brightness. In the latter case we find no light sum storage if we record the thermal de-excitation curve starting at liquid nitrogen temperature. The decay curves obtained for the same phosphors at a temperature of −132°C (Fig. 1b) have a similar appearance, with somewhat more pronounced hyperbolic portions. This is apparently due to an increase in the lifetime of electrons in traps at lower temperatures.

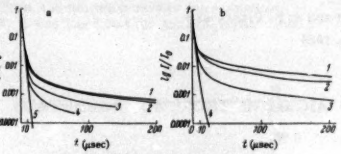


Fig. 1. Dependence of the decay curves of ZnS:Mn ($3 \times 10^{-3}$ gm/gm), Cl ($2 \times 10^{-5}$ gm/gm) phosphors on Ni concentration; (a) at room temperature; (b) at −132°C. Ni concentration (in gm/gm): curve 1—0; curve 2—$1 \times 10^{-7}$; curve 3—$1 \times 10^{-6}$; curve 4—$1 \times 10^{-5}$; curve 5—$1 \times 10^{-4}$.

When the Ni content of such samples is increased up to $1 \times 10^{-5}$ gm/gm, the brightness at the instant of excitation increases (curve 2, Fig. 2a) and decreases only for a further increase in Ni concentration. This effect is observed under different conditions of cathode ray excitation (voltage V, current density j) and also under photoexcitation ($\lambda_{exc}$ 313 and 365 mμ). It increases when the temperature is lowered to −132°C (Fig. 2b). It should be noted that the introduction of Ni into the ZnS:Mn does not change the luminescence spectrum.

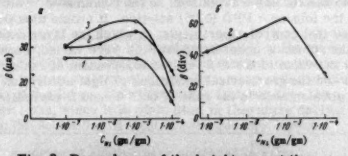


Fig. 2. Dependence of the brightness at the instant of excitation on Ni concentration for phosphors with different Cl content; (a) at room temperature; (b) at −132°C. Curve 1—ZnS:Mn, Cl ($\ll 2 \times 10^{-5}$ gm/gm); curve 2—ZnS:Mn, Cl ($\sim 2 \times 10^{-5}$ gm/gm); curve 3—ZnS:Mn, Cl ($> 2 \times 10^{-5}$ gm/gm).

To check the influence of flux on the observed brightness increase, we prepared a series of ZnS:Mn, Ni phosphors with 2% NaCl. This experiment confirmed the existence of a brightness increase in this case as well (curve 3, Fig. 2a). Thermal de-excitation of ZnS:Mn, Ni, Cl samples has shown that an increase in Ni concentration leads to a decrease in light sum storage at all capture levels (Fig. 3). In general the ZnS:Mn, Cl, Ni ($1 \times 10^{-4}$ gm/gm) sample does not store any appreciable amount of light energy. The behavior of the decay curves of this

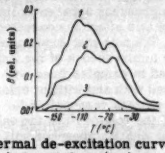


Fig. 3. Thermal de-excitation curves of ZnS:Mn, Cl ($> 2 \times 10^{-5}$ gm/gm) phosphors for different Ni concentration. Ni concentration (gm/gm): curve 1—0; curve 2—$1 \times 10^{-6}$; curve 3—$1 \times 10^{-5}$.

series of phosphors shows a dependence on Ni concentration similar to that described above (Figs. 4 and 5). It should be noted, however, that the afterglow curves of ZnS:Mn (2% NaCl) phosphors exhibit a somewhat more pronounced hyperbolic component (curve 1, Fig. 5).

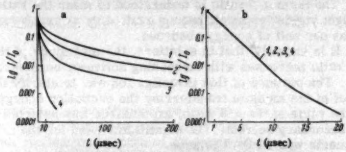


Fig. 4. Dependence of decay curves on Ni concentration: (a) for ZnS:Mn, Cl ($> 2 \times 10^{-5}$ gm/gm) phosphors; (b) for ZnS:Mn, Cl ($\ll 2 \times 10^{-5}$ gm/gm). Ni concentration (gm/gm): curve 1—0; curve 2—$1 \times 10^{-6}$; curve 3—$1 \times 10^{-5}$; curve 4—$1 \times 10^{-4}$.

We subsequently took steps to prevent getting chlorine into the samples obtained. This consisted in firing without a flux and also in a preliminary elimination of chlorine from the original ZnS by firing it in $NH_3$ at 900°C. The absence of chlorine was checked by chemical analysis. The ZnS:Mn, Ni samples obtained in this manner did not exhibit any brightness increase with increasing Ni concentration (curve 1, Fig. 2a). In this case we observed only quenching. These decay curves are exponential and differ considerably from those obtained for samples containing chlorine (Fig. 4b). The introduction of Ni into such phosphors does not affect the behavior of the decay curves, i.e., these curves coincide for samples with different Ni content (Fig. 4b).

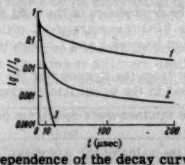


Fig. 5. Dependence of the decay curves of the ZnS:Mn phosphor on Cl concentration. Cl concentration (gm/gm): curve 1—$> 2 \times 10^{-5}$; curve 2—$\sim 2 \times 10^{-5}$; curve 3—$\ll 2 \times 10^{-5}$.

It should be noted that in view of the technique used in adding the activator, the samples studied should have contained oxygen. However, the absence of the hyperbolic component in the decay curves as well as the absence of light storage in such samples show that, in the absence of chlorine, oxygen does not form capture levels in this case.

The key to the explanation of the enhancing action of Ni in the ZnS:Mn phosphor apparently lies in the fact that the appearance of this effect is connected with the presence of chlorine. We note that Arpiarian[3] observed an enhancement in the luminescence of the ZnS:Au phosphor when Ni was added to samples fired with NaCl. The ZnS:Mn phosphors obtained with and without chlorides differ in the concentration of centers responsible for light sum storage. An explanation of the role of Ni in the enhancement of luminescence of the ZnS:Mn phosphor will obviously be possible only when the structure of these centers is ascertained.

In conclusion, the authors express their deep appreciation to M. V. Fok, M. D. Galanin, and Yu. M. Popov for valuable discussions in the course of this work.

REFERENCES

1. A. V. Lavrov. Doklady na VII Soveshchaniyu po Lyuminestsentsii. (Proceedings of Seventh Conference on Luminescence), Moscow, 1958.
2. A. I. Blazhevich and A. G. Zavrazhin. Doklady na VII Soveshchaniyu po Lyuminestsentsii. (Proceedings of Seventh Conference on Luminescence), Moscow, 1958.
3. N. Arpiarian. J. phys. radium, 17, 674 (1956).

## THE $\alpha/\beta$ RATIO IN A LIQUID SCINTILLATOR

Yu. A. Nemilov, G. N. Belozerskii and A. N. Pisarevskii

Received 13 July 1959

The term $\alpha/\beta$ ratio is understood to mean the ratio of light yields for scintillations excited by $\alpha$- and $\beta$-particles per unit of energy absorbed.

It is known[1-3] that in solutions, the magnitude of the $\alpha/\beta$ ratio increases with increasing activator concentration. The purpose of this investigation was to clarify the effect of the medium transferring the excitation energy on the value of the $\alpha/\beta$ ratio; naphthalene was selected as the secondary solvent. The scintillator used for the measurements was PPO* + toluene.

*PPO-2, 5-diphenyloxazole. All the reagents were of scintillation grade purity. The naphthalene was analytical reagent grade.

Thin sources of $Pu^{239}$ ($E_\alpha$ = 5.15 Mev) and $Cs^{137}$ ($E_\beta$ = 624 kev) were used for the measurements, in conjunction with an FEU-13 photomultiplier (the ballistic error due to the RC of the output circuit is less than 0.1%) and an AMA-3S[4] analyzer (according to the position of the total energy line).

The relationships obtained for the dependence of the light output and the value of the $\alpha/\beta$ ratio on PPO concentration for scintillators with and without naphthalene are plotted in Figs. 1-3.

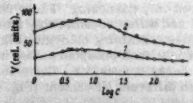


Fig. 1. The dependence of the light output value V on PPO concentration C with $\alpha$- and $\beta$-excitation (curves 1 and 2 respectively).

It is evident from the figures that the addition of a secondary solven* to the scintillator increases both the

*This leaves the luminescence spectrum practically unchanged.

light output and the value of the $\alpha/\beta$ ratio. In addition to this, the range of activator concentration in which changes in the $\alpha/\beta$ ratio are observed is increased up to 5 gm/liter.

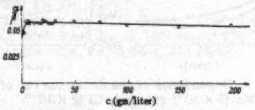


Fig. 2. The dependence of the $\alpha/\beta$ ratio on PPO concentration.

In addition to the main experiment described, supplementary measurements of these specified characteristics were carried out for the scintillator toluene + PPO + POPOP (0.1 gm/liter) [POPOP is 2, 5-p-phenylene-bis(5-phenyloxazole)]. These measurements were also conducted on the same scintillators in the form of gels (viscosity ~$10^3$ stokes) with polystyrene and crystals of stilbene. In solutions of toluene + PPO + POPOP, the value of the $\alpha/\beta$ ratio was approximately 10% less for all concentrations than in solutions without POPOP. Similar results were observed for the light yield. Furthermore, the results obtained for gels were identical to those for solutions. In the case of stilbene, the value of the $\alpha/\beta$ ratio has the same magnitude as the "saturated" value for the toluene + PPO (0.06) solution. It should also be noted that control experiments, in which the layer depths of the solutions under consideration were varied, showed that the value of the $\alpha/\beta$ ratio is independent of reabsorption and the geometrical conditions of light absorption by the photocathode in the case of both $\alpha$- and $\beta$-excitation.

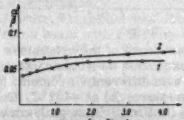


Fig. 3. Dependence of the value of the $\alpha/\beta$ ratio on PPO concentration. Curve 1—without naphthalene, curve 2—with naphthalene.

We now turn to a discussion of the results of the experiment.

The observed increase in the value of the $\alpha/\beta$ ratio with the addition of a secondary solvent (naphthalene) can be attributed to an increase in the duration of the excited state in naphthalene and a concomitant increase in the probability of an energy transfer in the direction:

solvent → secondary solvent → activator.

This increase has a more critical effect on the light output value under $\alpha$-excitation, inasmuch as the "cylinder of excitation" in this case is shorter, while the specific energy loss by the particle is appreciably greater. These hypotheses were confirmed by the observed increase in the value of the $\alpha/\beta$ ratio (in the case of naphthalene) up to high activator concentrations.

The decrease in the light output that was detected when POPOP was added (the luminescence spectrum of POPOP coincides better with the spectral characteristics of the photomultiplier than the PPO spectrum) can be attributed either to heavy losses during the transfer of energy from PPO to POPOP or to an exchange of energy between them.[5]

Thus, the following results were obtained:

1. It was found that the medium instrumental in transferring excitation energy has an effect on the $\alpha/\beta$ ratio.

2. It was shown that the viscosity of the scintillator (up to $10^2$ stokes) is not reflected in the value of the $\alpha/\beta$ ratio. This confirms a number of the conclusions of reference 2.

3. The "saturation" value of the $\alpha/\beta$ ratio obtained (0.06) (for the solution without naphthalene) is somewhat less than that cited in the literature[2] (0.08–0.1). For the solution with naphthalene the value is $\alpha/\beta = 0.07$.

REFERENCES

1. M. Furst and H. Kallmann. Phys. Rev. 85, 816 (1952).
2. M. D. Galanin and Z. A. Chizhikova. Opt. i Spektr. 4, 196 (1958).
3. G. T. Reynolds. Nucleonics 10, 46 (1952).
4. V. O. Vyazemskii. Doklady na Konf. po Yadernoi Elektronike. (Proceedings of the Conference on Nuclear Electronics), Moscow, 1959.
5. Kh. V. Protopopov and S. V. Butomo. Sovet. Arkheol. No. 2, 7 (1959).

# SCATTERING OF LIGHT IN MEDIA WITH VARIABLE OPTICAL PARAMETERS

A. P. Ivanov and E. B. Khodos

Received 22 July 1959

Two methods of determining the reflection and transmission coefficients of layers with optical parameters varying along the thickness are examined. For some particular cases, tables of values of reflection coefficients are compiled. Reflection spectra of mixtures of colored glass powders whose absorption constant varies with the thickness x by the law k = a + bx were studied experimentally. Good agreement between experimental and theoretical data is obtained.

A significant number of investigations have been devoted to the study of the scattering of light. In most of these studies cases were examined where the optical characteristics of the medium are the same at all points. Instead of these, however, in atmospheric optics and hydro-optics, spectrophotometry of scattering media, photochemistry, and other branches of science one encounters examples where there exists a dependence of optical constants and of the light regime on the depth of the layer.*

*The use of the term "optical constants" in the given case is not altogether fortuitous in a situation where these characteristics of the medium vary with the thickness of the layer. Notwithstanding this, we keep the given term, since it is often used in literature dealing with the scattering of light in homogeneous layers.

A series of studies have appeared in print recently in which attempts have been made to account for the influence on light scattering of the variation of scattering index with layer thickness,[1] the importance of the relation of emission and absorption coefficients,[2-4] and the concentration of scattering particles.[5-8] In spite of the fact that in those papers these particular questions are examined, the formulas obtained have a cumbersome form, and can be used only with difficulty.

In the present work the problem was set of determining the reflection and transmission coefficients of light-scattering layers by comparatively simple methods, in which the scattering and absorption constants vary with thickness by an arbitrary law.

The most precise investigation of a given problem is possible in principle on the basis of the solution of the equation of transmission of radiation (see, for example, reference 2). However, in the general case, this leads to practically insurmountable mathematical difficulties. Therefore, for the solution of the formulated problem certain simplifying assumptions are adopted.

One of the methods of calculation of reflection and transmission coefficients consists of a successive calculation of light scattering of different multiplicity. With this it is possible to present the light field in the medium in the form of two fluxes being propagated in opposite directions. Considering that the flux of any order of scattering which has arisen in an elementary volume is attenuated with distance by an exponential law, Chekalinskaya[9] has obtained a system of differential equations for determining the intensities of light of different multiplicities. If the scattering and absorbing properties of the medium are not the same at different depths in a plane parallel layer, then from the given equations for primary scattering, we find

$$R_1 = \int_0^{a_0} s\varepsilon^{-\vartheta\int_0^x p\,dx}\,dx, \quad T_1 = \varepsilon^{-\int_0^{a_0} p\,dx}\int_0^{a_0} t\,dx, \tag{1}$$

and for secondarily scattered light,

$$R_2 = 2\int_0^{x_0} se^{-2\int_0^x \rho dx} dx' \int_0^{x'} te^{-\int_0^x \rho dx} dx,$$

$$T_2 = e^{-\int_0^{x_0} \rho dx}\left[\int_0^{x_0} t'e^{-\int_0^{x'} \rho dx} dx' + \int_0^{x_0} s'e^{-3\int_0^{x'} \rho dx} dx' \int_0^{x'} s'e^{\int_0^{x'} \rho dx} dx'\right]. \quad (2)$$

Here, R and T are the reflection and transmission coefficients, respectively, s is the backward scattering constant per unit layer thickness, t is the forward scattering constant, $\rho$ is the attenuation constant equal to the sum of the parameters s, t, and k, which are assumed to be the same for the fluxes of different multiplicity of scattering, and $x_0$ is the thickness of the layer. Analogous expressions can be written for scattered light of higher orders.

It is possible to use the derived results for the calculation in closed form of (the intensity of) light reflected and transmitted by an object with varying optical constant s, t, and k.

We shall examine as an example the case of an infinitely thick layer where the absorption constant varies by the law K = a + bx, and s and t remain constant. In this case (taking into account secondary scattering), T = 0 and

$$R = \alpha\left(\beta + \sqrt{\pi}\,[0.5 - \beta\eta]\,[1 - \Phi(\eta)]\,e^{\eta^2}\right), \quad (3)$$

where

$$\alpha = \frac{s}{\sqrt{b}}, \quad \beta = \frac{t}{\sqrt{b}}, \quad \gamma = \frac{a}{\sqrt{b}}, \quad \eta = \alpha + \beta + \gamma,$$

and

$$\Phi(\eta) = \frac{2}{\sqrt{\pi}}\int_0^{\eta} e^{\xi^2} d\xi$$

is the probability integral.

For small $\eta$ formula (3) becomes

$$R = \frac{\sqrt{\pi}}{2}\alpha, \quad (4)$$

and for large $\eta$,

$$R = \frac{\alpha}{2\eta}\left(1 + \frac{\beta}{\eta}\right). \quad (5)$$

In the latter case, if the sample does not absorb light near the surface ($\gamma = 0$) then

$$R = \frac{2\frac{t}{s} + 1}{2\left(\frac{t}{s} + 1\right)^2},$$

i.e., the reflection coefficient depends only on the scattering capacity and for t/s = 1, it is equal to 37.5%.

For illustration of the dependence of the reflection coefficient on various parameters formula (3) was tabulated (Table 1).

Table 1

| γ | 0 | | | | | 1 | | | | 10 | | | 100 | |
|---|---|---|---|---|---|---|---|---|---|---|---|---|---|---|
| β \ α | 0.4 | 1 | 4 | 20 | 100 | 1 | 4 | 20 | 100 | 4 | 20 | 100 | 40 | 100 |
| 0 | 23.8 | 37.9 | 48.5 | 49.9 | 50 | 22.6 | 39.2 | 47.6 | 49.5 | 14.5 | 33.3 | 45.5 | 14.4 | 25.0 |
| 4 | 8.2 | 17.3 | 37.0 | 48.6 | 49.9 | 13.5 | 31.8 | 46.4 | 49.4 | 13.6 | 32.9 | 45.4 | 14.4 | 25.0 |
| 20 | — | 4.6 | 15.2 | 37.5 | 48.6 | 4.3 | 14.4 | 36.3 | 48.1 | 9.3 | 28.0 | 43.6 | 14.1 | 24.8 |
| 100 | — | — | 3.8 | 15.3 | 37.5 | — | 3.7 | 15.1 | 37.3 | 3.3 | 13.6 | 35.2 | 11.8 | 22.2 |

From the table it is seen that with increasing $\alpha$ and decreasing $\beta$ and $\gamma$, the reflectivity of the medium is increased. Considering only secondary scattering, the reflection coefficient cannot be greater than 50%.

The difficulty of computing higher orders of scattering and the impossibility of its application to a rather wide class of functions s(x), t(x), k(x) constitute the lack of a well defined method of calculation. Moreover, the method of successive multiplicities will give satisfactory accuracy only for strongly absorbing media of not very large optical thickness. Therefore, another method of solving the problem was investigated by us.

It is well known[10] that the reflection coefficient of a system of two plane parallel layers is equal to

$$R_{2+1} = R_2 + R_1\frac{T_2^2}{1 - R_1R_2}, \quad (6)$$

where $R_1$ and $R_2$ are the reflection coefficients of layers 1 and 2, and $T_2$ is the transmission coefficient of layer 2.

If the second layer is of infinitesimal thickness dx, then in this case $R_2 = sdx$ and $T_2 = 1 - (k + s)dx$, and from (6) it follows that

$$R_2 + dR = sdx + R_2\frac{[1 - 2(k + s)\,dx]}{1 - sdxR_2},$$

that is,

$$dR = [s(1 - R_1)^2 - 2R_1k]\,dx. \quad (7)$$

Formula (7), suitable for variation of k and s along the thickness, has already been found by Gurevich[10] for the case in which the scattering and absorption constants do not depend on x.

From (7) it is seen that if the reflection coefficient of layer 1 is known, then increasing it in thickness by dx, it is possible to find the increase dR of the reflection coefficient and, consequently, the reflection coefficient of the new layer $R_{2+1} = R_1 + dR$. Henceforth, the following method arises for calculation of the reflection coefficient of an object with constants s and k which vary along the thickness.

The layer of thickness $x_0$ is considered to consist of n equal parts such that the thickness of an elementary layer is equal to $x_0/n$. The choice of the number n is subject to conditions such as to make it possible to consider the magnitudes of k and s approximately constant within the boundaries of an elementary layer, and its reflection coefficient equal to $sx_0/n$. Knowing the magnitude of $R_1$ for the elementary layer farthest removed from the incident light, and substituting this value in (7), we find the value of dR and the magnitude of the reflection coefficient $R_{2+1}$ of the (first) two elementary layers. Thereupon, substituting again in (7) the value $R_{2+1}$, we determine the magnitude of $R_{3+2+1}$, etc. In an analogous manner it is possible to compute the reflectivity $R + R_{n+(n-1)+\ldots+1}$ of any object.

Knowing the dependence of R on the thickness, it is not difficult to determine also the transmission coefficient. Indeed, as it was shown by Gurevich,[10]

$$dT = -T(k + s - Rs)\,dx. \quad (8)$$

Henceforth it follows that

$$-\ln T(x_0) = \int_0^{x_0} (k(x) + s(x)[1 - R(x)])\,dx. \quad (9)$$

Replacing the integral by a sum, it is obviously easy to compute the value of T.

In order to determine more accurately the magnitudes of R and T, it is necessary to break up the original layer of thickness $x_0$ into a number of elementary layers, and with increase in the number n, the accuracy increases. The calculation continues until an increase in the number n no longer leads to any appreciable variation in the reflection and transmission coefficients. Our calculations showed that for the determination of the value of T, a

smaller number of increments is required than for determining the magnitude of R.

Naturally, we will use the well-known method in the case of nondependence of the constants s and k on the thickness of the layer. With this, less time is needed for the calculation than for computations by the exact Gurevich formula,[10] whereby all intermediate calculations do not require great accuracy.

We shall examine some examples of the application of formulas (7) and (9).

Let s be a constant magnitude and k = a + bx. In this case, expressions (7) and (9) become, respectively,

$$dR = [(1-R)^2 - 2R(\varphi + \psi y)]\, dy \qquad (10)$$

and

$$-\ln T(y_0) = \int_0^{y_0} (\varphi + \psi y + 1 - R)\, dy. \qquad (11)$$

Here $\varphi = a/s$, $\psi = b/s$, $y = sx$, and $y_0 = sx_0$.

In Fig. 1, curves of the dependence of the magnitudes of R and T on $y_0$ are presented for different values of $\varphi$ and $\psi$, based on formulas (10) and (11). From the graphs it is seen that with large $y_0$, the reflection and transmission coefficients are greatly decreased with an increase of $\varphi$ and $\psi$. In the region of small thicknesses the magnitudes of R and T depende initially only on $\varphi$ (the larger $\varphi$, the smaller R and T). With an increase of $y_0$ the influence of the magnitude of $\psi$ begins to be evident; it may occur that for a given thickness a sample with the smallest value of $\psi$ has the greatest value of reflection and transmission coefficients regardless of the magnitude of $\varphi$ (see curves 2 and 3; 2′ and 3′).

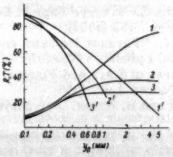


Fig. 1. Dependence of the magnitude of reflection coefficients R (1-3) and transmission coefficients T (1′-3′) on layer thickness $y_0$. Layer parameters: 1,1′—$\varphi = 0$, $\psi = 0.03$, 2,2′—$\varphi = 0.5$, $\psi = 0.03$, 3,3′—$\varphi = 0$, $\psi = 5$.

It is of interest to investigate the properties of an infinitely thick layer in a series of cases. By the method examined above it is possible to investigate only finite thicknesses. Therefore, it is necessary to know what thickness $x_0$ can still be finite yet will permit us to consider an object to be practically of infinite thickness. Depending on the law of variation of optical constants, the method of determining $x_0$ can be different. It is necessary only to choose a layer thickness with some provision for its validity. We shall examine some particular cases.

It is known[10] that with constant s and k

$$R = R_\infty \frac{1 - e^{-2z_0\sqrt{k^2+2kz}}}{1 - R_\infty^2 e^{-2z_0\sqrt{k^2+2kz}}}, \qquad (12)$$

where

$$R_\infty = 1 + \frac{k}{s} - \sqrt{\left(\frac{k}{s}\right)^2 + 2\frac{k}{s}} \qquad (13)$$

is the reflection coefficient of an infinitely thick layer. To compute the reflection coefficient with thickness up to $\lambda\%$ of $R_\infty$ setting $R = 0.01R_\infty$ in (12), we find

$$z_0 = \frac{\ln \dfrac{1 - 0.01\lambda R_\infty^2}{1 - 0.01\lambda}}{2\sqrt{k^2 + 2kz}}. \qquad (14)$$

Depending on the requirements of the problem $\lambda$ can be different.

Light penetrates deeper into the medium the smaller the scattering and absorption coefficients. Therefore, if the constants s and k vary with thickness by an arbitrary law but have small values $s_H$ and $k_H$ near the surface, then substituting these magnitudes in (14), it is easy to find $x_0$. By such an analysis a conservative estimate of an adequate thickness of the layer is provided. It is more difficult to compute $x_0$ if in the depth of the layer the scattering power and absorptivity are smaller than near the surface

The method of successive computation of values of R with different thicknesses can serve as the most general method of determining $x_0$. The smallest magnitude found for $x_0$, beyond which the value of the reflection coefficient practically does not change, obviously characterizes an infinitely thick layer.

With the aid of the described method, reflection coefficients of slabs were determined, which are characterized by different functions k(y) of variation of absorption with thickness, the scattering constant being considered fixed.

In Table 2, some results of the calculations carried out are presented (n = 20, $y_0 = 1$).

Table 2

| $\frac{K(y)}{S}$ | 3 | $-3y^2+3$ | $-3y+3$ | $2\sqrt{-y}+3$ | $2\sqrt{y}$ | $2y$ | $2y^2$ |
|---|---|---|---|---|---|---|---|
| R (%) | 12.5 | 12.9 | 14.2 | 21.7 | 24.2 | 32 | 40.2 |

With the aim of testing the derived model of the calculation, we investigated experimentally the case of an infinitely thick slab having s constant and k = a + bx. For comparison of the experimental data with the theoretical, reflection coefficients were computed with the aid of formula (10) and are compiled in Table 3. In each block of the table the upper number gives the reflection coefficient in percent and the lower number gives the number n of elementary layers into which it was required to divide the investigated layer of (thickness) $y_0 = sx_0$ in order to compute the magnitude of R. The thickness $y_0$ was varied from 0.2 (with $\varphi = 3$ and $\psi = 40$) to 20 (with $\varphi = 20$ and $\psi = 0.001$). Values of reflection coefficients shown in Table 3 differ from the true values by no more than 2%.

Table 3

| $\psi$ / $\varphi$ | | 0.001 | 0.01 | 0.1 | 0.5 | 3 | 10 | 40 |
|---|---|---|---|---|---|---|---|---|
| 0 | R (%) | 90 | 89.9 | 86.2 | 51.2 | 36.7 | 21.7 | 10.7 |
| | n | 20 | 15 | 15 | 15 | 10 | 10 | 5 |
| 0.03 | R (%) | 78.4 | 73.7 | 62.3 | 49.8 | 35.7 | 20.8 | 10.3 |
| | n | 20 | 15 | 10 | 10 | 10 | 5 | 5 |
| 0.2 | R (%) | 53.7 | 53.1 | 49.2 | 39.6 | 30.6 | 20.3 | 9.8 |
| | n | 15 | 10 | 10 | 10 | 10 | 5 | 5 |
| 0.5 | R (%) | 38.2 | 37.5 | 36.8 | 34 | 28.3 | 19.7 | 9.6 |
| | n | 15 | 10 | 10 | 10 | 10 | 5 | 5 |
| 1.5 | R (%) | 20.8 | 20.8 | 20.7 | 20.3 | 18.9 | 14.9 | 9 |
| | n | 10 | 10 | 10 | 5 | 5 | 5 | 5 |
| 3 | R (%) | 12.7 | 12.7 | 12.6 | 12.5 | 12.3 | 10.7 | 8.2 |
| | n | 5 | 5 | 5 | 5 | 5 | 5 | 5 |

The experimental determination of reflection coefficients was conducted with an SF-4 spectrophotometer provided with an attachment for measurement of diffuse reflection.[11]

Powdered glasses, types SS-4, ZS-6, and BS-10 served as the objects of the investigation. The powders were classified by particle size into narrow fractions by a sedimentation method. The average particle size was determined by measurements with a microscope. Light-scattering layers were obtained by a precipitation method in the following way. Colored powders of types SS-4 and ZS-6 were mixed in various proportions with white powder of type BS-10 having the same particle size. In this way mixtures of powders were obtained having different absorption for a single wavelength of light. If we are to begin with the assumption that absorption constants of the initial components obey an additive law, then the absorption constant of the mixture is equal to

$$k = k_1 c + (1 - c) k_2, \qquad (15)$$

where $k_1$ and $k_2$ are the absorption constants of the white and colored powders and c is the concentration of the white powder.

In the experimental procedure, pre-weighed amounts of powder were gathered together, which corresponded to the obtaining of single-layer screens.* Then a single-layer screen with very low concentration of white powder was laid upon a glass substrate. Onto the layer thus obtained, a new array of particles with a large quantity of BS-10 powder was precipitated. A similar process was continued until a screen was obtained near the surface layer which contained no colored glass. It is not difficult to show that if on transition from one elementary layer to another the concentration c increases by an amount $\Delta c$, then the absorption constant varies by a linear law. Thus, in the case of weak absorption and scattering[12]

$$a = k_1, \quad b = \frac{k_2 - k_1}{il}, \quad \varphi = \frac{k_1}{s}, \quad \psi = \left(\frac{k_2}{s} - \frac{k_1}{s}\right)\frac{1}{2r_0 i}. \qquad (16)$$

Here l is the particle size, $r_0$ is the reflection coefficient of the particle surface, equal in the given case to 0.05, and i is the serial number of the elementary layer. Using the values of measured reflection coefficients of the initial powders, and with the aid of formula (13) the magnitudes of the parameters $k_1/s$ and $k_2/s$ were determined.

Reflection spectra of the objects obtained were measured with and without a white substrate. It was shown that the white substrate did not change the reflectivity of the screens. On the basis of this it was possible to assume that the samples studied behaved practically the same as if they were infinitely thick.

The results of the investigation are presented in Figs. 2 and 3, where the reflection spectra of mixtures of powders of types ZS-6 and BS-10, and SS-4 and BS-10 are shown for different values of c (the solid curves correspond to experimental magnitudes, dashed curves to the theoretical). Analysis of the data obtained permits the assumption that on application of the indicated rough model of calculation satisfactory agreement is obtained between experiment and theory. It should be noted that, as shown experimentally, with large absorptivity calculated data differ significantly from experimental data (up to 15-17%). This is partly explained by the lack of complete fulfillment of the condition of additivity (15) and unsuitability of the examined theory for the investigation of strongly absorbing media. In spite of this, the method described can be used with success for the study of a wide class of objects with variable optical parameters.

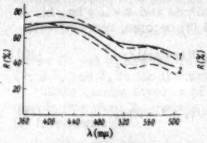


Fig. 2

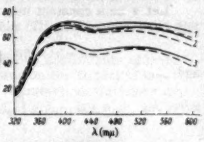


Fig. 3

Fig. 2. Reflection spectra of mixtures of powdered SS-4 and BS-10 glasses (particle size 25 microns). Solid curves—experimental, broken curves—theoretical. 1—$\Delta c$ = 2.5%, 2—$\Delta c$ = 10%.

Fig. 3. Reflection spectra of mixtures of powdered ZS-6 and BS-10 glasses (particle size 70 microns). Solid curves—experimental, broken curves—theoretical. 1—$\Delta c$ = 2.5%, 2—$\Delta c$ = 5%, 3—$\Delta c$ = 20%.

*A single-layer screen is one consisting of a single array of particles.

REFERENCES

1. S. D. Gutshabash. Uchenye Zapiski Leningrad Gosudarst. Univ., No. 153 (1952).
2. V. V. Sobolev. "Perenos luchistoi energii v atmospherakh zvezd i planet." (Transfer of Radiant Energy in Atmospheres of Stars and Planets), Gosudarst. Izd. Tekh.-Teoret. Lit., 1956.
3. C. Lundquist and H. Horak. Astrophys J. 121, 175 (1955).
4. C. Lundquist and H. Horak. Astrophys J. 121, 183 (1955).
5. V. A. Krat. Astron Zhur. 19, No. 1 (1942).
6. E. S. Kuznetsov. Isvest. Akad. Nauk SSSR, Ser. Geogr. i Geofiz. 7, 247 (1943).
7. P. Kubelka. J. Opt. Soc. Am. 44, 330 (1954).
8. V. V. Sobolev. Doklady Akad. Nauk SSSR 111, 1000 (1956).
9. Yu. I. Chekalinskaya. Trudy Inst. Fiz. i Mat., Akad. Nauk Belorus. SSR 1, 195 (1956).
10. M. M. Gurevich. Trudy Gosudarst. Opt. Inst., Leningrad 8, 1 (1931).
11. A. S. Toporets. Zhur. Opt.-Mekh. Prom. No. 2, 20 (1958).
12. B. I. Stepanov, Yu. I. Chekalinskaya, and O. P. Girin. Trudy Inst. Fiz. i Mat., Akad. Nauk Belorus. SSR 1 152 (1956).

# USE OF THE PHENOMENON OF "TOTAL EXTERNAL REFLECTION" FOR FILTERING THE CONTINUOUS SPECTRUM IN THE ULTRA-SOFT X-RAY REGION

A. P. Lukirskii and Yu. A. Omel'chenko

Received 9 July 1959

A method is described for filtering out the short wavelength part of ultra-soft X-radiation; this makes possible the use of the continuous spectrum as the source in the study of absorption spectra.

## INTRODUCTION

A continuous x-ray spectrum is ordinarily used as the radiation source in the investigation of x-ray spectra. The spectral intensity $I_\lambda$ of the continuous x-ray spectrum is given by the relation

$$I_\lambda = AZ\,\frac{1}{\lambda^2} j\,(V_0 - V_\lambda), \qquad (1)$$

where A is a constant, $\lambda$ the wavelength, j the current in the x-ray tube, Z the atomic number of the anode material, $V_0$ the voltage applied to the x-ray tube, and $V_\lambda = 12395/\lambda$ ($V_\lambda$ in volts and $\lambda$ in Angstrom units). In practice, the quantity $I_\lambda$, that is, the intensity present in the spectral interval $d\lambda = 1$, is not of interest, but rather the intensity $I_\nu$ which refers to the spectral interval $d\nu = 1$ expressed in volts. This is a consequence of the fact that when the value of the minimum resolved interval in volts ($\Delta V_{min}$) is used to specify the resolving power of spectral devices working in different wavelength regions, the value of $\Delta V_{min}$ is of the same order of magnitude at all wavelengths.

From Eq. (1) it is easy to obtain

$$I_\nu = BZj\,(V_0 - V_\lambda), \qquad (2)$$

where B is a constant.

In x-ray spectral devices a superposition of higher orders of reflection is usually produced; i.e., for given angles of reflection from a crystal or diffraction grating radiations with wavelengths $\lambda$, $\lambda/2$, $\lambda/3$, etc., are superimposed. In order to avoid this effect in working with the continuous spectrum (for studying absorption spectra), one selects the voltage on the x-ray tube so that $V_0 < 2V_\lambda$.

Let us assume that $V_0 = 1.5\,V_\lambda$. Then it is easy to obtain from (2) the equation,

$$I_\nu = BZj\,0.33\,V_0 = 0.33\,BZ \cdot P, \qquad (3)$$

where P is the power dissipated at the anode of the x-ray tube. For a given power P the intensity of the continuous spectrum will be the same, independent of the wavelength.

For ordinary x-radiation the value of P is limited only by the melting of the anode, and it is therefore possible to obtain an intensity in the continuous spectrum which is adequate for studying absorption spectra. However, in the case of ultrasoft x-radiation it is not possible to obtain high powers in the x-ray tube because of the effect of space charge. For example, to obtain a power of 1 kw dissipated at the anode in the 100 A region it would be necessary to produce a current of 5.5 amp with a voltage of 186 volts between the cathode and anode; this is impossible in practice. In view of these considerations the use of the continuous spectrum for absorption spectral studies in the ultrasoft radiation region is fraught with difficulties.

The use of other sources of radiation for absorption spectral studies is well known. These sources (condensed discharges in a vacuum[1] and in a capillary tube[2]) give a very intense line spectrum with a great number of lines. The chief drawback of these sources is the instability of both the relative and the absolute intensities. Spark sources have been used only in conjunction with the photographic method of recording the radiation; the accuracy of intensity measurements was therefore substantially lowered.

If the voltage on the x-ray tube is raised so that $V_0 \gg V_\lambda$, the limiting action of the space charge can be avoided and high radiation intensities can be obtained; however, the radiation cannot be used for absorption spectral studies without a selective weakening of the short wavelength part of the spectrum. Such a selective weakening was produced by Magnusson[3] using the fact that the short wavelength radiation is reflected only very weakly from a diffraction grating; he was then able to obtain absorption spectra in the 20-40 A region.

In the present investigation a method is described for filtering out the short wavelength part of the continuous spectrum using the phenomenon of "total external reflection." The intensity of the continuous spectrum in the wavelength region around 100 A was also estimated.

## FILTERING THE SHORT WAVELENGTH REGION OF THE CONTINUOUS SPECTRUM

Before describing the arrangement of the filter and its performance we will dwell a moment on the spectrometer and the method of producing the continuous spectrum. The investigation was carried out using a spectrometer with a focusing diffraction grating and a Geiger counter as detector. The kinematic design of the spectrometer was similar to one described previously.[4] The Geiger counter, the supply circuit for the x-ray tube, and the recorder circuit were entirely similar to those for a vacuum grating x-ray spectrometer described elsewhere.[5] The only difference was that in the present equipment the signal from the counter meter was recorded by a type PS1-01 electronic recorder.

The vacuum chamber of the spectrometer and the x-ray tube were evacuated separately with diffusion pumps, and were connected by a slit 0.3 mm wide. This system of pumping allowed a vacuum of approximately $1 \times 10^{-6}$ mm Hg to be easily maintained in the x-ray tube.

A tungsten anode was chosen as the source of the continuous spectrum; it consisted of a thin sheet of tungsten mounted on the body of the anode which was made of copper. In the course of the investigation it was found that the tungsten anode became rapidly coated with carbon, and that a stable continuous spectrum could be obtained only with a tungsten anode which had been preheated by electron bombardment to a temperature higher than 1000°C. The emission lines of tungsten served as a

criterion for the coating of the anode. At high anode temperatures, however, the anode was always coated to some extent with carbon, and this led to the appearance of carbon lines in the tungsten spectrum. The relative intensity of the carbon lines depended on the temperature to which the tungsten anode had been preheated and on the pressure in the x-ray tube. The continuous spectrum of tungsten obtained with the preheated anode is shown in Fig. 1, in which the intensity and the wavelength are plotted along the ordinate and the abscissa axis, respectively. The characteristic line of carbon in the first, second, and third orders ($C_k$I, $C_k$II, and $C_k$III) is superimposed on the continuous spectrum; thorium lines also appear since a thoriated tungsten cathode was used. Wavelength values for thorium and carbon were taken from handbook tables,[6] and for tungsten from reference 7. The drop in the intensity in the short wavelength region is due to the fact that the diffraction grating reflects the short wavelength radiation poorly (the angle of incidence of the beam on the grating was 5.5 deg). The intensity decrease at long wavelengths occurs in accordance with Eq. (1), and also because of an increase in the absorption of the window of the Geiger counter. In the region of the carbon line a rapid change in the absorption of the celluloid window of the Geiger counter may be observed.

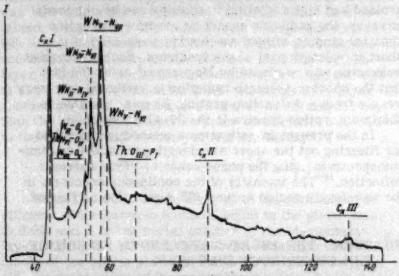


Fig. 1. The continuous spectrum from the tungsten anode.

To filter out the short wavelength part of the continuous spectrum we have used the phenomenon of "total external reflection" of x-radiation. The reflector O was located between the anode A of the x-ray tube and the entrance slit $S_1$ of the spectrometer (cf. Fig. 2, where P is the diffraction grating, D a diaphragm, $S_2$ the slit connecting the spectrometer chamber with the x-ray tube, and K the cathode). The reflector was mounted on a cylindrical rod which was brought out through the wall of the vacuum chamber of the tube and connected to a goniometer, so that different angles of reflection $\alpha$ could be set. The accuracy of the angle setting of the reflector was determined by the angle of divergence of the beam $\beta$ equal to about 0.5 deg.

Fig. 2. Schematic diagram of the filter.

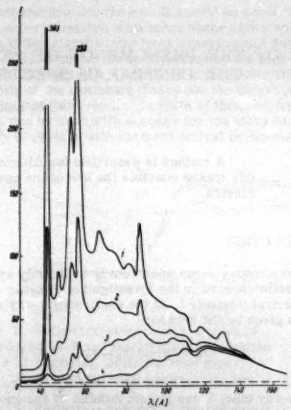


Fig. 3. The continuous spectrum of tungsten after filtering with a quartz reflector at various angles of reflection $\alpha$. Values of $\alpha$: curve 1—3°, curve 2—5.5°, curve 3—8°, curve 4—11°.

Two different reflectors, one of quartz and one of beryllium, were investigated at various angles. The curves in Fig. 3 show the wavelength dependence of the intensity $I_\lambda$ of the continuous spectrum for the quartz reflector placed at reflection angles of 3, 5.5, 8, and 11 deg; $I_\lambda$ is used here since the spectral interval defined by the slits of the spectrometer does not change as the detector is moved along the Rowland circle. The ordinates of the various curves were adjusted to give equal intensities at 150 A. It is apparent that the spectra contain a small percentage of stray radiation due to scattering from the grating and the diaphragms. The intensity of the background of stray radiation can be determined in the short wavelength region of the spectrum as follows. We note that the intensities on the short and long wavelength sides of the carbon line are very different. This difference is caused by absorption in the celluloid window of the Geiger counter. The ratio of these two intensities should remain practically unchanged as the angle of reflection is changed. If we designate this ratio by S, then

$$S = \frac{I_1 - I_b}{I_2 - I_b}, \qquad (4)$$

where $I_1$ and $I_2$ are the intensities on the long and short wavelength sides of the carbon line, respectively, and $I_b$ is the intensity of the background. If the expression for S is written down for several angles, the magnitude of $I_b$ can be easily determined. In addition, it is assumed that the value of the background intensity is constant in different parts of the spectrum. It must be noted that a decrease in the background intensity in the long wavelength region would be expected because in this case the detector is further away from the grating and the diaphragm. Since the relative magnitude of the background intensity in the long wavelength region is very small, the assumption of a constant background intensity does not introduce

a large error in the calculations; in Fig. 3 the background intensity is indicated by the dotted line.

For a better assessment of the filtering action Fig. 4 shows graphs of the dependence of $I_\alpha/I_{3^\circ}$ on the wavelength; $I_\alpha$ is the radiation intensity for a reflection angle $\alpha$ and $I_{3^\circ}$ is the intensity for the quartz reflection with $\alpha = 3^\circ$. The scales of the curves are adjusted to give equal ordinates at 150 A, using values of the intensities with the background intensity subtracted; corrections for higher orders of reflection have also been applied. The latter corrections were made by interpolation from data for the relative intensities of different orders of reflection obtained experimentally for the particular diffraction grating using the characteristic lines of carbon and boron. This crude method of calculation is quite satisfactory since the peak intensities of the characteristic lines in the higher orders of reflection are much less than the intensity in the first orders.

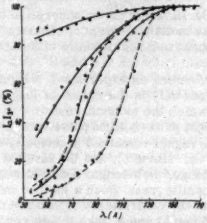


Fig. 4. Dependence of $I_\alpha/I_{3^\circ}$ on the wavelength for various angles of reflection $\alpha$. Values of $\alpha$: curve 1—4°, curve 2—5.5°, curve 3—5.9°, curve 4—7°, curve 5—7.7°. The solid curves refer to the quartz reflector, the dotted curves to the beryllium reflector.

The Table gives values of the ratio of the peak intensities in different orders for the diffraction grating used (600 grooves per mm, radius of curvature R = 1000 mm), which was ruled on glass and positioned with respect to the incident ray at a grazing angle of 5.5 deg.

| Relative intensity | $\lambda$ | |
|---|---|---|
| | $C_K$ (44 A) | $B_K$ (67 A) |
| $\frac{I_I}{I_{II}}$ | 8.4 | 90 |
| $\frac{I_I}{I_{III}}$ | 40 | 66 |
| $\frac{I_I}{I_{IV}}$ | 98 | — |

The solid curves in Fig. 4 refer to the reflection from quartz, the dotted curves to the reflection from beryllium.

## DISCUSSION OF THE RESULTS

The curves shown in Fig. 4 can be considered as giving, only in a first approximation, the dependence of the reflected radiation as a function of the wavelength. The first reason for this is that in the cases considered the intensity of the radiation is given relative to the intensity reflected at an angle of 3°. This is occasioned by the fact that all the data which we have cited on the intensity of the continuous spectrum as a function of the wavelength with different angles of reflection were obtained with one and the same x-ray tube and under the same conditions, while nothing can be said about the continuous spectrum which would have been obtained without the reflector. We note, however, that the value of $I_\alpha/I_{3^\circ}$ should differ from the value of $I_\alpha/I_0$ (where $I_0$ is the intensity of the unfiltered radiation) chiefly in the region of the short wavelength radiation, but not too strongly even there.

The other reason is the divergence of the beam $\beta$, as determined by the slit and the diaphragm (Fig. 2). As a consequence of the divergence the value of $I_\alpha/I_{3^\circ}$ changes with wavelength somewhat more smoothly than it should. However, the results quoted were obtained under actual working conditions of the spectrometer, and should therefore be regarded preferably as characteristics of the filter.

It follows from the curves given in Fig. 4 that, with the proper choice of the angle of reflection, it is possible to weaken the second order reflection by approximately seven times; the higher orders are weakened still more.

We note that the dependence of $I_\lambda/I_{3^\circ}$ on $\lambda$ for the beryllium reflector differs from that for quartz in that the graphs are somewhat more curved, and also displaced toward longer wavelengths.

The intensities of the continuous spectra for various angles of reflection were obtained with a current in the x-ray tube of 100 ma, a voltage of 5.2 kv, and a diameter of the focal spot of 5 mm. Under these conditions and with a width of 15 $\mu$ for the entrance and exit slits of the spectrometer, and using a diffraction grating with 600 rulings per mm and a radius of curvature of 1000 mm, the intensity of the continuous spectrum in the region of 100 A as registered by the Geiger counter was equal to approximately 50 counts/sec. If it is considered that the maximum power which can be dissipated at the tungsten anode is 200 watts/mm², then with the dimensions used for the focal spot the power obtainable could be increased from 320 watts to 3600 watts; this would give about 500 counts/sec for the spectral intensity in the 100 a region. With intensity values of this order the continuous spectrum could be used for spectral absorption studies.

The authors express their indebtedness to Academician A. A. Lebedev for discussions and his interest in this investigation.

## REFERENCES

1. H. W. B. Skinner and J. E. Johnston. Proc. Roy. Soc. (London) **A161**, 420 (1937).
2. D. H. Tomboulian and E. M. Pell. Phys. Rev. **83**, 1196 (1951).
3. T. Magnusson. Nova Acta Regiae Soc. Sci. Upsaliensis, Ser. IV, 11, (1938).
4. A. P. Lukirskii. Radiotekh. i Elektron. **2**, 328 (1957).
5. A. P. Lukirskii, M. A. Rumsh, and L. A. Smirnov. Opt. i Spektr. (in press).
6. Spravochnye tablitsy po rentgenovski spectroskopii. (Reference Tables for X-ray Spectroscopy), Izvest. Akad. Nauk SSSR, Moscow, 1953.
7. J. L. Rogers and F. G. Chalkin. Proc. Phys. Soc. (London) **B67**, 348, 412 (1954).

*SHORT COMMUNICATIONS*

# ON THE ABSORPTION OF ULTRAVIOLET RADIATION BEHIND A SHOCKWAVE IN THE AIR

S. A. Losev, N. A. Generalov, and L. B. Terebenina

Received 4 August 1959

Communications 1-3 reported the results of experimental investigations of the optical properties of air in the ultraviolet region of the spectrum behind a shockwave reflected from the back wall of a shock tube. Wurster and others[1, 2] have obtained the emission and absorption spectra of air at a temperature of $4\text{-}5 \times 10^3$ deg and a density approaching atmospheric. They have found that under these conditions, the spectrum is due to the presence of molecular oxygen and nitric oxide (the Shumann-Runge band system of $O_2$ and the $\gamma$-band system of NO). However, the absorption coefficient of heated air, which would be important in the evaluation of band intensities, was not measured in any of the above-mentioned investigations.

In the present work, we measured the absorption coefficient of heated air in the ultraviolet region of the spectrum behind the moving shockwave in a shock tube. Experiments were performed with the air pressure in front of the shockwave (in the low-pressure compartment) equal to 7.6-76 mm of mercury (0.01 to 0.1 atm). Hydrogen was used at pressures of 12 to 80 atm in the high-pressure compartment of the shock tube. On rupture of the diaphragm separating the air from the hydrogen, a shockwave was propagated through the air. Depending on the initial difference in pressures, the velocity of the shockwave ranged from 2 to 3.5 km/sec, and the temperature of the gas behind the shockwave front varied from 2 to 3.3 $\times 10^3$ deg.

The following arrangement was used for registering the absorption of ultraviolet radiation. Light from the source—a DKSSh-1000 lamp—passed through quartz windows in a direction perpendicular to the axis of the shock tube, at a distance of 2.5 meters from the diaphragm, and fell on the entrance slit of a quartz monochromator equipped with a 60° Cornu prism. An FEU-18 photomultiplier was placed at the exit slit of the monochromator; the signal from the photomultiplier was fed into an OK-17M oscilloscope. In order to imprive the signal-to-noise ratio, the DKSSh-1000 lamp was pulsed by means of discharges from a battary of high capacitance condensers, synchronized with passage of the shockwave past the quartz windows in the shock tube. The length of the light path inside the shock tube was 5 cm.

The absorption coefficient of air behind the shockwave front was measured over the wavelength range 2250 to 3400 A; the width of the spectral interval isolated by the monochromator varied from 9 to 19 A in different experiments. Analysis showed that the slit function of the instrument used was practically trapezoidal in shape, the ratio of the lower base to the upper base usually being 3:2 (sometimes 3:5 and 7:5).

Figure 1 shows a typical oscillogram. The lower line is the zero line; at the moment of passage of the first shockwave front, there occurs a sharp decrease in the signal (due to absorption of light by the heated air). Control experiments showed that emission by the gas itself or by any impurity was not recorded by the photomultiplier for the spectral interval and the experimental conditions chosen by us. The level of scattered radiation was controlled with the help of light filters BS in the following way. After performing an experiment, a light filter BS which transmitted only in the region of longer wavelengths than those for which the monochromator was set was placed in the light path. A light pulse was then emitted (the level of the signal remained practically constant in each series of experiments), and the level of scattered light from the longer wavelength spectral region was recorded on the oscillogram. Such a method makes it possible to evaluate the contribution of scattered radiation to the observed signal and to take it into account in calculating the experimental error. Experiments showed that scattering of radiation was mainly due to some kind of clouding of the optics, since after cleaning, the fraction of radiation scattered decreased. It was found that scattered radiation is important at the short wavelength end of the spectral region investigated (5-15% of the signal), but is relatively small elsewhere (less than 5% of the signal).

Fig. 1. Oscillogram of the absorption of ultraviolet radiation behind a shockwave front propagating at a velocity of 2.5 km/sec.

Since cold air is transparent in the spectral region investigated, the absorption coefficient of air behind the shockwave front appears in this case as the ratio of the intensity of absorbed radiation to the intensity of radiation passing through the observation section of the shock tube before passage of a shockwave. Simultaneous measurement of the rate of propagation of the shockwave and of the absorption gave us the absorption coefficient as a function of temperature and pressure. It was assumed, in agreement with references 4 and 5, that the temperature and pressure behind the shockwave front approached the values calculated from Hugoniot's adiabatic curve, taking account of dissociation and the excitation of internal degrees of freedom of the molecule. The velocity of the shockwave was measured with the help of two photomultipliers registering the impulses due to the passage of the shockwave within the field of vision of a Toepler apparatus, between two slits placed 16 cm apart. The time interval between two impulses was measured from an oscillogram taken from the screen of an OK-17M oscilloscope. The error in the measured velocity was 3%, leading to an equal error in the values for temperature and pressure.

Figure 2 shows the experimental values of the absorption coefficient $\alpha$ as a function of wavelength for a number of experiments performed under similar conditions of temperature and pressure. The scatter in the values of temperature for points plotted on the same graph did not exceed ±150°K in the majority of cases. The ab-

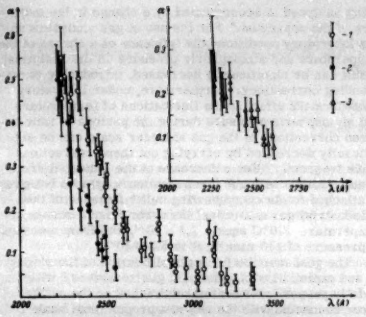


Fig. 2. Experimental values of the absorption coefficient $\alpha$ of air (path length 5 cm).
1—at T ≈ 2600°K and p ≈ 6.5(±0.5) atm;
2—at T ≈ 2200°K and p ≈ 5.0(±0.5) atm;
3—at T ≈ 3100°K and p ≈ 1.2(±0.2 atm.

solute values of the experimental errors (shown in the figure as vertical lines) were calculated taking into consideration the noise in the photomultiplier load, the finite line-width on the oscillograms, and the influence of scattered radiation.

Experiments showed that the absorption coefficient of air decreased with increasing wavelength. From Fig. 2 it can be seen that between 2800 and 3200 A (at T ≈ 2600°K and p ≈ 6.5 atm) this decrease is not monotonic: separate absorption maxima are evident in the graph. The heights of these absorption maxima exceed the experimental error.

Thus, our experimental investigation detected a noticeable absorption of ultraviolet radiation over a path length of 5 cm, by air heated by a shockwave. The absorption coefficient increased with increasing pressure and temperature; when the pressure and temperature were increased, absorption became noticeable even in the long wavelength region of the spectrum. Analysis of existing data[1, 2, 6] indicated that the main cause for the absorption of light in the spectral region investigated was the existence of oxygen and nitric oxide bands.

REFERENCES

1. W. Wurster and H. Glick. J. Chem. Phys. 27, 5, 1218 (1957).
2. W. Wurster, C. Treanor, and H. Glick. J. Chem. Phys. 29, 1, 250 (1958).
3. I. Keck, B. Kivel, and T. Wentink. Preprint. Inst. of Heat Transfer and Fluid Mechanics, 1957.
4. F. S. Faizullov, N. N. Sobolev, and E. M. Kudryavtsev. Doklady Akad. Nauk SSSR 127, 3, 541 (1959).
5. J. Clouston, A. Gaydon, and I. Glass. Proc. Roy. Soc. A248, 1255, 429 (1958).
6. S. A. Losev. Nauch. Doklady Vyssh. Shkoly, Fiz.-Mat. Nauk. No. 5, 197 (1958).

# CALCULATION OF THE ERRORS OF AN ABSORPTION ANALYZER OF GASEOUS OR LIQUID MIXTURES

A. O. Sall'

Received 14 September 1958

In order to decrease the errors in absorption analysis based on the measurement of the fraction of the radiation absorbed by a specific component of the mixture of gases or liquids being analyzed,[1-3] the compensating change of the reference intensity in the absorptiometer examined in references 3-8 is accomplished by a change of the thickness of the layer of the compensating mixture. The concentration of the specific component in the mixture analyzed is then determined by the thickness of the layer of the compensating mixture, for which the signal at the output of the radiation detector vanishes. Let us calculate the relative error of such an absorptiometer. Let us examine, for example, the optico-acoustic gas analyzer with gas compensation.[4-6] We will take the numerical values of the parameters of an industrial gas analyzer[7, 8] as those determining the magnitude of the errors.[4, 5]

The expression for the radiation intensity I transmitted by the apparatus containing the analyzed mixture and detected by the radiation detector, can be written in the form:[5]

$$I = I_0 [(1 - \delta) e^{-D} + \delta],$$

where $I_0$ is the intensity transmitted by the apparatus in the absence of a component absorbing radiation, D is the optical density, $\delta$ is the ratio of the share of the "ballast radiation" to the total intensity.

We denote by $\gamma$ the ratio of the threshold sensitivity of the radiation detector to the value of the intensity $I_0$. Then, for a threshold sensitivity $\Delta C$, determined by the noise and impedance of the detector, we have

$$\frac{d}{dc} [(1 - \delta) e^{-D} + \delta] \Delta c = \gamma,$$

from which, for the corresponding component error, we have

$$\left(\frac{\Delta c}{c}\right)_\gamma = \gamma e^D D^{-1} (1 - \delta)^{-1}.$$

For $\gamma = 10^{-4}$, $\delta = 0.5$, and $D = 0.5$ we get

$$\left(\frac{\Delta c}{c}\right)_\gamma \simeq 7 \cdot 10^{-4}.$$

The minimum possible measurement of the change of the radiation intensity, limited by a series of factors (nonidentical changes of the beams being compared, the presence of a remaining source signal in absorptiometers with attenuation of the beams, fluctuation of the number of quanta falling on the detector) generally establishes a magnitude of the order of a thousandth part of the current (i.e., $\alpha = 10^{-3}$).[4, 6] Using the conclusions of reference 5

and putting $\delta = 0.5$ and $D = 0.5$, we obtain for the corresponding relative error

$$\left(\frac{\Delta c}{c}\right)_{\kappa} = 5.3 \cdot 10^{-3}.$$

The component error, determined by the error of the compensating and recording equipment, can also be found by formulas obtained in reference 5. Then

$$\beta \simeq \sqrt{\beta_1^2 + \beta_2^2},$$

where $\beta_1$ is the ratio of the error in the shift of the reflecting surface (produced, for example, by a lift in the sliding system) to the magnitude of the total shift; $\beta_2$ is the relative error of the determination of the magnitude of the shift of the reflecting surface relative to the recording apparatus. A numerical value of the coefficient $\varepsilon$ can be found,[5] considering that for a change of the length of the light path in the compensating cell of 3 mm, the relative change of the compensating beam, determined by the change of the geometry of the light path,[5] does not exceed 0.01. If the length of the light beam in the gas layer is expressed in mm, and the concentration of the specific component in volume percent, then generally $K \geq 10^{-2}$ (mm %)$^{-1}$. With such a value of K (and the compensating cell filled with the pure component being analyzed), it is possible to attain a value $D_K \simeq 3$ mm $\times 100\% \times 0.01$ (mm %)$^{-1} \simeq 3$. In this case

$$\varepsilon \simeq \frac{0.01}{3} \simeq 3 \cdot 10^{-3}.$$

Considering also that $\beta \simeq 5 \times 10^{-3}$ [5] for $D \simeq 0.5$, we have

$$\left(\frac{\Delta c}{c}\right)_{\beta} \simeq \beta \simeq 5 \cdot 10^{-3}.$$

The error of a chemical control analysis of gas mixtures (by which a calibration and correction of an apparatus is produced) for a relatively large concentration of the component determined does not generally exceed 0.01. U Usually, one aims for a relative error of calibration and establishment of the scale of a gas analyzer of $5 \times 10^{-3}$. Using the derived numerical values, we find the following quantity for the square error

$$\sqrt{(7 \cdot 10^{-4})^2 + (5.3 \cdot 10^{-3})^2 + (5 \cdot 10^{-3})^2 + (10^{-2}) + (5 \cdot 10^{-3})^2} \simeq 0.013,$$

i.e., 1.3% (relative) of an upper division of measurement of the gas analyzer.

If the scale of the gas analyzer is graduated in volume percent, then a change in the density of the gas mixture being analyzed is accompanied by a change in the indicators of the apparatus.[6] For the use of gas analyzers under laboratory conditions the influence of a change of the temperature and atmospheric pressure on the analytical result can be significantly decreased, introducing corresponding corrections. Furthermore, under laboratory conditions the effect of the fluctuations of temperature and atmospheric pressure during the periods of time between corrections of the gas analyzer scale can be significantly decreased by carrying out these corrections more frequently. For a decrease of the indicated error in apparatuses with gas compensation a sylphon bellows is attached to the compensating cell.[6] Because of this, in industrial gas analyzers[7] the error from a change of temperature $\pm 10°C$ equals $1.3 \times 10^{-3}$, and from a change of pressure of $\pm 10$ mm Hg it is $5.3 \times 10^{-3}$.

The goal must be for a simplification of the setting up and exploitation of industrial gas analyzers,[7] with strictly proportional scales established on them. The error connected with the use of a proportional scale[5, 6] generally does not exceed 0.015. In this case it is possible to neglect the error of calibration and preparation of the scale. As a result of the presence in the complete gas analyzer of an electronic recorder,[7] the value of $\beta$ increases to 0.01. Thus, the square error of industrial apparatuses for $D \simeq 0.5$ and $\delta \simeq 0.5$ has a magnitude of the order of 2-3% (relative).

## REFERENCES

1. V. M. Chulanovskii and N. P. Lenkin. Izvest. Akad. Nauk SSSR 15, 206 (1945).
2. M. V. Savost'yanova. Izvest. Akad. Nauk SSSR, Ser. Fiz. 11, 424 (1947).
3. V. M. Chulanovskii. "Vvedenie v Molekulyarnyi Analiz." (Introduction to Molecular Analysis), Gosudarst. Izd. Tekh.-Teoret. Lit., Moscow-Leningrad, 1951.
4. A. O. Sall'. Priborostroenie No. 6, 14 (1956).
5. A. O. Sall'. Opt. i Spektr. 5, 316 (1958).
6. A. O. Sall'. Zhur. Tekh. Fiz. 29, 330 (1959).
7. V. A. Pavlenko. Pribory dlya Avtomaticheskovo Kontrolya Analiza Gazov i Mass-Spektrometry, in "Teploenergetickeskie i Khimiko-Teknologicheskie Pribory i Regulyatory." (Apparatuses for the automatic control of gas analysis and of mass spectrometers, in 'Thermoelectric and Chemical-Technological Apparatuses and Regulators") Mashgiz, M.-L., 1959.
8. A. O. Sall'. Opt. i Spektr. 7, 432 (1959).

# THE STRUCTURE AND NATURE OF EXCITATION OF THE MAGNESIUM OXIDATION SPECTRUM

V. A. Sokolov and N. A. Nazimov

Received 1 October 1959

MgO is one of the white oxides said to possess the property of candoluminescence.[1] The unusual brightness of the flame accompanying the oxidation (burning) of magnesium is also associated with the concept of candoluminescence.

Recently, it was shown that true candoluminescence of oxides which have the properties of crystalline phosphors is possible only at relatively low temperatures (below the quenching temperatures of luminescence).[2] One would therefore expect that at the ignition temperature of magnesium (>1400°), the solid particles of the oxide created during the burning process would be merely pure thermal radiators.

We carried out an investigation of the spectrum of burning magnesium in order to understand its excitation mechanism.

As a result of this investigation, it was established that the continuous spectrum of the magnesium flame is approximately the same as the thermal radiation spectrum of MgO (Fig. 1).* An analysis of the spectrum according to the method described in reference 3 shows that it obeys Kirchhof's law.

*The oxidation spectrum of magnesium was simply obtained by photographing the flame of metallic magnesium slowly burning in air. The thermal radiation spectrum of the oxide was obtained by placing a solid MgO sample in front of the spectrograph and heating it with the help of an electric oven.

This indicates that the luminescence of burning magnesium is determined to a large extent by the thermal radiation of the hot particles formed by the oxidation reaction. The unusual brightness of these particles is due to the selectivity of the thermal radiation of MgO.

The thermal radiation of solid fragments of oxide is the principal cause of the visible radiation of the magnesium flame, but it is not the only cause. Thus, particularly in the case of an energetic and short-lived flash, one sees a clearly defined electron-vibrational structure of the MgO molecule (shown on a magnified scale in Fig. 2) superimposed on the continuum in the green portion of the spectrum. This structure appears because of the presence of gaseous MgO, and is due to either thermal excitation alone or to processes related to chemiluminescence.

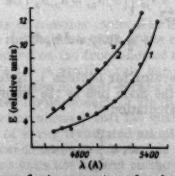


Fig. 1. Curve 1—temperature luminescence spectrum of MgO; curve 2—oxidation spectrum of Magnesium (x—the position of the vibrational structure of MgO molecules).

In order to explain this, the band intensities $I_{v',v''}$ were determined for the electron vibrational spectrum shown in Fig. 2, and the vibrational transition probabilities $A^{*}_{v',v''}$ were computed (using Manneback's method[3]). The distribution law

$$I_{v'v''} = A^{*}_{v'v''} C e^{-\frac{E_{v'}}{kT}}$$

was applied in the logarithmic form

$$\lg I_{v'v''} = \lg A^{*}_{v'v''} + \lg C - \frac{E_{v'}}{kT} \lg e.$$

This is the equation of a straight line in coordinates $\lg I/A^{*}$ and $E_{v'}$ (the energy of the upper vibrational level) with the slope

$$a = \frac{1}{kT} \lg e.$$

The graphical dependence of these quantities as shown in Fig. 3 shows that the points obtained deviate only slightly from a straight line. This, in turn, means that in the spectrum investigated, the distribution of the vibrational states is practically an equilibrium distribution, i.e., the excitation of the electron vibrational spectrum in this case has almost no connection with the processes of chemiluminescence. In addition, if one considers the fact that the continuous emission spectrum of the oxidation obeys Kirchhof's law, as was mentioned before, it appears that general thermodynamic equilibrium exists in the flame of burning magnesium.

Thus, the unusual brightness of the magnesium flame is caused not only by the thermal emission of solid fragments of the oxide formed which radiate selectively, but also by the thermal emission of MgO molecules in the gaseous phase.

It should also be mentioned that some atomic lines of magnesium are seen in the spectrum of the magnesium flame. However, the amount of atomic radiation in the oxidation spectrum of magnesium is insignificant in comparison with the factors considered above.

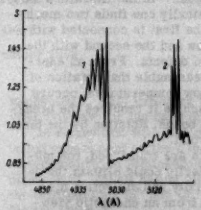


Fig. 2

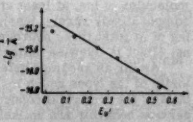


Fig. 3

Fig. 2. Curve 1—electron vibrational structure of MgO molecule in the oxidation spectrum of magnesium; curve 2—magnesium lines.

Fig. 3. Graph of $-\lg I/A^{*}$ as a function of $E_{v'}$.

REFERENCES

1. L. T. Minchin. Trans. Faraday Soc. 35, 163 (1939).
2. V. A. Sokolov. Opt. i Spektr. 4, 409 (1958).
3. V. A. Sokolov, I. S. Grozina, and A. N. Gorban. Opt. i Spektr. 3, 92 (1957).
4. G. Liebman. Z. Physik 65, 404 (1930).
5. C. Manneback. Physica 17, 1001 (1952).

# THE INFLUENCE OF PROTON MOBILITY ON NUCLEAR MAGNETIC RESONANCE LINE WIDTH IN CRYSTALS

I. V. Aleksandrov, N. N. Korst, and N. D. Sokolov

Received 10 October 1959

Mobility of hydrogen atoms (protons) in a condensed phase may be occasioned by internal rotation or by translational jumps of the atoms (protons) from one equilibrium position to another. The application of nuclear magnetic resonance (NMR) of protons constitutes one of the effective methods for studying this mobility. NMR has been used to investigate internal rotation in many solids (see, for example, reference 1).

The investigation of translational jumps of protons, particularly in hydrogen bonds, is no less important a problem, being one whose solution has great significance, for example, in the theory of protonic semiconductors, protolytic reactions, and the mobility of protons in adsorbed films and in certain polymers—albumins and others.

Ice is one of the substances for which the role and mechanism of proton transfer has not been decided.

In 1936 Pauling, in analyzing the reasons for the existence of residual entropy in ice, concluded that there is a disordered distribution of hydrogen atoms among the possible equilibrium positions in hydrogen bonds. He showed that in ice there is a well defined number of equivalent distributions consistent with the requirement that each oxygen atom has two hydrogen neighbors. However it is still an open question whether each such proton configuration occurs statistically or whether transitions are occurring between one such configuration and another, i.e., do hydrogen atoms (protons) jump from one equilibrium position to another? Neutron diffraction data[2] will not be able to answer this question, since they agree equally with both models.

Obviously jumps do occur in some temperature range; the question arises, at what temperature do they begin and by what mechanism do they occur? In the literature (see, for example, reference 4) basically one finds two mechanisms for proton mobility: the first is connected with the rotation of water molecules and the second with the occurrence of various kinds of defects. From an energetic point of view it seems reasonable that rotation of molecules in ice, at least at low temperatures, occurs comparatively rarely, inasmuch as it requires the breaking of at least three hydrogen bonds. Rotation by the tunnel effect is likewise unimportant.

As far as assumed defects are concerned, the majority of the types which formerlly could explain the details of the electrical conductivity and dielectric dispersion behavior are unlikely from an energetic viewpoint. For the most part, proton exchange through defects should take place slowly. It is still possible that collective jumps of protons along hydrogen bonds play a more important role, these hydrogen bonds forming rings of several (≥6) links. Such jumps, coupled with changes in the proton configuration, may form an important link in the explanation of various properties of ice.

The choice between the statistical model of ice and the model involving proton jumps can be made by studying the second moment of the NMR signal from the ice protons. An investigation of its temperature dependence should give information about whether the proton exchange occurs classically or by the tunnel effect.

In order to calculate the second moment, we shall assume that in the presence of exchange, the frequency with which one proton distribution changes into another equivalent one is much greater than the line width (expressed in cycles per second). Under these conditions, classical and quantum (tunneling) mechanisms will obviously lead to exactly the same result. We shall consider this assumption to apply equally to the possible rotations of molecules (assuming that they occur sufficiently rapidly), as well as to translational jumps in rings. Obviously, changes in the proton configuration through defects can occur only slowly and need not be considered in the calculation.

Under the assumed conditions for calculation of the second moment we can use the method of Gutowsky and Pake.[4] In our case it is restricted to the use of a Hamiltonian averaged over all the proton positions in calculating the second moment of the line by the method of Van Vleck.[5]

$$\mathcal{H} = -\gamma\hbar H_0 \sum_j S_{jz} + A + B + C, \qquad (1)$$

where

$$A = \frac{\gamma^2\hbar^2}{2} \sum_{k>j} r_{jk}^{-3} [3\cos^2\theta_{jk} - 1][(S_j S_k) - 3S_{kj} S_{jk}],$$

$$B = -\frac{3}{2}\gamma^2\hbar^2 \sum_{k>j} r_{jk}^{-3} \left\{ [S_j^+ S_{kz} + S_{kj} S_k^+] \sin\theta_{jk}\cos\theta_{jk} e^{-i\varphi_{jk}} + \frac{1}{2} S_k^+ S_j^+ \sin^2\theta_{jk} e^{-2i\varphi_{jk}} \right\},$$

$$C = -\frac{3}{2}\gamma^2\hbar^2 \sum_{k>j} r_{jk}^{-3} \left\{ [S_j^- S_{kz} + S_{kj} S_k^-] \sin\theta_{jk}\cos\theta_{jk} e^{i\varphi_{jk}} + \frac{1}{2} S_k^- S_j^- \sin^2\theta_{jk} e^{2i\varphi_{jk}} \right\};$$

$S_j$ is the spin operator for nucleus j. Note that in analyzing the shape of the main line by the method of moments (that is, in the calculation of

$$M_n = \int_0^\infty \nu^n g(\nu)\, d\nu,$$

where $g(\nu)$ is the line shape) it is necessary to exclude the subsidiary lines arizing from terms B and C, inasmuch as they make a large contribution to the second moment, despite their small intensities, because of their

great separation in frequency from the main line. Thus terms B and C must be omitted from the Hamiltonian.

The difficulty of the calculation is eliminated in calculating the geometry of the proton distribution. Taking the six nearest protons into account, and handling the protons in the next layer by means of an integration, we obtain the following result:

For rapid exchange in a single crystal

$$\langle \Delta\omega^2 \rangle = 0.32\hbar^2\gamma^4 r^{-6}\,[3.0 - 1.8F(\theta, \varphi)];$$

in a polycrystalline sample,

$$\langle \Delta\omega^2 \rangle = 0.63\hbar^2\gamma^4 r^{-6}$$

(substitution of numerical values gives $\langle \Delta\omega^2 \rangle \simeq 20$ gauss$^2$). In the absence of exchange (or with slow exchange) for a single crystal

$$\langle \Delta\omega^2 \rangle = 0.32\hbar^2\gamma^4 r^{-6}\,[3.9 - 2.4F(\theta, \varphi)];$$

for a powder

$$\langle \Delta\omega^2 \rangle = 0.80\hbar^2\gamma^4 r^{-6}$$

(substitution of numerical values gives $\langle \Delta\omega^2 \rangle \simeq 25$ gauss$^2$). Here

$$F(\theta, \varphi) = \cos^4\theta + \sin^4\theta\,(1.5 - \cos^4\varphi - \sin^4\varphi),$$

where r is the separation of the nearest protons (1.65 A), and $\theta$ and $\phi$ are the angles defined by the direction of the constant magnetic field H with respect to the crystal axes.

This calculation is evidently applicable at temperatures sufficiently low that the concentration of defects is small and they give rise only to slow exchange. These formulas are of course not applicable in the vicinity of 0°C. Preliminary measurements, made at our request by A. G. Lundin at the Institute of Physics of the Siberian branch of the Academy of Sciences of the USSR, gave $\langle \Delta\omega^2 \rangle = 12$ gauss$^2$. Now it is important to follow the dependence of second moment on temperature. We may expect that the second moment will approach a limit. The qualitative observations of Bloembergen, Purcell, and Pound[6] on the line width of the NMR in ice testify to this fact. If the limiting value turns out to be 25 gauss$^2$ (statistical model or slow exchange), it means that at higher temperatures rapid exchange occurs classically, if, on the other hand, the limiting value turns out to be 20 gauss$^2$, it means that both at very low temperatures and near 0°C the motion of protons is basically by a tunneling mechanism. It would at the same time mean that rotation and defects, at least at low temperatures, do not play a notable role in changing the proton configuration.

We have carried out a similar calculation for the carbonic acid crystal, consisting of dimeric molecules held together by hydrogen bonds. In this case only two protons were considered—the oned involved in the two hydrogen bonds of the dimer. This pair of protons can reorient in a plane defined by the angle $\theta$ between the normal to this plane and the direction of the field H (synchronous transitions of protons in adjacent potential wells). In the presence of rapid reorientation the calculation gives, for a single crystal,

$$\langle \Delta\omega^2 \rangle = \frac{9}{16}\gamma^4 r^{-6}\hbar^2 \left[3\sin^2\theta\left(\sin^2\varphi\cos^2\frac{\delta}{2} + \cos^2\varphi\cdot\sin^2\frac{\delta}{2}\right) - 1\right];$$

for a powder

$$\langle \Delta\omega^2 \rangle = \frac{9}{80}\hbar^2\gamma^4 r^{-6}\,(1 + 3\cos^2\delta)$$

($\delta$ is the angle between the two possible directions of the vector r which connects the pair of protons.)

In this manner, a comparison of experimental data with the results of calculations can provide an answer to the question of the presence or absence of rapid jumps of protons in crystals containing hydrogen bonds.

REFERENCES

1. H. Gutowsky and G. Pake. J. Chem. Phys. 18, 162 (1950).
2. L. Pauling. J. Am. Chem. Soc. 57, 2680 (1935).
3. S. W. Peterson and H. A. Levy. Acta Cryst. 10, 70 (1957).
4. A discussion on the physics of water and ice. Proc. Roy. Soc. A247, 421 (1958).
5. J. Van Vleck. Phys. Rev. 74, 1168 (1948).
6. N. Bloembergen, E. M. Purcell, and R. V. Pound. Phys. Rev. 73, 679 (1948).

# THE STEP-SHAPED DEPENDENCE OF THE RECOMBINATION LUMINESCENCE QUANTUM YIELD OF ALKALI HALIDE CRYSTAL PHOSPHORS ON THE FREQUENCY OF THE EXCITING LIGHT

I. V. Yaek

Received 3 November 1959

For solutions of complex molecules the fluorescence quantum yield in the Stokes region of the excitation spectrum does not depend on the frequency of the exciting light (Vavilov's law).[1] A similar rule has been established both in the Stokes and anti-Stokes regions for the short, intra-center luminescence of alkali halide crystal phosphors.[2,3] Zaitov showed[4] that the quantum yield of the optical flash of x-ray irradiated alkali halide crystals within the boundaries of each excited elementary absorption band also does not depend on the frequency of the stimulating light.

The phosphorescence excitation spectra of alkali halide crystals measured in references 2, 5, and 6 differ somewhat from the excitation spectra of steady-state luminescence. This indicates that there is a departure from Vavilov's law for the case of recombination luminescence.

In connection with this problem we conducted a detailed experiment on the dependence of the quantum yield of recombination luminescence on the frequency of the exciting light. Alkali halide single crystals activated with the leadlike ions $In^+$ and $Ga^+$ were chosen as the materials for the study.

The measurements were conducted at room temperature in an automatically recording photoelectric photometer. The excitation was accomplished with light from a hydrogen lamp or an SVDSh-250 lamp passed through the monochromator of an SF-4 spectrophotometer.

The quantum yield of recombination luminescence

$\eta_p$ is defined as

$$\eta_p(\nu_3) = \frac{n_p}{n(\nu_3)},$$

where $n_p$ is the number of quanta emitted in the process of recombination luminescence, $n(\nu_3)$ is the number of quanta with frequency $\nu_3$ that are absorbed. In the steady state $n_p$ and $n(\nu_3)$ can be referred to a unit of time,[7] i.e., replaced by $dn_p/dt$ and $dn(\nu_3)/dt$ respectively. It is difficult to directly determine $I_p = dn_p/dt$ at the time of the excitation. For this reason we measured the phosphorescence intensity at a definite stage of its decay (1 sec after the excitation ceased). If the quantum yield of the steady-state luminescence is constant then the intensity of the steady-state luminescence is

$$I_{st.}(\nu_3) \sim \frac{dn(\nu_3)}{dt}.$$

Thus, the recombination luminescence yield can be calculated as

$$\eta_p(\nu_3) = \left[\frac{I_p}{I_{st.}}\right]_{\nu_3}.$$

If the intensity of the exciting light is varied in such a way that at all frequencies the steady-state luminescence intensity remains constant, then the function $I_p(\nu_3)$ gives the quantum yield spectrum of the recombination luminescence directly without further corrections.

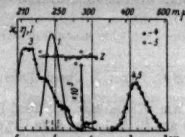


We rechecked and confirmed that the $\eta_{lt.}(\nu_3) = \text{const.}$ condition was fulfilled. The data for the phosphor KBr-In are plotted in curve 2 of the Figure. The spectrum of the recombination luminescence quantum yield that was obtained for this phosphor (curve 3) has an unusual shape. As the frequency of the exciting light is increased a steplike growth in recombination luminescence is observed. The absorption spectrum of KBr-In with low activator concentration is shown in the same figure (curve 1). As can be seen, the lowest value of recombination luminescence quantum yield is in the region of the absorption bands at 4.23 ev and 4.08 ev (the electron transitions $^1S_0 \rightarrow {}^3P_1$ and $^1S_0 \rightarrow {}^3P_0$ in $In^+$ ions). Here it is less by a factor of 7000 than the highest yield in the band having a maximum at 5.08 ev (the electron transition $^1S_0 \rightarrow {}^1P_1$ in the $In^+$ ions).

Within the boundaries of the $^1S_0 - {}^1P_1$ band two regions are observed which have constant but unequal yields. These two regions are located at the edges of the absorption band.

Still another higher plateau is observed in the yield spectrum on the short wavelength side of the $^1S_0 \rightarrow {}^1P_1$ band. This plateau is apparently associated with the $n^1S_0 \rightarrow (n+1)^1S_0$ electron transition in the activator ion.

The recombination luminescence quantum yield spectra of the phosphors KcL-In, NaCl-In, and KBr-Ga have a similar steplike character.

Blinger[2] expressed the hypothesis that the variability of the phosphorescence yield of KCl-Tl can be explained by overlapping of the absorption bands of phosphorescence and fluorescence centers which are different in nature. Such an explanation contradicts the over-all superposition of the fluorescence and recombination luminescence spectra that we established (see curves 4 and 5 in the Figure).

We associate the growth of the recombination luminescence yield in the direction of the short wavelength bands with its excitation by a two-step process that is photothermal in nature. This assumption is in good agreement with the fact of the general decrease of the recombination luminescence yield and the redistribution of the yields toward the short wavelength bands when the temperature is reduced.[8] The variability of the yield within the boundaries of the $^1S_0 \rightarrow {}^1P_1$ band is explained by the fact that this band is not an elementary one but is composed of three subbands corresponding to the splitting of the $^1P_1$ level into 2J + 1 components in the field of the crystal lattice.[8] Because of the photothermal nature of the excitation of recombination luminescence the yield for the short wavelength subbands must be greater than for the long wavelength subbands. The difference in the yields of the different components of the $^1S_0 \rightarrow {}^1P_1$ band depends on the degree of splitting which is not the same for different activators. A conclusive relationship actually observed is that the degree of splitting and differences in yields of subbands grow in a parallel way in the series of activators $Tl^+ \rightarrow In^+ \rightarrow Ga^+$.

If one resolves the contour of the $^1S_0 \rightarrow {}^1P_1$ absorption band of the KBr-In phosphor into three components having Gaussian shape, and if one assumes that the yield of each of the components is constant but greater for the short wavelength subband than for the long wavelength ones, then after plotting the yield for the total band one obtains a picture that agrees with the experimental curve. We estimated the spacing between maxima of adjacent components of the splitting of the $^1P_1$ level by a method of this kind. It is noted in the Figure by a dotted line and amounts 0.13-0.14 ev.

The data presented in this report show that the quantum yield of recombination luminescence is constant in regions of discrete, elementary absorption bands of luminescence centers, but in the general case is different for different elementary bands.

We think that after photoexcitation which transfers it to a specific electron state a luminescence center very quickly comes to equilibrium with the surrounding crystal lattice with respect to vibrational energy. After this thermal ionization of the excited center (or some other process[9]) takes place, which leads to the stimulation of recombination luminescence. However, the equilibrium between the different electron states in the general case does not have time to become established during the lifetime of a center in an excited state.

In conclusion we express our profound gratitude to Ch. B. Lyshchik for his guidance in this work.

REFERENCES

1. S. I. Vavilov. Z. Physik **22**, 266 (1924)(see also the collection of papers. Ibid. 1, 150); Z. Physik **42**, 311 (1927)(see the collection of papers. Ibid. 1, 222); S. S. Solomin. Doklady Akad. Nauk SSSR 31, 741 (1941).
2. W. Bunger. Z. Physik **66**, 311 (1930).
3. K. K. Shvarts. Materialy VII Soveshchaniya po Lyuminestsentsii, Moscow. (Papers of the Seventh Conference on Luminescence), Moscow, 1958.
4. F. N. Zaitov. Opt. i Spektr. **4**, 102 (1958).
5. M. L. Kats. Doklady Akad. Nauk SSSR **32**, 178 (1941); M. Kato. Sci. Paper Inst. Phys. Chem. Research (Tokyo) **42**, 95 (1944); Ch. B. Lushchik, Kh. F. Kvaembre and I. V. Yaek. Materialy VII Soveshchaniya po Lyuminestsentsii,

Moscow. (Papers of the Seventh Conference on Luminescence), Moscow, 1958.
6. I. V. Yaek. Trudy Inst. Fiz. i Astron., Akad. Nauk Eston. No. 10, 166 (1959).
7. B. I. Stepanov. "Lyuminestsentsiya slozhnykh molekul." (The Luminescence of Complex Molecules), Minsk, 1955.
8. Ch. B. Lushchik and N. E. Lushchik. Trudy Inst. Fiz. i Astron., Akad Nauk Eston. No. 6, 5 (1957).
9. Ch. B. Lushchik, G. G. Liid'ya, I. V. Yaek, and E. S. Elisler. Opt. i Spektr. (in print).

# A METHOD OF STRUCTURAL-GROUP ANALYSIS BY INFRARED SPECTRA. DETERMINATION OF MONO-OLEFINIC STRUCTURES OF THE PRODUCTS OF THE GAMMA-RADIOLYSIS OF n-HEPTANE

B. A. Smirnov

Received 9 November 1959

We determined quantitatively the types of mono-olefins in the product of the gamma-radiolysis of n-haptane obtained from Kolbanovskii,[1] using a double-beam spectrophotometer IKS-14 equipped with a NaCl prism, in the 9-16 $\mu$ region. The characteristic frequencies of the corresponding structures and the averages of the $E_{1a}$ (moles/ml/cm), taken from the literature,[2] are given in the Table. Results obtained with our instrument on the vinylidene structure RR'C = $CH_2$ and heptene-1 were in good agreement with the values from the literature. In the case of the above two structures, we took our values for the characteristic frequencies and the $E_{1a}$.

| Structure | $\lambda(\mu)$, $\nu(cm^{-1})$ | $E_{1a}$ 10³ (moles/cm²/cm) | Moles/ml·10⁶ | Mole % calculated on basis of $C_7$ |
|---|---|---|---|---|
| RCH=CHR' trans-olefin | 10.25—10.37 (976—964) | 10 | 39.0 | 5.5 |
| RCH=$CH_2$ α-olefin | 10.90—11.00 (917—909) | 10.8 | 12.35 | 1.7 |
| RR'C=$CH_2$ vinylidene | 11.21—11.30 (892—885) | 14.5 | 7.82 | 1.1 |
| RCH=C—R' $CH_3$ | 12.01—12.38 (833—808) | 4.0 | 4.2 | 0.6 |

Scattered light was eliminated through the use of scatter plates in the instrument. The rate of scanning was 14 min/rev and the scanning was linear with respect to wavelength, since in the region $\lambda > 10$ $\mu$, it guarantees a greater accuracy in recording relative to scanning linear in wave number.

In order to obtain the most accurate possible results, the analysis was performed in the following way. The cell thickness d was about 0.25 mm because of the following consideration: since in the double-beam method, the absorption due to the unsaturated product is eliminated, then, the thicker the sample, the more prominent will be the characteristic frequencies of the structures sought. The width of the cell containing the sample can be increased to a total transmission $T_\Sigma = T_{C_7} + T_{unsatd.}$, of not less than 30%, without infraction of the linearity of the recording part of the spectrophotometer. For $T_\Sigma <$ 30%, linearity is disturbed, which fact was substantiated in our instrument by means of direct measurement.

Furthermore, when the thickness of the cell with the irradiated heptane was equal to the thickness of the cell with pure heptane—d = 0.261 mm—we determined from the infrared spectra the qualitative structural-group composition of the unsaturated part of the products. The approximate total amount of unsaturated structures was calculated to be about 9 mole % on the basis of $C_7$. After After this, the measurements were repeated with a sample cell of thickness d = 0.281 mm—about 9% thicker than the reference cell with n-heptane. In this manner we excluded the influence of the background due to the saturated part of the products. The final calculations were based on this last spectrum. The application of this method to the given sample gave a correction of 20% for the α-olefins in the direction of increase in their concentration and permitted us to detect very clearly the structure RCH=CR'R", thus vindicating our method.

Preliminary experiments with products which received integral doses of about $10^{18}$ev/ml and about $10^{20}$ ev/ml, respectively, showed that reliable determination of the main unsaturated component can be performed only beginning with doses of about $10^{21}$ev/ml.

We studied a sample of n-haptane which had received a dose of $1.8 \times 10^{22}$ev/ml. In this case, the following four types of unsaturated structures could be determined with certainty: trans-olefins, α-olefins, vinylidene structure RCH=CR'R", whose concentrations were in the ratios of 9:3:2:1 within the limits of experimental error, with a total concentration of the unsaturated compounds $63.3 \pm 3.5 \times 10^{-3}$ moles/ml or $8.9 \pm 0.5$ mole % calculated on the basis of $C_7$.

It must be noted that the infrared method does not allow the determination of cis-unsaturated compounds in the presence of considerable quantities of n-paraffins, because of the strong absorption by the latter in the region of 13.7 to 14.7 $\mu$ caused by deformation vibrations of the chain $-(CH_2)_{n>2}-$, and hence their presence in the irradiated product is still an open question. The same situation occurs in the case of tetrasubstituted olefins of the type RR'C=CR"R"' which, in general, are not analyzed by infrared spectroscopy.

In conclusion, the author would like to express his gratitude to Iu. A. Kolbanovskii for his exceptionally valuable help in the realization of the present investigation.

## REFERENCES

1. A. M. Brodsky. I. A. Kolbanovski, E. D. Filatova, and A. S. Tschernysheva. Intern. J. Appl. Radiation and Isotopes 5, 57 (1959).
2. H. L. McMurrey and V. Thornton. Anal. Chem. 24, No. 2, 318 (1952).

# I-J INTERACTION IN THE $CH_3I$ MOLECULE

B. D. Osipov

Received 13 November 1959

The interaction of nuclear spin with the magnet field of a molecule in a $^1\Sigma$ state (I-J interaction) has been observed and measured for a whole series of linear molecules. For a symmetric top molecule the I-J interaction has been studied adequately only for $NH_3$.[1] The energy of the I-J interaction for a nucleus lying on the axis of the symmetric top has the following form:[2]

$$W_m = \frac{F(F+1)-J(J+1)-I(I+1)}{2}\left[a+(b-a)\frac{K^2}{J(J+1)}\right], \quad (1)$$

where F is the total angular momentum quantum number, J is the rotational quantum number, K is the projection of J on the axis of the molecule, and a and b are constants of the I-J interaction.

In the presence of quadrupole hyperfine structure the J degeneracy is removed by the quadrupole interaction, and the presence of I-J interaction leads only to a shift of the energy levels by the amount $W_m$.

In the present investigation the I-J interaction in the $CH_3I$ molecule was studied. The method of double resonance[3] was used to observe transitions between the quadrupole hyperfine structure levels of the rotational spectrum of the molecule. The results of the measurement of the frequencies of the most intense transitions with J = K are given in the Table. Because of the large magnitude of the quadrupole coupling constant of the iodine nucleus in the $CH_3I$ molecule, the calculation of the quadrupole hyperfine structure had to be carried out correct to third order perturbation theory.[4] The calculated values of the third order correction are also given in the Table.

The change in the frequency of the transition F → F + 1, $\Delta J = 0$, due to the magnetic interaction, is given by the formula

$$\delta W_m = \pm(F+1)\left[a+(b-a)\frac{K^2}{J(J+1)}\right]. \quad (2)$$

where the ± sign depends on the relative positions of the F and F + 1 levels.

Each pair of transitions with J = 2 and 3, as seen from the Table, comprises a positive as well as a negative shift $\delta W_m$; this gives the possibility of determining independently the quadrupole coupling constant $(eqQ)_I$ and the energy of the I-J interaction. The determination of the constants a and b is shown in the diagram. The error of the measurements permits the establishment of only an upper limit for the value of the constant a ≤ 1.04 kc; however, since a is positive (the sign of a is determined by the sign of the magnetic moment of the molecule), the constant b can be determined fairly accurately: b = 19.9 ± 0.5 kc. It is possible to establish a lower limit for the ratio b/a ≥ 19.6, which agrees well with the ratio of the rotational constants of the $CH_3I$ molecule, which is equal to 20.

| J, K | F → F + 1 | Transition Frequency (kc) | Third order correction (kc) | $(eqQ)_I$ (kc) | $\frac{\lvert\delta W_m\rvert}{F+1}$ (kc) |
|---|---|---|---|---|---|
| 1 | $\frac{3}{2}\rightarrow\frac{5}{2}$ | 292 417 ± 2 | − 0.1 | — | 4.7 ± 0.40 * |
| 2 | $\frac{3}{2}\rightarrow\frac{5}{2}$ | 276 885 ± 3 | − 1.0 | 1 934 030 ± 20 | 6.8 ± 0.44 |
| | $\frac{7}{2}\rightarrow\frac{9}{2}$ | 374 915 ± 3 | −18.9 | — | — |
| 3 | $\frac{3}{2}\rightarrow\frac{5}{2}$ | 281 600 ± 3 | − 3.2 | 1 933 994 ± 20 | 7.8 ± 0.41 |
| | $\frac{9}{2}\rightarrow\frac{11}{2}$ | 444 662 ± 2 | −12.6 | — | — |

*Calculated for eqQ = 1934012 kc.

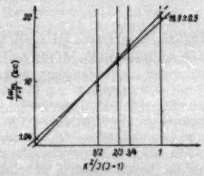


## REFERENCES

1. R. L. White. Revs. Modern Phys. 27, 276 (1955).
2. R. S. Henderson and J. H. Van Vleck. Phys. Rev. 74, 106 (1948).
3. N. G. Basov and B. D. Osipov. Opt. i Spektr. 4, 795 (1954).
4. L. Landau and E. Lifshits. "Kvantovaya mekhanika." (Quantum Mechanics), Pt. I, p. 162, 1948.

# HIGH-SPEED SPECTROMETER WITH SPECTRUM SCANNING BY MEANS OF A ROTATING DISK WITH A SPIRAL SLOT AS EXIT SLIT

V. V. Kolt'sov

Received 28 December 1959

There is a broad range of problems for whose solution the possibility of fast spectrum measurements under laboratory and field conditions has great significance.[1]

In the device reported, a rotating disk with a spiral slot as shown in Fig. 1 is used as the exit slit. During the rotation of the disk the slot is displaced over the spectrum and finally the light flux is collected onto a detector. The use of a rotating disk with spiral slot as the exit slit has, in a number of cases, a substantial advantage compared with the methods of scanning spectra described in the literature.[2] Variation of the form of the spiral and the width of the slit in conformity with the dispersion curve of the monochromator allows a spectrum scanned linearly by wavelength and a uniform slit width through the scanned part of the spectrum to be obtained. In diffraction grating monochromators the use of a slot in the form of an Archimedean spiral $\rho = \rho_0 + k\varphi$ allows a satisfactory linear scan in wavelength to be obtained. The exit slit had a slope relative to the spectrum which impairs the resolution of the device. The greater the radius $\rho$ of the spiral and the smaller the spectrum height h, the smaller this distortion. The location of the axis of the rotating disk above (or below) the spectrum, the decrease in height of the exit slit, and in the same way the use of cylindrical lenses or a cylindrical diffraction grating and a cylindrical lens (mirror) for reducing the height of the spectrum decrease this distortion. Figure 2 shows the dependence $\Delta\lambda = f(\lambda)$ obtained experimentally for various spectrum heights h and computed for h = 0 at $\rho_0$ = 30 mm ($\varphi$ = 0); $\rho_{max}$ = 64 mm ($\varphi$ = 177°).

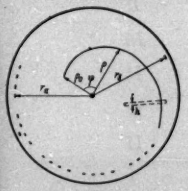

Fig. 1

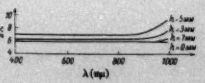

Fig. 2

The exit slit is conveniently placed in one half of the disk, the other half being used for the wavelength calibration and for the production of the dark current lines on the oscillograph screen. To enable this to be done apertures are made in the second half of the disk at a distance $r_s$ from the center greater than the largest value of $\rho$ for the spiral slot. Light from a small illuminator passes through these apertures either to the same detector used for the spectrum being studied, or to an auxiliary detector connected in parallel with it. For the superposition of the wavelength calibration marks on the oscillograph spectrum, the oscillograph scans twice in one revolution of the disk. For this, two apertures are made on a disk diameter at a distance $r_k > r_s$ from the center. Light from a second illuminator passes through these apertures onto a germanium photodiode, which controls the synchronization of the scanning beam of the oscillograph with the scanning spectrum. The proposed method of calibration, in contrast to reference 3, does not require the use of a double beam oscillograph.

The method described of scanning spectra was used in a high-speed spectrometer constructed in 1958 for the study of the intensity of natural objects under normal conditions. A replica reflection diffraction grating of the echelette type of 600 lines/mm and a photomultiplier as detector were used in this device. In the scanning, the "porosity"

$$Z = \frac{\Delta t_{free}}{\Delta t_{lab.}} = 1.02,$$

$\Delta t$ = 0.01 sec, and the recorded spectrum interval is $\Delta\lambda$ = 0.6$\mu$ (in the region 0.4-1 $\mu$), allowing the possibility of a spectrometer P ≈ 120 (for $\lambda$ = 0.7 $\mu$).

In Fig. 3 an oscillogram of a typical transmission interference filter is shown.

Fig. 3

In the necessary application to spectrometric detectors where the time constant is limited by the scanning frequency, it is expedient to make Z ≈ 0, for which it is possible to place a slot in both halves of the rotating disk, or to make one slot over the whole disk. The rotational motion of the spectrum scanning device, which possesses low "porosity," creates favorable conditions for magnetic recording of spectra. The simplicity of the constructional solution of the spectrum scanning device allowed the making of a portable and economical power supply that was of particular value for measurements outside the laboratory. The use of a rotating disk to scan the spectrum facilitates its mechanical coupling to a movie camera used simultaneously for recording the oscillogram and the photographic ties to the object under study.

## REFERENCES

1. V. V. Kolt'sov. Trudy Lab. Aerometod. Akad. Nauk SSSR 7, (1958).
2. O. D. Dmitrivskii, B. S. Neporent, and V. A. Nikitin. Uspekhi Fiz. Nauk 64, 445 (1958).
3. B. W. Bullock and S. Silverman. J. Opt. Soc. Am. 40, 608 (1950).

## CORRECTIONS

Vol. VII, issue 4, p. 307, paper by E. N. Boitsov and A. I. Finkel'shtein, table on p. 308. The compounds and their formulas in the first column "Compound" should be rearranged as follows: melamine, ammeline, ammelide, cyanuric acid.

---

The other two corrections given in this Russian issue (VIII, #4) were made to the articles in the translation issues concerned.

## *TRANSLITERATION OF CYRILLIC CHARACTERS*

**used by the Optical Society of America**

| | | | | | |
|---|---|---|---|---|---|
| А | а | a | Р | р | r |
| Б | б | b | С | с | s |
| В | в | v | Т | т | t |
| Г | г | g | У | у | u |
| Д | д | d | Ф | ф | f |
| Е | е | e | Х | х | kh |
| Ж | ж | zh | Ц | ц | ts |
| З | з | z | Ч | ч | ch |
| И | и | i | Ш | ш | sh |
| Й | й | i | Щ | щ | shch |
| К | к | k | Ъ | ъ | ″ |
| Л | л | l | Ы | ы | y |
| М | м | m | Ь | ь | ′ |
| Н | н | n | Э | э | e |
| О | о | o | Ю | ю | yu |
| П | п | p | Я | я | ya |

# THE OPTICAL SOCIETY OF AMERICA

**Why should you join OSA?**

There is no other association of opticists in existence to promote and disseminate knowledge in this field. The Optical Society of America was organized in 1916 "to increase and diffuse the knowledge of optics in all its branches pure and applied, to promote the mutual interests of investigators of optical problems, of designers, manufacturers and users of optical instruments and apparatus of all kinds, and to encourage co-operation among them".

**What about the advantages of membership?**

You receive three monthly publications:

**THE JOURNAL OF THE OPTICAL SOCIETY OF AMERICA:** *This is the official publication of OSA*

**OPTICS AND SPECTROSCOPY:** *an English translation of the leading scientific journal of the USSR Academy of Sciences in this field*

**PHYSICS TODAY:** *as OSA is a member society of the American Institute of Physics, OSA members receive this publication**

From JOSA and OPTICS AND SPECTROSCOPY you will not only learn what your American colleagues are doing, but also discover what the Russians are working on in your field. Together these two journals publish the work of American and Russian scientists in all branches of optics and spectroscopy, including X-ray, ultraviolet, visible, infrared and microwave, filters, lens design, thin layer optics, geometric optics, electron optics, diffraction gratings, electroluminescence, wave mechanics, thermal radiation backgrounds, detectors, infrared polarizers, and their many applications in science and industry.

You will also receive announcements and programmes of all meetings (OSA holds at least two a year) and, even if you cannot attend many of these, you will know what is going on in your area. And you can submit a paper and have it given by proxy.

**Who can join?**

OSA invites to membership all who are interested in any branch of optics, either in research, in teaching, in optical applications, in the manufacture and distribution of optical equipment of all kinds, or in physiological and medical optics.

**What are the membership dues?** $13.00 per annum.

**How can you join?**

Write Dr. Mary E. Warge, Executive Secretary, Optical Society of America, 1155 16th Street, N. W., Washington 6, D. C., for an application form.

*OSA members may also subscribe to other AIP publications at a reduced rate.

OPTICAL SOCIETY *of* AMERICA
1155 SIXTEENTH STREET, N. W. WASHINGTON 6, D. C.

SHORT COMMUNICATIONS

On the Absorption of Ultraviolet Radiation Behind a Shockwave in the Air . . . . . S. A. Losev, N. A. Generalov, and L. B. Terebenina 300

Calculation of the Errors of an Absorption Analyzer of Gaseous or Liquid Mixtures . . . . . A. O. Sall' 301

The Structure and Nature of Excitation of the Magnesium Oxidation Spectrum . . . . . V. A. Sokolov and N. A. Nazimov 303

The Influence of Proton Mobility on Nuclear Magnetic Resonance Line Width in Crystals . . . . . I. V. Aleksandrov, N. N. Korst, and N. D. Sokolov 304

The Step-Shaped Dependence of the Recombination Luminescence Quantum Yield of Alkali Halide Crystal Phosphors on the Frequency of the Exciting Light . . . . . I. V. Yaek 305

A Method of Structural-Group Analysis by Infrared Spectra. Determination of Mono-Olefinic Structures of the Products of the Gamma-Radiolysis of n-Heptane . . . . . B. A. Smirnov 307

I-J Interaction in the $CH_3I$ Molecule . . . . . B. D. Osipov 309

High-Speed Spectrometer with Spectrum Scanning by Means of a Rotating Disk with a Spiral Slot as Exit Slit . . . . . V. V. Kolt'sov 309

Corrections . . . . . 310

EDITOR'S NOTE

Comments on the scientific content of the translated Russian articles published in OPTICS AND SPECTROSCOPY are invited. They should be addressed as a Letter to the Editor of the Journal of the Optical Society of America and forwarded to the Editor of that journal, Dr. W. R. Brode, National Bureau of Standards, Washington 25, D.C.

VOL. VIII, NO. 4 APRIL 1960

CONTENTS

Ninetieth Anniversary of V. I. Lenin's Birthday ..... 229
On the Calculation of Photoionization Absorption. L. M. Biberman and G. E. Norman 230
Spark Discharge Emission in Helium M. P. Vanyukov, A. A. Mak, and V. P. Muratov 233
Isotope Shift in the Spectrum of Molybdenum Yu. P. Dontsov 236
Isotopic Band Shifts in the Electronic-Vibrational Spectra of Some Diatomic Molecules R. R. Shvangiradze, K. A. Oganezov, and B. Ya. Chikhladze 239
Calculation of the Polarizability of Conjugated Molecules taking into Account the Electrostatic Interaction of π-Electrons T. K. Rebane 242
Frequencies and Intensities in the Infrared Spectrum of Bromoform N. E. Gaponova, M. P. Lisitsa, and Yu. P. Tsyashchenko 245
The Indicatrix of the Raman Scattering of Light L. L. Kondilenko, P. A. Korotkov, and V. L. Strizhevskii 249
The Anti-Stokes Component of the Raman Spectrum for Hydrogen-Bonded Compounds L. N. Ovander 252
Infrared Spectra of Chlorophyll and its Analogues A. N. Sidorov and A. N. Terenin 254
Study of Infrared Absorption Spectra of Dicyclic Hydrocarbons S. V. Markova, P. A. Bazhulin, A. F. Plate, and V. I. Stanko 260
Infrared Absorption Spectra of Hydroxyfluoroboric Complexes of Potassium and Sodium M. V. Aknmanova and G. E. Kurilchikova 264
Vibrational Spectra of the Modifications of Germanium Dioxide V. V. Obukhov-Denisov, N. N. Sobolev, and V. P. Cheremisinov 267
Vibrational Spectra of Alkoxysilanes and Siloxanes. II. Vibrations of the $SiO_4$ Groups in the Spectra of Tetraalkoxysilanes A. N. Lazarev 270
Investigation of the Absorption Spectra of Zinc Sulfide Crystals E. F. Gross, L. G. Suslina, and K. F. Komarovskikh 273
The Luminescence Spectra of Diamonds G. O. Gomon 275
The Mechanism of Scintillations in Organic Substances I. M. Rozman 277
Effect of High-Temperature Annealing on the Luminescence and Coloration of X-Rayed Quartz Crystals M. N. D'Yachenko 281
Luminescence Properties of Cesium Iodide Crystals Grown from a Superheated Melt Yu. A. Tsirlin, V. I. Startsev, and L. M. Soifer 283
Temperature Dependence of the Luminescence of NaI(Tl) Crystals at Temperatures between 0° and 270°C V. I. Startsev, Z. B. Baturicheva, and Yu. A. Tsirlin 286
Temperature Effect on Infrared Quenching K. S. K. Rebane and E. Sakarinen 288
The Properties of ZnS:Mn, Ni, Cl Phosphors under Cathode Ray Excitation A. I. Blazhevich, A. G. Zavrazhin, and A. V. Lavrov 290
The α/β Ratio in a Liquid Scintillator Yu. A. Nemilov, G. N. Belozerskii and A. N. Pisarevskii 292
Scattering of Light in Media with Variable Optical Parameters A. P. Ivanov and E. B. Khodos 293
Use of the Phenomenon of "Total External Reflection" for Filtering the Continuous Spectrum in the Ultra-Soft X-Ray Region A. P. Lukirskii and Yu. A. Omel'chenko 297

*(Contents continued on inside back cover)*